Universitat de Lleida

Measuring the availability of metals in large mixtures with diffusive gradients in thin-films technique (DGT) devices

Jordi Sans Duñó

Universitat de Lleida

VRIJE UNIVERSITEIT BRUSSEL

TESI DOCTORAL EN COTUTELA

MEASURING THE AVAILABILITY OF METALS IN LARGE MIXTURES WITH DIFFUSIVE GRADIENTS IN THIN FILMS (DGT) DEVICES.

Jordi Sans Duñó

Memòria presentada per optar al grau de Doctor per la Universitat de Lleida

Programa de Doctorat en Electroquímica Ciència i Tecnología

Doctoral program of sciences

Directors/a

Jaume Puy Llorens

Joan Cecília Averós

Yue Gao

Tutors/a

Jaume Puy Llorens

Agraïments

El procés per poder produir una tesi és un camí llarg i amb tota mena de reptes dintre de l'àmbit científic i personal. És per això que estic molt agraït amb totes les persones de les quals parlaré a continuació. Vosaltres m'heu brindat les eines i tot el suport emocional per poder realitzar aquest treball amb la major qualitat possible.

Als Drs. Jaume Puy i Joan Cecília que han estat els meus tutors de tesis des de un bon principi d'aquest camí i m'han donat les eines per poder afrontar els reptes científics de la millor manera possible.

Als Drs Yue Gao i Willy Baeyens per dirigir les activitats de recerca durant la meva estada de investigació a l'AMGC. Estic agraït amb la confiança que em van donar quan em van proposar de fer una tesi en règim de co-tutela per tal de poder ampliar el temps d'investigació dintre el grup, conjuntament amb el suport financer que m'han donat.

Als Drs. Josep Galceran, Encarna Companys, Carlos Rey per la seva ajuda i els seus consells que m'han ajudat a resoldre problemes d'àmbit científic.

Al Dr. Calin David per aportar el seu enginy tecnològic per la millora de les tècniques de mesura.

A la Sílvia, per els seus consells en el procés experimental que requereix el maneig de solucions de metalls traça que han de ser analitzades per ICP.

Al Dr. Vincent Perrot i la Tianhui Ma per tot el temps dedicat en ensenyar-me les tècniques de mesura del Hg i a millorar el treball d'investigació que hem estat fent conjuntament a l'AMGC

A la Dr. Martine per donar-me la oportunitat de formar part de l'expedició de mostreig amb el vaixell Belgica.

A la Mingyue Luo, la Wendy i la Delphine amb qui ha estat un plaer treballar conjuntament en diferents tasques de recerca.

A la Maria, el Paulo, l'Antonio, el Fede i la Merche que van fer que l'adaptació a Lleida fos d'allò més ràpida i agradable.

Al Ricardo, L'Anna i la Ruth que van fer l'àmbit de treball un lloc agradable durant l'època del COVID.

Al Kevin, la Lucía, el Joao, l'Adnívia, la Lauren i l'Arné per fer més amè el dia a dia en l'etapa post-COVID.

Als companys de feina del grup AMGC de la VUB, els agraeixo la seva gran acollida al grup d'investigació on m'han fet sentir pràcticament com a casa.
A tots els amics del grup de les pinyes que els vaig conèixer pràcticament només arribar i han fet que viure a Lleida sigui un plaer enorme.
Als meus amics de química per totes les videotrucades que ens hem fet durant el confinament en l'època més severa del COVID i els viatges que hem fet plegats aquests últims anys, un cop les restriccions ho anat permetent.
Als amics del poble que tot i anar per allà cada cop menys freqüentment quan ens trobem és com si el temps no hagués passat.
A la Carol per tota l'estima i el seu suport que m'ha donat durant l'etapa final del doctorat.
A la meva mare, al meu pare i a la meva germana per tot el suport i empenta que m'han donat des de el començament fins al final del doctorat.

Table of Contents

Abstract

The distribution of trace-metal compounds and the physicochemical processes in which these species are involved are key factors to understand bioavailability. Diffusive gradients in thin-films technique (DGT) is a dynamic analytical technique that measures the analyte available after a certain deployment time. It allows to define a DGT-labile concentration of the sample (c_{DGT}) from the knowledge of the metal diffusion coefficient as the only one specific parameter of the analyte. Since c_{DGT} is an effective metal concentration, a relationship with the concentration of the real species was derived by introducing the lability and mobility of each species. Accordingly, methods to measure these physicochemical parameters, as well as, to study their dependence on the composition of the system and the characteristics of the DGT devices are desired.

In this thesis, we have contributed to this aim by studying the dependence of the lability of the species on the geometrical characteristics of the DGT device. Both, rigorous numerical simulations and laboratory experiments have been conducted and complemented with measurements in natural waters.

The influence of the sequential complexation in the availability of Ni in presence of NTA has been studied with DGT devices with different thickness of the diffusive gel and resin layer in laboratory experiments.

New strategies have been provided to measure diffusion coefficients of free metal ions and complexes both in the linear and in the finite volume regimes with diffusion cell devices. Special attention has been devoted to the measurement of the lability degree as well as to the dissociation rate constant of complexes from the mass accumulated in a back resin disc when DGT devices with a stack of two resin discs are used. From first principles, expressions considering a homogeneous or an heterogenous distribution of the resin beads have been developed to determine dissociate rate constants.

The deployment of 3 sets of DGT devices with different configurations has allowed the determination of the lability and diffusivity of a pool of inorganic Zn complexes in the Osor stream.

Finally, the speciation and availability of Hg in solutions with natural organic matter have been studied. A global discussion of the relationship between the reducible Hg fraction, the DGT-labile Hg concentration and the Hg bound to the carboxylic and phenolic sites of SRHA or SRFA has been provided.

Samenvatting

De distributie van sporemetaalverbindingen en de fysisch-chemische processen waarbij deze species betrokken zijn, zijn sleutelfactoren om de biologische beschikbaarheid te begrijpen. Diffusieve gradiënten in dunne-film techniek (DGT) is een dynamische analytische techniek die de beschikbare chemische stof meet na een bepaalde onderdompelingstijd in de oplossing. Het maakt het mogelijk een DGT-labiele concentratie van het monster (c_{DGT}) te bepalen op basis van de kennis van de metaaldiffusiecoëfficiënt als enige specifieke parameter van de chemische stof. Aangezien (c_{DGT}) een effectieve metaalconcentratie is, werd een relatie met de echte species concentratie afgeleid door de labiliteit en mobiliteit van elke species in te voeren. Bijgevolg zijn methoden gewenst om deze fysisch-chemische parameters te meten, alsook om hun afhankelijkheid van de samenstelling van de oplossing en de kenmerken van het DGT-toestel te bestuderen.

In dit proefschrift hebben wij hiertoe bijgedragen door de labiliteit van de species als functie van de geometrische eigenschappen van het DGT-toestel te bestuderen. Zowel rigoureuze numerieke simulaties als laboratoriumexperimenten zijn uitgevoerd en aangevuld met metingen in aquatische systemen.

De invloed van de sequentiële complexatie op de beschikbaarheid van nikkel in aanwezigheid van NTA is bestudeerd met DGT-toestellen met verschillende diffusieve gel en harslaag diktes via laboratoriumexperimenten.

Er zijn nieuwe strategieën ontwikkeld om de diffusiecoëfficiënten van vrije metaalionen en complexen te meten in verschillende omstandigheden met diffusiecellen.

Speciale aandacht is besteed aan de meting van de labiliteitsgraad en de dissociatiesnelheidsconstante van complexen uit de geaccumuleerde massa in de achterste harslaag van een DGT met 2 harslagen. Vanuit de basisbeginselen zijn uitdrukkingen ontwikkeld voor een homogene of heterogene verdeling van de harskorrels om de dissociatiesnelheidsconstanten te bepalen.

Het gebruik van 3 sets DGT-toestellen met verschillende configuraties heeft de bepaling van de labiliteit en diffusiviteit van een pool van anorganische Zn-complexen in de Osor-stroom mogelijk gemaakt.

Tenslotte zijn de speciatie en beschikbaarheid van Hg in oplossingen met natuurlijk organisch materiaal bestudeerd. Een algemene bespreking van het verband tussen de reduceerbare Hg-

fractie, de DGT-labiele Hg-concentratie en het Hg dat gebonden is aan de carboxyl- en fenolische sites van humuszuur of fulvinezuur werd verstrekt.

Resumen

La distribución de compuestos metálicos traza y los procesos fisicoquímicos en los que intervienen estas especies son factores clave para comprender la biodisponibilidad. La técnica "Diffusive gradients in thin-films technique" (DGT) es una técnica analítica dinámica que mide el analito disponible tras un determinado tiempo deposición. Permite definir una concentración DGT-lábil de la muestra (c_{DGT}) a partir del conocimiento del coeficiente de difusión del metal como único parámetro específico del analito. Dado que c_{DGT} es una concentración efectiva de metal, se derivó una relación de la concentración de las especies reales con la labilidad y la movilidad de cada especie. En consecuencia, se desea disponer de métodos para medir estos parámetros fisicoquímicos, así como, estudiar su dependencia de la composición del sistema y de las características de los dispositivos DGT.

En esta tesis, hemos contribuido a este objetivo estudiando la dependencia de la labilidad de las especies con las características geométricas del dispositivo DGT. Se han realizado simulaciones numéricas rigurosas y experimentos de laboratorio que se han complementado con medidas en aguas naturales.

Se ha estudiado la influencia de la complejación secuencial en la disponibilidad de Ni en presencia de NTA con dispositivos DGT con diferentes grosores del gel difusor y de la capa de resina en experimentos de laboratorio.

Se han proporcionado nuevas estrategias para medir los coeficientes de difusión de iones metálicos libres y complejos tanto en el régimen lineal como en el de volumen finito con dispositivos de celdas de difusión.

Se ha prestado especial atención a la medición del grado de labilidad, así como a la constante de velocidad de disociación de los complejos a partir de la masa acumulada en un disco de resina posterior cuando se utilizan dispositivos DGT con una pila de dos discos de resina. A partir de primeros principios, se han desarrollado expresiones considerando una distribución homogénea o heterogénea de las perlas de resina para determinar las constantes de velocidad de disociación.

La deposición de 3 conjuntos de dispositivos DGT con diferentes configuraciones ha permitido determinar la labilidad y difusividad de un conjunto de complejos inorgánicos de Zn en el río Osor.

Finalmente, se ha estudiado la especiación y disponibilidad de Hg en soluciones con materia orgánica natural. Se ha proporcionado una discusión global de la relación entre la fracción de

Hg reducible, la concentración de Hg lábil por DGT y el Hg enlazado a los sitios carboxílicos y fenólicos de SRHA o SRFA

Resum

La distribució de compostos metàl·lics traça i els processos fisicoquímics en els que intervenen aquestes espècies són factors clau per a comprendre la biodisponibilitat. La tècnica “Diffusive gradients in thin-films technique” (DGT) és un tècnica analítica dinàmica que permet mesurar el analit disponible després d’un temps determinat de mesura. A partir del coneixement del coeficient de difusió del metall com a únic paràmetre específic del analit es pot definir la concentració DGT-làbil de la mostra (c_{DGT}). Donat que (c_{DGT}) és una concentració efectiva de metall, se ha demostrat un relació de les espècies reals introduint la labilitat i la mobilitat de cada espècie. En conseqüència, es vol disposar de mètodes per mesurar els paràmetres fisicoquímics, així com, estudiar la seva dependència de la composició del sistema i de les característiques dels dispositius DGT.

En aquesta tesi, per tal d’assolir l’objectiu hem estudiat la dependència de la labilitat de les espècies amb les característiques geomètriques del dispositiu DGT. S’han realitzat simulacions numèriques rigoroses i experiments del laboratori que s’han complementat amb les mesures en aigües naturals.

S’ha dut a terme l’estudi de la influència de la complexació seqüencial de la disponibilitat de Ni en presència de NTA amb els dispositius DGT amb diferents gruixos de gel difusiu i de la capa de resina en experiments de laboratori.

S’han proporcionat noves estratègies per mesurar els coeficients de difusió d’ions metàl·lics i complexes tan en el règim lineal com en el règim de volum finit amb la cel·la de difusió.

S’ha donat especial atenció a la mesura del grau de labilitat, així com a la constant de velocitat de dissociació dels complexes a partir de la massa acumulada en un disc de resina posterior quan s’utilitzen dispositius DGT amb 2 discs de resina apilats. A partir de primers principis, s’han desenvolupat expressions considerant una distribució homogènia o heterogènia de les perles de resina per a determinar les constants de velocitat de dissociació.

La deposició de 3 conjunts de dispositiu DGT amb diferents configuracions ha permès determinar la labilitat i difusivitat d’un conjunt de complexes inorgànics de Zn en el riu Osor.

Finalment, s’ha estudiat la especiació i la disponibilitat de Hg en solucions que contenen matèria orgànica natural. S’ha proporcionat la discussió global de la relació entre la fracció de Hg reduïble, la concentració de Hg làbil per DGT i el Hg enllaçat als setis carboxílics i als fenòlics de SRHA o SRFA.

1 Introduction

Natural waters are highly complex systems in terms of chemical, physical and biological processes [1]. The fate and transport of trace-metal ions depend on inherent characteristics of the natural water defined by their chemical composition and type of physical processes that occur. The knowledge of these processes is relevant to unravel the chemical cycle of an element as well as to understand the mechanisms that produce the biomagnification of a trace-metal element along the food chain [2]. In general, the activity of a free metal ion is regulated by inorganic ligands (such as phosphates, chlorides, carbonates, etc), organic ligands such as fulvic or humic acids, polysaccharides, colloids or suspended particulate matter [3]. The distribution of trace-metal compounds among these variety of species is a key factor to understand the uptake of these elements by biota [4]. In general, only the free metal ion is able to be internalized by some proteins present at the cell membrane. Thus, the use of total concentrations has been proven to be a poor predictor of toxicity for biota.

The uptake process is characterized by different steps including at least the transport to the membrane surface and the internalization. When the metal uptake is rate limited by the internalization step, the free metal ion is able to predict the toxicity of a trace-metal [5-7]. However, this dependence might not be valid for other trace-metals whose transport across the biota membrane is fast enough to produce a metal depletion close to the consuming surface so that the internalization is no longer the rate limiting step in the uptake process. In these conditions, a concentration gradient develops and all the species tend to buffer the metal consumption contributing in this way to the uptake [8-9].

The above overview indicates that the uptake is not only dependent on the process that allow the crossing of the free metal ion through the consuming membrane but it is the result of a set of coupled processes in which many species take part: free metal, complexes and other species that can support the metal consumption. The transport of all these species, usually determined by diffusion, and the interchange reactions (dissociation of complexes) are also relevant determining altogether the toxic or nutritive properties of the media. Accordingly, there is a need to measure the concentration of the different species in which a trace-metal is involved together with the corresponding physicochemical parameters among which diffusion coefficients and dissociation rate constants are the most relevant. Unfortunately, this information is not accessible in many cases since there are large mixtures of ligands in natural media and even not all the ligands present in the media may be known.

Simplifications based on the use of pools or fractions of compounds are many times required to approach the global system and the knowledge of the characteristics of these fractions require a set of independent measurements.

In this thesis, we have focused on the development of a dynamic analytical technique called diffusive gradients in thin-films (DGT). This technique was invented around 1994 [10]. Since then, it has been extensively used by environmental researchers to monitor the concentration of trace-metals in all types of natural waters [11-14].

The idea to develop the DGT technique came from a need to improve the sensitivity of Diffusive Equilibrium in thin-films (DET) for trace-metals in porewaters. But its first application was tested in sea water [10]. The application of the DGT technique has evolved in order to be able to monitor the concentration of trace-metals in soils and sediments [15-16 17 18].

Among the main advantages of DGT devices are the ability to work “on site” avoiding contaminations of the sample, an easy manipulation, accumulations independent of the flow of external water in streams, as well as, a simple interpretation. DGT devices mimic the uptake processes of biota in limiting diffusion conditions so that DGT labile concentrations are expected to be interesting parameters to predict bioavailability.

1.1 The DGT technique

1.1.1 Manufacture and measurement in natural waters

A DGT device is composed of a piston, a resin layer that works as a binding agent, a diffusive gel placed on top of the resin layer, a filter and a cap with a circular hole as indicated in Figure 1.1.

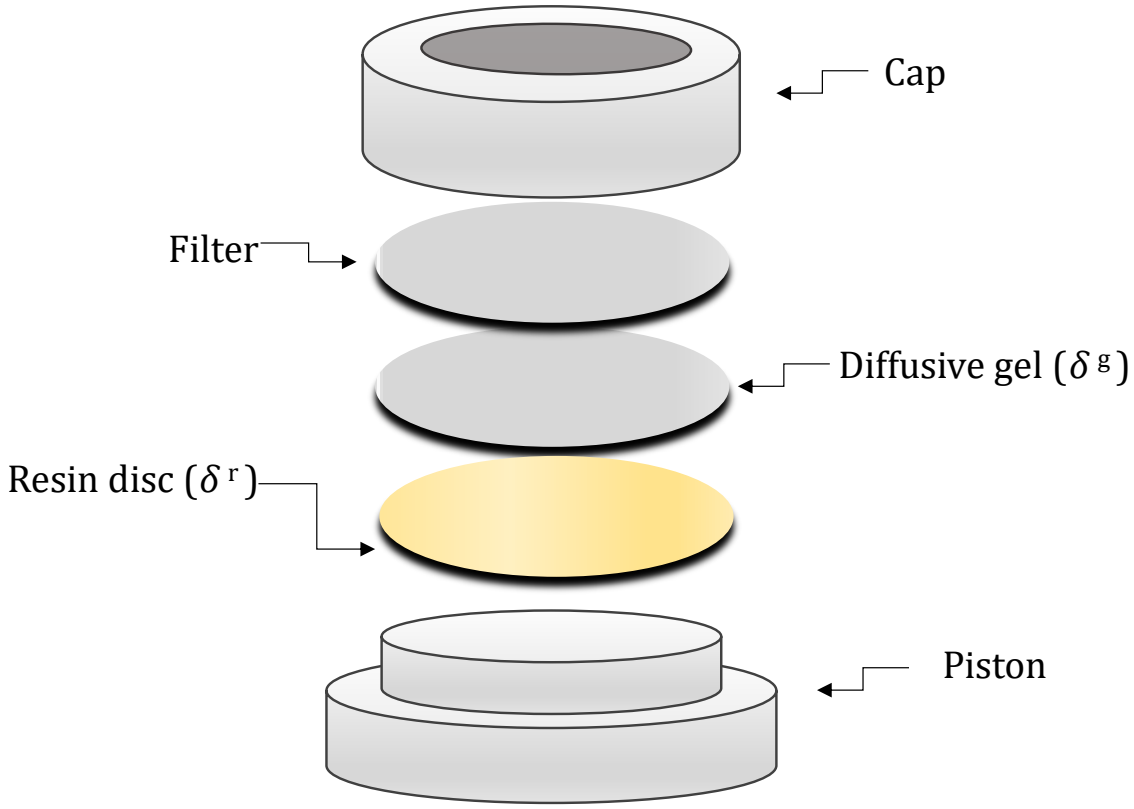

Figure 1.1 Schematic representation of components of a DGT device.

The resin disc is made of the same polymeric matrix than the diffusive gel layer but it includes a dispersion of a fast and strong binding agent of the target analyte. For metal measurements, Chelex 100, a styrene divinylbenzene copolymer containing paired iminodiacetate ions, is usually used as binding agent. It has been proven that Chelex 100 reacts efficiently with free metal ions like Pb^{+2}, Ni^{+2}, Zn^{+2}, Cu^{+2}, Co^{+2} etc [19]. Nevertheless, for other trace-metals elements such as Hg^{+2}, Chelex 100 has shown a kinetic limitation due to a lack of affinity between Hg^{+2} and the iminodiacetic groups [20]. This problem has been solved using other binding agents based on mercaptans such as 3-mercaptopropyl functionalized silica [21].

Binding agents used in DGT devices aim to generate a full depletion of the free trace-metal of interest at the interface of the resin-diffusive gel (perfect sink conditions). The geometrical

characteristics, size of the window and thickness of the diffusive gel and resin were designed to accumulate in natural samples a mass of the target element high-enough for a quantification of the element with ICP-OES or ICP-MS after deployments in the range of hours or days.

When only free metal is present in the solution, after a transient regime lasting of the order of 20 min, a quasi-steady-state is reached with a linear metal concentration profile along the diffusive layer [10]. For deployments lasting hours or days, a very good approximation is based on assuming instantaneous steady-state. Accordingly, the First Fick law allow to write the metal accumulation as:

$$n = At\frac{D_{\mathrm{M}}c_{\mathrm{M}}^{*}}{\delta^{g}} \qquad (1)$$

where n stands for the number of moles of the target accumulated in the resin disc, A is the geometric area, δ^{g} the thickness of the diffusive layer, c_{M}^{*} the metal concentration in the bulk solution, D_{M} the metal diffusion coefficient and t the deployment time.

In presence of complexes, the metal concentration profile in the diffusive gel is no longer linear due to the buffering of the complexes, but using the model outlined above, a DGT-labile concentration, c_{DGT}, can be defined as:

$$n = At\frac{D_{\mathrm{M}}c_{\mathrm{DGT}}}{\delta^{g}} \qquad (2)$$

The DGT labile concentration, c_{DGT}, is then the effective concentration of a sample that, containing only free metal, would give the same accumulation as our system.

According to Eq (2) the interpretation of a DGT accumulation in terms of a labile concentration requires the knowledge of only one parameter specific of the metal: the diffusion coefficient. No detailed knowledge is required on the reaction rate constants between the metal and the binding agent, whenever this binding is fast and strong enough to drop the metal concentration to zero at the diffusive gel/resin interface (perfect sink conditions).

However, close to the interface between the filter and sample solution, the diffusion domain penetrates into the solution in what is called, the diffusive boundary layer (DBL) [22]. When the DBL is considered, Eq (2) assumes that δ^{g} stands for the composed thickness of the diffusive gel, filter and DBL. It has been shown that the diffusion coefficient in the diffusive gel is not far different from that in the filter so that only one layer with the common diffusion

coefficient needs to be considered. In many cases, the external flow of the water where the DGT devices are deployed makes the DBL negligible with respect to the composed thickness of diffusive gel and filter. In these conditions, Eq (2), applies. Otherwise, to improve the quality of the measurement or in cases where the sample is stagnant, the deployment of devices with different thickness of diffusive gel allow to calculate the thickness of the DBL by the linear regression of the inverse of the mass accumulated vs the inverse of the thickness of the gel layer. In stagnant waters (e.g lakes, wells), its determination is almost compulsory to ensure a good measurement, because the flow of water is slow enough to produce a DBL comparable to the thickness of the DGT device [23].

When the binding agent dispersed in the resin domain is electrically charged (for instance, in resin discs prepared with Chelex 100) the immobilized charges in the volume of the resin layer may produce an electric field leading to a migration flux that adds to the diffusive one for electrically charged species. For instance, for negatively charged complexes, the electric field induces a migration flux in the opposite direction to the diffusive flux, thus reducing the metal accumulation in the resin layer at low ionic strengths [24]. When this scenario occurs, a Donnan potential can be calculated by considering that the net charge from the resin layer is neutralized by the trace metal and the concentration of the background salt in the resin domain. In media with a high ionic strength the Boltzmann factors are close to 1 and these characteristics do not play an important role on the measurement of a flux since the electrical charges of the resin are screened by the background salt. However at high ionic strengths, the kinetics and stability of the binding between metal cations and Chelex can also decrease leading to situations where Eq (1) is not valid. In these cases, the kinetics of the binding needs to be considered [24].

In natural waters, as explained in the previous section, the free metal ion is distributed among diverse species involving inorganic, organic, colloids or particulate matter. The species diffuse inside the DGT gels when they are smaller than the pore size of filter and the pore size of the diffusive gel layer. When the free metal ion reaches the resin domain it binds to the resin beads so that the free metal concentration profile in the resin domain is negligible. The consumption of the free metal shifts the complexes towards dissociation. When a complex is able to achieve full dissociation at the interface of the resin-diffusive gel layer, the complex is called labile, whereas a complex that does not dissociate at all along the resin domain is called inert. The complexes that their dissociation rate process is kinetically limited

but they achieve a certain degree of dissociation at the interface of the resin layer are called partially labile complexes. These set of processes are depicted in the following figure:

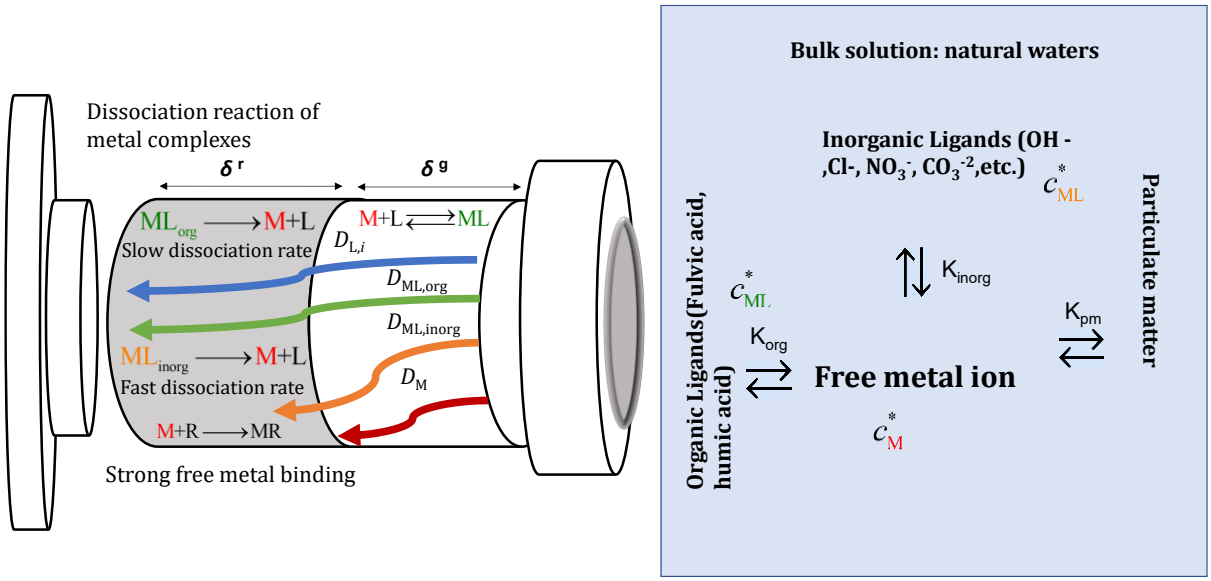

Figure 1.2 Schematic representation of diffusion-reaction processes of different metal species in the bulk solution. A free metal ion (red) together with a set of inorganic complexes (yellow) and organic complexes (green) are included in the figure. A particular diffusion coefficient for each ligand is considered and labelled as $D_{L,i}$ *. In the figure, it is also assumed that the particulate matter cannot cross the filter.*

Figure 1.2 provides an overview of the diffusion-reaction processes in the DGT device for a set of species including a metal and different complexes. The binding of the free metal ion at the interface of the resin-gel layer produces a diffusion gradient of the free metal concentration that penetrates until the bulk solution. Complexes that are labile achieve complete dissociation at the interface of the resin-gel layer. However, partially labile complexes penetrate and dissociate along the resin layer. In the case of inert complexes, although they penetrate in the resin layer, their dissociation is negligible and accordingly, they do not contribute to the metal accumulation.

An overview of a theoretical framework that models the set of diffusion-reaction process taking place in the DGT device together with some results reported in the literature are briefly reviewed in the following section.

1.1.2 Theoretical framework

Eq (2) defines c_{DGT} as an effective concentration. In order to understand the functioning of natural systems, an interpretation of Eq (2) in terms of the real species present in the system has been developed [25 26]. In this framework, when the system contains a set of complexes ML_i with a set of ligands L_i, the accumulation in a DGT sensor can be written as:

$$n = \frac{At}{\delta^g}\left(D_{\mathrm{M}} c_{\mathrm{M}}^{*} + \sum_{i=1}^{h} D_{\mathrm{ML}_i} c_{\mathrm{ML}_i}^{*} \xi_i \right) \tag{3}$$

where ξ_i stands for the lability degree of the complex ML_i which can be identified with:

$$\xi_i = 1 - \frac{c_{\mathrm{ML}_i}^{\mathrm{r}}}{c_{\mathrm{ML}_i}^{*}} \tag{4}$$

where $c_{\mathrm{ML}_i}^{\mathrm{r}}$ stands for the concentration of the complex ML_i at the resin-diffusive gel interface and $c_{\mathrm{ML}_i}^{*}$ labels the complex concentration in the bulk solution

Notice that $0 < \xi_i < 1$. In the case of inert complexes, $\xi_i = 0$, $c_{\mathrm{ML}_i}^{\mathrm{r}} = c_{\mathrm{ML}_i}^{*}$, indicating that there is no dissociation of the complex at the interface diffusive gel/resin even though the free metal concentration at this spatial position drops to zero. The labile complexes are defined in the other limit, $\xi_i = 1$ which implies that $c_{\mathrm{ML}_i}^{\mathrm{r}} = 0$, indicating that the dissociation of the complex is complete and they have reached a local equilibrium with the free metal along the diffusive gel. These complexes are known as labile. Complexes with intermediate dissociation degrees are known as partially labile complexes.

As defined in Eq.(5), the lability degree of a complex in a mixture cannot be experimentally measured.

In addition to the particular lability degree of each complex, a global lability degree of a metal in a system can be defined as:

$$\xi = \frac{J - J_{\mathrm{free}}}{J_{\mathrm{labile}} - J_{\mathrm{free}}} = \frac{\dfrac{n}{At} - \dfrac{D_{\mathrm{M}} c_{\mathrm{M}}^{*}}{\delta^{\mathrm{g}}}}{\displaystyle\sum_{i=1}^{h} \frac{D_{\mathrm{ML}_i} c_{\mathrm{ML}_i}^{*} \xi_i}{\delta^{\mathrm{g}}}} \tag{5}$$

where the flux of free metal is described as:

$$J_{\mathrm{free}} = D_{\mathrm{M}} \frac{c_{\mathrm{M}}^{*}}{\delta^{\mathrm{g}}} \tag{6}$$

and J_{labile}, the hypothetical flux in the system when all the complexes were labile can be written as:

$$J_{\mathrm{labile}} = \sum_{i=1}^{h} D_{\mathrm{ML}_i} \frac{c_{\mathrm{ML}_i}^{*}}{\delta^{\mathrm{g}}} \tag{7}$$

Notice that Eq (5) indicates that the lability degree is related to the contribution of the complexes to the metal flux. It can be defined as the increase of the metal flux due to the

presence of complexes ($J - J_{\text{free}}$) with respect to the maximum contribution of the complexes to the metal flux ($J_{\text{labile}} - J_{\text{free}}$) which would arise when all complexes were fully labile, i.e., $\xi_i = 1 \quad \forall i$.

In a system with only one complex, Eq (5) indicates that the lability degree of this complex is experimentally accessible from the accumulation of metal in a DGT device (*n*)

$$\xi_i = \frac{\frac{n}{At} - \frac{D_{\text{M}} c^*_{\text{M}}}{\delta^g}}{\frac{D_{\text{ML}_i} c^*_{\text{ML}_i}}{\delta^g}} \qquad (8)$$

whenever the speciation and the diffusion coefficients of both free metal and complex are known.

The interpretation of the physical meaning of Eq (3) is now very simple: the total flux is the addition of the flux of free metal in the solution plus a contribution from all the complexes equal to the fraction of the maximum contribution indicated by the respective lability degree. Eq (3) also indicates that in addition to geometric characteristics of the DGT device, the accumulation depends on the mobilities (D_{i}) and labilities (ξ_i) of all the species [27] [28-29].

A main question around the lability degree remains: Is it an intrinsic property of a complex or is it dependent on the device and on the composition of the media?. Several works have been devoted to answer this question as well as to describe these dependences. It has been shown that the lability degree depends on the thickness of the diffusive gel and the resin disc. Increasing both thicknesses, the lability degree tends to increase since partially labile complexes have more time to dissociate while travelling by diffusion across both discs (see Figure 2). The same argument suggests that the lability degree also tends to increase as the diffusion coefficient of the complex decreases. Approximate analytical expressions for this dependence in systems with only one complex have been reported both when the electrostatic effects originated by the charge of the resin beads are negligible [30] or when these effects are relevant and are modelled through a Donnan model [31].

The dependence of the lability degree on the concentration of the ligand in a system with only one ligand has also been studied. It has been shown that an increase of the ligand concentration tends to decrease the lability degree of the complex in the range of ligand excess but this is a mild dependence in comparison with the same influence in other sensors. Conversely, in absence of ligand excess, i. e., when the free ligand concentration profile is

not flat along the DGT device, an increase of the ligand concentration tends to increase the lability degree of the complex.

Studies of the dependence of the lability degree of a complex on the concentration of other ligands are still scarce. Previous results have suggested that although the influence of the system composition on the lability degree of a complex could be relevant, the use of the lability degree measured in single ligand solutions in the prediction of the flux of the mixtures has only small deviations since mutual influences between the lability degrees of a couple of complexes are on the opposite sense and tend to cancel[32].

It seems then pertinent to try to increase the knowledge of the dependence of the lability degree on the composition of the system in ligand mixtures as well as to focus on the determination of intrinsic physicochemical parameters like diffusion coefficients and dissociation rate constants in order to increase our knowledge on the functioning of natural system.

1.2 Outline of the thesis

In this thesis, we have aimed to further develop this theoretical framework by:

1) Developing a rigorous numerical code that applies the Finite Element Method (FEM) to solve the diffusion-reaction equations (PDE) that are involved in the accumulation of trace-metal ions in a DGT device in presence of ligands.

2) Setting up new strategies to determine diffusion coefficients of free metal ion and complexes from experimental measurements in a diffusion cell device:
    a. We would like to model the transport of a set of species that interact among them to quantitatively interpret the processes in a diffusion cell. We would like to apply this model to determine the diffusion coefficients of free metal cations and complexes using experiments at different ligand concentrations.
    b. We would also like to model the transport in the diffusion cell when effects of the finite volume of both cells are non-negligible. With this model, we aim to determine the diffusion coefficient of a set of free metal ions.

3) In natural waters, the free metal ions endure several complexation reactions that may modify their contribution to the uptake by biota. With some hypothesis, in chapter 4, this problem has shown to be formally identical to the one of a single ML complex by just defining a formal complex species with an apparent dissociation rate constant and an apparent diffusion coefficient. In consequence, the formula of the lability degree in excess of ligand, perfect sink and steady-state conditions can be applied to reproduce the experimental results when Ni endures successive complexation with NTA. The use of different DGT configurations are employed to show the dependency of the lability degree with the thickness of the resin and gel layer.

4) The use of DGT devices with a stack of 2 resins have been proved to be useful to elucidate the presence of partially labile complexes and to determine the dissociation rate constant[33]. Nevertheless, the casting of the Chelex 100 resin produces a heterogeneous distribution of the resin layer. From first principles, in chapter 5 we have developed a model for a double heterogeneous resin layer considering that half of the volume of the resin disc is empty. The dissociation rate constant of a metal complex has been obtained from the application of this model in controlled laboratory experiments and in natural

waters. From these results, the contribution of these complexes to the biouptake by biota has been assessed in diffusion limited conditions.

5) Hg is a trace-metal element that has been extensively studied because its toxicity and bioaccumulation along the food chain represents a hazard to human health [34]. However, the accumulation of Hg in DGT devices in presence of organic matter is still far from being understood. For a further insight into this problem, we compare the measurements of different Hg fractions: reducible and non-reducible Hg, labile and non-labile Hg and the Hg bound to phenolic and carboxylic sites in experiments in presence of Suwanee river humic acid (SRHA) and Suwanee river fulvic acid (SRFA).

6) A stream located in Girona, Catalonia, where former mining activity contaminated the river water [35] has been sampled with several analytical techniques to obtain complementary data about Zn concentration and its speciation. In chapter 7 we report the results obtained when the measurements of c_{DGT} with different DGT devices ae used in order to determine the physicochemical properties of Zinc complexes in Osor stream (i.e the diffusion coefficient and the dissociation rate constant).

1.3 References

1. Buffle, J., *Complexation Reactions in Aquatic Systems. An Analytical Approach.* Ellis Horwood Limited: Chichester, 1988.
2. Amyot.M, M. F. M. M. K. A. M. L., The Chemical Cycle and Bioaccumulation of Mercury. *Annu. Rev. Ecol. Syst* **1998,** *29*, 543-566.
3. Buffle, J., Introduction. In *Complexations reactions in aquatic systems: An analytical approach*, Ellis Horwood Limited: 1988; pp 1-11.
4. Worms, I.; Simon, D. F.; Hassler, C. S.; Wilkinson, K. J., Bioavailability of trace metals to aquatic microorganisms: importance of chemical, biological and physical processes on biouptake. *Biochimie* **2006,** *88* (11), 1721-1731.
5. Galceran, J.; van Leeuwen, H. P., Dynamics of biouptake processes: the role of transport, adsorption and internalisation. In *Physicochemical kinetics and transport at chemical-biological surfaces. IUPAC Series on Analytical and Physical Chemistry of Environmental Systems*, van Leeuwen, H. P.; Koester, W., Eds. John Wiley: Chichester (UK), 2004; Vol. 9, pp 147-203.
6. Paquin, P. R.; Gorsuch, J. W.; Apte, S.; Batley, G. E.; Bowles, K. C.; Campbell, P. G. C.; Delos, C. G.; Di Toro, D. M.; Dwyer, R. L.; Galvez, F.; Gensemer, R. W.; Goss, G. G.; Hogstrand, C.; Janssen, C. R.; McGeer, J. C.; Naddy, R. B.; Playle, R. C.; Santore, R. C.; Schneider, U.; Stubblefield, W. A.; Wood, C. M.; Wu, K. B., The biotic ligand model: a historical overview. *Comparative Biochemistry and Physiology C-Toxicology & Pharmacology* **2002,** *133* (1-2), 3-35.
7. Heijerick, D. G.; De Schamphelaere, K. A. C.; Janssen, C. R., Biotic ligand model development predicting Zn toxicity to the alga Pseudokirchneriella subcapitata: possibilities and limitations. *Comparative Biochemistry and Physiology C-Toxicology & Pharmacology* **2002,** *133* (1-2), 207-218.
8. Degryse, F.; Smolders, E.; Merckx, R., Labile Cd complexes increase Cd availability to plants. *Environmental Science and Technology* **2006,** *40* (3), 830-836.
9. Degryse, F.; Smolders, E.; Parker, D. R., Metal complexes increase uptake of Zn and Cu by plants: implications for uptake and deficiency studies in chelator-buffered solutions. *Plant and Soil* **2006,** *289* (1-2), 171-185.
10. Davison, W.; Zhang, H., In-situ speciation measurements of trace components in natural- waters using thin-film gels. *Nature* **1994,** *367* (6463), 546-548.
11. Sigg, L.; Black, F.; Buffle, J.; Cao, J.; Cleven, R.; Davison, W.; Galceran, J.; Gunkel, P.; Kalis, E.; Kistler, D.; Martin, M.; Noel, S.; Nur, Y.; Odzak, N.; Puy, J.; Van Riemsdijk, W.; Temminghoff, E.; Tercier-Waeber, M. L.; Toepperwien, S.; Town, R. M.; Unsworth, E.; Warnken, K. W.; Weng, L. P.; Xue, H. B.; Zhang, H., Comparison of analytical techniques for dynamic trace metal speciation in natural freshwaters. *Environmental Science & Technology* **2006,** *40* (6), 1934-1941.
12. Gao, Y.; Zhou, C. Y.; Gaulier, C.; Bratkic, A.; Galceran, J.; Puy, J.; Zhang, H.; Leermakers, M.; Baeyens, W., Labile trace metal concentration measurements in marine environments: From coastal to open ocean areas. *Trac-Trends in Analytical Chemistry* **2019,** *116*, 92-101.
13. Gimpel, J.; Zhang, H.; Davison, W.; Edwards, A. C., In situ trace metal speciation in lake surface waters using DGT, dialysis, and filtration. *Environmental Science and Technology* **2003,** *37* (1), 138-146.
14. Menegario, A. A.; Yabuki, L. N. M.; Luko, K. S.; Williams, P. N.; Blackburn, D. M., Use of diffusive gradient in thin films for in situ measurements: A review on the progress in

chemical fractionation, speciation and bioavailability of metals in waters. *Analytica Chimica Acta* **2017,** *983*, 54-66.
15. Harper, M. P.; Davison, W.; Zhang, H.; Tych, W., Kinetics of metal exchange between solids and solutions in sediments and soils interpreted from DGT measured fluxes. *Geochimica Et Cosmochimica Acta* **1998,** *62* (16), 2757-2770.
16. Harper, M. P.; Davison, W.; Tych, W., DIFS - a modelling and simulation tool for DGT induced trace metal remobilisation in sediments and soils. *Environmental Modelling & Software* **2000,** *15* (1), 55-66.
17. Lehto, N. J., Principles and application in soils and sediments. In *Diffusive Gradients in Thin-Films for environmental measurements*, Davison, W., Ed. Cambridge University Press: Cambridge, 2016; pp 146-173.
18. Marrugo-Madrid, S., Turull, M. Zhang,H. Diez, S., Diffusive gradients in thin-films for the measurement of labile metal species in water and soils: a review. *Environmental Chemistry Letters* **2021,** *19*, 3761-3788.
19. Bennett, W. W.; Arsic., M.; Panther, J. G.; Welsh, D. T.; Teasdale, P. R., Binding Layer Properties. In *Diffusive Gradients in Thin-films for environmental measurements*, First ed.; Davison, W., Ed. Cambridge University Press: Cambridge, 2016; pp 66-92.
20. Docekalova, H.; Divis, P., Application of diffusive gradient in thin films technique (DGT) to measurement of mercury in aquatic systems. *Talanta* **2005,** *65* (5), 1174-1178.
21. Gao, Y.; De Canck, E.; Leermakers, M.; Baeyens, W.; Van Der Voort, P., Synthesized mercaptopropyl nanoporous resins in DGT probes for determining dissolved mercury concentrations. *Talanta* **2011,** *87*, 262-267.
22. Warnken, K. W.; Zhang, H.; Davison, W., Accuracy of the diffusive gradients in thin-films technique: Diffusive boundary layer and effective sampling area considerations. *Analytical Chemistry* **2006,** *78* (11), 3780-3787.
23. Santos, C. A.; Gemeiner, H.; Menegario, A. A.; Galceran, J.; Teixeira Zanatta, M. B.; Chang, H. K., A new approach to improve the accuracy of DGT (Diffusive Gradients in Thin-films) measurements in monitoring wells. *Talanta* **2022,** *238*, 123044.
24. Altier, A.; Jimenez-Piedrahita, M.; Rey-Castro, C.; Cecilia, J.; Galceran, J.; Puy, J., Accumulation of Mg to diffusive gradients in thin films (DGT) devices: kinetic and thermodynamic effects of the ionic strength. *Analytical Chemistry* **2016,** *88* (20), 10245-10251.
25. Galceran, J.; Puy, J., Interpretation of diffusion gradients in thin films (DGT) measurements: a systematic approach. *Environmental Chemistry* **2015,** *12* (2), 112-122.
26. Baeyens, W.; Gao, Y.; Davison, W.; Galceran, J.; Leermakers, M.; Puy, J.; Superville, P. J.; Beguery, L., In situ measurements of micronutrient dynamics in open seawater show that complex dissociation rates may limit diatom growth. *Scientific Reports* **2018,** *8*.
27. Galceran, J.; Puy, J.; Salvador, J.; Cecília, J.; Mas, F.; Garcés, J. L., Lability and mobility effects on mixtures of ligands under steady-state conditions. *Phys. Chem. Chem. Phys.* **2003,** *5*, 5091-5100.
28. Salvador, J.; Garcés, J. L.; Galceran, J.; Puy, J., Lability of a mixture of metal complexes under steady-state planar diffusion in a finite domain. *Journal of Physical Chemistry B* **2006,** *110* (27), 13661-13669.
29. Salvador, J.; Puy, J.; Cecilia, J.; Galceran, J., Lability of complexes in steady state finite planar diffusion. *Journal of Electroanalytical Chemistry* **2006,** *588*, 303-313.
30. Puy, J.; Mongin, S.; Uribe, R.; Cecilia, J.; Galceran, J.; Zhang, H.; Davison, W. In ***Key role of the resin thickness on the metal flux and lability degree of complexes measured with diffusion gradients in thin films (DGT)***, SETAC Europe 21st Annual Meeting. Ecosystem Protection in a Sustainable World: A challenge for Science and Regulation, Milano (Italy), Milano (Italy), 2011; pp Conference book of abstracts ET12A-1 (p57).

31. Puy, J.; Galceran, J.; Cruz-Gonzalez, S.; David, C. A.; Uribe, R.; Lin, C.; Zhang, H.; Davison, W., Metal accumulation in DGT: Impact of ionic strength and kinetics of dissociation of complexes in the resin domain. *Anal. Chem.* **2014,** *86*, 7740-7748.
32. Altier, A.; Jimenez-Piedrahita, M.; Uribe, R.; Rey-Castro, C.; Cecilia, J.; Galceran, J.; Puy, J., Effects of a mixture of ligands on metal accumulation in diffusive gradients in thin films (DGT). *Environmental Chemistry* **2018,** *15* (3), 183-193.
33. Jimenez-Piedrahita, M.; Altier, A.; Cecilia, J.; Rey-Castro, C.; Galceran, J.; Puy, J., Influence of the settling of the resin beads on Diffusion Gradients in Thin films measurements. *Analytica Chimica Acta* **2015,** *885*, 148-155.
34. Mason, R. P.; Fitzgerald, W. F.; Morel, F. M. M., The Biogeochemical Cycling OF Elemental Mercury - Anthropogenic Influences. *Geochimica Et Cosmochimica Acta* **1994,** *58* (15), 3191-3198.
35. Navarro, A.; Font, X.; Viladevall, M., Metal Mobilization and Zinc-Rich Circumneutral Mine Drainage from the Abandoned Mining Area of Osor (Girona, NE Spain). *Mine Water and the Environment* **2015,** *34* (3), 329-342.

2 Numerical procedure to solve the diffusion-reaction equations (PDE) of metal binding to DGT devices in presences of ligands.

2.1 Description of the problem

The transport of the metal species inside the DGT device is described by the diffusion-reaction equations (PDE). In many practical situations, the system of partial differential equations that describes the motion of the species cannot be uncoupled [1]. Thus, it is not possible to derive an analytical solution that describes the transport of the species in that specific situation. As a result, a usual way to solve PDE is by using numerical methods that transform a system of partial differential equations into an algebraic system of equations [2]. We aim to find the solution of a system of diffusion-reaction PDE under a set of specific boundary values that model the physicochemical behaviour of a DGT device. The diffusion transport in this device mainly occurs along the DGT axis, because the free metal ion strongly binds to the resin layer. Thus, the solution of the boundary problem in one dimension is enough to understand the transport of the metal ions in a DGT device. A one dimensional representation of the system is given by the following figure:

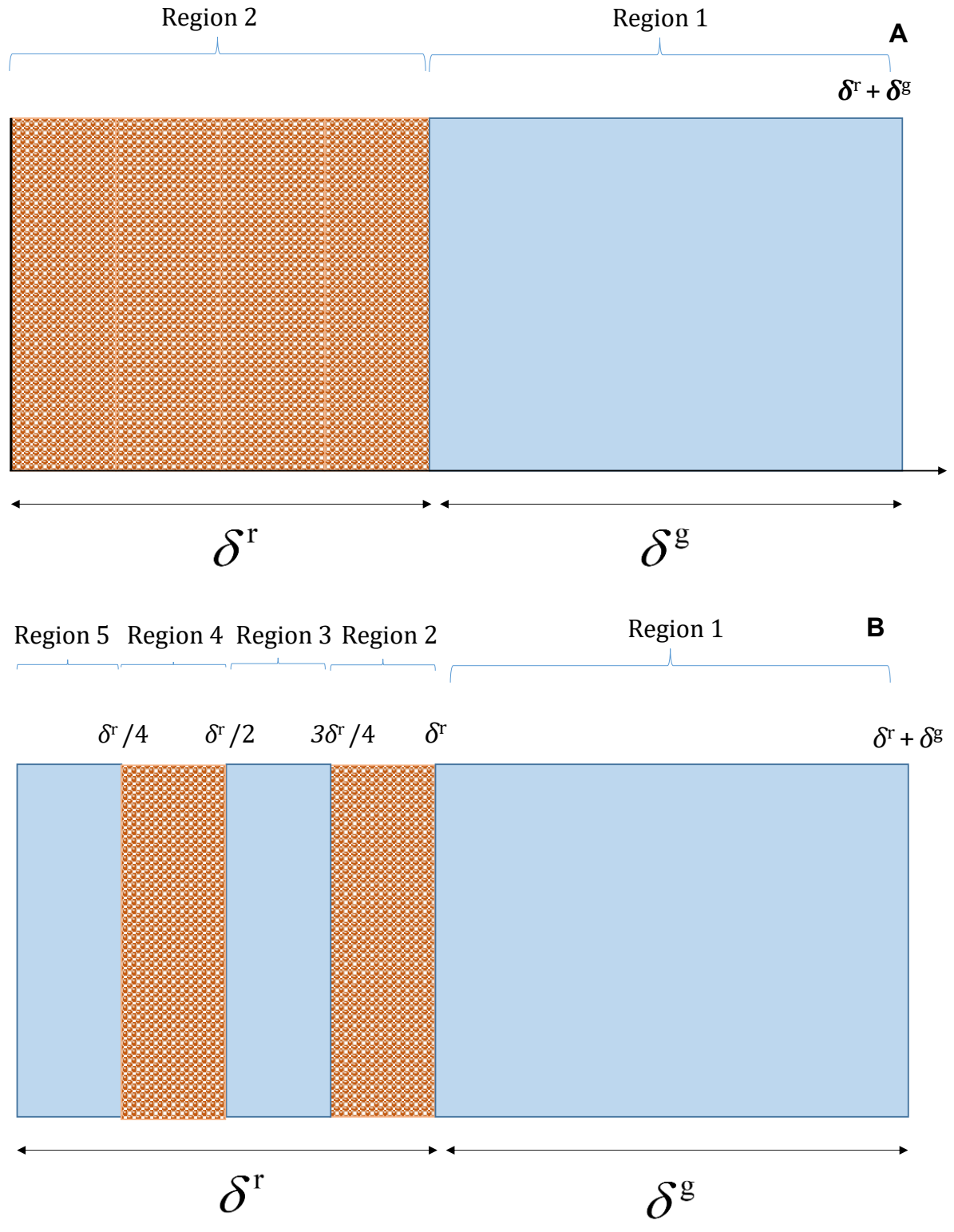

Figure 2.1 schematic representation of the regions of a DGT device for an homogeneous resin (Panel A) heterogeneous resin (Panel B). In both cases δ^g includes the gel layer, filter and DBL where is assumed that the species have the same diffusion coefficient.

In Figure 2.1 is displayed a one dimensional representation along the DGT axis. It defines the domain to solve the diffusion-reaction motion of a metal in presence of *h* ligands where each

ligand can endure *n* successive reactions. Additionally, side reactions of the ligand with other reactants can be considered (e.g protonation of the ligand). Nevertheless, the reactions that are considered in the program must have the following form:

$$A + B \underset{k_d}{\overset{k_a}{\rightleftharpoons}} C \tag{2.1}$$

Where k_a is the association reaction rate constant and k_d is the dissociation reaction rate constant in the gel layer and bulk solution. Whereas k_d^R is the dissociation reaction rate constant in the resin layer. The equilibrium constant is defined by $K = \frac{k_a}{k_d}$. When the species are in equilibrium their concentrations become c_A^*, c_B^*, c_C^*, and fulfil the equilibrium constant by $K = \frac{c_C^*}{c_A^* c_B^*}$.

In the resin domain, we have considered different types of distribution among the resin beads. A homogeneous distribution implies that the resin beads are placed along the whole domain from $0>x>\delta^r$. An heterogeneous distribution of the resin layer is modelled in a way that the resin beads are placed from $\delta^r/2>x>\delta^r$ and from $0>x>\delta^r/2$ there are no resin beads. For a stack of 2 resin discs, the regions where there are resin beads are from $\delta^r/2>x>\delta^r$ and from $\delta^r/4>x>\delta^r./2$. In these regions, the metal ions may endure a reaction with the resin beads, in the following way:

$$\mathrm{M} + \mathrm{R} \underset{k_{d,R}}{\overset{k_{a,R}}{\rightleftharpoons}} \mathrm{MR} \tag{2.2}$$

Where $k_{a,R}$ is the association reaction rate constant and $k_{d,R}$ is the dissociation reaction rate constant which equilibrium constant is defined by $K_R = \frac{k_{a,R}}{k_{d,R}}$.

Considering the previous specifications of the problem the diffusion-reaction equations that are going to be solved are:

$$\frac{\partial c_i}{\partial t} = \begin{Bmatrix} D_i \\ D_i^R \end{Bmatrix} \frac{\partial^2 c_i}{\partial x^2} + \sum_{j=1}^{Nreac} reaction\ terms \tag{2.3}$$

Where D_i and D_i^{R} are the diffusion coefficients in the gel layer and in the resin layer respectively. *Nreac* defines the total number of reactions that the species *i* is enduring with the form $A + B \underset{k_{\mathrm{d}}}{\overset{k_{\mathrm{a}}}{\rightleftharpoons}} C$. Therefore for a general system of the following form:

$$
\begin{aligned}
& c_{L_{11}} + c_{L_{12}} \underset{k_{\mathrm{d}1}}{\overset{k_{\mathrm{a}1}}{\rightleftharpoons}} c_{L_{13}} \\
& c_{L_{21}} + c_{L_{22}} \underset{k_{\mathrm{d}2}}{\overset{k_{\mathrm{a}2}}{\rightleftharpoons}} c_{L_{23}} \\
& \quad \cdots \\
& c_{L_{j,1}} + c_{L_{j,2}} \underset{k_{\mathrm{d},j}}{\overset{k_{\mathrm{a},j}}{\rightleftharpoons}} c_{L_{j,3}} \\
& \quad \cdots \\
& c_{L_{h,1}} + c_{L_{h,2}} \underset{k_{\mathrm{d},h}}{\overset{k_{\mathrm{a},h}}{\rightleftharpoons}} c_{L_{h,3}}
\end{aligned}
\qquad (2.4)
$$

We need to define an index matrix ($\boldsymbol{M}_{\mathrm{reac}}$) that keeps track of the set of reactions that endure each species in our system. Where the dimension of $\boldsymbol{M}_{\mathrm{reac}}$ is *N*x3 and in general it has the following shape:

$$
M_{\mathrm{reac}} = \begin{pmatrix}
L_{11} & L_{12} & L_{13} \\
L_{21} & L_{22} & L_{23} \\
 & \cdots & \\
L_{j1} & L_{j2} & L_{j3} \\
 & \cdots & \\
L_{h1} & L_{h2} & L_{h3}
\end{pmatrix}
\qquad (2.5)
$$

Where the values $L_{i,j}$ are integer numbers that label each species that is having a reaction, and in the program are used to indicate the concentration of the species that are reacting with the species *i*.

The matrix that stores the kinetic reaction constants ($\boldsymbol{k}_{\mathrm{reac}}$) has the same number of rows and columns than $\boldsymbol{M}_{\mathrm{reac}}$, because it stores the value of k_{a}, k_{d} and $k_{\mathrm{d}}^{\mathrm{R}}$. Thus ,

$$k_{\text{reac}} = \begin{pmatrix} k_{\text{a},1} & k_{\text{d},1} & k_{\text{d},1}^{\text{R}} \\ k_{\text{a},2} & k_{\text{d},2} & k_{\text{d},2}^{\text{R}} \\ & & \\ k_{\text{a},j} & k_{\text{d},j} & k_{\text{d},j}^{\text{R}} \\ & \cdots & \\ k_{\text{a,N}} & k_{\text{d,N}} & k_{\text{d,N}}^{\text{R}} \end{pmatrix} \tag{2.6}$$

Once $\boldsymbol{M}_{\text{reac}}$ and $\boldsymbol{k}_{\text{reac}}$ have been defined a general definition of the system of diffusion reaction PDE equations can be done and for the species A and B in the gel layer would be:

$$\frac{\partial c_i}{\partial t} = D_i \frac{\partial^2 c_i}{\partial x^2} + \sum_{j=1}^{Nreac} \left(-k_{\text{reac}(j,1)} c_{M_{\text{reac}}(j,1)} c_{M_{\text{reac}}(j,2)} + k_{\text{reac}(j,2)} c_{M_{\text{reac}}(j,3)} \right) \tag{2.7}$$

Whereas for the species C the sign in the reaction is the opposite to the species A and B , thus:

$$\frac{\partial c_i}{\partial t} = D_i \frac{\partial^2 c_i}{\partial x^2} + \sum_{j=1}^{Nreac} \left(k_{\text{reac}(j,1)} c_{M_{\text{reac}}(j,1)} c_{M_{\text{reac}}(j,2)} - k_{\text{reac}(j,2)} c_{M_{\text{reac}}(j,3)} \right) \tag{2.8}$$

To formulate the transport equation in the resin domain for the species A or B, the term $c_{\boldsymbol{M}\text{reac}(j,3)}$ should be multiplied by $\boldsymbol{k}_{\text{reac}(j,3)}$ and D_i changed for D_i^{R} and the transport equation is written as:

$$\frac{\partial c_i}{\partial t} = D_i^{\text{R}} \frac{\partial^2 c_i}{\partial x^2} + \sum_{j=1}^{Nreac} \left(k_{\text{reac}(j,1)} c_{M_{\text{reac}}(j,1)} c_{M_{\text{reac}}(j,2)} + k_{\text{reac}(j,3)} c_{M_{\text{reac}}(j,3)} \right) \tag{2.9}$$

For the species C, the sign in the reaction term $\boldsymbol{k}_{\text{reac}(j,3) \text{ and } c_{\text{M, reac}(j,3)}}$ is the opposite to the species A and B as explained above:

$$\frac{\partial c_i}{\partial t} = D_i^{\text{R}} \frac{\partial^2 c_i}{\partial x^2} + \sum_{j=1}^{Nreac} \left(k_{\text{reac}(j,1)} c_{M_{\text{reac}}(j,1)} c_{M_{\text{reac}}(j,2)} - k_{\text{reac}(j,3)} c_{M_{\text{reac}}(j,3)} \right) \tag{2.10}$$

To have a better understanding of how works the matrix $\boldsymbol{M}_{\text{reac}}$, let us consider a particular case where a metal (M) reacts with a 2 different ligands (^{1}L, ^{2}L) and each ligand endures 2 successive complexation reactions (M^1L_1 , M^1L_2) and (M^2L_1 , M^2L_2). Then, the set of chemical reactions to consider are :

$$
\begin{aligned}
&M + {}^{1}L \underset{k_{d1}}{\overset{k_{a1}}{\rightleftharpoons}} M^{1}L \\
&M + {}^{2}L \underset{k_{d,2}}{\overset{k_{a,2}}{\rightleftharpoons}} M^{2}L \\
&M^{1}L + {}^{1}L \underset{k_{d,3}}{\overset{k_{a,3}}{\rightleftharpoons}} M^{1}L_{2} \\
&M^{2}L + {}^{2}L \underset{k_{d,4}}{\overset{k_{a,4}}{\rightleftharpoons}} M^{2}L_{2}
\end{aligned}
\tag{2.11}
$$

Assigning a new integer number every time a new species appears in the set of reactions, the matrix $\boldsymbol{M}_{\text{reac}}$ for the last example would become:

$$
M_{\text{reac}} = \begin{pmatrix} 1 & 2 & 3 \\ 1 & 4 & 5 \\ 3 & 2 & 6 \\ 5 & 4 & 7 \end{pmatrix} \tag{2.12}
$$

Where the labels of the species for the metal M is “1” , the ligand ^{1}L is “2”, the complex $M^{1}L$ is “3”, the ligand ^{2}L is “4”, the complex $M^{2}L$ is “5”, the complex $M^{1}L_{2}$ is “6” and the complex $M^{2}L_{2}$ is “7”. Notice that to keep track of the species of the first 2 complexations reactions (first and second row of Eq (2.12)), we don’t need 6 numbers to label each species, because the same metal (with label “1”) is reacting with 2 different ligands. For the successive complexation reactions (rows 3 and 4), we use the integer numbers that have been already assigned to the complex $M^{1}L$, $M^{2}L$ and their ligands ^{1}L , ^{2}L, but the species produced ($M^{1}L_{2}$, $M^{2}L_{2}$) are labelled with a new integer number.

2.2 Initial and boundary conditions

The formulation of our boundary problem requires to impose a set of boundary values and initial conditions to the partial differential equations. In particular, to solve these set of equations we need to impose the equilibrium condition at the bulk solution which requires to solve the equilibrium problem from a set of total metal and ligand concentrations for a given pH and in a given temperature. The speciation code VMINTEQ has been applied to obtain these set of equilibrium concentrations, as well as, their equilibrium constants.
The DGT device is considered to be empty at t=0, thus :

$$c_i(t=0, 0<x<\delta^{r}+\delta^{g})=0 \tag{2.13}$$

and the bulk solution is considered well-agitated so the concentration of the species at the interface between the DGT device and the bulk solution is considered to be in equilibrium, therefore:

$$c_i(t\geq 0, x=\delta^{r}+\delta^{g})=c_i^{*} \tag{2.14}$$

Also, at the bottom of the DGT device there is a piston that is assumed to be impermeable and does not endure any binding reaction, thus, there is no flux of matter across the piston:

$$\left.\frac{\partial c_i}{\partial x}\right|_{x=0}=0 \tag{2.15}$$

The transfer of matter from the gel layer to the resin layer is considered by the flux equality at the interface of the resin layer. Nevertheless, we consider to apply the Donnan potential to take into account the electrostatic effects due to the charged resin beads inside the resin. Thus, the boundary condition for the flux is :

$$D_i\left.\frac{\partial c_i}{\partial x}\right|_{x=\delta^{r-}}=D_i\left.\frac{\partial c_i}{\partial x}\right|_{x=\delta^{r+}} \tag{2.16}$$

And the continuity of the concentrations is given by:

$$\left.c_i^{r}\right|_{x=\delta^{r+}}=\Pi^{z_i}\left.c_i^{r}\right|_{x=\delta^{r-}} \tag{2.17}$$

Where Π^{z_i} stands for the electrostatic effect given by the Donnan potential at the interface of the resin-layer:

$$\Pi^{z_i} = \exp\left(\frac{z_i F \psi_D}{RT}\right) \quad (2.18)$$

2.3 Non-dimensional variables

The set of partial differential equation that comprise our problem are characterized by the set of concentrations, diffusion coefficients and reaction constants that define our system. The differences between the numerical values that have the concentrations and diffusion coefficients of the different species may cause computational issues when making operations. Thus, we are going to change the variables of the system of partial differential equations into a system with non-dimensional variables, by applying the following operations:
The concentration of the species considered are going to be divided by its equilibrium concentration in the bulk solution:

$$q_i = \frac{c_i}{c_i^*} \tag{2.19}$$

We are going to re-scale the spatial dimension of the problem by changing the spatial coordinate variable :

$$x = \frac{z}{\sqrt{D_{\max}}} \tag{2.20}$$

Where $D_{\max}$ is the largest diffusion coefficient of all species. Then, the second spatial derivative is changed as follows:

$$\frac{\partial^2 c}{\partial x^2} = \frac{1}{D_{\max}} \cdot \frac{\partial^2 c}{\partial z^2} \tag{2.21}$$

Thus applying this change to the partial differential equation that describes the transport of a species A the diffusion coefficient $d_{\mathrm{A}} = \frac{D_{\mathrm{A}}}{D_{\max}}$ and $d_{\mathrm{A}}^{\mathrm{R}} = \frac{D_{\mathrm{A}}^{\mathrm{R}}}{D_{\max}}$.

Assuming that species A endures a simple complexation reaction $A + B \underset{k_d}{\overset{k_a}{\rightleftharpoons}} C$ inside the DGT device and dividing by the equilibrium concentration ($c_{\mathrm{A}}{}^*$). Where we assume that this particular species reacts with the beads of the resin layer.
Now, it is needed to change the variables for the rest of the concentrations, which is done by multiplying and dividing by $c_{\mathrm{i}}{}^*$ where $i \neq \mathrm{A}$.

$$\frac{\partial q_{\mathrm{A}}}{\partial t}=\begin{Bmatrix} d_{\mathrm{A}} \\ d_{\mathrm{A}}^{\mathrm{R}} \end{Bmatrix}\frac{\partial^2 q_{\mathrm{A}}}{\partial z^2}-k_{\mathrm{a}}q_{\mathrm{A}}q_{\mathrm{B}}c_{\mathrm{B}}^{*}+q_{\mathrm{C}}\frac{k_{\mathrm{d}}c_{\mathrm{C}}^{*}}{c_{\mathrm{A}}^{*}}-k_{\mathrm{a,R}}q_{\mathrm{A}}q_{\mathrm{R}}c_{\mathrm{R}}^{*}+q_{\mathrm{AR}}\frac{k_{\mathrm{d,R}}c_{\mathrm{R}}^{*}}{c_{\mathrm{A}}^{*}} \tag{2.22}$$

Applying the same operations to the transport equations of species B and C, assuming that they do not endure a reaction with the resin layer:

$$\frac{\partial q_{\mathrm{B}}}{\partial t}=\begin{Bmatrix} d_{\mathrm{B}} \\ d_{\mathrm{B}}^{\mathrm{R}} \end{Bmatrix}\frac{\partial^2 q_{\mathrm{B}}}{\partial z^2}-k_{\mathrm{a}}q_{\mathrm{A}}q_{\mathrm{B}}c_{\mathrm{A}}^{*}+q_{\mathrm{C}}\frac{k_{\mathrm{d}}c_{\mathrm{C}}^{*}}{c_{\mathrm{B}}^{*}} \tag{2.23}$$

$$\frac{\partial q_{\mathrm{C}}}{\partial t}=\begin{Bmatrix} d_{\mathrm{C}} \\ d_{\mathrm{C}}^{\mathrm{R}} \end{Bmatrix}\frac{\partial^2 q_{\mathrm{C}}}{\partial z^2}-q_{\mathrm{A}}q_{\mathrm{B}}\frac{k_{\mathrm{a}}c_{\mathrm{A}}^{*}c_{\mathrm{B}}^{*}}{c_{\mathrm{C}}^{*}}+k_{\mathrm{d}}q_{\mathrm{C}} \tag{2.24}$$

For the sake of simplicity, in subsection “Weak formulation” and onwards, the derivation of the matrix notation from the variational formulation is going to be done for the Eqs (2.22)-(2.24) instead of using the general formulation implemented earlier.

2.4 Solving the transient problem

In this section is explained with a flowchart the set of operations that convert the equilibrium concentrations, dissociation reaction rates, association reaction rates of the set of species of the system into the concentration profiles and other output values. Moreover, the spatial discretization of the domain is explained in detail.

2.4.1 General algorithm

A general scheme of the program is provided to have a general understanding about the inputs required, the outputs of the program and the key operations that are done.

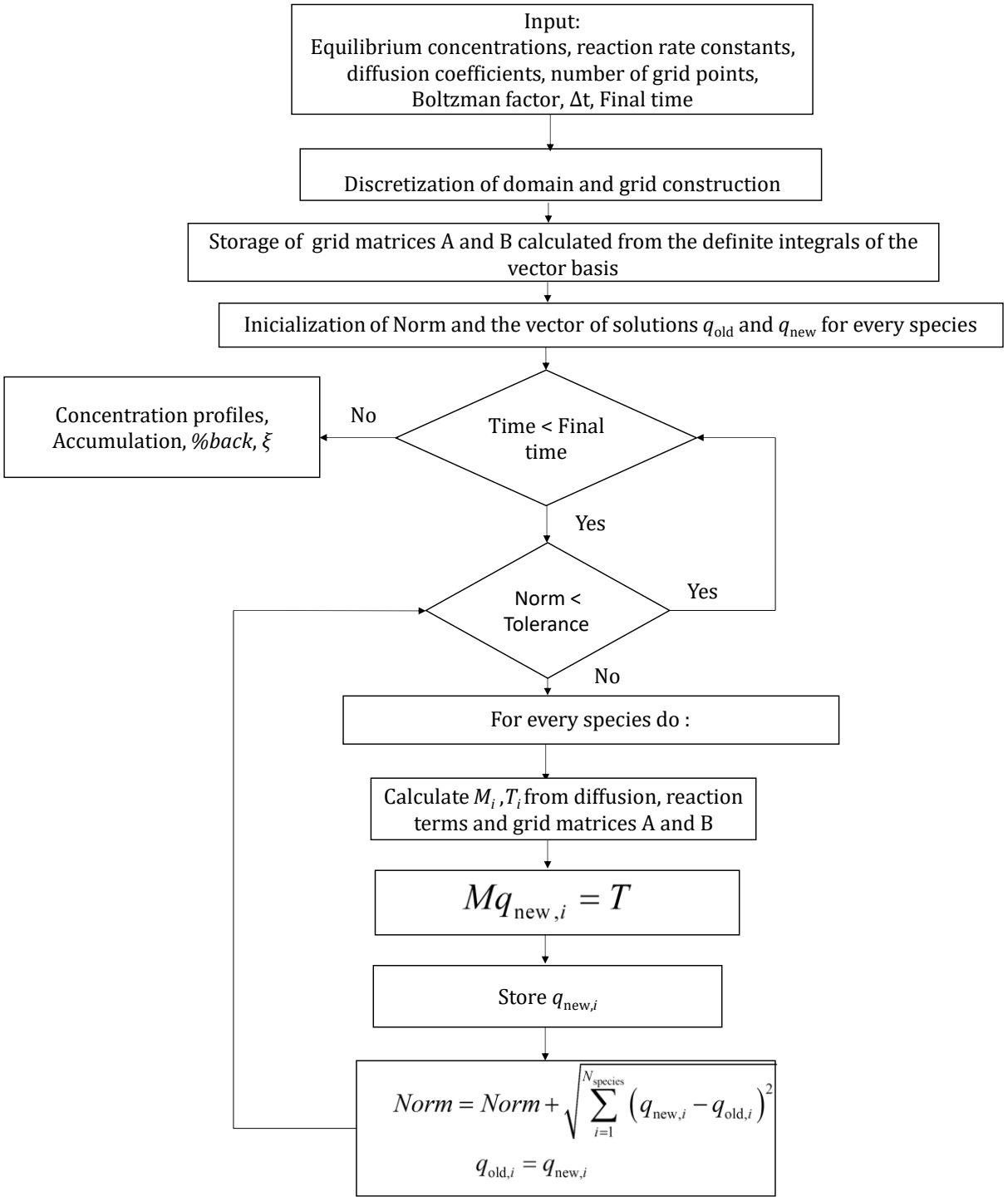

Figure 2.2 Flowchart of the program to compute the concentration profiles, the accumulation, ξ and %back

In Figure 2.2 are summarized the key steps that follow our program to compute the concentration profiles. From a set of input values, the program iteratively solves a set of unknowns $q_{new,i}$ that are the normalized concentrations for the set of transport equations of the species considered. The input values are the equilibrium concentrations, reaction rate constants, diffusion coefficients, Boltzmann factors and other internal parameters (such as Δt,

number of grid points, final time etc). The approximate solution of the unknowns $q(t)_{new,i}$ are considered correct for every species, for a given time "t", when the norm of the normalized concentrations satisfies a given tolerance. In the case that the final time has been reached the program gives the output values described in Figure 2.2, otherwise computes the new solution for the next time step $q(t+\Delta t)_{new,i}$.

2.4.2 Spatial discretization

The discretization of the domain is key factor to obtain accurate results when applying numerical methods. In our case we apply the finite element method to obtain approximate solutions of a set of PDE in a discrete domain. The grid is build to have NR+NG+1 points for a homogeneous resin. Where NR is the number of points in the resin and NG is the number of points in the gel. For a heterogeneous resin, the total number of grid points can be equal to the homogeneous case, but there are 4 different regions: from ($0>z>\delta^r/4$) with a number of points labelled as NR1, from ($\delta^r/4>z>\delta^r/2$) with a number of points NR2, from ($\delta^r/2>z>3\delta^r/4$) with a number of points NR3, from ($3\delta^r/4>z>\delta^r$) with a number of points NR4. The total number of points in the heterogeneous case is given by NR1+NR2+NR3+NR4+NG+1. In both cases, the interval of the grid is variable (h_i) and to avoid any confusion, as this definition is arbitrary, its length is defined between the points z_i and z_{i+1}.

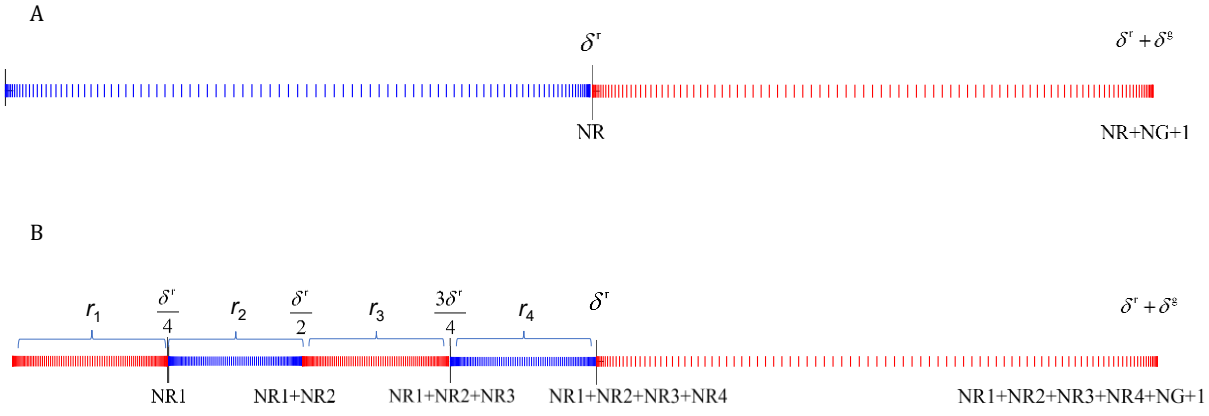

Figure 2.3 Panel A discretization of the domain for the case of a homogeneous resin layer. Panel B discretization of the domain in the case of a heterogeneous resin layer.

Figure 2.3 shows the grid that is used to discretize the domain of the DGT device, for a homogeneous case (Panel A) and for a heterogeneous case (Panel B). Notice that length of the interval h_i is narrower in the positions near the boundary points between different regions. Because, it is considered that the derivatives of the solution near to these point are going to experience sharper changes. Whereas the interval length is wider in the middle of the regions

where the derivatives of the solution are smoother. To build the grid for a DGT device with a heterogeneous resin it has been used the following formula:

$$\left.\begin{aligned} z_i &= \frac{r_1}{2}\left(1-\cos\left(\frac{\Pi i}{NR1}\right)\right) \text{ for } 0<i<NR1 \\ z_i &= r_1+\frac{r_2}{2}\left(1-\cos\left(\frac{\Pi\, i}{NR2}\right)\right) \text{ for } 0<i<NR2 \\ z_i &= r_1+r_2+\frac{r_3}{2}\left(1-\cos\left(\frac{\Pi i}{NR3}\right)\right) \text{ for } 0<i<NR3 \\ z_i &= r_1+r_2+r_3+\frac{r_4}{2}\left(1-\cos\left(\frac{\Pi i}{NR4}\right)\right) \text{ for } 0<i<NR4 \\ z_i &= r_1+r_2+r_3+r_4+\frac{g}{2}\left(1-\cos\left(\frac{\Pi i}{NG}\right)\right) \text{ for } 0<i<NG \end{aligned}\right\} \quad (2.25)$$

In this case, r_1, r_2 , r_3 and r_4 correspond to a fourth part of the total thickness of the resin and they encompass the regions described in Figure 2.3 and the thickness of the gel corresponds to *g*. Notice that when *i*=0, the grid function (z_i), becomes 0, thus it is the beginning of the grid. In between regions, when *i*=0 the grid function is defined in the previous region. For the fifth region, when *i* is equal to the total number of grid points, the grid function have the thickness "r_1"). Whereas for the other regions, the grid function is equal to the length of that region plus the length of the previous regions. In the case that the resin is homogeneous, the same grid function is applied but only 1 region is considered for the resin layer and 1 region for the gel layer.

2.4.3 Weak formulation

To obtain an approximate solution related to the boundary problem, we use the finite element method (FEM) which is based on the weak formulation of a system of partial differential equation for a finite vector basis that corresponds to a discrete domain [3].

Previous to derive the weak formulation, let us show the variational formulation of the problem for species A, B and C.

$$0=\int_0^{\delta^r+\delta^g}\left(\frac{\partial q_{\mathrm{A}}}{\partial t}-\begin{Bmatrix} d_{\mathrm{A}} \\ d_{\mathrm{A}}^{\mathrm{R}} \end{Bmatrix}\frac{\partial^2 q_{\mathrm{A}}}{\partial z^2}+k_{\mathrm{a}}q_{\mathrm{A}}q_{\mathrm{B}}c_{\mathrm{B}}^{*}-q_{\mathrm{C}}\frac{k_{\mathrm{d}}c_{\mathrm{C}}^{*}}{c_{\mathrm{A}}^{*}}+k_{\mathrm{a,R}}q_{\mathrm{A}}q_{\mathrm{R}}c_{\mathrm{R}}^{*}-q_{\mathrm{AR}}\frac{k_{\mathrm{d,R}}c_{\mathrm{R}}^{*}}{c_{\mathrm{A}}^{*}}\right)\phi\, dz \quad (2.26)$$

Where ϕ is any function that belongs to the Hilbert space containing the solutions, then it is enough that this property holds for any basis. [3].

To proceed to derive the weak formulation, we have to use the linear properties of the integral operator:

$$0=\int_0^{\delta^r+\delta^g}\frac{\partial q_A}{\partial t}\phi dz-\int_0^{\delta^r+\delta^g}\begin{Bmatrix}d_A\\ d_A^R\end{Bmatrix}\frac{\partial^2 q_A}{\partial z^2}\phi dz+\int_0^{\delta^r+\delta^g}k_a q_A q_B c_B^*\phi dz-\int_0^{\delta^r+\delta^g}q_C\frac{k_d c_C^*}{c_A^*}\phi dz+\int_0^{\delta^r+\delta^g}k_{a,R}q_A q_R c_R^*\phi dz-\int_0^{\delta^r+\delta^g}q_{AR}\frac{k_{d,R}c_R^*}{c_A^*}\phi dz \quad (2.27)$$

Now, we can integrate by parts the diffusive term which contains second order spatial derivatives by applying :

$$\int_0^{\delta^r+\delta^g}udv\,dz=uv\Big|_0^{\delta^r+\delta^g}-\int_0^{\delta^r+\delta^g}vdu\,dz \quad (2.28)$$

Where the term u in Eq (2.28) is equal to the basis function $u=\phi$, thus its derivative is du=dϕ . The term dv in Eq (2.28) is equal to the diffusive term in Eq (2.27) that have second order partial derivative over x. Thus,

$$dv=\frac{\partial^2 q_A}{\partial z^2};v=\int\frac{\partial^2 q_A}{\partial z^2}dz;v=\frac{\partial\, q_A}{\partial z} \quad (2.29)$$

Now by substituting the terms u, du, dv, v into Eq (2.28), we obtain:

$$\int_0^{\delta^r+\delta^g}\phi\frac{\partial^2 q_A}{\partial z^2}dz=\phi\frac{\partial\, q_A}{\partial z}\Big|_0^{\delta^r+\delta^g}-\int_0^{\delta^r+\delta^g}\phi'\frac{\partial\, q_A}{\partial z}dz \quad (2.30)$$

Where the first term is equal 0 because $\phi(x=\delta^r+\delta^g)=0$ to satisfy the Dirichlet boundary [3] conditions at $\delta^r+\delta^g$ and because there is no flux of matter across the piston $\frac{\partial\, q_A}{\partial z}\Big|_{x=0}=0$.

Thus, Eq (2.30) becomes:

$$\int_0^{\delta^r+\delta^g}\phi\frac{\partial^2 q_A}{\partial z^2}dz=-\int_0^{\delta^r+\delta^g}\phi'\frac{\partial\, q_A}{\partial z}dz \quad (2.31)$$

Substituting this equation into Eq (2.27), we obtain:

$$0=\int_0^{\delta^r+\delta^g}\frac{\partial q_A}{\partial t}\phi dz+\begin{Bmatrix}d_A\\ d_A^R\end{Bmatrix}\int_0^{\delta^r+\delta^g}\phi'\frac{\partial\ q_A}{\partial z}dz+k_a c_B^*\int_0^{\delta^r+\delta^g}q_A q_B\phi dz-\frac{k_d c_C^*}{c_A^*}\int_0^{\delta^r+\delta^g}q_C\phi dz+k_{a,R}c_R^*\int_0^{\delta^r+\delta^g}q_A q_R\phi dz-\frac{k_{d,R}c_R^*}{c_A^*}\int_0^{\delta^r+\delta^g}q_{AR}\phi dz \quad (2.32)$$

Eq (2.32) corresponds to the weak formulation of the boundary value problem for the species A. Applying the same procedure, we obtain the weak formulation for species B and C:

$$0=\int_0^{\delta^r+\delta^g}\frac{\partial q_B}{\partial t}\phi dz+\begin{Bmatrix}d_B\\ d_B^R\end{Bmatrix}\int_0^{\delta^r+\delta^g}\phi'\frac{\partial\ q_B}{\partial z}dz+k_a c_A^*\int_0^{\delta^r+\delta^g}q_A q_B\phi dz-\frac{k_d c_C^*}{c_B^*}\int_0^{\delta^r+\delta^g}q_C\phi dz \quad (2.33)$$

$$0=\int_0^{\delta^r+\delta^g}\frac{\partial q_C}{\partial t}\phi dz+\begin{Bmatrix}d_C\\ d_C^R\end{Bmatrix}\int_0^{\delta^r+\delta^g}\phi'\frac{\partial\ q_C}{\partial z}dz-\frac{k_a c_B^* c_A^*}{c_C^*}\int_0^{\delta^r+\delta^g}q_A q_B\phi dz+k_d\int_0^{\delta^r+\delta^g}q_C\phi dz \quad (2.34)$$

:

2.4.4 Development of continuous functions in terms of basis functions

In this section, we approximate the vector basis functions ϕ into a basis set $\phi^h\in\phi$ with *N* components that correspond to the discretization of the with a length *h* that is variable along the domain.

2.4.4.1 Basis functions (Galerkin method)

Following the Galerkin approach, the unknown trial functions q_A, q_B and q_C that belong to the solution space are going to be developed in terms of a finite vector basis functions with *N* elements that correspond to the number of grid points (for an homogeneous resin *N=NR+NG* and for a heterogeneous resin *N= NR1+NR2+NR3+NR4+NG*).

Thus, we can define our vector of unknows as function of a finite vector basis functions that describes the discretized domain [4].

$$q_A(t,z)\ =\sum_{i=1}^{N}q_{A,i}(t)\phi_i(z)\ +q_{A,N+1}(t) \quad (2.35)$$

$$\frac{\partial q_A(t,z)}{\partial z}=\sum_{i=1}^{N}q_{A,i}(t)\phi_i'(z) \quad (2.36)$$

$$\frac{\partial q_A(t,z)}{\partial t} = \sum_{i=1}^{N} \frac{\partial q_{A,i}(t)}{\partial t} \phi_i(z) \tag{2.37}$$

$$q_A(t,z) q_B(t,z) = \sum_{i=1}^{N} q_A(t) q_B(t) \phi_i(z) \tag{2.38}$$

$$q_{\mathrm{B}}(t,z) = \sum_{i=1}^{N} q_{\mathrm{B},i}(t) \phi_i(z) + q_{\mathrm{B,N+1}}(t) \tag{2.39}$$

$$\frac{\partial q_B(t,z)}{\partial z} = \sum_{i=1}^{N} q_{B,i}(t) \phi_i'(z) \tag{2.40}$$

$$\frac{\partial q_{\mathrm{B}}(t,z)}{\partial t} = \sum_{i=1}^{N} \frac{\partial q_{\mathrm{B},i}(t)}{\partial t} \phi_i(z) \tag{2.41}$$

$$q_{\mathrm{C}}(t,z) = \sum_{i=1}^{N} q_{\mathrm{C},i}(t) \phi_i(z) + q_{\mathrm{C,N+1}}(t) \tag{2.42}$$

$$\frac{\partial q_{\mathrm{C}}(t,z)}{\partial t} = \sum_{i=1}^{N} \frac{\partial q_{\mathrm{C},i}(t)}{\partial t} \phi_i(z) \tag{2.43}$$

Now, we can define the weak formulation of our system of equations in terms of basis functions where the time contribution is carried by nodal values and the spatial contribution by the shape functions. The Galerkin formulation for each species is :

$$0 = \frac{\partial q_{\mathrm{A}}}{\partial t} \int_0^{\delta^{\mathrm{r}}+\delta^{\mathrm{g}}} \sum_{i=1}^{N} \phi_i \phi_j dz + \begin{Bmatrix} d_{\mathrm{A}} \\ d_{\mathrm{A}}^{\mathrm{R}} \end{Bmatrix} q_A \int_0^{\delta^{\mathrm{r}}+\delta^{\mathrm{g}}} \sum_{i=1}^{N} \phi_i' \phi_j' dz + k_{\mathrm{a}} c_{\mathrm{B}}^* q_{\mathrm{A}} q_{\mathrm{B}} \int_0^{\delta^{\mathrm{r}}+\delta^{\mathrm{g}}} \sum_{i=1}^{N} \phi_i \phi_j dz - \frac{k_{\mathrm{d}} c_{\mathrm{C}}^*}{c_{\mathrm{A}}^*} q_{\mathrm{C}} \int_0^{\delta^{\mathrm{r}}+\delta^{\mathrm{g}}} \sum_{i=1}^{N} \phi_i \phi_j dz + k_{\mathrm{a,R}} c_{\mathrm{R}}^* q_{\mathrm{A}} q_{\mathrm{R}} \int_0^{\delta^{\mathrm{r}}+\delta^{\mathrm{g}}} \sum_{i=1}^{N} \phi_i \phi_j dz - \frac{k_{\mathrm{d,R}} c_{\mathrm{R}}^*}{c_{\mathrm{A}}^*} q_{\mathrm{AR}} \int_0^{\delta^{\mathrm{r}}+\delta^{\mathrm{g}}} \sum_{i=1}^{N} \phi_i \phi_j dz \tag{2.44}$$

$$0 = \frac{\partial q_{\mathrm{B}}}{\partial t} \int_0^{\delta^{\mathrm{r}}+\delta^{\mathrm{g}}} \sum_{i=1}^{N} \phi_i \phi_j dz + \begin{Bmatrix} d_{\mathrm{B}} \\ d_{\mathrm{B}}^{\mathrm{R}} \end{Bmatrix} q_{\mathrm{B}} \int_0^{\delta^{\mathrm{r}}+\delta^{\mathrm{g}}} \sum_{i=1}^{N} \phi_i' \phi_j' dz + k_{\mathrm{a}} c_{\mathrm{A}}^* q_{\mathrm{A}} q_{\mathrm{B}} \int_0^{\delta^{\mathrm{r}}+\delta^{\mathrm{g}}} \sum_{i=1}^{N} \phi_i \phi_j dz - \frac{k_{\mathrm{d}} c_{\mathrm{C}}^*}{c_{\mathrm{B}}^*} q_{\mathrm{C}} \int_0^{\delta^{\mathrm{r}}+\delta^{\mathrm{g}}} \sum_{i=1}^{N} \phi_i \phi_j dz \tag{2.45}$$

$$0 = \frac{\partial q_{\mathrm{C}}}{\partial t}\int_0^{\delta^{\mathrm{r}}+\delta^{\mathrm{g}}}\sum_{i=1}^{N}\phi_i\,\phi_j\,dz + \begin{Bmatrix} d_{\mathrm{C}} \\ d_{\mathrm{C}}^{\mathrm{R}} \end{Bmatrix} q_{\mathrm{C}}\int_0^{\delta^{\mathrm{r}}+\delta^{\mathrm{g}}}\sum_{i=1}^{N}\phi_i'\phi_j'dz - \frac{k_{\mathrm{a}}c_{\mathrm{B}}^{*}c_{\mathrm{A}}^{*}}{c_{\mathrm{C}}^{*}}q_{\mathrm{A}}q_{\mathrm{B}}\int_0^{\delta^{\mathrm{r}}+\delta^{\mathrm{g}}}\sum_{i=1}^{N}\phi_i\,\phi_j\,dz + k_{\mathrm{d}}q_{\mathrm{C}}\int_0^{\delta^{\mathrm{r}}+\delta^{\mathrm{g}}}\sum_{i=1}^{N}\phi_i\,\phi_j\,dz \quad (2.46)$$

The shape functions (ϕ(z)) are piecewise linear functions that behave as a kronecker delta, thus the functions are equal to 1 at the i^{th} position and 0 when $j \neq i$. A type of functions that fulfil this behaviour are first order Lagrange polynomial, which we use to define our shape functions.

$$\phi(z) = \begin{cases} \dfrac{z - z_{i-1}}{z_i - z_{i-1}} & z_{i-1} < z < z_i \\ \dfrac{z_{i+1} - z}{z_{i+1} - z_i} & z_i < z < z_{i+1} \\ 0 & \textit{elsewhere} \end{cases} \quad (2.47)$$

And their first derivative is equal to a step function whose value is the inverse of the thickness of the grid between the nodes i^{th} and i^{th}-1 or i^{th} +1 and i^{th}.

$$\phi'(z) = \begin{cases} \dfrac{1}{z_i - z_{i-1}} & z_{i-1} < z < z_i \\ \dfrac{-1}{z_{i+1} - z_i} & z_i < z < z_{i+1} \\ 0 & \textit{elsewhere} \end{cases} \quad (2.48)$$

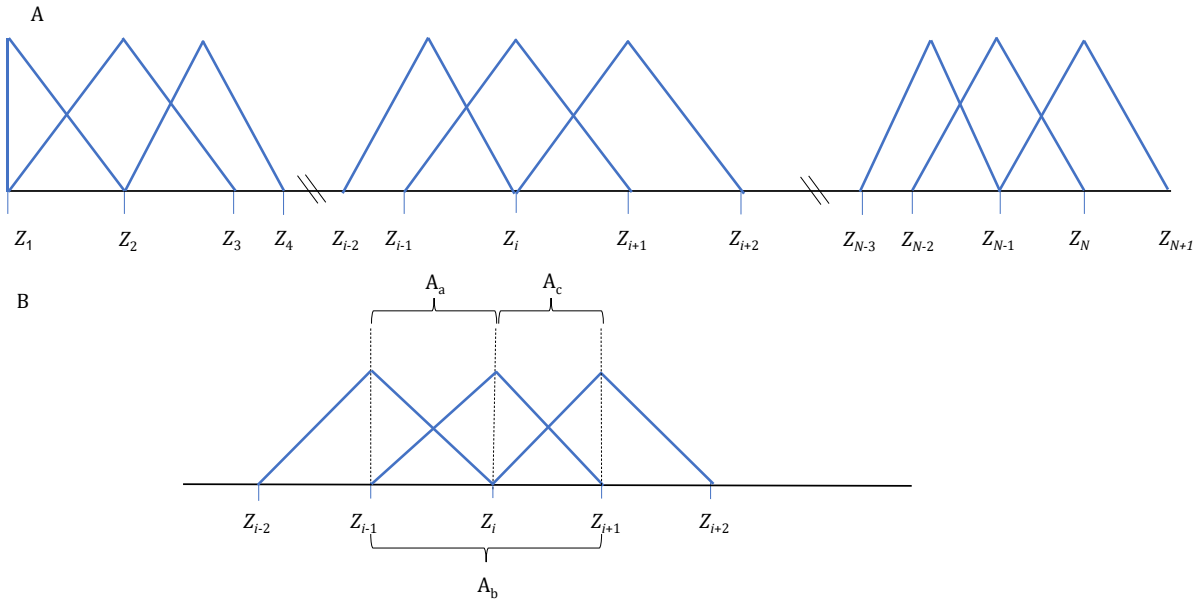

Figure 2.4 Panel A displays the shape of the basis functions at the beginning, at the end and at the i^{th} location of the grid. Panel B depicts the domain of integration between the product of two shape function which belong to the lower diagonal position and upper diagonal position (A_a and A_c). For the case of A_b, the picture depicts the domain of integration of the square of the shape function at the i^{th} position of the grid.

In Panel A Figure 2.4 is displayed the shape functions according to different positions of the grid. Notice that in the position z_1 the hat function is cutted in half, because is the end of the domain. Whereas in position z_N, the hat function finishes at the position z_{N+1} where there is the boundary condition. The domains of integration are depicted in Panel B Figure 2.4 of the hat functions which are between z_{i-1} to z_i and between z_i to z_{i+1} . Then, three different type of integral come into play:

$$A_b = \int_{z_{i-1}}^{z_{i+1}} \phi_i \phi_i dz = \int_{z_{i-1}}^{z_i} \phi_i \phi_i dz + \int_{z_i}^{z_{i+1}} \phi_i \phi_i dz = \int_{z_{i-1}}^{z_i} \left(\frac{z - z_{i-1}}{z_i - z_{i-1}} \right) \left(\frac{z - z_{i-1}}{z_i - z_{i-1}} \right) dz + \int_{z_i}^{z_{i+1}} \left(\frac{z_{i+1} - z}{z_{i+1} - z_i} \right) \left(\frac{z_{i+1} - z}{z_{i+1} - z_i} \right) dz \tag{2.49}$$

$$A_a = \int_{z_{i-1}}^{z_i} \phi_i \phi_{i-1} dz = \int_{z_{i-1}}^{z_i} \left(\frac{z - z_{i-1}}{z_i - z_{i-1}} \right) \left(\frac{z_i - z}{z_i - z_{i-1}} \right) dz \tag{2.50}$$

$$A_c = \int_{z_i}^{z_{i+1}} \phi_i \phi_{i+1} dz = \int_{z_i}^{z_{i+1}} \left(\frac{z_{i+1} - z}{z_{i+1} - z_i} \right) \left(\frac{z - z_i}{z_{i+1} - z_i} \right) dz \tag{2.51}$$

A tridiagonal matrix (A) describes the result of the integration of the product of basis functions at each point of the grid. The fact that the matrix is tridiagonal arises from the definition of the basis functions in Eq (2.47). The subindexes a,b,c are referred to lower diagonal, main diagonal and upper diagonal positions of a tridiagonal matrix. In Eq (2.50)which corresponds to the lower diagonal position of the matrix A is defined by the product of the vector basis function ϕ_i by ϕ_{i-1}. The function ϕ_i is defined in Eq (2.47) and the function ϕ_{i-1} is the equivalent of the function ϕ_i (in the domain $z_{i-1}<z< z_i$) with a negative slope and ending at the position z_i. In Eq (2.51)the function ϕ_i now has the expression of the domain $z_i<z< z_{i+1}$ and the function ϕ_{i+1} is the equivalent of ϕ_i (in the domain $z_i<z< z_{i+1}$) but with a positive slope and starting at the position z_i.

Moreover, we have another type of matrix to consider that come out from applying the integration by parts on the diffusive term. This second matrix (let us call it B), comes from the definite integral of the product of the derivatives of two basis functions described in Eq (2.48) . Therefore, this matrix is also tridiagonal and we are going to use the subindexes b, a and c to refer to the main diagonal, the lower diagonal and the upper diagonal respectively.

$$B_b = \int_{z_{i-1}}^{z_{i+1}} \phi_i' \phi_i' dz = \int_{z_{i-1}}^{z_i} \phi_i' \phi_i' dz + \int_{z_i}^{z_{i+1}} \phi_i' \phi_i' dz = \int_{z_{i-1}}^{z_i} \left(\frac{1}{z_i - z_{i-1}} \right) \left(\frac{1}{z_i - z_{i-1}} \right) dz + \int_{z_i}^{z_{i+1}} \left(\frac{-1}{z_{i+1} - z_i} \right) \left(\frac{-1}{z_{i+1} - z_i} \right) dz \quad (2.52)$$

$$B_a = \int_{z_{i-1}}^{z_i} \phi_i' \phi_{i-1}' dz = \int_{z_{i-1}}^{z_i} \left(\frac{1}{z_i - z_{i-1}} \right) \left(\frac{-1}{z_i - z_{i-1}} \right) dz \quad (2.53)$$

$$B_c = \int_{z_i}^{z_{i+1}} \phi_i' \phi_{i+1}' dz = \int_{z_i}^{z_{i+1}} \left(\frac{-1}{z_{i+1} - z_i} \right) \left(\frac{1}{z_{i+1} - z_i} \right) dz \quad (2.54)$$

The result of the integrals A_b (Eq (2.49)), A_a (Eq (2.50)), A_c (Eq (2.51))and B_b (Eq (2.52)) B_a (Eq (2.53)) and B_c (Eq (2.54)) are:

$$A_b = \frac{h_{i-1}}{3} + \frac{h_i}{3} \quad (2.55)$$

$$A_a = \frac{h_{i-1}}{2} \quad (2.56)$$

$$A_c = \frac{h_i}{2} \tag{2.57}$$

$$B_b = \frac{1}{h_{i-1}} + \frac{1}{h_i} \tag{2.58}$$

$$B_a = \frac{-1}{h_{i-1}} \tag{2.59}$$

$$B_c = -\frac{1}{h_i} \tag{2.60}$$

The matrices A, B in the matrix notation are:

$$A = \begin{pmatrix} \frac{h_1}{3} & \frac{h_1}{2} & 0 & 0 & 0 & 0 & 0 \\ \frac{h_1}{2} & \frac{h_1}{3}+\frac{h_2}{3} & \frac{h_2}{2} & 0 & 0 & 0 & 0 \\ 0 & ... & ... & ... & 0 & 0 & 0 \\ 0 & 0 & \frac{h_{i-1}}{2} & \frac{h_{i-1}}{3}+\frac{h_i}{3} & \frac{h_i}{2} & 0 & 0 \\ 0 & 0 & 0 & ... & ... & ... & 0 \\ 0 & 0 & 0 & 0 & \frac{h_{N-2}}{2} & \frac{h_{N-2}}{3}+\frac{h_{N-1}}{3} & \frac{h_{N-1}}{2} \\ 0 & 0 & 0 & 0 & 0 & \frac{h_{N-1}}{2} & \frac{h_{N-1}}{3} \end{pmatrix} \tag{2.61}$$

$$B=\begin{pmatrix} \frac{1}{h_1} & \frac{-1}{h_1} & 0 & 0 & 0 & 0 & 0 \\ \frac{-1}{h_1} & \frac{1}{h_1}+\frac{1}{h_2} & \frac{-1}{h_2} & 0 & 0 & 0 & 0 \\ 0 & ... & ... & ... & 0 & 0 & 0 \\ 0 & 0 & \frac{-1}{h_{i-1}} & \frac{1}{h_{i-1}}+\frac{1}{h_i} & \frac{-1}{h_i} & 0 & 0 \\ 0 & 0 & 0 & ... & ... & ... & 0 \\ 0 & 0 & 0 & 0 & \frac{-1}{h_{N-2}} & \frac{1}{h_{N-2}}+\frac{1}{h_{N-1}} & \frac{-1}{h_{N-1}} \\ 0 & 0 & 0 & 0 & 0 & \frac{-1}{h_{N-1}} & \frac{1}{h_{N-1}} \end{pmatrix} \quad (2.62)$$

Notice that in Eq (2.61) and Eq (2.62) the first and last element of the matrices A_b and B_b correspond to half of the integral, because, as said before the first and last element correspond to a half of the shape function.

2.4.5 System of partial differential equations expressed in terms of basis functions.

From the Galerkin approximation, after applying the definite integrals, we proceed to derive the matrix notation of our system of PDE, in a first step, we substitute the definite integrals by the corresponding matrices Eq (2.61) and Eq (2.62):

$$0=\frac{\partial q_A}{\partial t}\sum_{i=1}^{N}A_{ij}+\begin{Bmatrix} d_A \\ d_A^R \end{Bmatrix} q_A\sum_{i=1}^{N}B_{ij}+k_a c_B^* q_A q_B\sum_{i=1}^{N}A_{ij}-\frac{k_d c_C^*}{c_A^*}q_C\sum_{i=1}^{N}A_{ij}+k_{a,R}c_R^* q_A q_R\sum_{i=1}^{N}A_{ij}-\frac{k_{d,R}c_{AR}^*}{c_A^*}q_{AR}\sum_{i=1}^{N}A_{ij}$$

(2.63)

To proceed to solve this system of Equations we apply the Implicit Euler method which is considered to be a simple numerical method that has unconditional stability respect to Δt and an accuracy of order 1 [5]. In the Implicit Euler method the time partial derivative is treated as:

$$\frac{\partial q_i}{\partial t}=\frac{q_i(t+\Delta t)-q_i(t)}{\Delta t}=F(q_i(t+\Delta t),t) \quad (2.64)$$

Then, to apply the implicit Euler method we need to discretize the time differentiation as in Eq (2.64) and substitute q_A for q_A(t+1) on the other terms of Eq (2.63), so we obtain:

$$0=\left(\frac{q_A(t+\Delta t)-q_A(t)}{\Delta t}\right)\sum_{i=1}^{N}A_{ij}+\begin{Bmatrix}d_{\mathrm{A}}\\ d_{\mathrm{A}}^{\mathrm{R}}\end{Bmatrix}q_A(t+\Delta t)\sum_{i=1}^{N}B_{ij}+k_{\mathrm{a}}c_{\mathrm{B}}^{*}q_{\mathrm{A}}(t+\Delta t)q_{\mathrm{B}}(t+\Delta t)\sum_{i=1}^{N}A_{ij}-\frac{k_{\mathrm{d}}c_{\mathrm{C}}^{*}}{c_{\mathrm{A}}^{*}}q_{\mathrm{C}}(t+\Delta t)\sum_{i=1}^{N}A_{ij}+$$
$$k_{\mathrm{a,R}}c_{\mathrm{R}}^{*}q_{\mathrm{A}}(t+\Delta t)q_{\mathrm{R}}(t+\Delta t)\sum_{i=1}^{N}A_{ij}-\frac{k_{\mathrm{d,R}}c_{\mathrm{R}}^{*}}{c_{\mathrm{A}}^{*}}q_{\mathrm{AR}}(t+\Delta t)\sum_{i=1}^{N}A_{ij} \qquad (2.65)$$

The system of equations shown in Eq (2.65) has N unknowns that correspond to $q_{\mathrm{A}}(t+1)$ from i=1, N in the grid position. Thus, in order to derive the matrix notation of our system of equations, we need to isolate $q_{\mathrm{A}}(t+\Delta t)$ in Eq (2.65)

$$\left[\sum_{i=1}^{N}A_{ij}+\Delta t\left(\begin{Bmatrix}d_{\mathrm{A}}\\ d_{\mathrm{A}}^{\mathrm{R}}\end{Bmatrix}\sum_{i=1}^{N}B_{ij}+k_{\mathrm{a}}c_{\mathrm{B}}^{*}q_{\mathrm{B}}(t+\Delta t)\sum_{i=1}^{N}A_{ij}+k_{\mathrm{a,R}}c_{\mathrm{R}}^{*}q_{\mathrm{R}}(t+\Delta t)\sum_{i=1}^{N}A_{ij}\right)\right]q_A(t+\Delta t)=q_{\mathrm{A}}(t)\sum_{i=1}^{N}A_{ij}+\Delta t\left(\frac{k_{\mathrm{d}}c_{\mathrm{C}}^{*}}{c_{\mathrm{A}}^{*}}q_{\mathrm{C}}(t+\Delta t)\sum_{i=1}^{N}A_{ij}-\frac{k_{\mathrm{d,R}}c_{\mathrm{R}}^{*}}{c_{\mathrm{A}}^{*}}q_{\mathrm{AR}}(t+\Delta t)\sum_{i=1}^{N}A_{ij}\right) \qquad (2.66)$$

Our objective is to solve the previous linear system of equations that expressed in matrix in notation becomes:

$$Mq=T \qquad (2.67)$$

This linear system of equations is iteratively solved until the approximate solution of the non-linear system of equation satisfies a certain tolerance (i.e the approximate solution is good enough to obtain the results).

From the comparison with a Matrix notation $M_{ij}q_i=T_i$, we can assign our system of equations displayed in Eq (2.66) to M and T as:

$$M_{\mathrm{A}}=\left[\sum_{i=1}^{N}A_{ij}+\Delta t\left(\begin{Bmatrix}d_{\mathrm{A}}\\ d_{\mathrm{A}}^{\mathrm{R}}\end{Bmatrix}\sum_{i=1}^{N}B_{ij}+k_{\mathrm{a}}c_{\mathrm{B}}^{*}q_{\mathrm{B}}(t+\Delta t)\sum_{i=1}^{N}A_{ij}+k_{\mathrm{a,R}}c_{\mathrm{R}}^{*}q_{\mathrm{R}}(t+\Delta t)\sum_{i=1}^{N}A_{ij}\right)\right] \qquad (2.68)$$

$$T_{\mathrm{A}}=q_{\mathrm{A}}(t)\sum_{i=1}^{N}A_{ij}+\Delta t\left(\frac{k_{\mathrm{d}}c_{\mathrm{C}}^{*}}{c_{\mathrm{A}}^{*}}q_{\mathrm{C}}(t+\Delta t)\sum_{i=1}^{N}A_{ij}-\frac{k_{\mathrm{d,R}}c_{\mathrm{AR}}^{*}}{c_{\mathrm{A}}^{*}}q_{\mathrm{AR}}(t+\Delta t)\sum_{i=1}^{N}A_{ij}\right) \qquad (2.69)$$

Applying the same procedure to the weak formulation of the transport equations of species B and C in Eqs (2.33)-(2.34), the matrix notation for species B and C is:

$$M_{\mathrm{B}}=\left[\sum_{i=1}^{N}A_{ij}+\Delta t\left(\begin{Bmatrix}d_{\mathrm{B}}\\ d_{\mathrm{B}}^{\mathrm{R}}\end{Bmatrix}\sum_{i=1}^{N}B_{ij}+k_{\mathrm{a}}c_{\mathrm{A}}^{*}q_{\mathrm{A}}(t+\Delta t)\sum_{i=1}^{N}A_{ij}\right)\right] \qquad (2.70)$$

$$T_{\mathrm{B}}=q_{\mathrm{B}}(t)\sum_{i=1}^{N}A_{ij}+\Delta t\left(\frac{k_{\mathrm{d}}c_{\mathrm{C}}^{*}}{c_{\mathrm{B}}^{*}}q_{\mathrm{C}}(t+\Delta t)\sum_{i=1}^{N}A_{ij}\right) \qquad (2.71)$$

$$M_{\mathrm{C}} = \left[\sum_{i=1}^{N} A_{ij} + \Delta t \left(\begin{Bmatrix} d_{\mathrm{C}} \\ d_{\mathrm{C}}^{\mathrm{R}} \end{Bmatrix} \sum_{i=1}^{N} B_{ij} + k_{\mathrm{d}} \sum_{i=1}^{N} A_{ij} \right) \right] \tag{2.72}$$

$$T_{\mathrm{C}} = q_{\mathrm{C}}(t) \sum_{i=1}^{N} A_{ij} + \Delta t \left(k_{\mathrm{a}} \frac{c_{\mathrm{A}}^{*} c_{\mathrm{B}}^{*}}{c_{\mathrm{C}}^{*}} q_{\mathrm{A}}(t+\Delta t) q_{\mathrm{B}}(t+\Delta t) \sum_{i=1}^{N} A_{ij} \right) \tag{2.73}$$

The shape of the Matrix M_{A}, M_{B}, M_{C} are tridiagonal. Thus, Eq (2.68)-(2.72) can be written in a vector format. To show that we are going to use the matrix of species A (M_{A}). Where main diagonal is labelled as $M_{\mathrm{A}_{i,\mathrm{b}}}$, the term of the upper diagonal $M_{\mathrm{A}_{i,\mathrm{c}}}$ and the term of the lower diagonal $M_{\mathrm{A}_{i,\mathrm{a}}}$:

$$M_{\mathrm{A}_{i,\mathrm{a}}} = \left[\sum_{i=2}^{N} A_{i,\mathrm{a}} + \Delta t \left(\begin{Bmatrix} d_{\mathrm{A}} \\ d_{\mathrm{A}}^{\mathrm{R}} \end{Bmatrix} \sum_{i=2}^{N} B_{i,\mathrm{a}} + k_{\mathrm{a}} c_{\mathrm{B}}^{*} q_{\mathrm{B}}(t+\Delta t) \sum_{i=2}^{N} A_{i,\mathrm{a}} + k_{\mathrm{a,R}} c_{\mathrm{R}}^{*} q_{\mathrm{R}}(t+\Delta t) \sum_{i=2}^{N} A_{i,\mathrm{a}} \right) \right] \tag{2.74}$$

$$M_{\mathrm{A}_{i,\mathrm{b}}} = \left[\sum_{i=1}^{N} A_{i,\mathrm{b}} + \Delta t \left(\begin{Bmatrix} d_{\mathrm{A}} \\ d_{\mathrm{A}}^{\mathrm{R}} \end{Bmatrix} \sum_{i=1}^{N} B_{i,\mathrm{b}} + k_{\mathrm{a}} c_{\mathrm{B}}^{*} q_{\mathrm{B}}(t+\Delta t) \sum_{i=1}^{N} A_{i,\mathrm{b}} + k_{\mathrm{a,R}} c_{\mathrm{R}}^{*} q_{\mathrm{R}}(t+\Delta t) \sum_{i=1}^{N} A_{i,\mathrm{b}} \right) \right] \tag{2.75}$$

$$M_{\mathrm{A}_{i,\mathrm{c}}} = \left[\sum_{i=1}^{N-1} A_{i,\mathrm{c}} + \Delta t \left(\begin{Bmatrix} d_{\mathrm{A}} \\ d_{\mathrm{A}}^{\mathrm{R}} \end{Bmatrix} \sum_{i=1}^{N-1} B_{i,\mathrm{c}} + k_{\mathrm{a}} c_{\mathrm{B}}^{*} q_{\mathrm{B}}(t+\Delta t) \sum_{i=1}^{N-1} A_{i,\mathrm{c}} + k_{\mathrm{a,R}} c_{\mathrm{R}}^{*} q_{\mathrm{R}}(t+\Delta t) \sum_{i=1}^{N-1} A_{i,\mathrm{c}} \right) \right] \tag{2.76}$$

These equations (Eq (2.74)-(2.76)) can be stored in 3 different vectors which we need as an input along with Eq (2.69) to solve the linear system of equations. To do that we use a Fortran subroutine from numerical recipes called tridagdp which performs a LU decomposition and solves the system of equations with back substitution [6].

To have a full understanding in relation to the code, it is useful to expand the terms in Eq (2.74)-(2.76) in the key positions of the grids i.e (i=1, i=Nfin and i=j^{th}) in the resin and gel layer, as well as, it is important to show how to take into account the Donnan potential in the flux equality at i=NR [7].

In the first position of the grid are only needed Eq (2.69), Eq(2.75) and Eq (2.76) which are displayed as :

$$M_{\mathrm{A}_{1,\mathrm{b}}} = \left[A_{1,\mathrm{b}} + \Delta t \left(d_{\mathrm{A}}^{\mathrm{R}} B_{1,\mathrm{b}} + k_{\mathrm{a}} c_{\mathrm{B}}^{*} q_{\mathrm{B}}(t+\Delta t) A_{1,\mathrm{b}} + k_{\mathrm{a,R}} c_{\mathrm{R}}^{*} q_{\mathrm{R}}(t+\Delta t) A_{1,\mathrm{b}} \right) \right] \tag{2.77}$$

$$M_{\mathrm{A}_{1,\mathrm{c}}} = \left[A_{1,\mathrm{c}} + \Delta t \left(d_{\mathrm{A}}^{\mathrm{R}} B_{1,\mathrm{c}} + k_{\mathrm{a}} c_{\mathrm{B}}^{*} q_{\mathrm{B}}(t+\Delta t) A_{1,\mathrm{c}} + k_{\mathrm{a,R}} c_{\mathrm{R}}^{*} q_{\mathrm{R}}(t+\Delta t) A_{1,\mathrm{c}} \right) \right] \tag{2.78}$$

$$T_{\mathrm{A}_1} = q_{\mathrm{A}}(t)\left(A_{1,\mathrm{b}} + A_{1,\mathrm{c}}\right) + \Delta t \left(\frac{k_{\mathrm{d}} c_{\mathrm{C}}^{*}}{c_{\mathrm{A}}^{*}} q_{\mathrm{C}}(t+\Delta t)\left(A_{1,\mathrm{b}} + A_{1,\mathrm{c}}\right) + \frac{k_{\mathrm{d,R}} c_{\mathrm{AR}}^{*}}{c_{\mathrm{A}}^{*}} q_{\mathrm{AR}}(t+\Delta t)\left(A_{1,\mathrm{b}} + A_{1,\mathrm{c}}\right) \right) \tag{2.79}$$

In the i^{th} position of the grid assuming that it corresponds to a position between 2 and NR-1 Eq (2.68) and (2.69) become:

$$M_{\mathrm{A}_{i,\mathrm{b}}} = \left[A_{i,\mathrm{b}} + \Delta t \left(d_{\mathrm{A}}^{\mathrm{R}} B_{i,\mathrm{b}} + k_{\mathrm{a}} c_{\mathrm{B}}^{*} q_{\mathrm{B}}(t+\Delta t) A_{i,\mathrm{b}} + k_{\mathrm{a,R}} c_{\mathrm{R}}^{*} q_{\mathrm{R}}(t+\Delta t) A_{i,\mathrm{b}} \right) \right] \tag{2.80}$$

$$M_{\mathrm{A}_{i,a}} = \left[A_{i,\mathrm{a}} + \Delta t \left(d_{\mathrm{A}}^{\mathrm{R}} B_{i,a} + k_{\mathrm{a}} c_{\mathrm{B}}^{*} q_{\mathrm{B}}(t+\Delta t) A_{i,\mathrm{a}} + k_{\mathrm{a,R}} c_{\mathrm{R}}^{*} q_{\mathrm{R}}(t+\Delta t) A_{i,\mathrm{a}} \right) \right] \tag{2.81}$$

$$M_{\mathrm{A}_{i,\mathrm{c}}} = \left[A_{i,\mathrm{c}} + \Delta t \left(d_{\mathrm{A}}^{\mathrm{R}} B_{i,\mathrm{c}} + k_{\mathrm{a}} c_{\mathrm{B}}^{*} q_{\mathrm{B}}(t+\Delta t) A_{i,\mathrm{c}} + k_{\mathrm{a,R}} c_{\mathrm{R}}^{*} q_{\mathrm{R}}(t+\Delta t) A_{i,\mathrm{c}} \right) \right] \tag{2.82}$$

$$T_{\mathrm{A}_i} = q_{\mathrm{A}}(t)\left(A_{i,a} + A_{i,\mathrm{b}} + A_{i,\mathrm{c}}\right) + \Delta t \left(\frac{k_{\mathrm{d}} c_{\mathrm{C}}^{*}}{c_{\mathrm{A}}^{*}} q_{\mathrm{C}}(t+\Delta t)\left(A_{i,a} + A_{1,\mathrm{b}} + A_{1,\mathrm{c}}\right) + \frac{k_{\mathrm{d,R}} c_{\mathrm{AR}}^{*}}{c_{\mathrm{A}}^{*}} q_{\mathrm{AR}}(t+\Delta t)\left(A_{i,a} + A_{1,\mathrm{b}} + A_{1,\mathrm{c}}\right) \right) \tag{2.83}$$

At the position NR, it has to be considered the flux equality from Eq (2.16) and apply finite differences as:

$$\frac{D_{\mathrm{A}}^{\mathrm{R}}\left(q_{\mathrm{A}}(\mathrm{NR}) - q_{\mathrm{A}}(\mathrm{NR\text{-}1})\right)}{h(\mathrm{NR\text{-}1})} = \frac{D_{\mathrm{A}}\left(q_{\mathrm{A}}(\mathrm{NR}) - q_{\mathrm{A}}(\mathrm{NR+1})\right)}{h(\mathrm{NR})} \tag{2.84}$$

In our case, we have applied the Donnan potential model to describe the electrostatic effect in the resin beads which is described in Eq (2.17). Notice that the concentration inside the resin is Π^{z} times proportional to the concentration outside the resin, to the power of the charge (z) of the species "A", thus Eq(2.84) becomes:

$$\frac{D_{\mathrm{A}}^{\mathrm{R}}\left(\Pi^{z_i} q_{\mathrm{A}}(\mathrm{NR}) - q_{\mathrm{A}}(\mathrm{NR\text{-}1})\right)}{h(\mathrm{NR\text{-}1})} = \frac{D_{\mathrm{A}}\left(q_{\mathrm{A}}(\mathrm{NR}) - q_{\mathrm{A}}(\mathrm{NR+1})\right)}{h(\mathrm{NR})} \tag{2.85}$$

Then, after some operations, we obtain:

$$q(\mathrm{NR})\left(\frac{D_{\mathrm{a}}^{\mathrm{R}}\, h(\mathrm{NR})}{D_{\mathrm{a}}\, h(\mathrm{NR\text{-}1})} \Pi^{z_i} + 1 \right) - \frac{D_{\mathrm{a}}^{\mathrm{R}} h(\mathrm{NR})}{D_{\mathrm{a}}^{\mathrm{R}} h(\mathrm{NR\text{-}1})} q(\mathrm{NR\text{-}1}) - q(\mathrm{NR+1}) = 0 \tag{2.86}$$

Therefore, the Matrix a, b and c at the position NR become:

$$M_{\mathrm{NR,b}} = \left(\frac{D^{\mathrm{R}} h(\mathrm{NR})}{D\, h(\mathrm{NR\text{-}1})} \Pi^{z_i} + 1 \right) \tag{2.87}$$

$$M_{\mathrm{NR,a}} = -\left(\frac{D^{\mathrm{R}} h(\mathrm{NR})}{D\ h(\mathrm{NR\text{-}1})} \right) \tag{2.88}$$

$$M_{\mathrm{NR,c}} = 1 \tag{2.89}$$

$$T_{\mathrm{NR}} = 0 \tag{2.90}$$

To fulfil the boundary condition (Eq (2.17)) it is also required that the equation corresponding to the matrix $M_{\mathrm{NR\text{-}1,c}}$ is multiplied by Π^{z}. Because it also corresponds to the position $q(\mathrm{NR})$ of the vector of solutions, so that $M_{\mathrm{NR\text{-}1,c}}$ becomes:

$$. M_{\mathrm{NR\text{-}1,c}} = \Pi^{z_i} \left[A_{\mathrm{NR\text{-}1,c}} + \Delta t \left(d_{\mathrm{A}}^{\mathrm{R}} B_{\mathrm{NR\text{-}1,c}} + k_{\mathrm{a}} c_{\mathrm{B}}^{*} q_{\mathrm{B}}(t+\Delta t) A_{i,\mathrm{c}} + k_{\mathrm{a,R}} c_{\mathrm{R}}^{*} q_{\mathrm{R}}(t+\Delta t) A_{\mathrm{NR\text{-}1,c}} \right) \right] \tag{2.91}$$

In the gel layer, the Eq (2.74)-(2.76) at a position between NR+1 and N-1 become:

$$M_{\mathrm{A}_{i,\mathrm{b}}} = \left[A_{i,\mathrm{b}} + \Delta t \left(d_{\mathrm{A}} B_{i,\mathrm{b}} + k_{\mathrm{a}} c_{\mathrm{B}}^{*} q_{\mathrm{B}}(t+\Delta t) A_{i,\mathrm{b}} \right) \right] \tag{2.92}$$

$$M_{\mathrm{A}_{i,a}} = \left[A_{i,\mathrm{a}} + \Delta t \left(d_{\mathrm{A}} B_{i,a} + k_{\mathrm{a}} c_{\mathrm{B}}^{*} q_{\mathrm{B}}(t+\Delta t) A_{i,\mathrm{a}} \right) \right] \tag{2.93}$$

$$M_{\mathrm{A}_{i,\mathrm{c}}} = \left[A_{i,\mathrm{c}} + \Delta t \left(d_{\mathrm{A}} B_{i,\mathrm{c}} + k_{\mathrm{a}} c_{\mathrm{B}}^{*} q_{\mathrm{B}}(t+\Delta t) A_{i,\mathrm{c}} \right) \right] \tag{2.94}$$

$$T_{\mathrm{A}_i} = q_{\mathrm{A}}(t) \left(A_{i,a} + A_{i,\mathrm{b}} + A_{i,\mathrm{c}} \right) - \Delta t \left(\frac{k_{\mathrm{d}} c_{\mathrm{C}}^{*}}{c_{\mathrm{A}}^{*}} q_{\mathrm{C}}(t+\Delta t) \left(A_{i,a} + A_{i,\mathrm{b}} + A_{i,\mathrm{c}} \right) \right) \tag{2.95}$$

Notice that Eqs ((2.92)-(2.95)) no longer have present the term of the reaction between the species A and the resin beads, also, the diffusion coefficient corresponds to the gel phase. The equations at the last point of the grid have the particularity of including the information that belongs to the boundary condition at the position $\delta^{\mathrm{r}} + \delta^{\mathrm{g}}$.

$$M_{\mathrm{A}_{N,\mathrm{b}}} = \left[A_{N,\mathrm{b}} + \Delta t \left(d_{\mathrm{A}} B_{N,\mathrm{b}} + k_{\mathrm{a}} c_{\mathrm{B}}^{*} q_{\mathrm{B}}(t+\Delta t) A_{N,\mathrm{b}} \right) \right] \tag{2.96}$$

$$M_{\mathrm{A}_{N,\mathrm{a}}} = \left[A_{N,\mathrm{a}} + \Delta t \left(d_{\mathrm{A}} B_{N,a} + k_{\mathrm{a}} c_{\mathrm{B}}^{*} q_{\mathrm{B}}(t+\Delta t) A_{N,\mathrm{a}} \right) \right] \tag{2.97}$$

$$M_{\mathrm{A}_{N,\mathrm{c}}} = \left[A_{N,\mathrm{c}} + \Delta t \left(d_{\mathrm{A}} B_{N,\mathrm{c}} + k_{\mathrm{a}} c_{\mathrm{B}}^{*} q_{\mathrm{B}}(t+\Delta t) A_{N,\mathrm{c}} \right) \right] \tag{2.98}$$

$$T_{A_N} = q_A(t)\left(A_{N,a} + A_{N,b} + A_{N,c}\right) + \Delta t\left(\frac{k_d c_C^*}{c_A^*} q_C(t+\Delta t)\left(A_{N,a} + A_{N,b} + A_{N,c}\right)\right) \quad (2.99)$$

Where $q_A(t+1)=q_B(t+1)=q_C(t+1)=1$ in Eq (2.98) and equilibrium conditions are also fulfilled. Thus, Eq (2.98) goes to the independent term and the equations become:

$$M_{A_{N,b}} = \left[A_{N,b} + \Delta t\left(d_A B_{N,b} + k_a c_B^* q_B(t+\Delta t) A_{N,b}\right)\right] \quad (2.100)$$

$$M_{A_{N,a}} = \left[A_{N,a} + \Delta t\left(d_A B_{N,a} + k_a c_B^* q_B(t+\Delta t) A_{N,a}\right)\right] \quad (2.101)$$

$$T_{A_N} = \left(A_{N,a} + A_{N,b}\right) + \Delta t\left(k_a c_B^*\left(A_{N,a} + A_{N,b}\right)\right) - \left[\Delta t\left(d_A B_{N,c}\right)\right] \quad (2.102)$$

The development of the equations for the species B and C that have been done in this section follows the same procedure but we have to use instead Eq (2.45) and Eq (2.46).

2.4.6 Solver for non-mobile species

The species that are non-mobile in a DGT device are the beads of resin that are fixed in the gel polymeric matrix. In consequence, these equations do not have the diffusive term and there is no need to apply the finite element method to solve them.

$$\frac{\partial q_R}{\partial t} = -k_{a,R} q_A q_R c_A^* + q_{AR} k_{d,R} \quad (2.103)$$

$$\frac{\partial q_{AR}}{\partial t} = q_A q_R k_{a,R} c_A^* - k_{d,R} q_{AR} \quad (2.104)$$

A way to proceed is the application of the inverse Euler method (Eq (2.64)) on Eqs(2.103)-(2.104).Therefore:

$$\frac{q_R(t+\Delta t) - q_R(t)}{\Delta t} = -k_{a,R} q_A(t+\Delta t) q_R(t+\Delta t) c_A^* + q_{AR}(t+\Delta t) k_{d,R} \quad (2.105)$$

$$\frac{q_{AR}(t+\Delta t) - q_{AR}(t)}{\Delta t} = q_A(t+\Delta t) q_R(t+\Delta t) k_{a,R} c_A^* - k_{d,R} q_{AR}(t+\Delta t) \quad (2.106)$$

Then, isolating for $q_R(t+\Delta t)$ in Eq (2.103) and for $q_{AR}(t+\Delta t)$ in Eq (2.104), we obtain :

$$q_R(t+\Delta t)(1+\Delta t k_{a,R} q_A(t) c_A^*) = q_R(t+\Delta t) + q_{AR}(t+\Delta t) k_{d,R} \quad (2.107)$$

$$q_{AR}(t+\Delta t)\left(1+\Delta t k_{d,R}\right) = \Delta t q_A(t) q_R(t+\Delta t) k_{a,R} c_A^* + q_{AR}(t+\Delta t) \quad (2.108)$$

The initial conditions necessary to solve this system of equations are $q_{AR}(t)=0$ and $q_R(t)=1$.This system of equations is solved along the resin layer, for an homogeneous resin layer they would be solved for the grid points 1 to NR. For a heterogeneous resin layer they

would be solved for the grid points NR1 to NR1+NR2 and for NR1+NR2+NR3 to NR1+NR2+NR3+NR4. No reaction with the resin beads would be observed from 0 to NR1-1 and from NR1+NR2+1 to NR1+NR2+NR3-1.

2.5 Accumulation, lability degree and *%back*

DGT devices are dynamic sensors that measure a flux of metal by the elution of the resin disc or other experimental procedures. In presence of ligands from the metal flux at the resin layer the contribution of the complexes in solution to the total accumulation can be understood by calculating the global lability degree of the metal species in solution.

Another strategy to unravel the presence of partially labile complexes is by measuring the percentage between the back accumulation and the total accumulation (i.e *%back*) with a DGT devices with a stack of 2 resins. Both the lability degree and the *%back* are experimental measurements that can be employed to determine the dissociation rate constant of a complex.

Thus, from the solution of the concentration profiles this experimental variables can be calculated in a simulation which allow to predict or understand the behaviour of diffusion-reaction systems.

This procedure can be done by integrating the concentration of metal that has reacted with the resin beads (i.e q_{AR}) at the last simulation time :

$$n_M = A\int_0^{\delta^r} q_{MR}(z,t_n)dz \qquad (2.109)$$

Where A is the area of the DGT device, q_{MR} is the concentration of metal bound to the resin at the last time of the simulation, δ^r is the thickness of the resin disc. Considering a DGT device with 2 resin layers, this integration can be performed numerically by the trapezoidal rule and Eq (2.109) becomes:

$$n_M = A2c_R^*\left(\sum_{i=1}^{NR}\frac{(q_{MR}(z_i,t_n)+q_{MR}(z_{i+1},t_n))}{2}\Delta z_i\sqrt{D_{max}}\right) \qquad (2.110)$$

Where $\Delta x_i = \Delta z_i\sqrt{D_{max}}$ is the spatial coordinates in the international units and c_R^* is the total concentration of the resin beads, which has been used previously to solve the problem with non-dimensional variables.

The back accumulation can be calculated in a very similar way :

$$n_{back} = Ac_R^*\int_0^{\frac{\delta^r}{2}} q_{MR}(z,t_n)dz = Ac_R^*\left(\sum_{i=1}^{NR/2}\frac{q_{MR}(z_i,t_n)+q_{MR}(z_{i+1},t_n)}{2}\Delta z_i\sqrt{D_{max}}\right) \qquad (2.111)$$

Thus, the *%back* is computed straightforward from the division of Eq (2.111) by Eq (2.110).

$$\%back = \frac{n_{\text{back}}}{n_{\text{T,M}}} \tag{2.112}$$

The global lability degree is computed from [8]:

$$\xi = \frac{J\big|_{x=\delta^{\text{r}}} - J_{\text{free}}\big|_{x=\delta^{\text{r}}}}{J_{\max}\big|_{x=\delta^{\text{r}}} - J_{\text{free}}\big|_{x=\delta^{\text{r}}}} \tag{2.113}$$

By applying forward differences to $J\big|_{x=\delta^{\text{r}}}$ and $J_{\text{free}}\big|_{x=\delta^{\text{r}}}$ and substituting by:

$$J_{\max}\big|_{x=\delta^{\text{r}}} = \frac{D_{\text{M}} c_{\text{M}}}{\delta^{\text{g}}} + \sum_{i=1}^{h} \frac{D_{\text{M}^i\text{L}} c_{\text{M}^i\text{L}}}{\delta^{\text{g}}} + \sum_{j=1}^{n} \frac{D_{\text{ML}_j} c_{\text{ML}_j}}{\delta^{\text{g}}} \tag{2.114}$$

The global lability degree is computed as :

$$\xi = \frac{\sqrt{D_{\max}}\left(\sum_{i=1}^{h} c^{*}_{\text{M}^i\text{L}} \frac{q_{\text{M}^i\text{L}}(\text{NR}) - q_{\text{M}^i\text{L}}(\text{NR}-1)}{h(\text{NR})} + \sum_{i=1}^{n} c^{*}_{\text{ML}_j} \frac{q_{\text{ML}_j}(\text{NR}) - q_{\text{ML}_j}(\text{NR}-1)}{h(\text{NR})} \right)}{\frac{D_{\text{M}} c^{*}_{\text{M}}}{\delta^{\text{g}}} + \sum_{i=1}^{h} \frac{D_{\text{M}^i\text{L}} c^{*}_{\text{M}^i\text{L}}}{\delta^{\text{g}}} + \sum_{j=1}^{n} \frac{D_{\text{ML}_j} c^{*}_{\text{ML}_j}}{\delta^{\text{g}}} - \sqrt{D_{\max}} \frac{q_{\text{M}}(\text{NR}) - q_{\text{M}}(\text{NR}-1)}{h(\text{NR})}} \tag{2.115}$$

Whereas for each species the lability degree is computed as:

$$\xi_i = 1 - q_i(\text{NR}) \tag{2.116}$$

2.6 References

1. Crank, J., *The Mathematics of Diffusion*. 2nd ed.; Clarendon Press: Oxford, UK, 1975.
2. Morton, K. W. a. M., D., *Numerical Solution of Partial Differential Equations*. Cambridge University Press: 2005.
3. Hughes, T. J. R., Fundamental Concepts; a simple one-dimensional boundary-value problem. In *The Finite Element Method: Linear Static and Dynamic Finite Element Analysis*, Prentice Hall: Englewood Cliffs,N.J., 1987.
4. Hughes, T. J. R., Formulation of Parabolic, Hyperbolic and Elliptic-Eigenvalue Problems. In *The Finite Element Method: Linear Static and Dynamic Finite Element Analysis*, Prentice Hall: Englewood Cliffs,N.J., 1987; pp 418-458.
5. Hughes, T. J. R., Algorithms for Parabolic problems. In *The Finite Element Method: Linear Static and Dynamic Finite Element Analysis*, Prentice Hall: Englewood Cliffs,N.J., 1987; pp 459-489.
6. Press, W. H.; Flannery, B. P.; Teukolsky, S. A.; Vetterling, W. T., *Numerical Recipes*. Cambridge University Press: Cambridge, 1986.
7. Altier, A.; Jimenez-Piedrahita, M.; Rey-Castro, C.; Cecilia, J.; Galceran, J.; Puy, J., Accumulation of Mg to diffusive gradients in thin films (DGT) devices: kinetic and thermodynamic effects of the ionic strength. *Analytical Chemistry* **2016,** *88* (20), 10245-10251.
8. Uribe, R.; Mongin, S.; Puy, J.; Cecilia, J.; Galceran, J.; Zhang, H.; Davison, W., Contribution of partially labile complexes to the DGT metal flux. *Environmental Science and Technology* **2011,** *45* (12), 5317-5322.

3 Determination of diffusion coefficients of complexes and free metal ions in gel layers from diffusion cell experiments.

3.1 Introduction

The (bio)availability of trace metals in natural waters depends, in general, on the chemical speciation as well as on the mobility and reactivity of all the metal species [1]. Convection is the main transport phenomena responsible for the dissemination of metal species. However, close to the consuming surfaces of algae and microorganisms, under laminar conditions, the mobility of the species is determined by diffusion [2]. In these conditions, when the free metal is the only one species able to be internalized, the metal flux at the consuming interface depends on the respective diffusivities and labilities of the set of species present. In recent years, several dynamic analytical techniques have been developed with the purpose to mimic the uptake by biota. Among them, GIME (Gel integrated Microelectrode) and DGT has been presented to measure trace-metal ions *in situ* by diffusion through a hydrogel[3-4].

The wide use of these analytical techniques relies on their simplicity and their ability to be used on site. Their interpretation in terms of the species present requires the knowledge of the diffusion coefficients in hydrogels through independent experimental measurements. The characteristics of the diffusion cell offer a way to obtain reliable values of diffusion coefficients in hydrogels [5-7]. A diffusion cell is composed of an acceptor and a donor compartments connected with the gel layer through which we are interested in measuring the diffusion coefficients. After a transient time, the accumulation in the acceptor cell is linear with time allowing the determination of the diffusion coefficient from first Fick's law. This approach is only valid at short time measurements, because it neglects the decrease of the metal flux that is caused by a depletion of the concentration in the donor cell and the consequent increase of the concentration in the acceptor cell.

In some cases, the concentration in the donor cell is limited by precipitation phenomena, especially when we want to do the measurements at a pH close to the natural waters. When the concentration in the donor is low, we have to wait long times to have measurable concentrations in the acceptor cell and the effects of finite volume of the cells cannot be neglected.

Considering pH values close to the natural systems also requires to be aware of the presence of metal hydroxo-complexes that can exhibit different diffusion coefficients to that of the metal. Actually, the determination of diffusion coefficients of metal complexes is a subject of intrinsic interest which has been little explored up to now, since the metal availability in natural samples depends on the mobility of each species as stated above[6, 8].

In this chapter, we start considering measurements of diffusion coefficients using different stirring rates in the donor and acceptor solutions in order to evaluate the influence and the convenience of considering a DBL on both sides of the gel layer when using a diffusion cell to measure diffusion coefficients.

We also aim to determine diffusion coefficients of metal complexes in mixtures. When there is more than one metal species in the donor solution, the diffusion flux to the acceptor depends on the diffusion coefficients of all the species, and a set of experiments with different concentrations can be required to determine the diffusion coefficient of each species.

Finally, we have derived an expression that allows determining diffusion coefficients of trace-metals in conditions of finite volume regime, which can be useful in cases where the concentration of free metals in the donor compartment is close to the limit of detection since the concentration in the acceptor should also be above the LOD and accordingly, it is non-negligible with respect to the concentration in the donor cell.

3.2 Materials and Reagents.

The diffusion cell is composed of two compartments (donor and acceptor) of 100 mL each one connected through a circular hole of 2 cm^2 (0.80 cm radius). See Figure 3.1 for a scheme of the cell.

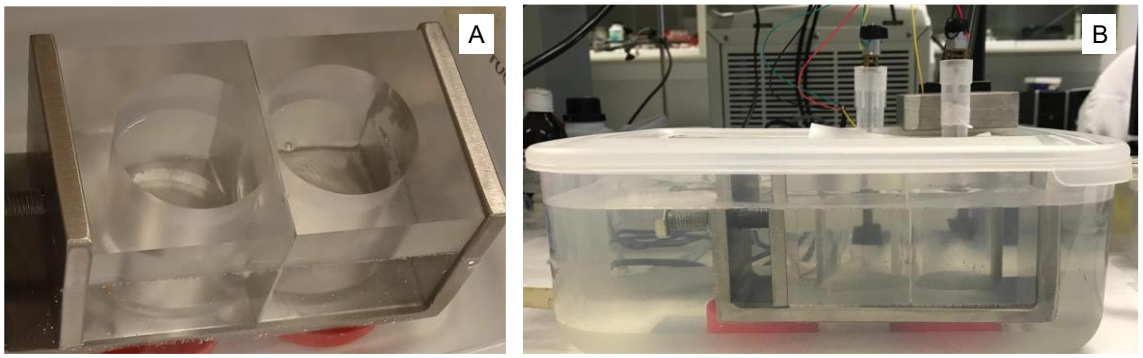

Figure 3.1 Diffusion cell instrument employed to perform the experiments in Table 3.1 (Panel A). In Panel B is depicted the diffusion cell inside a recipient with an external flow of water to keep constant the temperature, as well as, a couple of rotors to maintain a selected constant agitation.

Both cells are connected by the gel layer and separated by a plastic (with a hole with the same area of the gel layer) to avoid compression damage of the APA gel that is placed on the connecting area between both compartments. The thickness of the gel is 0.629 mm and has an area of 4.91 cm^2 (1.25 cm radius). Both compartments are clamped together and placed in a thermostatic bath to maintain a constant temperature. For long term experiments, an APA gel with an area of 8.04 cm^2 (1.6 cm radius) has been employed.

The donor compartment is filled with a solution of a given concentration of the analytes whose diffusion coefficients need to be determined. The solution of the acceptor compartment is free from the analyte but shares a similar ionic strength, pH and volume with the donor solution to ensure that only diffusion controls the transport of the target cations from the donor to the acceptor cells.

In both compartments there is a stirring paddle which homogenizes both solutions. The stirring paddle frequency can be modulated by applying a certain potential difference. For an applied potential of 3.5V, 5V and 7.5V a frequency of 140, 243 rpm and 400 rpm is obtained. The temperature has been maintained constant with a thermostatic bath at 25°C.

The solutions in the donor compartment have been prepared from certified reagents of Cd, Zn and Pb at 1000 mg/L 2% HNO_3 Précis, Lithium standard for ICP 1004 mg/L ± 2 mg/L, Ni 1000 µg/mL 2% HNO_3 SPEX certiprep, Rb 1000mg/L 2% HNO_3 Assurance. In another type

of experiments, the donor solutions have been prepared from certified reagents TraceCERT which contain Ag 10 mg/L, Al 10 mg/L, Ba 10 mg/L, Be 10 mg/L, Bi 10mg/L, Ca 100mg/L, Cd 10 mg/L, Co 10 mg/L, Cr 10 mg/L, Cs 10 mg/L, Cu 10 mg/L, Fe 100 mg/L, Ga 10 mg/L, In 10 mg/L, K 100 mg/L, Li 10 mg/L, Mg 10 mg/L, Mn 10 mg/L, Mo 10 mg/L, Na 100 mg/L, Ni 10 mg/L, Pb 10 mg/L, Rb 10 mg/L, Sr 10 mg/L, Tl 10 mg/L,V 10 mg/L, Zn 10mg/L with a 10% w/w HNO3. The analysis of the trace-metals in solution has been done by ICP-MS.

Table 3.1 Experimental conditions and concentrations of the analytes in the donor cell are quoted as columns in the Table. The concentration of the analytes in the acceptor cell at t=0s was negligible. The salt background in the acceptor cell is NaNO3 and it has the same concentration as in the donor compartment. Stirring rate was the same at the donor and acceptor cells and the values are indicated in the Table. Temperature was set at 25ºC, the volume of the donor and acceptor solution cells was 0.1 L and the sampling volume at different times for measurement of the concentration evolution is reported in the Table.

	Donor solution							
c_{NaNO3} (mol m^{-3})	5	5	5	10	100	101	101	5
$c_{T,NTA}$(mol m^{-3})	$2x10^{-1}$	-	-	-	$1x10^{-1}$	0.05	-	-
c_{Ni} (mol m^{-3})	0.0078	0.185	0.176	0.186	0.001	0.05	0.57	0.185
c_{Zn} (mol m^{-3})	0.0073	0.165	0.15	0.155	-	-	-	0.165
c_{Pb} (mol m^{-3})	0.0022	0.054	0.052	0.053	-	-	-	0.054
c_{cu}(mol m^{-3})	0.0087	-	-	-	-	-	-	-
c_{co}(mol m^{-3})	0.0087	-	-	-	-	-	-	-
c_{Cd} (mol m^{-3})	0.041	0.096	0.09	0.093	-	-	-	0.096
c_{Rb} (mol m^{-3})	0.0058	0.12	0.11	0.12	0.071	-	-	0.12
c_{K} (mol m^{-3})	0.165	-	-	-	-	-	-	0.26
c_{Li} (mol m^{-3})	0.072	1.426	1.36	1.47	-	-	-	1.43
$c_{Glycina}$ (mol m^{-3})	-	-	-	-	0.04	-	-	-
c_{Hepes} (mol m^{-3})	-	-	-	-	-	40	2	-
Stirring rate (rpm)	243	243	400	140	243	243	243	243
pH	3.96	3.00	2.49	4.23	8.77	7.56	7.48	2.38
$V_{aliquot}$ (µL)	500	500	50	35	100	150	150	200
Time (h)	2.9	2.9	54.0	149.7	2.9	3.5	3.0	50.1

3.3 Methodology

The donor cell is filled with the solution of the metal ion. Aliquots of the acceptor solution of the volumes indicated in Table 3.1 are extracted and analysed for the metal content by ICP-MS at different times. Let us assume that the free metal is the only one relevant metal species in the donor with a concentration that can be considered time independent during the experiment, while the metal concentration in the acceptor is negligible. Assuming instantaneous steady-state and perfect mixing in the acceptor side, the accumulation in the acceptor solution is described by Eq (3.1) [6]:

$$n_{\mathrm{M}} = \frac{D_{\mathrm{M}}\, c_{\mathrm{M}}^{*} A t}{\delta^{\mathrm{g}}} \qquad (3.1)$$

Where n_{M} is the number of moles of metal in the acceptor solution, c_{M}^{*} is the total metal concentration at the donor solution, A is the geometric area, D_{M}, the diffusion coefficient of the free hydrated metal and δ^{g} is the thickness of the gel layer. The previous equation considers that the gel thickness is the current diffusion path of the analyte ($\delta^{\mathrm{DBL}} << \delta^{\mathrm{g}}$) so that the existence of a DBL is neglected in comparison to δ^{g} [9]. However, if the diffusion coefficient of the metal in the gel is not far different from that in water, Eq (3.1) is still valid assuming that δ^{g} stands for the thickness of the gel plus the δ^{DBL} at both sides of the gel, in the donor and in the acceptor cells.

3.3.1 Measurement of the DBL thickness from diffusion-cell experiments

Figure 3.2 shows a schematic representation of the diffusion layers of a diffusion cell instrument and the steady-state concentration profile when only the free metal is present in the solution :

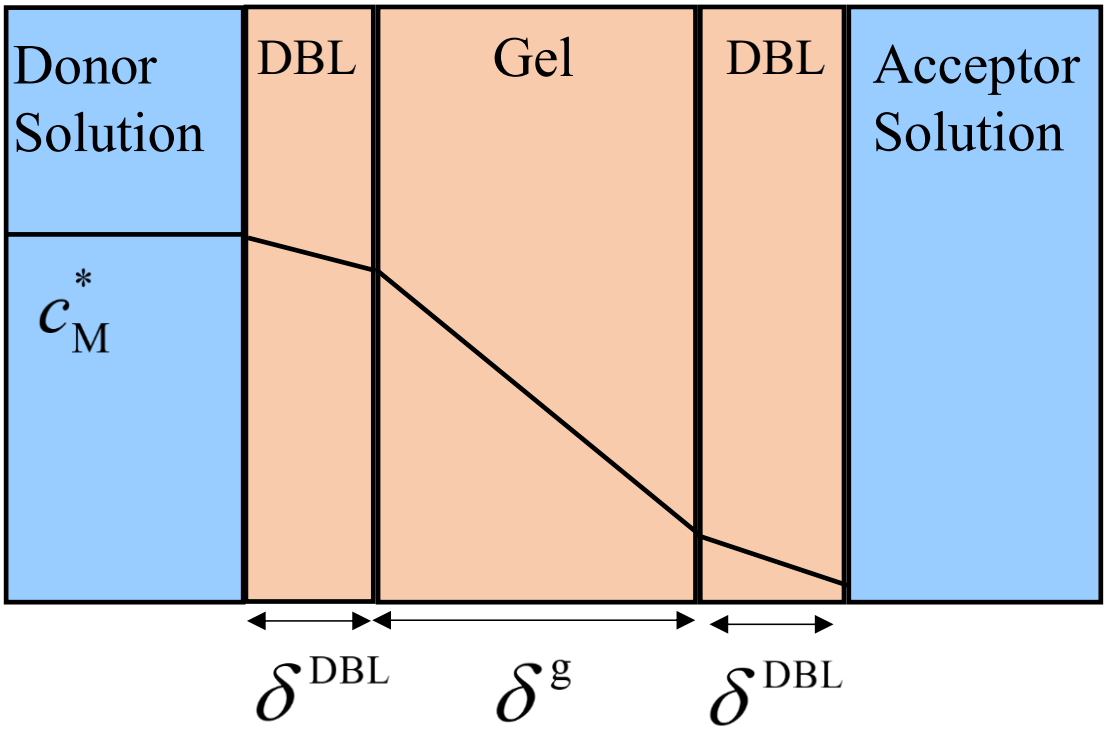

Figure 3.2 Domains considered in the diffusion cell along with the steady-state concentration profile for a trace-metal with a donor concentration (c_M^*).

Figure 3.2 includes a DBL with thickness δ^{DBL} in each side of the diffusive gel layer. The slope of the metal concentration profile is smaller in these layers assuming that the diffusion coefficient is higher in water than in the gel layer.

In well-stirred donor and acceptor solutions, it is a fair assumption to neglect δ^{DBL} and then Eq.(3.1) can be used to calculate the diffusion coefficient. However, when the stirring is not vigorous enough the experimental measurement of the diffusion coefficients through Eq.(3.1) can yield to underestimated values.

Since δ^{DBL} decreases as the stirring increases, when an increase of the stirring rate does not yield a significant increase of the accumulation in the acceptor cell we can accept that δ^{DBL} is negligible with respect to δ^{g} and the diffusion coefficient obtained with the simple Eq.(3.1) can be accepted.

Alternatively, δ^{DBL} can be calculated at any stirring rate assuming as true a reference value of the diffusion coefficient of a given metal. Values reported in DGT research can be used to this aim. For instance, we compute an operational δ^{DBL} from a trace-metal element (e.g Cd)

added in the donor solution with the application of Eq (3.2). Once δ^{DBL} is known, the diffusion coefficients of the rest of trace-metals can be obtained from the acceptor data. Under steady-state and perfect sink conditions, and assuming a common diffusion coefficient of the metal in the gel layer and in the DBL, the accumulation in the acceptor cell coming from a diffusive flux can be described as:

$$n_M = \frac{D_M c_M^* A t}{\delta^g + 2\delta^{DBL}} \quad (3.2)$$

Where c_M^* is the total metal concentration at the donor solution, A is the geometric area, D_M, the diffusion coefficient of the free hydrated metal, δ^g the thickness of the gel layer and δ^{DBL} the diffusive boundary layer (considered identical in both compartments of the diffusion cell when the rotation frequency is the same in both cells). Then, from Eq (3.2), δ^{DBL} can be determined as:

$$\delta^{DBL} = \frac{D_M c_M^* A - s\delta^g}{2s} \quad (3.3)$$

where s is the slope of the linear regression of the plot of the mass of the reference cation (Cd) accumulated in the acceptor cell vs time, D_M is the diffusion coefficient of Cd in the APA gel reported by DGT research at the temperature of interest and c_M^* the Cd concentration in the donor solution. Once this operational value of δ^{DBL} is determined at the stirring frequency of interest, the diffusion coefficient of other metals can be determined at that stirring frequency using Eq (3.2).

3.3.2 Measurement of diffusion coefficients of metal complexes from a mixture of metals in excess of ligand conditions.

When the donor solution contains metal complexes, the flux of metal towards the acceptor solution depends on the diffusive motion of both, free metal and complexes. It can be seen (See supporting information) that when diffusion takes place in steady-state and in a finite domain, the total metal flux is derived from an independent diffusion of the species. Assuming steady-state conditions, $c_M(x=0)=0$, $c_{ML}(x=0)=0$ (perfect sink conditions) and c_{ML}

($x=\delta^{g}+2\,\delta^{DBL}$)= c^{*}_{ML}, c_M ($x=\delta^{g}+2\,\delta^{DBL}$)= c^{*}_{M} the mass of metal accumulated in the acceptor solution can be written as:

$$n_M = \frac{D_M c^{*}_M + \sum_i^n D_{MLi} c^{*}_{MLi}}{\delta^{g} + 2\delta^{DBL}} At \qquad (3.4)$$

Which corresponds to a case with only one ligand that yields to successive metal complexes. In Eq (3.4), D_{MLi} and c^{*}_{MLi} label the diffusion coefficient and the concentration of the metal complex, n is the maximum stoichiometric metal-to-ligand ratio and i refers to the i^{th} complexation reaction.

Taking advantage of the independent diffusion of species, the application of Eq.(3.4) is a good strategy to determine the diffusion coefficients of complexes through experiments at different ligand concentration. Diffusion coefficients and δ^{DBL} can be determined solving a system of equations built from measuring the accumulation in systems with different speciation. The equilibrium concentrations of all the species in a laboratory system can be assessed using a speciation code (e.g VMINTEQ) from $c_{T,M}$, $c_{T,L}$, pH and the temperature of the system. To reduce the number of unknowns, an additional independent experiment at the same pH, ionic strength and stirring rate, can be used to determine δ^{DBL}, as explained in the above section.

For example, for a case where there is a single complexation reaction Eq (3.4) becomes :

$$n = \frac{D_M c^{*}_M + D_{ML} c^{*}_{ML}}{\delta^{g} + 2\delta^{DBL}} At \qquad (3.5)$$

and the diffusion coefficient of the complex can be determined as,

$$D_{ML} = \frac{s(\delta^{g} + 2\delta^{DBL}) - A D_M c^{*}_M}{A c^{*}_{ML}} \qquad (3.6)$$

once δ^{DBL} is known. If both diffusion coefficients, D_M and D_{ML}, have to be determined, a couple of experiments using different concentrations of metal and/or complex in the donor solution are required.

Something similar happens when complexes with stoichiometry ML and ML_2 are present. In this case, Eq (3.4) becomes:

$$n = \frac{D_M c_M^* + D_{ML} c_{ML}^* + D_{ML2} c_{ML2}^*}{\delta^g + 2\delta^{DBL}} At \quad (3.7)$$

and the number of unknowns increases up to 4 (D_M, D_{ML}, D_{ML2} and δ^{DBL}). In these conditions, the simplest approach to determine D_{ML2} is to have previously determined δ^{DBL}, D_M and D_{ML} using experiments in which the concentration of ML_2 is negligible. In this way, only one additional experiment is needed to obtain D_{ML2}.

Thus, when D_M and D_{ML} are known, D_{ML2} can be obtained as:

$$D_{ML2} = \frac{s\left(\delta^g + 2\delta^{DBL}\right) - A\left(D_M c_M^* + D_{ML} c_{ML}^*\right)}{A c_{ML2}^*} \quad (3.8)$$

where D_{ML2} is the diffusion coefficient of the complex that comes from the second complexation reaction.

3.3.3 Calculation of diffusion coefficients when a finite volume regime applies

When metal concentrations in the bulk solution are of the order of nM, the linear regime does not hold during a time long enough to have a measurable concentration in the acceptor cell since the metal concentration in the donor cell is depleted during the experiment while the metal concentration in the acceptor cell increases. For this case, we have developed an approximate model to determine the diffusion coefficient from the evolution of the concentration in the acceptor cell with time.

When the flux is not steady-state, the variation of the donor and acceptor concentrations with time can be written as:

$$c_D(t) = c_D^* - \frac{A}{V_D}\int_0^t J dt \quad (3.9)$$

and

$$c_A(t) = \frac{A}{V_A}\int_0^t J dt \quad (3.10)$$

Assuming that concentrations at both sides of the gel layer are time dependent, but that the metal profile is close to linear between both surfaces as would be if steady state was reached, when first Fick's law is applied the flux becomes:

$$J(t) = D_M \frac{c_D(t) - c_A(t)}{g} \quad (3.11)$$

We will refer to the approximation of the flux as done in Eq (3.11) as instantaneous steady state approximation. This is a good approximation when the change of the concentrations at the limiting surfaces of the gel layer is slow in comparison to the time to reach steady-state for time independent concentrations at the gel surfaces. This means that we are facing effects of the finite volume of the donor and acceptor cells but these effects are mild.
After substituting Eq (3.9) and Eq (3.10) into Eq (3.11) we obtain :

$$J(t) = \frac{D_M A}{\Delta g}\left(\frac{1}{V_A} + \frac{1}{V_D}\right)\int_0^t J(t)dt \tag{3.12}$$

Then, the time derivative of the flux becomes:

$$\frac{dJ(t)}{dt} = -\frac{D_M}{\Delta g}\left(\frac{A}{V_A} + \frac{A}{V_D}\right)J(t) \tag{3.13}$$

Once we integrate on both sides respect to the flux and time we obtain:

$$J(t) = J_0 \exp\left(-\frac{D_M}{g}\left(\frac{A}{V_A} + \frac{A}{V_D}\right)t\right) \tag{3.14}$$

Substituting Eq (3.14) in Eq (3.9) and Eq (3.10) and integrating respect to time, we obtain an expression for the concentration in the donor and acceptor cell:

$$c_A(t) = \frac{c_D^* V_D}{V_A + V_D} - \frac{c_D^* V_D}{V_A + V_D}\exp\left(-\frac{D_M A}{\Delta g}\left(\frac{V_A + V_D}{V_A V_D}\right)t\right) \tag{3.15}$$

$$c_D(t) = c_D^* - \frac{c_D^* V_D}{V_A + V_D} - \frac{c_D^* V_D}{V_A + V_D}\exp\left(-\frac{D_M A}{\Delta g}\left(\frac{V_A + V_D}{V_A V_D}\right)t\right) \tag{3.16}$$

Eq (3.15) can be rewritten as

$$\ln\left(\frac{c_D^* V_D}{V_A + V_D} - c_A(t)\right) = -\frac{D_M A}{\Delta g}\left(\frac{V_A + V_D}{V_A V_D}\right)t + \ln\left(\frac{c_D^* V_D}{V_A + V_D}\right) \tag{3.17}$$

which allows us to determine the metal diffusion coefficient from the slope of the linear fitting of $\ln\left(\frac{c_D^* V_D}{V_A + V_D} - c_A(t)\right)$ vs t since the slope can be identified with $-\frac{D_M A}{\Delta g}\left(\frac{V_A + V_D}{V_A V_D}\right)$.

From Eq (3.17) D_M can be easily fitted from the experimental data, when finite volume effects take place.

3.4 Results

3.4.1 Estimation of the DBL thickness from experiments in a diffusion cell

It has been done a set of experiments with increasing applied voltage to the stirring paddle, 3.5V, 5V and 7.5V which correspond to stirring frequencies of 140 rpm, 243 rpm, 400 rpm respectively. For DGT accumulation measurements, a well-stirred solution is considered when a rotation frequency of 100 rpm is applied to the deployment solution [9]. Our purpose is to revise if similar results apply to measurements in the diffusion cell.

The experimental results of the accumulation vs time for each stirring rate are shown in Figure 3.3.

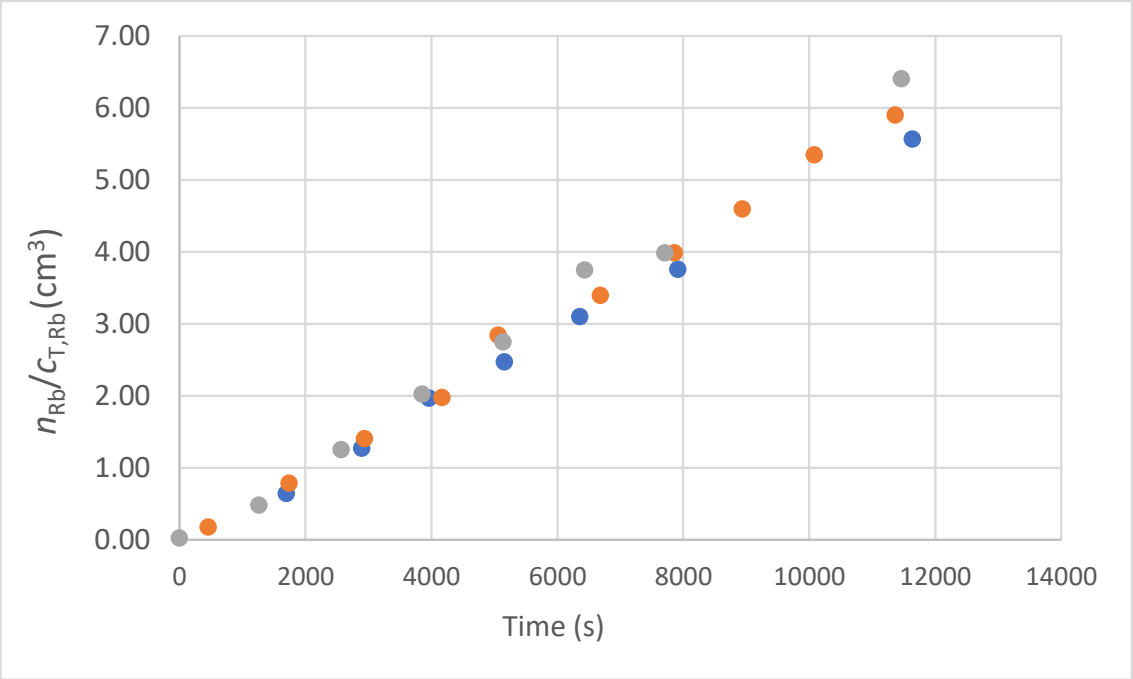

Figure 3.3 Normalized accumulation in the acceptor cell against time for 3 experiments with stirring rates 400 rpm (gray dots), 243 rpm (orange dots) and 140 rpm (blue dots).

With the purpose to show the differences with the stirring rate, it has been plotted in Figure 3.3 the accumulation of rubidium at the acceptor cell vs time. This figure shows a very mild increase of the accumulation in the acceptor cell as the stirring rate increases. As a result, the slope of the accumulation vs time in an experiment that belongs to a stirring rate of 400 rpm is greater than the slope of an experiment that has been done at 140 rpm. According to Eq (3.2), this increase is compatible with a decrease of δ^{DBL} so that the diffusion domain is shortened and the flux increases. Thus, introducing into Eq (3.3) the diffusion coefficient of

Cd, δ^{DBL}-values for each stirring can be determined. The results of this procedure based on the Cd diffusion coefficient reported in the website of DGT-research can be found in column 1 of Table 3.2 . Alternatively, the experiment at 400 rpm can be used to determine D_{Cd} by assuming a negligible $\delta^{DBL} = 0$. Thus, with $\delta^{DBL} = 0$ the analysis of the concentrations on the acceptor cell lead to D_{Cd} = 4.97x10^{-10} m^2 s^{-1} which, used in the rest of experiments reported in Table 3.2 lead to the δ^{DBL}-values for each stirring rate indicated in column 2 of Table 3.2 . The δ^{DBL}-values reported in Table 3.2 should be useful for each metal cation within the model that δ^{DBL} depends on the physical characteristics of the transport on both compartments of the cell but not on the chemical composition of the solutions.

Different rows in Table 3.2 have different stirring rates so that differences between δ^{DBL} in the last column of Table 3.2 are expected.

Table 3.2 Values of δ^{DBL} determined for each stirring rate from the regression of the plot of accumulation vs time and using Eq (3.4) for each experiment reported in the different rows. The δ^{DBL} values reported in column 1 come from introducing D_{Cd}=6.09x10^{-10} m^2 s^{-1} into Eq (3.4) as reported for T=25ºC in the website of DGT research. δ^{DBL} values reported in column 2 come from applying Eq (3.4) with D_{Cd}=4.97x10^{-10} m^2 s^{-1} obtained from the data at 400 rpm assuming a negligible δ^{DBL} at such stirring rate. Other data: T = 25°C and δ^{g} =6.29x10^{-4}(m).

δ^{DBL} (m) / Stirring rate(rpm)	Cd	Cd	$<\delta^{DBL}>$ (m)
140	2.04x10^{-4}	8.54x10^{-5}	1.45 x10^{-4}
243 (Exp Abril 2021)	3.12x10^{-4}	1.97x10^{-4}	2.54 x10^{-4}
400 (Exp Agost 2022)	1.46x10^{-4}	4.02x10^{-5}	8.57x10^{-5}
400 (Exp Juny 2021)	7.09x10^{-5}	-	

A decrease of δ^{DBL} as the stirring rate increases, is expected. Although there is a trend in this sense, data of Table 3.2 do not allow to corroborate this dependence. At 400 rpm, the lowest δ^{DBL} is reported. However δ^{DBL} corresponding to 140 and 243 rpm do not show the expected trend.

Once $<\delta^{DBL}>$ have been determined, we calculate the diffusion coefficient of the free metal elements (e.g Ni, Cd, Zn, Pb) and compare these values with the data available in the DGT website.

Table 3.3 Set of diffusion coefficients determined from Eq (3.4) using the value reported of δ^{DBL} corresponding to the labelled stirring rate reported in the previous table .

Element	*D* (m^2 s^{-1}) at 25 °C (140 rpm)	*D* (m^2 s^{-1}) at 25 °C (243 rpm)	*D* (m^2 s^{-1}) at 25 °C (400 rpm) Exp Juny 2021	*D* (m^2 s^{-1}) at 25 °C (400 rpm) Exp Agost 2022	D from DGT research at 25 °C
Pb	$6.48x10^{-10}$	$6.68x10^{-10}$	$6.52x10^{-10}$	-	$8.03x10^{-10}$
Pb	$7.94x10^{-10}$	$8.19x10^{-10}$	$7.99x10^{-10}$	$7.59x10^{-10}$	
Zn	-	$6.71x10^{-10}$	-	-	$6.08x10^{-10}$
Zn	-	$8.00x10^{-10}$	-	$6.68x10^{-10}$	
Ni	$4.69x10^{-10}$	$5.52x10^{-10}$	$4.65x10^{-10}$	-	$5.77x10^{-10}$
Ni	$5.74x10^{-10}$	$6.76x10^{-10}$	$5.70x10^{-10}$	$5.88x10^{-10}$	

The methodology shown in the section “Measurement of the DBL thickness from diffusion-cell experiments Measurement of the DBL thickness from diffusion-cell experiments” allows to determine very similar results than those reported in DGT research. Moreover, the results given for the diffusion coefficients are consistent when the stirring rate is changed.

3.5 Determination of diffusion coefficients from a mixture of metals with partial complexation with NTA.

Depending on the molecular size, diffusion coefficients of metal complexes can differ from that of the free metal. In many cases, complexes show diffusion coefficients lower than free hydrated metal ions. For example, this behaviour has been reported for metal complexes such as NiNTA, CdNTA, CoNTA and PbNTA. Whereas, the opposite case has been observed for iodide complexes showing a higher diffusion coefficient than the free metal [10]. Thus, the speciation of the trace-metal ion will influence the rate of mass transport when the process is controlled by diffusion.

In this section, we use the methodology described in "Measurement of diffusion coefficients of metal complexes from a mixture of metals in excess of ligand conditions" to measure the diffusion coefficient of M-NTA complexes in the APA gel.

We apply this methodology to experiments where we have different ligand concentrations with a cocktail of metal ions (i.e Cd, Co and Pb) or with a single trace-metal (i.e Ni). In the cases of Cd and Co, the speciation includes a relevant fraction of free metal ion, being this fraction greater for Cd than for the case of Co. In the case of Pb, the trace-metal ion has an affinity for the ligand higher than other trace-metals ions present in the system and accordingly, it achieved a very high degree of complexation. For Ni, we have compositions of the donor solution where the main Ni species is the complex NiNTA but in other cases, the concentration of $Ni(NTA)_2$ is not negligible.

Figure 3.4 evidences that the speciation plays a relevant role in the rate of accumulation in the acceptor cell, in particular for Cd, Co and Pb:

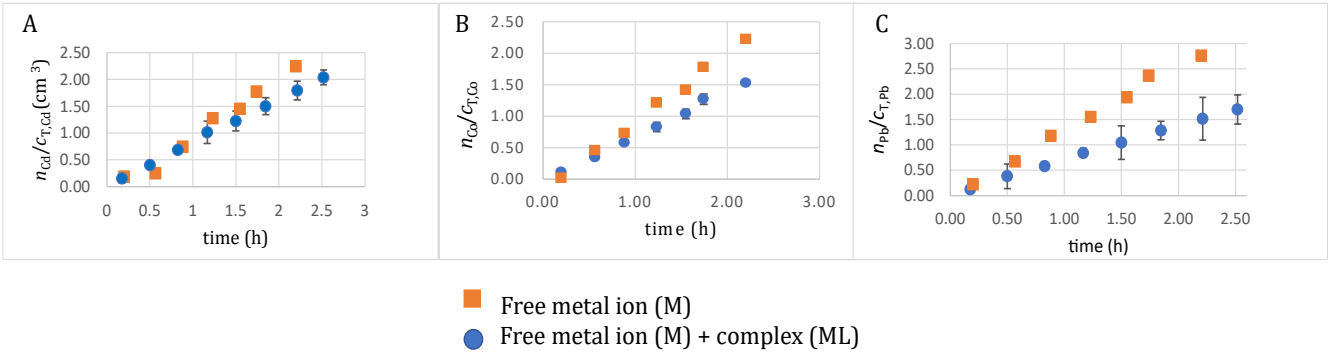

Figure 3.4 Panel A Cd accumulation in the acceptor cell vs time for an experiment which solution contained a cocktail of metal ions in absence of ligands (orange squares) compared to an experiment which solution contained a cocktail of metals in presence of NTA (blue dots). Total concentrations are reported in Table 3.1 column 2 and column 1 respectively.

Panel B As in panel A for the Co transport in the same solutions

Panel C: As in panel A replacing Cd with Pb.

Figure 3.4, panel A reports in orange squares a plot of the normalized accumulation of Cd in the acceptor cell vs time when the donor solution contains Cd together with a cocktail of metal ions in absence of ligands (orange squares). In blue dots, a donor solution which contains the same mixture of metal ions but in presence of NTA. According to VMINTEQ in the first case the speciation of Cd in solution corresponding to orange squares mainly corresponded to the free metal ion. Whereas in the second case corresponding to the blue circles, the speciation of Cd according to VMINTEQ was shared between the free Cd (55%) and CdNTA(45%). As seen in the Figure 3.4, the accumulation in the acceptor cell when the donor contains the mixture tends to decrease with respect to the accumulation when there is only free Cd in the donor solution. This trend suggests a smaller diffusion coefficient of CdNTA than that of Cd.

Figure 3.4, panel B, shows more clearly that the slope of the accumulation in the acceptor cell decreases when there is a 76% of the total Co as Co-NTA and a 24% of free Co (according to VMINTEQ) in the donor solution with respect to the accumulation when the donor solution only contains free Co. A quantitative analysis of this effect allows to compute the ratio between the diffusion coefficient of the complex and the free metal ion for the case of CoNTA (ε_{CoNTA}=0.65). The calculation of D_{ML} (therefore, ε) is straightforward from the slope of the linear accumulation in the acceptor cell vs time, when EqAcctotM (3.6) is considered. Since EqAcctotM (3.6) includes two unknowns, D_M and D_{ML}, two independent experiments involving different concentrations of free metal and/or ligand are required, as explained in

section “Measurement of diffusion coefficients of metal complexes from a mixture of metals in excess of ligand conditions”. When in one experiment only the free metal is relevant (as it is the case of column 2 in Table 3.1 where there is no ligand in the solution) the determination of D_M is independent of that of D_{ML}. Then, and a second experiment, with concentrations selected so that the presence of CoNTA is high enough that the diffusion of the complex has an important impact on the accumulation in the acceptor cell (e. g., column 1 in Table 3.1) can be used to obtain D_{ML}. In both experiments, the slope of the linear regression of the accumulation in the acceptor cell vs time allow the calculation of the diffusion coefficient whenever the equilibrium concentrations in the donor solution (c_M^* and c_{ML}^*) are provided by VMINTEQ .

In Figure 3.4 panel C, we can observe that for the case of Pb, where the 97% of Pb is complexed, the accumulation of the mixture has a much smaller slope than the accumulation of the free metal ion. Thus proving that the complex diffuses at slower rate than the free metal ion. Notice that, in this case, there is no need to use Eq (3.6) . Instead, Eq (3.2) can be used because the concentration of PbNTA is close to 100% and in consequence the diffusive flux corresponds to this species. The result for D_{PbNTA} is reported in Table 3.4.

Let us now consider the accumulation of Ni in the acceptor solution in 3 independent experiments with increasing NTA concentration in the donor solution. In presence of NTA, Ni can yield to free Ni, NiNTA and $Ni(NTA)_2$.

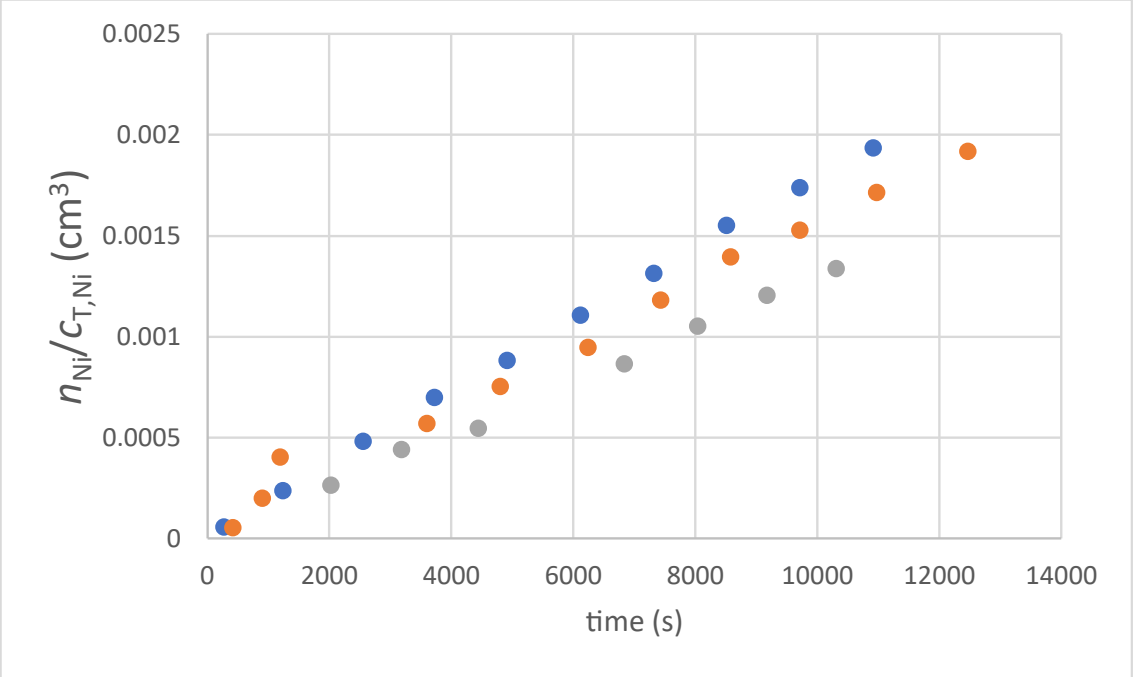

Figure 3.5 Normalized accumulation with $c_{T,Ni}$ in the acceptor cell of 3 independent experiments. In blue dots is represented a case which the donor solution contained only Ni which experimental conditions are in Table 3.1 column 7. In Orange dots is represented a case which the donor solution contained Ni in presence of NTA which $c_{T,Ni}$, $c_{T,NTA}$ and other experimental parameters are given in Table 3.1 column 6. In gray dots the donor solution contained Ni in presence of NTA which $c_{T,NTA}$ and pH were higher than the prior cases, see Table 3.1 column 5.

In Figure 3.5, we gather the results of 3 independent experiments with increasing concentrations of total NTA in the donor solution. The blue dots represent an experiment with a donor solution containing only Ni whose speciation results indicate that almost all the Ni is present as free metal ion. The orange dots represent a case for a donor solution containing Ni +NTA with total concentrations specified at column 6 of Table 3.1. According to VMINTEQ, the addition of NTA in the solution implies a change in the speciation where 97% of Ni becomes complexed as NiNTA. Grey dots correspond to a donor solution containing Ni+NTA, where $c_{T,NTA}$ and pH have increased respect to the orange markers, with concentrations specified in column 5 of Table 3.1

The speciation results show that eventhough the $c_{T,NTA}$ increases from 0.05 to $1x10^{-1}$ mol m^{-3}, the concentration of $NiNTA_2$ would not increase from a 3% to a 30% unless the pH of the solution had been changed from 7.6 to 8.8. Because, $c_{NTA}{}^{-3}$ is buffered by the protonation reaction, at pH=7.6, a great percentage of NTA is still protonated. Thus, at pH=7.6 there is not enough $c_{NTA}{}^{-3}$ to achieve a great percentage of $NiNTA_2$ in the solution and pH needs to be increased to 8.8 to increase the NTA^{-3} available for a consecutive Ni complexation.

Going back to Figure 3.5 , the difference between slopes (orange and gray dots) show that the complex formed from the second successive complexation reaction ($Ni(NTA)_2(H2O)_4$) has a smaller diffusion coefficient than the complex produced in the first complexation reaction $NiNTA(H2O)_5$ as suggested by a decrease of the slope of the gray dots compared to the orange ones. However the difference is small because $Ni(NTA)_2$ contain only 30% of the total Ni while NiNTA is still the main species with a 70% of $c_{T,Ni}$. The application of Eqs ((3.6) -(3.8) yields to D_{NiNTA2}=1.38x10^{-10} m^2/s (see Table 3.4) which has strongly decreased in comparison to D_{NiNTA} = 3.78 x10^{-10} m^2/s.

To sum up, this methodology offers a new way to measure diffusion coeficients in thin gels such as APA gel with the diffusion cell. A task that is difficult to achieve from accumulation experiment in DGT devices, because the dissociation of complexes is coupled to the diffusion process for partially labile complexes. In consequence when performing these measurements with DGT there can be an understimation of the diffusion coeficient of the complex in the case that there is not a correct assesment of the lability of the complex.

Table 3.4 Values reported for the diffusion coefficients of metal complexes obtained applying the methodology described, as well as, the values for ε and speciation of metal complexes.The values employed of δ^{g} =6.29x10^{-4}(m) and δ^{DBL}=.7.09x10^{-5} m. The diffusion coefficients of the free metals used for calculating ε and D_{ML} (When necessary) are: D_{Co}= 5.94x10^{-10}m^2 s^{-1}and D_{Cd} =6.09x10^{-10}m^2 s^{-1}, D_{Pb}=7.07x10^{-10} m^2 s^{-1},D_{Ni}=4.34x10^{-10} m^2 s^{-1}, D_{Cu}=6.23x10^{-10} m^2 s^{-1}, D_{Zn}=6.08 x10^{-10} m^2 s^{-1}.

Exp	D (Experimental) m^2 s^{-1}	ε (Experimental)	Speciation (Experiment)	D m^2 s^{-1} (Literature)	ε (literature)
CuNTA	4.36x10^{-10}	0.70	99.3 %	5.37x10^{-10}	0.86
PbNTA	4.53x10^{-10}	0.64	97%	5.95x10^{-10}	0.74
CoNTA	4.09x10^{-10}	0.69	76.3 %	-	-
NiNTA	3.78x10^{-10}	0.87	97.7 %	4.75x10^{-10}	0.82
NiNTA$_2$	1.38x10^{-10}	0.40	30%	-	-
ZnNTA	6.14x10^{-10}	1.00	82.95 %	-	-
CdNTA	4.15x10^{-10}	0.68	45%	3.99x10^{-10} at 22°C	0.65

3.6 Determination of diffusion coefficients from a finite volume regime

3.6.1 Physical details about the finite volume regime

We have done a set of experiments out of the linear regime in the diffusion cell and different stirring rates (140 and 400 rpm) (see Table 3.1, columns 3,4) to show that at a certain point in time the diffusion gradient decreases because the concentration in the acceptor cell after some accumulation time is comparable to the concentration in the donor cell.

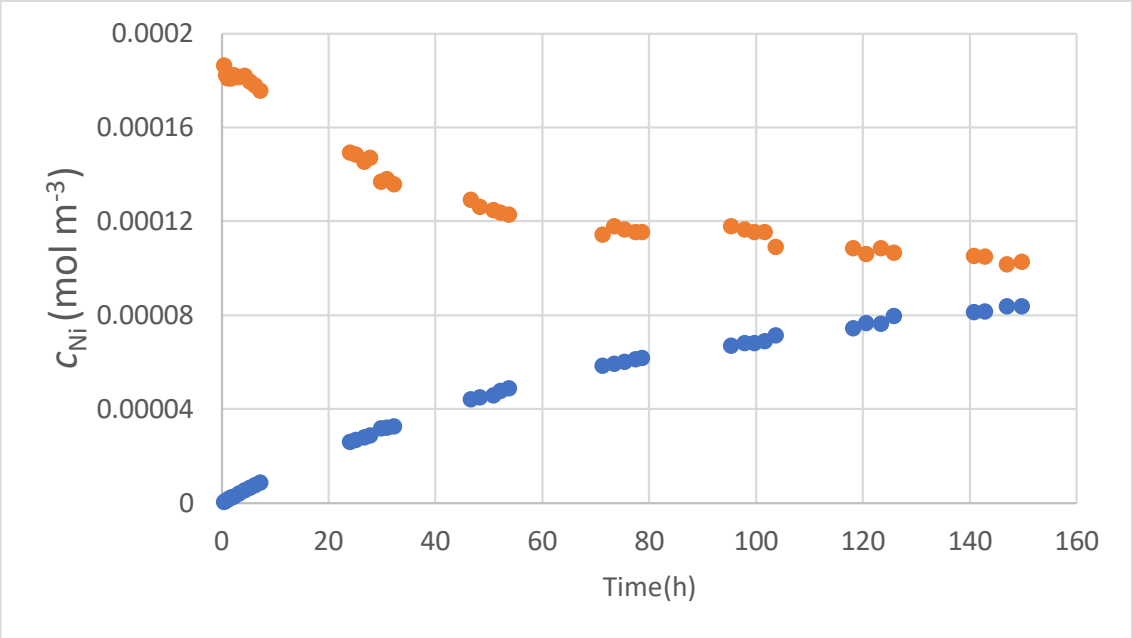

Figure 3.6 Evolution of the Ni concentration in the donor cell (orange dots) and acceptor cell (blue dots) for a stirring rate of 140 rpm.

Figure 3.6 shows that the metal concentration in the acceptor cell is linear in a short period of time (close to 10 hours) when the decrease of c_{Ni} in the donor cell is negligible compared to the concentration in the acceptor cell. After that period of time, the accumulation in the acceptor cell is no longer linear because the mass transfer by diffusion is slowed down due to a lower diffusion gradient. Nearby to the end of the experiment, after 138.9 h, as it can be observed the concentration in acceptor and the donor cell are almost constant in time indicating that the system is close to reach the equilibrium.

A numerical simulation of the concentration profiles, to show the change of diffusion gradient over time has been done with a MATLAB built-in subroutine (ODE-15s) to integrate the diffusion partial differential equation with the boundary conditions of the diffusion cell.

The idea is to simulate and reproduce the change in concentration (in the donor and acceptor cell) that occur in the experiment shown in Figure 3.6.

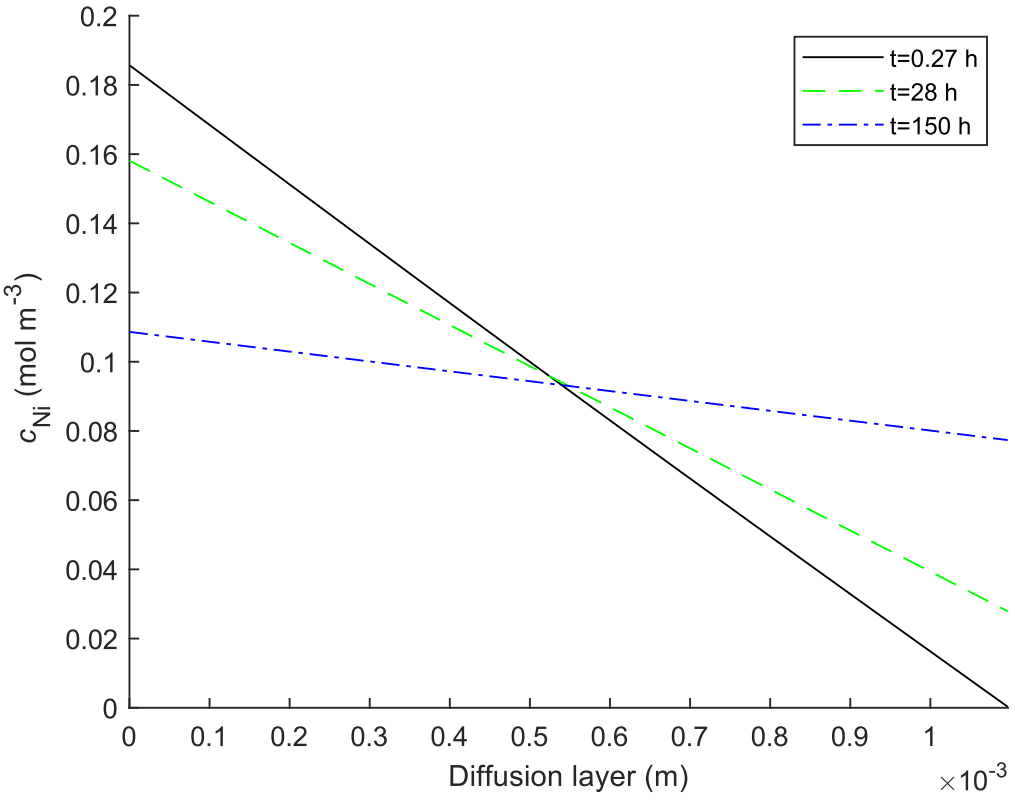

Figure 3.7 Shows the concentration profile of Ni along the diffusion layer (Δg +2 ΔDBL) at 3 different times 0.27 h (black line), 28h (green dashed line) and 150h (green dashed and dotted line) using the following parameters :Δg=6.29x10^{-4} m, ΔDBL=2.34x10^{-4} m, D_{Ni} =5.77x10^{-10} m^2 s^{-1}, V_A=V_D=1x10^{-4} m^3, c^*_{Ni} =0.186 mol m^{-3},t=5400000s .

Figure 3.7 displays the Ni concentration profile along the gel that connects both compartments of the diffusion cell in the experiment described in column 4 of Table 3.1 for 3 different times (0.27 h, 28h and 150h). In Figure 3.7, the concentration at the donor cell is depicted at x=0.Whereas, the concentration in the acceptor cell is depicted in the rightmost part of Figure 3.7, when x=1.097x10^{-3} m. The decrease of the concentration along the gel layer indicates the arising of a diffusive flux between both compartments that is independent of de x-plane considered since the profile is linear. As time goes on, Figure 3.7 indicates that the gradient decreases since the slope of the linear concentration profile decreases. The black line corresponds the concentration profile related to a quasi steady-state when 0.27h have passed. In this case, the concentration in the donor solution $c_{D,Ni}$ (at x=0) (see black line) is equal to c^*_{Ni} and the concentration in the acceptor cell is negligible. This quasi steady-state

lasts less than 7 hours (what is called the linear regime, see Figure 3.6), more or less when the concentration in the acceptor cell would reach a value close to 0.01 mol m^{-3}. At 28 hours, the diffusion gradient decreases which can be observed by a decrease in the slope of the straight line respect the to the simulation at t=0.27 h. Thus the accumulation in the acceptor cell vs time has already become non-linear (see Figure 3.6). At 150 h, the diffusion gradient is so small that the amount of mass that comes from diffusion tends to 0 and thus in the experiment (see Figure 3.6) the concentration in the acceptor cell vs time is almost constant (from 138h to 150h).

3.6.2 Determination of diffusion coefficients for trace-metals with natural abundance

The natural abundance of some trace-metal elements (e.g Zn) challenges the measurement of physicochemical parameters (e.g D_{Zn}), because the amount of metal measured in the acceptor cell at short times (3h) is of the same order as the amount of metal present in the blanks. One way to solve this problem is to perform an experiment in a larger period of time. In the case that the period of time is large enough and the donor concentration is not high enough to consider the acceptor concentration negligible, the accumulation with time will become non-linear due to finite volume effects. In such conditions, it is possible to use our model developed at section "Calculation of diffusion coefficients when a finite volume regime applies" in order to determine the diffusion coefficient of such trace-metal elements.
To verify this behaviour, let us compare the evolution of the concentration in the acceptor cell in the linear regime with the finite volume regime.

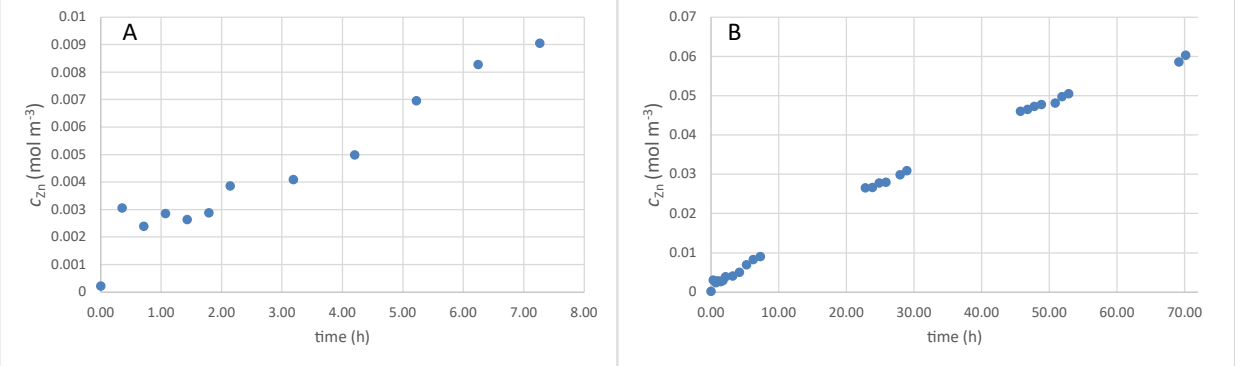

Figure 3.8 Comparison of the evolution of Zinc concentration in the acceptor cell in the linear regime (panel A) with the finite volume regime (panel B).

Figure 3.8, panel A shows that during the linear regime when 3 hours of experiment have been reached is not possible to determine D_{Zn}, because the background concentration of Zn in the acceptor cell is higher than the concentration of zinc produced by the mass accumulated

by transport by diffusion of zinc ions. It is true that this behaviour is no longer observed from 3h to 7.5 h and during this time-span a linear fitting of the data can be done to determine D_{Zn}.. Nonetheless, it may also happen that in experiments with lower initial donor concentrations this linear regime may not be observed. Moreover our model grants access to a set of data points that were not able to be interpreted using the linear model.

In order to extract information about the diffusion coefficient in this finite volume regime, we can linearize the experimental data from the acceptor cell by applying two operations, which consist on subtracting $\frac{c_{Zn}(V_A+V_D)}{V_D} = 2c_{Zn}$ (when $V_A = V_D$) to c^*_{Zn} in the acceptor cell and to apply natural logarithm. These operations are reflected on the linearization process of Eq (3.15) .After that, we get:

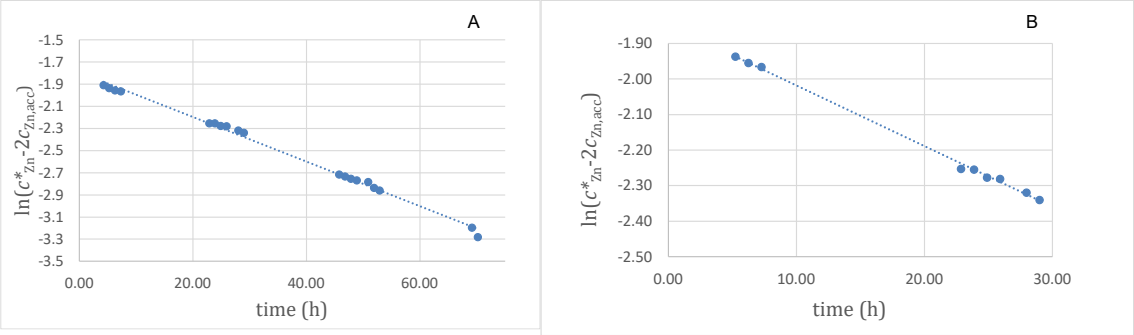

Figure 3.9 Linearized experimental data of the Zn concentration in the acceptor cell vs time for a stirring rate of 400 rpm (until 80h) (Panel A) and using the same experimental data, it is linearized until 30h of accumulation in the acceptor cell (Panel B)

The comparison of panel A and panel B in Figure 3.9 is done with the purpose to show that the fitting of the diffusion coefficient using data at very long times can lead to overestimated result. One reason might be that the experimental data is not accurate enough at very long times, because the gel layer might suffer some damage from the vibration that is created caused by the stirring motion. Another reason is that towards to the end of the experiment, the acceptor concentration tends to a value that is half of the donor concentration, but the measured concentration in the acceptor cell may oscillate around that value or even be a bit greater than that concentration.

For the reasons above, using the slope of the linear regression of the data displayed in Figure 3.9 Panel B (using seconds instead of hours), the calculation of D_{Zn} is straightforward using Eq(3.17) (This calculation has also been performed for the elements Ni, Cd and Pb). From

experimental data obtained at 400 rpm and 140 rpm (see Table 3.1, columns 3 and 4 respectively), we obtain the following diffusion coefficients:

Table 3.5 Diffusion coefficients values obtained through a fitting of the experimental data of 400 rpm and 140 rpm using Eq(3.17) in a finite volume regime. Parameters used: δ^{g} =6.29x10^{4}(m), δ^{DBL} =7.09 x10^{5} (m), A=3.14x10^{-4} m^{2}.

Frequency (rpm)	D (m^2/s) (140 rpm)	D (m^2/s) (400 rpm)
Ni	4.53x10^{-10}	5.05x10^{-10}
Pb	7.50x10^{-10}	8.90x10^{-10}
Cd	4.75x10^{-10}	5.51x10^{-10}
Zn	4.42x10^{-10}	5.82x10^{-10}

The diffusion coefficients obtained in Table 3.5 show a good agreement with the results obtained in the linear regime (see Table 3.2). Therefore, this methodology can be considered adequate to determine diffusion coefficients in particular cases when the linear regime is not able to provide a good estimation. For example, when there is a natural abundance of a trace-metal ion.

3.7 References

1. Buffle, J., Introduction. In *Complexations reactions in aquatic systems: An analytical approach*, Ellis Horwood Limited: 1988; pp 1-11.
2. Degryse, F.; Smolders, E., DGT and bioavailability. In *Diffusive Gradients in Thin-Films for environmental measurements*, Davison, W., Ed. Cambridge University Press: Cambridge, 2016; pp 216-262.
3. van Leeuwen, H. P.; Town, R. M.; Buffle, J.; Cleven, R.; Davison, W.; Puy, J.; van Riemsdijk, W. H.; Sigg, L., Dynamic speciation analysis and bioavailability of metals in Aquatic Systems. *Environmental Science and Technology* **2005,** *39*, 8545-8585.
4. Unsworth, E. R.; Warnken, K. W.; Zhang, H.; Davison, W.; Black, F.; Buffle, J.; Cao, J.; Cleven, R.; Galceran, J.; Gunkel, P.; Kalis, E.; Kistler, D.; van Leeuwen, H. P.; Martin, M.; Noel, S.; Nur, Y.; Odzak, N.; Puy, J.; van Riemsdijk, W. H.; Sigg, L.; Temminghoff, E.; Tercier-Waeber, M. L.; Toepperwien, S.; Town, R. M.; Weng, L. P.; Xue, H. B., Model predictions of metal speciation in freshwaters compared to measurements by in situ techniques. *Environmental Science and Technology* **2006,** *40* (6), 1942-1949.
5. Shiva, A. H.; Teasdale, P. R.; Bennett, W. W.; Welsh, D. T., A systematic determination of diffusion coefficients of trace elements in open and restricted diffusive layers used by the diffusive gradients in a thin film technique. *Analytica Chimica Acta* **2015,** *888*, 146-154.
6. Scally, S.; Davison, W.; Zhang, H., Diffusion coefficients of metals and metal complexes in hydrogels used in diffusive gradients in thin films. *Analytica Chimica Acta* **2006,** *558* (1-2), 222-229.
7. Garmo, O. A.; Royset, O.; Steinnes, E.; Flaten, T. P., Performance study of diffusive gradients in thin films for 55 elements. *Analytical Chemistry* **2003,** *75* (14), 3573-3580.
8. Unsworth, E. R.; Zhang, H.; Davison, W., Use of diffusive gradients in thin films to measure cadmium speciation in solutions with synthetic and natural ligands: Comparison with model predictions. *Environmental Science and Technology* **2005,** *39* (2), 624-630.
9. Warnken, K. W.; Zhang, H.; Davison, W., Accuracy of the diffusive gradients in thin-films technique: Diffusive boundary layer and effective sampling area considerations. *Analytical Chemistry* **2006,** *78* (11), 3780-3787.
10. Serrano, N.; Díaz-Cruz, J. M.; Ariño, C.; Esteban, M.; Puy, J.; Companys, E.; Galceran, J.; Cecilia, J., Full-wave analysis of stripping chronopotentiograms at scanned deposition potential (SSCP) as a tool for heavy metal speciation: Theoretical development and application to Cd(II)-phthalate and Cd(II)-iodide systems. *JOURNAL OF ELECTROANALYTICAL CHEMISTRY* **2007,** *600*, 275-284.

3.8 Supporting information of: Determination of diffusion coefficients of complexes and free metal ions in gel layers from diffusion cell experiments.

3.8.1 Steady-state model of the processes in a diffusion cell for a system with a metal in presence of a ligand which endures *n* sequential complexation reactions.

Let us consider that we have in the donor compartment of a diffusion cell device (see Figure 3.2 of the main text) a system where a free metal (M) endures *n* complexations reactions with a Ligand (L) :

$$\mathrm{M+L} \underset{k_\mathrm{d}}{\overset{k_\mathrm{a}}{\rightleftarrows}} \mathrm{ML+L} \underset{k_\mathrm{d}}{\overset{k_\mathrm{a}}{\rightleftarrows}} \mathrm{ML_2} \ \ldots\ \mathrm{ML}_{i-1}\mathrm{+L} \underset{k_\mathrm{d}}{\overset{k_\mathrm{a}}{\rightleftarrows}} \mathrm{ML}_i\mathrm{+L} \underset{k_\mathrm{d}}{\overset{k_\mathrm{a}}{\rightleftarrows}} \mathrm{ML}_{i+1} \ \ldots\ \mathrm{ML}_{n-1}\mathrm{+L} \underset{k_\mathrm{d}}{\overset{k_\mathrm{a}}{\rightleftarrows}} \mathrm{ML}_i$$

Assuming that each species has a common diffusion coefficient in the DBL and the diffusive gel layer, the transport of the species to the acceptor cell in steady-state conditions is described by:

$$0 = D_\mathrm{M} \frac{\partial^2 c_\mathrm{M}}{\partial x^2} - k_\mathrm{a} c_\mathrm{M} c_\mathrm{L} + k_\mathrm{d} c_\mathrm{ML}$$

$$0 = D_\mathrm{ML} \frac{\partial^2 c_\mathrm{ML}}{\partial x^2} + k_\mathrm{a} c_\mathrm{M} c_\mathrm{L} - k_\mathrm{d} c_\mathrm{ML} - k_{\mathrm{a}2} c_\mathrm{ML} c_\mathrm{L} + k_{\mathrm{d}2} c_{\mathrm{ML}_2}$$

...

$$0 = D_{\mathrm{ML}_i} \frac{\partial^2 c_{\mathrm{ML}_i}}{\partial x^2} + k_\mathrm{a} c_{\mathrm{ML}_{i-1}} c_\mathrm{L} - k_\mathrm{d} c_{\mathrm{ML}_i} - k_\mathrm{a} c_{\mathrm{ML}_i} c_\mathrm{L} + k_\mathrm{d} c_{\mathrm{ML}_{i+1}} \qquad \text{(S3.1)}$$

...

$$0 = D_{\mathrm{ML}_{n-1}} \frac{\partial^2 c_{\mathrm{ML}_{n-1}}}{\partial x^2} + k_\mathrm{a} c_{\mathrm{ML}_{n-2}} c_\mathrm{L} - k_\mathrm{d} c_{\mathrm{ML}_{n-1}} - k_\mathrm{a} c_{\mathrm{ML}_{n-1}} c_\mathrm{L} + k_\mathrm{d} c_{\mathrm{ML}_n}$$

$$0 = D_{\mathrm{ML}_n} \frac{\partial^2 c_{\mathrm{ML}_n}}{\partial x^2} + k_\mathrm{a} c_{\mathrm{ML}_{n-1}} c_\mathrm{L} - k_\mathrm{d} c_{\mathrm{ML}_n}$$

The boundary conditions of the system can be written as:

$$c_i\big|_{x=\delta^\mathrm{g}+2\delta^\mathrm{DBL}} = c_i^* \qquad \text{(S3.2)}$$

$$c_i\big|_{x=0} = 0 \qquad \text{(S3.3)}$$

where *i* refers to each species in the donor solution and $\delta^\mathrm{g} + 2\delta^\mathrm{DBL}$ is the whole thickness of the gel that connects both compartments and the diffusion boundary layers at each side of the gel. The donor side corresponds to *x*=0 while the acceptor side to $x = \delta^\mathrm{g} + 2\delta^\mathrm{DBL}$

SI Chapter 3.Determination of diffusion coefficients with diffusive cell device

The sum of the system of ordinary differential equations defined in Eq (S3.1) becomes:

$$0 = D_{\mathrm{M}} \frac{\partial^2 c_{\mathrm{M}}}{\partial x^2} + \sum_{i=1}^{n} D_{\mathrm{ML}_i} \frac{\partial^2 c_{\mathrm{ML}_i}}{\partial x^2} \tag{S3.4}$$

Eq (S3.4) can be written as:

$$0 = \frac{d^2}{dx^2}\left(D_{\mathrm{M}} c_{\mathrm{M}} + \sum_{i=1}^{n} D_{\mathrm{ML}_i} c_{\mathrm{ML}_i} \right) \tag{S3.5}$$

By integration of the Eq (S3.5), the general solution of the differential equation can be written as:

$$Ax + B = \left(D_{\mathrm{M}} c_{\mathrm{M}} + \sum_{i=1}^{n} D_{\mathrm{ML}_i} c_{\mathrm{ML}_i} \right) \tag{S3.6}$$

where A and B are integration constants.
Applying the boundary conditions Eq(S3.2) and Eq(S3.3) in Eq (S3.6) a solution for the integration constants A and B is obtained:

$$A = \frac{D_{\mathrm{M}} c_{\mathrm{M}}^{*} + \sum_{i=1}^{n} D_{\mathrm{ML}_i} c_{\mathrm{ML}_i}^{*}}{\delta^{\mathrm{g}} + 2\delta^{\mathrm{DBL}}} \tag{S3.7}$$

$$B = 0 \tag{S3.8}$$

Thus, the total flux of metal in steady-state conditions at x=0 (acceptor cell) defined as

$$J_{\mathrm{M}} = \left[\frac{d}{dx}\left(D_{\mathrm{M}} c_{\mathrm{M}} + \sum_{i=1}^{n} D_{\mathrm{ML}_i} c_{\mathrm{ML}_i} \right) \right]_{x=0} \tag{S3.9}$$

is given by :

$$J_{\mathrm{M}} = \frac{D_{\mathrm{M}} c_{\mathrm{M}}^{*} + \sum_{i=1}^{n} D_{\mathrm{ML}_i} c_{\mathrm{ML}_i}^{*}}{\delta^{\mathrm{g}} + 2\delta^{\mathrm{DBL}}} \tag{S3.10}$$

Which indicates that the total flux of M from the donor to the acceptor solution is just the addition of the flux of each metal species independently of the chemical reactions between them.

3.8.2 Numerical program build with MATLAB to solve the partial differential equation by using the method of lines (MOL): modelling the evolution of concentrations in the diffusion cell when finite volume effects of the compartments are non-negligible

The program considers a simple system with only free metal in the donor solution of the diffusion cell. Thus, the transport equation is:.

$$\frac{\partial c_{\mathrm{M}}}{\partial t} = \left\{ \begin{array}{c} D_{\mathrm{M}}^{\mathrm{g}} \\ D_{\mathrm{M}}^{\mathrm{DBL}} \end{array} \right\} \frac{\partial^2 c_{\mathrm{M}}}{\partial x^2} \tag{S3.11}$$

Where $D_{\mathrm{M}}^{\mathrm{g}}$ and $D_{\mathrm{M}}^{\mathrm{DBL}}$ are the diffusion coefficients of the free metal ion at the diffusive gel and the DBL respectively.

The initial and boundary conditions are:

$$c_{\mathrm{M}}(t=0, x=\delta^{\mathrm{g}}+2\delta^{\mathrm{DBL}}) = c_{\mathrm{M}}^{*} \tag{S3.12}$$

$$c_{\mathrm{M}}(t=0, 0<x<\delta^{\mathrm{g}}+2\delta^{\mathrm{DBL}}) = 0 \tag{S3.13}$$

$$c_{\mathrm{M}}(t, x=0) = \frac{A}{V_{\mathrm{A}}}\int_0^t J dt \tag{S3.14}$$

$$c_{\mathrm{M}}(t, x=\delta^{\mathrm{g}}+2\delta^{\mathrm{DBL}}) = c_{\mathrm{M}}^{*} - \frac{A}{V_{\mathrm{A}}}\int_0^t J dt \tag{S3.15}$$

The spatial domain is discretized by N_{DBL1}, N_{DBL2} and N_{G} points resulting in step intervals for each domain given by:

$$\Delta\mathrm{DBL}_1 = \frac{\delta^{\mathrm{DBL}}}{N_{\mathrm{DBL}_1}} \tag{S3.16}$$

$$\Delta\mathrm{g} = \frac{\delta^{\mathrm{g}}}{N_{\mathrm{G}}} \tag{S3.17}$$

$$\Delta\mathrm{DBL}_2 = \frac{\delta^{\mathrm{DBL}}}{N_{\mathrm{DBL}_2}} \tag{S3.18}$$

The method of lines is based on discretising the spatial variable of a PDE to transform the spatial derivatives in an algebraic approximation 1. Once this operation is done, the spatial

variable of the PDE is not stated explicitly. Applying a finite differences scheme in the spatial derivative, Eq(S3.11) within the MOL framework becomes :

$$\frac{\partial c_{\mathrm{M},i}}{\partial t} = \left\{ \begin{array}{c} D_{\mathrm{M}}^{\mathrm{g}} \\ D_{\mathrm{M}}^{\mathrm{DBL}} \end{array} \right\} \frac{c_{\mathrm{M},i-1} - 2c_{\mathrm{M},i} + c_{\mathrm{M},i+1}}{\Delta x^2} \tag{S3.19}$$

which can be solved applying an ODE integrator.

The MATLAB subroutine ODE-15S uses a variable order method to integrate the algebraic system of equations. It requires the time points at which the PDE needs to be solved, as well as the initial conditions that have been specified in Eq (S3.12) and Eq (S3.13).

The vector of solutions, when ODE-15s is employed, is defined as:

$$c_{\mathrm{M,sol}}[t, c_{\mathrm{M}}] = ode15s(@\,\mathrm{algdiffcell}, tspan, \mathrm{initial\ conditions}) \tag{S3.20}$$

Where @algdiffcell is the subroutine needed to specify the spatial discretization at each point of the domain and *tspan* refers to the time points at which we want to know our solution.

Now, we are going to specify the equations required in the subroutine @algdiffcell in relation to the discretization applied in each region:

In the first and last point of the domain :

$$\frac{\partial c_{\mathrm{M},1}}{\partial t} = \frac{A}{V} \frac{D_{\mathrm{M}}^{\mathrm{DBL}} \left(c_{\mathrm{M},1} - c_{\mathrm{M},2} \right)}{\Delta \mathrm{DBL}_1} \tag{S3.21}$$

$$\frac{\partial c_{\mathrm{M},1}}{\partial t} = \frac{A}{V} \frac{D_{\mathrm{M}}^{\mathrm{DBL}} \left(c_{\mathrm{M},Nfin-1} - c_{\mathrm{M},Nfin} \right)}{\Delta \mathrm{DBL}_2} \tag{S3.22}$$

Where Eq(S3.21) has negative sign in the first point of the domain and positive sign in the last point of the domain (N_{fin}=N_{DBL1}+N_{G}+N_{DBL2}).

In the region DBL1:

$$\frac{\partial c_{\mathrm{M},i}}{\partial t} = \frac{D_{\mathrm{M}}^{\mathrm{DBL}}}{\Delta \mathrm{DBL}_1^{\,2}} \left(c_{\mathrm{M},i-1} - 2c_{\mathrm{M},i} + c_{\mathrm{M},i+1} \right) \tag{S3.23}$$

In the gel domain:

$$\frac{\partial c_{\mathrm{M},i}}{\partial t} = \frac{D_{\mathrm{M}}^{\mathrm{g}}}{\Delta \mathrm{g}_1^{\,2}} \left(c_{\mathrm{M},i-1} - 2c_{\mathrm{M},i} + c_{\mathrm{M},i+1} \right) \tag{S3.24}$$

In the second DBL domain:

$$\frac{\partial c_{\mathrm{M},i}}{\partial t} = \frac{D_{\mathrm{M}}^{\mathrm{DBL}}}{\Delta \mathrm{DBL}_2^{2}} \left(c_{\mathrm{M},i-1} - 2c_{\mathrm{M},i} + c_{\mathrm{M},i+1} \right) \tag{S3.25}$$

At the interface between the DBL and the gel layer, the continuity of the flux has to be taken into account. Thus the following equalities need to be considered,

$$\frac{D_{\mathrm{M}}^{\mathrm{DBL}}}{\Delta \mathrm{DBL}_1}\left(c_{\mathrm{M},i-1}-c_{\mathrm{M},i}\right)=\frac{D_{\mathrm{M}}}{\Delta g}\left(c_{\mathrm{M},i+1}-c_{\mathrm{M},i}\right) \tag{S3.26}$$

$$\frac{D_{\mathrm{M}}}{\Delta g}\left(c_{\mathrm{M},i\text{-}1}-c_{\mathrm{M},i}\right)=\frac{D_{\mathrm{M}}^{\mathrm{DBL}}}{\Delta \mathrm{DBL}_2}\left(c_{\mathrm{M},i+1}-c_{\mathrm{M},i}\right) \tag{S3.27}$$

Using Eq (S3.26) to replace $c_{\mathrm{M,i+1}}$ in Eq (S3.23):

$$\frac{\partial c_{\mathrm{M},N_{\mathrm{DBL2}}+N_{\mathrm{G}}}}{\partial t}=\frac{2D_{\mathrm{M}}^{\mathrm{DBL}}}{\Delta \mathrm{DBL}_1\left(\Delta \mathrm{g}+\Delta \mathrm{DBL}_1\right)}\left(c_{\mathrm{M},N_{\mathrm{DBL2}}+N_{\mathrm{G}}+1}-c_{\mathrm{M},N_{\mathrm{DBL2}}+N_{\mathrm{G}}}\right)-\frac{2D_{\mathrm{M}}^{\mathrm{g}}}{\Delta \mathrm{g}\left(\Delta \mathrm{g}+\Delta \mathrm{DBL}_1\right)}\left(c_{\mathrm{M},N_{\mathrm{G}}+N_{\mathrm{DBL}_1}}-c_{\mathrm{M},N_{\mathrm{G}}+N_{\mathrm{DBL}_1}-1}\right) \tag{S3.28}$$

The same procedure has to be followed at the other interface but in this case, the substitution of $c_{\mathrm{M,i+1}}$ has to be done in Eq (S3.24) using the flux equality from Eq(S3.27) [2]. This leads to the following expression:

$$\frac{\partial c_{\mathrm{M},N_{\mathrm{DBL2}}+N_{\mathrm{G}}}}{\partial t}=\frac{2D_{\mathrm{M}}^{\mathrm{g}}}{\Delta \mathrm{g}\left(\Delta \mathrm{g}+\Delta \mathrm{DBL}_2\right)}\left(c_{\mathrm{M},N_{\mathrm{DBL}_2}}-c_{\mathrm{M},N_{\mathrm{DBL}_2}+1}\right)-\frac{2D_{\mathrm{M}}^{\mathrm{DBL}}}{\Delta \mathrm{DBL}_2\left(\Delta \mathrm{g}+\Delta \mathrm{DBL}_2\right)}\left(c_{\mathrm{M},N_{\mathrm{DBL}_2}}-c_{\mathrm{M},N_{\mathrm{DBL}_2}-1}\right) \tag{S3.29}$$

Notice that ODE15-S only requires information about the discretization of the spatial variable at every point of the domain.

3.8.3 References

1. Samir , H. e. a., Method of lines. *Scholarpedia* **2007,** *2(7)*.
2. Crank, J., *The Mathematics of Diffusion*. 2nd ed.; Clarendon Press: Oxford, UK, 1975.

4 Availability of metals to DGT devices with different configurations. The case of sequential Ni complexation.

Jordi Sans-Duñó[a], Joan Cecilia[b], Josep Galceran[a], Jaume Puy[a]*

[a]*Departament de Química,* [b]*Departament de Matemàtica, Universitat de Lleida and AGROTECNIO-CERCA, Rovira Roure 191, 25198, Lleida, Spain*

* Corresponding author. E-mail address: jpuy@quimica.udl.cat, Phone 34 973 702529, Fax 34 973 702924

This chapter has been published in STOTEN:
https://doi.org/10.1016/j.scitotenv.2021.146277

Chapter 4. Availability of metals to DGT devices with different configurations. The case of sequential Ni complexation.

4.1 ABSTRACT

The analytical technique DGT (Diffusive Gradients in Thin films) is able to gain access to a wealth of information by carefully interpreting accumulation data from passive samplers with different configurations (i.e. different thicknesses of its constituent layers). A set of DGT devices were simultaneously deployed in solutions of Ni and nitrilotriacetic acid (NTA) of different concentrations to measure the availability of Ni in these solutions. Accumulations indicate that the availability of Ni depends on both the thickness of the resin and the thickness of the diffusive gel. In both cases, the lability degree increases as the thickness increases. As the formation of successive complexes (such as $Ni(NTA)_2$) proceeds, the availability of the metal decreases, which is quantitatively explained by reducing the formulation to a case with only one complex, but with an effective dissociation rate constant that decreases as the concentration of NTA increases. Simple analytical expressions are reported to quantify the lability degree in the different DGT configurations. These results indicate that a set of different DGT devices can characterize the availability of a cation in a natural sample with uptake processes at different spatial or time scales. Alternatively, and from a more fundamental point of view, information on speciation, mobilities and labilities of the species present in natural samples can be obtained with a set of DGT configurations.

Keywords: DGT, lability degree, stoichiometry effects, thickness of diffusion, thickness of resin, NiNTA

4.2 Highlights

- Independent information is easily obtained with DGT devices with different thicknesses
- Lability increases as the diffusive gel or the resin thickness increase
- Simple expressions quantify the influence of the thickness on the availability
- The formation of successive complexes reduces their availability
- Speciation, mobilities and labilities of a mixture can be solved with a set of DGT data

4.3 INTRODUCTION

Despite many efforts, the measurement of trace metal speciation in freshwaters is still challenging. Different types of analytical techniques have been developed to gain insight into the equilibrium and dynamic speciation of natural waters. Some of them are based on quantifying the concentration of the free ion in solution, such as Ion selective electrodes, Absence of Gradients and Nernstian Equilibrium Stripping (AGNES) or the Donnan Membrane Technique (DMT) [1-5]. Alternatively, other techniques provide a quantification of a labile fraction, which includes the contribution of the free ion plus an extra contribution of some complexes. For example, the Gel Integrated Microelectrodes (GIME) were designed [6] to provide *in situ* measurements of some labile fraction of metal compounds able to dissociate in a well-defined diffusion layer. Anodic stripping voltammetry (ASV) and other stripping voltammetric techniques can also measure a labile fraction dependent on the electrode size [7-8]. Permeation Liquid Membrane (PLM) and Polymer Inclusion Membrane (PIM) also determine a labile fraction, but they can be tuned to reduce this fraction up to the concentration of the free ion [9-11].

It has been shown that the span of dynamic analytical techniques provides complementary data as a consequence of the spatio-temporal scale of the measurement process involved in each technique [12]. These measurements can mimic the uptake of some nutrients or contaminants by living organisms, when the uptake process is selective for the free metal ion and evolves under diffusion-controlled conditions [13]. Thus, chemical availabilities measured in a set of sensors can predict metal bioavailability to microorganisms and algae in natural media and they can be consistently used in pollution prevention laws and policies.

DGT (Diffusive Gradients in Thin films) is a dynamic technique that is readily used for *in situ* measurements [14-17]. It accumulates metals in a binding layer (resin disc) after they have diffused through a hydrogel (diffusive gel disc). The binding to the resin disc is ideally so fast and strong that perfect sink conditions apply [18]. The flux of metal bound is calculated from the metal accumulated during the whole deployment time, which is typically of the order of days and it constitutes a time weighted average concentration [19-20]. Different chemical species can contribute to the accumulation, but DGT provides only an integrated value and it does not allow to identify the contribution of a specific species which depends on its mobility and lability. Lability refers to the

capability of complexes to dissociate and reach local equilibrium along the diffusion domain [21-22]. Net dissociation occurs in a region (the so-called reaction layer) where the complex concentration does not reach equilibrium with the free metal and ligand. In DGT, the reaction layer comprises part of the diffusive gel, but it extends into the resin domain where a negligible concentration of free metal drives partially labile complexes to dissociate [23-24]. Thus, complexes are far more labile in DGT than in voltammetric sensors, where penetration into the electrode is not allowed. The dependence of the lability on the thickness of the diffusive and resin gels in DGT opens the way to obtain complementary information on the availability of a metal cation in a natural sample which can be summarized in a kinetic signature, i.e., a set of availabilities at different spatial and time scales covered by the set of sensors [12, 25]. Furthermore, this information can be used to assess which are the complexes that contribute to the metal availability and, eventually, to determine the speciation, dissociation rate constants or diffusion coefficients of the species present in a natural sample [26] which is an important task to understand the functioning of natural systems.

Up to now, there have been few attempts to determine mobilities, concentrations and labilities of the species present in a natural system [25-28]. The procedure is based on using a set of DGT devices equipped with different gels and/or resins. A set of lability degrees for all the target analytes is, thus, obtained. These lability degrees can be written in terms of the speciation, physicochemical and geometrical parameters, when a convenient relationship is known. The resulting set of equations allow, then, to solve for the unknowns. An analytical expression, derived for a complex under ligand excess conditions is available [24]. In this paper, this expression is extended to consider electrostatic effects of the resin charge typical in freshwaters and it is applied to a model system that contains Ni and nitrilotriacetic (NTA) acid at different total NTA concentrations. One aim of this work is to check the accuracy of this expression in a controlled system, which is a necessary step prior to its application in natural samples.

In many cases, complexes with a stoichiometric relationship between metal and ligand 1: n with n>1 arise. Despite such complexes being common for most ligands, they have seldom been considered in the DGT literature. Since Ni and NTA form a complex of stoichiometry $Ni(NTA)_2$ at some concentrations ratios, this situation is also considered

in this paper, evidencing why trace metals become less available when successive complexes are formed.

4.4 Chemical availability of metal cations in presence of ligands using DGT: the lability degree.

The lability degree, ξ, of a set of complexes of an element M has been defined [21-22, 29] as:

$$\xi \equiv \frac{J - J_{\text{free}}}{J_{\text{labile}} - J_{\text{free}}} \tag{4.1}$$

where J stands for the total flux of metal accumulated in the resin disc, and J_{free} and J_{labile} are defined below. J_{free} is the flux due to the free metal in solution (as if complex dissociation was frozen), which in steady state and perfect sink conditions, as typically met in DGT deployments, becomes

$$J_{\text{free}} = D_{\text{M}} \frac{c_{\text{M}}^{*}}{\delta^{\text{g}}} \tag{4.2}$$

where c_{M}^{*} is the bulk concentration of free metal in solution, D_{M} is the metal diffusion coefficient, δ^{g} is the integrated thickness of the diffusive gel, filter and diffusive boundary layer (DBL), where common diffusion coefficients for each species are assumed to apply. When only one ligand is present in the solution, but successive complexes with stoichiometric relationships metal-to-ligand 1:1,... , 1:*n* can be formed, J_{labile} is defined as:

$$J_{\text{labile}} = \sum_{i=1}^{n} D_{\text{ML}_i} \frac{c_{\text{ML}_i}^{*}}{\delta^{\text{g}}} + J_{\text{free}} \tag{4.3}$$

where $c_{\text{ML}_i}^{*}$ stands for the bulk concentration of the complex ML_i generated by one M ion and i ligands (L) and D_{ML_i} is its corresponding diffusion coefficient. J_{labile} is the steady state flux when dissociation of all the complexes is so fast that equilibrium with the free metal is reached at all the relevant spatial domain. Equation (4.3) can be extended to systems with different ligands by adding an extra summation for all the ligands present.

According to Eqs. (4.1)-(4.3), the lability degree of a system stands for the fraction that relates the actual contribution of complexes to the metal flux, $J - J_{\text{free}}$, with the maximum contribution, $J_{\text{labile}} - J_{\text{free}}$, reached if all the complexes were labile [15, 22].

The global lability degree of a set of complexes of an element in a system is experimentally accessible with Eq. (4.1) when the bulk concentrations and the diffusion coefficients are known. The particular lability degree of a given complex, ξ_{ML_i}, is not experimentally accessible, since only the total accumulation is measurable. However, it is a measure of the complex consumption by dissociation and it can be defined [30-31] as

$$\xi_{\text{ML}_i} \equiv 1 - \frac{c_{\text{ML}_i}^{\text{r}^+}}{c_{\text{ML}_i}^{*}} \tag{4.4}$$

where $c_{\text{ML}_i}^{\text{r}^+}$ stands for the complex concentration at the diffusive gel side of the resin-diffusive gel interface ($x=\delta^{\text{r}}$, see Fig S4.1 in the Supporting Information). Obviously, $0 \le \xi_{\text{ML}_i} \le 1$.

When only one complex is present, ξ_{ML} (we omit the subscript i=1, since it is no longer necessary)is given by Eq. (4.1), and when $J_{\text{free}} << J$,

$$\xi_{\text{ML}} = \frac{J}{J_{\text{labile}}} = \frac{n_{\text{M}}/At}{D_{\text{ML}}\left(\frac{c_{\text{ML}}^{*}}{\delta^{g}}\right)} \tag{4.5}$$

where n_{M} stands for the accumulation (moles) of metal M, A is the area of the DGT device and t the deployment time [32]. Eq (4.5) allows the measurement of the lability degree of ML complexes in systems where only one relevant complex in solution is present.

Alternatively, in excess of ligand conditions, ξ_{ML} can be written in terms of physicochemical parameters [32] as:

$$\xi = 1 - \frac{\left(1+\varepsilon K^{'}\right)}{\varepsilon K^{'} + \frac{\delta^{g}}{m}\coth\left(\frac{\delta^{g}}{m}\right) + \frac{\delta^{g}\Pi^{z_{ML}}\left(1+\varepsilon K^{'}\right)}{\lambda_{ML}}\frac{D_{ML}^{R}}{D_{ML}}\tanh\left(\frac{\delta^{r}}{\lambda_{ML}}\right)} \quad (4.6)$$

where $\varepsilon = \frac{D_{ML}}{D_{M}}$ is the normalized diffusion coefficient. In Eq (4.6), z_{ML} stands for the charge of the ML complex,

$$m = \sqrt{\frac{D_{ML}}{k_{d}\left(1+K^{'}\right)}} \quad (4.7)$$

$$\lambda_{ML} = \sqrt{\frac{D_{ML}^{R}}{k_{d}}} \quad (4.8)$$

$$\Pi^{z_{ML}} = \frac{c_{ML}^{r^{-}}}{c_{ML}^{r^{+}}} = \exp\left(\frac{z_{ML}F\Psi}{RT}\right) \quad (4.9)$$

where R and F label the gas and the Faraday constants, respectively, T labels the temperature and Ψ stands for the electrostatic potential difference between the diffusive gel and the resin.

From now on, the superscript R denotes the value of a magnitude in the resin domain, while the absence of this superscript denotes magnitudes in diffusion domains other than the resin disc. Thus, D_{ML}^{R} labels the diffusion coefficient in the resin domain (we are interested in allowing different diffusion coefficients in the resin and diffusive gel domains as we will see later on), $K = \frac{k_{a}}{k_{d}}$ stands for the stability constant, $K' = \frac{k_{a}c_{L}^{*}}{k_{d}} = \frac{k_{a}^{'}}{k_{d}} = \frac{c_{ML}^{*}}{c_{M}^{*}}$ and k_a and k_d are the association and dissociation rate constants.

The Boltzmann factor Π stands for the electrostatic partitioning of a monovalent positively charged species at the resin/diffusive gel interface, due to the negative charge of the resin. This effect implies that the concentration profiles of charged species at the resin-diffusive gel interface suffer a discontinuity which depends on the ionic strength and the charge of the species [32-33].

Eq (4.6) indicates that the lability degree depends on the ligand concentration as well as on the geometrical parameters of the DGT device, increasing when δ^{g} or δ^{r} increase. The lability degree decreases as the ligand concentration increases, since this increase shifts the equilibrium of complexation towards association. However, in DGT devices most of the metal bound to the resin comes from the complex dissociation inside the resin domain where, under perfect sink conditions, the free metal concentration is negligible [34-35], but where the complexes that are not fully labile can have a relevant concentration. Since the shift of the equilibrium as the ligand concentration increases cannot take place in absence of metal, the lability degree in DGT devices becomes almost independent of the ligand concentration in ligand excess conditions.

In a system that contains a mixture of ligands, ξ_{ML} differs from the corresponding value in a single ligand system sharing in common the complex and free ligand concentrations, $\xi_{ML}^{h=1}$. However, the use of $\xi_{ML}^{h=1}$ measured in single ligand systems provides reasonably approximate values when predicting metal accumulation in mixtures [30, 36] due to opposite mutual effects that tend to cancel.

4.5 Materials and Methods

4.5.1 Experimental set-up for DGT measurements.

Diffusive and resin gels were acquired from DGT research Limited (https://www.dgtresearch.com). A total number of 15 DGT devices were used. In order to assay DGT devices with different resin and diffusive gel thickness, 5 groups of 3 units were prepared containing: 1 filter, 1 diffusive gel and 1 resin disc (labelled as configuration 1R1G); 1 filter, 1 diffusive gel and 2 resin discs (2R1G); 1 filter, 2 diffusive gels and 1 resin disc (1R 2G) and 3 filters, 1 diffusive gel and 1 resin disc (1R1G3F). A last group containing 1 filter, 1 diffusive gel and 1 resin disc was used for blank measurements.

DGT holders (piston type, 2 cm diameter window), polyacrylamide gel discs (diffusive disc, 0.779 mm thick and resin disc 0.4 mm thick) and polyethersulfone (PES) filters (0.45 µm pore size, 150 µm thick) were used. Once assembled, they were rinsed in a preconditioning solution at the same ionic strength (100 mmol L^{-1}) of the solutions for at least 24 hours.

Deployments: 2 L of solutions corresponding to the experimental conditions of either column 1 (Exp A) or column 2 (Exp B) of Table 4.1 were left to equilibrate in a 5L polyethylene exposure bucket thermostatized at 25 °C during 3 h and stirring rate 240 rpm. Three DGT devices of each type were deployed in each solution (see working conditions in Table 4.1). Deployment time lasted for 20 hours and pH was measured at the beginning and end of the accumulation. Three aliquots of 0.9 mL were extracted from the solution before and after the deployment in order to measure total Ni concentration with ICP-MS (7700 Series, Agilent).

Table 4.1 Total concentrations of Ni, NTA, HEPES and physical parameters for DGT experiments Exp A and Exp B.

	Exp A		Exp B
$c_{T,Ni}$ (mmol L^{-1})	3.50×10^{-2}		3.50×10^{-2}
$c_{T,NTA}$ (mmol L^{-1})	5.50×10^{-2}		1.14
HEPES (mmol L^{-1})	0.200		0.200
$NaNO_3$ (mmol L^{-1})	100		100
pH	7.7		7.6
T(°C)	25		25
% NiNTA	99%		62%
% $Ni(NTA)_2$	1%		38%

After the deployment, DGT devices were disassembled, resin discs were extracted using clean tweezers and eluted using 1 mL HNO_3 20 %, to ensure an efficient metal extraction procedure (elution factor equal to 1 was used). More details are described elsewhere [37].

4.5.2 Experimental set-up for measurements with diffusion cell.

Stock solutions of Ni ($Ni(NO_3)_2\cdot6H_2O$, Sigma-Aldrich,puriss p.a) 100 mmol L^{-1}, NTA (Fluka, analytical grade) 3×10^{-1} mmol L^{-1}, HEPES (4-(2-hydroxyethyl)-1-piperazineethanesulfonic acid), High purity grade Amresco, at pH 8.4, adjusted by dropwise addition of 10^3 mmol L^{-1} NaOH or HNO_3 (Fluka ACS reagent) 250 mmol $L^{-1}$and glycine(Sigma-Aldrich, puriss. p.a) 25 mmol L^{-1}were prepared. Solutions were left to equilibrate for 24 h with stirring and T=24.9ºC. In experiment 4 (Table 4.2.) glycine were used instead of HEPES due to its buffer capacity in a different pH range [38].

A set of four experiments were done in a diffusion cell to measure the diffusion coefficients of NiNTA and $Ni(NTA)_2$ across the diffusive gel. The two compartments (donor and acceptor) of the diffusion cell were connected through a diffusive gel placed in the communication 2 cm^2 circular hole. See experimental details in the SI. Concentrations of the solutions are gathered in Table 4.2. The acceptor cell contains the buffer and background electrolyte at the same concentrations as the corresponding donor

solution in the experiment. In all experiments, sodium nitrate (Fluka, puriss. p.a) was used as background electrolyte to reach an ionic strength I=100 mmol L^{-1}.

4.5.3 Determination of diffusion coefficients

Diffusion coefficients were determined from the measurement of the slope of the plot of the mass of Ni in the acceptor solution of the diffusion cell against time [39-40]. The mass of Ni in the acceptor solution was determined by analysing at different times aliquots of the acceptor solution with ICP-MS, resulting in a linear increase with time as reported in the SI.

Table 4.2. Experimental conditions (for experiments 1 to 4) which have been employed in donor and acceptor diffusion cells respectively.

Parameters	Donor				Acceptor			
	Exp 1	Exp2	Exp 3	Exp 4	Exp 1		Exp 3	Exp 4
$c_{T,Ni}$ (mmol L^{-1})	5.69×10^{-2}	4.6×10^{-2}	1×10^{-2}	3.77×10^{-2}	-	-	-	-
$c_{T,NTA}$ (mmol L^{-1})		5×10^{-2}	1×10^{-1}		-	-	-	-
$c_{T,Hepes}$(mmol L^{-1})	0.2	0.2	-	0.2	0.2	0.2	-	0.2
$c_{T,Glycine}$(mmol L^{-1})			1×10^{-1}				1×10^{-1}	
$NaNO_3$(mmol L^{-1})	100	100	100	100	100	100	100	100
pH	7.44	7.60	8.66	7.04	7.42	7.48	8.87	6.97
T(°C)	24.9	24.9	24.9	24.9	24.9	24.9	24.9	24.9
Volume (L)	0.100	0.088	0.100	0.092	0.100	0.088	0.100	0.092
Total time (s)	11700	10380	10320	11460	11700	10380	10320	11460

Assuming: i) that the concentrations of M and ML in the acceptor are at any time negligible with respect to those in the donor solution, ii) a common diffusion coefficient

for each species in water and gel solutions and iii) steady-state diffusion, then the mass of metal in the acceptor solution, n_M, can be written as:

$$n_M = \frac{\sum_i^n D_{ML_i} c^*_{ML_i}}{\delta^g + \delta^{DBL}} At \quad (4.10)$$

where δ^{DBL} stands for the total DBL thickness at both sites of the diffusive gel, so that in this previous formula δ^g stands just for the gel thickness.

For *n*=2, at least two experiments are required to determine D_{ML} and D_{ML_2}. Total concentrations of the performed experiments are detailed in Table 4.2. Concentrations of $c^*_{ML_1}$ and $c^*_{ML_2}$ were calculated using the speciation software VMinteq [41]. The parameter δ^{DBL} was determined from an experiment with only free metal, also included in Table 4.2. , using D_{Ni} =5.77×10^{-10} m^2 s^{-1} as reported by DGT Research. The mass of Ni in the acceptor solution, n_M, was determined by analysing samples with ICP-MS from both diffusion cell compartments Table 4.2. Exp 4 (see Table 4.4) was used to verify the Ni diffusion coefficient in a stack of two diffusive gels. See SI for more details.

4.5.4 Determination of the lability degree of the Ni complexes in the different DGT devices

When there are two relevant Ni complexes in the sample solution (Exp B in Table 4.1), 62 % of NiNTA and 38 % of Ni(NTA)$_2$), the global lability degree of Ni complexes in the different DGT devices is assessed with Eq (4.1) (theoretically estimating J_{labile} with Eq (4.3) and J_{free} -which becomes negligible- with Eq (4.2)). When only one Ni complex is present (Exp A in Table 4.1, 99% of Ni as NiNTA), the lability degree is computed with the particular Eq ((4.5)). In both cases, speciation is estimated with VMinteq and the diffusion coefficients are determined as described in Section "Determination of diffusion coefficients". The thickness of the diffusion domain is particular for each DGT configuration. The thickness of an individual diffusive gel, resin and filter are 0.629mm

, $\delta^r = 0.4\text{mm}$ and $\delta^f = 0.150\text{mm}$, respectively. Due to the vigorous stirring, the DBL thickness in DGT experiments is neglected.

4.5.5 Determination of kinetic constants.

In Exp A (Table 4.1), NiNTA is the only relevant Ni species.

Table 4.3. Experimental diffusion coefficients and the regression coefficient obtained in this work from the number of accumulated moles vs. time, using the conditions of Table 4.2. .

Experiment	Diffusion Coefficient in the gel phase (in m^2s^{-1})	R^2
Exp 2	$D_{\text{NiNTA}} = 5.06\times10^{-10}$	0.9996
Exp 3	$D_{\text{Ni(NTA)}_2} = 2.25\times10^{-10}$	0.9976
Exp 4 (using 2 diffusion gels)	$D_{\text{Ni}} = 4.60\times10^{-10}$	0.9989

In order to evaluate whether Eq (4.6) accurately predicts the lability degree of the NiNTA in the different DGT devices and different concentrations, we need to estimate the dissociation rate constant of the NiNTA. In this task, the experimental value of ξ_{NiNTA} for 1R1G devices is used as input value and solving Eq (4.6), with an iterative procedure described in the SI, $k_{d,1}$ (for NiNTA dissociation) is obtained.

Notice that using ξ_{NiNTA} from 1R1G DGT, instead of that from other geometrical configurations, is an arbitrary choice, but it has been checked that using ξ_{NiNTA} from other DGT configurations as an input, a very close output $k_{d,1}$ is retrieved, which suggests the suitability of ξ_{NiNTA} given by Eq (4.6).

In Exp B, both NiNTA and $Ni(NTA)_2$ concentrations are relevant and the values of $k_{a,1}$, $k_{d,1}$, $k_{a,2}$, and $k_{d,2}$ are required to run the numerical simulations (see next section). $k_{a,i}$ and

$k_{d,i}$ label, respectively, the association and dissociation rate constants of the process $ML_{i-1} + L \rightleftarrows ML_i$.

In general, in a set of successive complexes, the dissociation of ML into M and L is usually the rate limiting step [42-43]. Assuming that the dissociation of ML is the rate limiting step, ML and ML_2 will be in equilibrium along all the spatial domain, but not with M. The particular values of the rate constants $k_{a,2}$ and $k_{d,2}$ are, then, not necessary whenever their ratio fulfils the stability constant of $Ni(NTA)_2$ (which was taken from VMinteq) and are large enough for the concentrations of both NiNTA and $Ni(NTA)_2$ to satisfy equilibrium. Accordingly, a dissociation rate constant for ML_2 higher than 100-fold that of ML was used after checking that a further increase did not modify the accumulation, securing that the rate limiting step is the ML dissociation process.

4.5.6 Numerical simulation of concentrations profiles and accumulations.

A further step in the quantitative understanding of the system behaviour has been gained by using a rigorous numerical code, that solves the system of diffusion-reaction equations taking into account the specific DGT initial and boundary conditions, to obtain theoretical expected values of the lability degree (see details in Section 4.10.1 of this SI or Section 2 in the SI of reference [44]). Speciation calculations with VMinteq for total Ni and NTA concentrations of each case indicate that Ni, NiNTA, $NiNTA_2$, NTA and HNTA are the relevant species, while the rest of species have negligible concentrations (see Section 4.10.4 of the SI). Accordingly, only these relevant species have been considered in the numerical simulation code. Rate constants and diffusion coefficients determined as commented above were used. Notice that the acid base equilibrium $NTA + H \rightleftharpoons HNTA$ is included in the simulation considering equilibrium between these species. Association and dissociation kinetic constants for the proton binding to the NTA are then assumed large enough, while the ratio fulfils the equilibrium constant.

In conditions of low ionic strength, the negative charge of the resin can induce a migration flux resulting from the gradient of the electrical potential at the resin-gel interphase. In the simulation code, this physical phenomenon is modelled using the Donnan partition

model which considers the electrical potential as a step function located at the resin-gel interphase (See Section 1 of the SI). Accordingly, a Boltzmann factor (Π) as defined in Eq (4.9) is considered for the electrostatic partitioning of the charged species. The Boltzmann factor for each species was evaluated from the experimental determination of the rubidium Boltzmann factor. Rubidium chloride was added into the solution at a concentration of 3.92×10^{-3} mmol L^{-1}. and because the specific binding of Rb to the resin sites is expected to be negligible, as other alkali metals such as Na, all the Rb mass eluted from the resin disc corresponds to the electrostatic binding. Accordingly, the Boltzmann factor for Rb can be computed dividing the bulk Rb concentration by the concentration of rubidium in the resin disc as Eq. (4.9) indicates [20, 45]. For any other species with charge z_i, the factor $(\Pi)^{z_i}$ applies.

4.6 Results and discussion.

4.6.1 Characterization of the solutions described in Table 1

The first experiment detailed in Table 4.2. (Exp 1) aims to calculate δ^{DBL} in the diffusion cell. This calculation uses the tabulated value 5.77×10^{-10} m^2s^{-1} from DGT research limited (https://www.dgtresearch.com/diffusion-coefficients) for DNi at 25ºC. Once δ^{DBL} is known, Eq. AccM(4.10) allows the determination of D_{NiNTA} and D_{NiNTA_2} from the rest of experiments. Diffusion coefficients of NiNTA and $Ni(NTA)_2$ measured with the diffusion cell are reported in Table 4.3. The obtained diffusion coefficient of $Ni(NTA)_2$ is smaller than that of NiNTA indicating an increase of the size of the $Ni(NTA)_2$ complex. Exp 4 in Table 4.2. also allows the determination of the Ni diffusion coefficient in a stack of two diffusive gels. The diffusion coefficient is expected to be independent of the thickness of the diffusive gel, but the experimental measurement yielded D_{Ni} $=4.60\times10^{-10}$ m^2s^{-1}, a value lower than the tabulated value at DGT research limited, indicating that a kind of extra resistance to diffusion appears when a stack of diffusive gels is used. We speculate that this extra resistance might be due to a change in the size of the gel pores at the surface of the gel.

The Boltzmann factor for the Donnan partitioning at the resin diffusive gel interface, obtained by adding Rb into the system, of $\Pi=1.13$ is very small, indicating an important screening of the resin charges by the salt background. However, species with electrical charge z_i will have Boltzmann factors Π^{z_i}. Since $Ni(NTA)_2$ and NTA have a high electrical charge (-4 and -3, respectively) the resulting Boltzmann factors are non-negligible (1.6 and 1.4, respectively) advising the explicit consideration of the electrostatic effects. These Boltzmann factors can be applied to all experiments of Table 4.1, since they share a common ionic strength.

The dissociation rate constant of NiNTA, fitted with the numerical simulation from the experimental lability degree in Exp A (Table 4.1), is $k_{d,1}$(NiNTA) $=1.43\times10^{-3}$ s^{-1}.

4.6.2 Dependence of the accumulation and lability degree on the geometrical parameters of the DGT device

Figure 4.1 plots the accumulation and the lability degree vs the thickness of the diffusive gel or the thickness of the resin gel. The lines in Figure 4.1 correspond to values computed with Eq (4.6) for a complex whose diffusion coefficient, stability and rate dissociation constant coincide with the above values determined for NiNTA. As shown in Figure 4.1a, an increase of δ^{g} decreases the accumulation, since the diffusion domain becomes thicker, the source of complex moves away and the flux decreases. Conversely, an increase of δ^{r} increases the accumulation, since the complexes NiNTA and $Ni(NTA)_2$ inside the resin have more time and volume for dissociation.

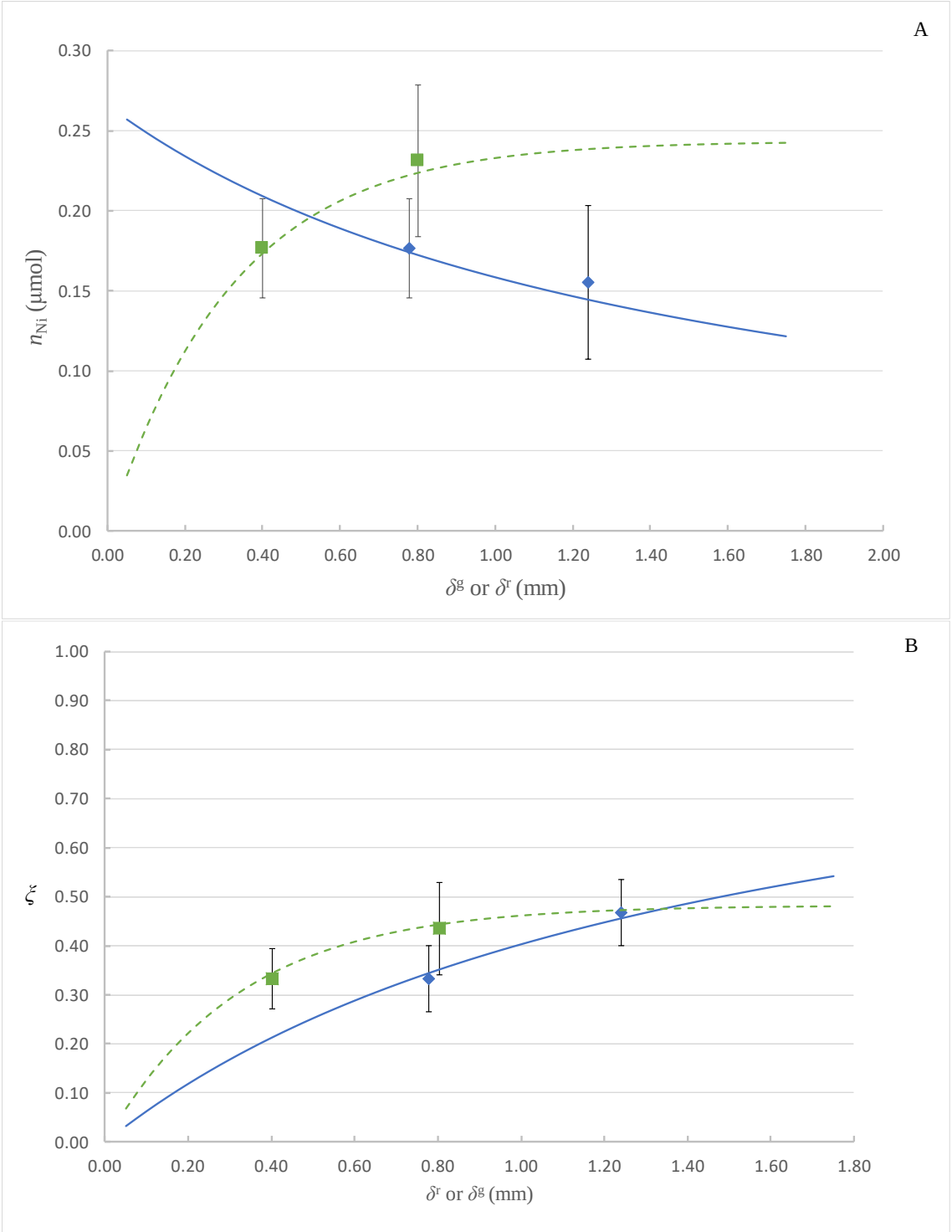
A
0.30
0.25
0.20
0.15
0.10
0.05
0.00
n_{Ni} (µmol)
0.00 0.20 0.40 0.60 0.80 1.00 1.20 1.40 1.60 1.80 2.00
δ^g or δ^r (mm)
B
1.00
0.90
0.80
0.70
0.60
0.50
0.40
0.30
0.20
0.10
0.00
ξ
0.00 0.20 0.40 0.60 0.80 1.00 1.20 1.40 1.60 1.80
δ^r or δ^g (mm)

Figure 4.1. Dependence of the accumulation (panel a) or the lability degree (panel b) either on the gel thickness (dashed green line) or on the resin thickness (solid blue line) computed with Eq ((4.6)). Parameters used in Eq ((4.6)) are the values for NiNTA resulting from Eqs. ((4.11))-eqPieff(4.16). Markers for panels a and b correspond to the experimental measurements of Exp B in Table 4.1. Lines and markers (green squares) corresponding to the dependence on δ^g have δ^r = 0.4mm. Lines and markers (blue diamonds) corresponding to the dependence on δ^r have δ^g = 0.779 mm. Errors bars correspond to standard deviations of accumulation (Fig.1A) or lability degree (Fig.1B) as reported in Table .

Figure 4.1b depicts the dependence of the lability degree on the thickness of the diffusive gel or the thickness of the resin gel. As seen in the figure, an increase of either δ^r or δ^g increases ξ. However, the influence of δ^r is more pronounced at low thicknesses, but it plateaus beyond a certain resin thickness, while a sufficiently large increase of δ^g is able to bring the complex to full lability. Indeed, an increase in δ^r increases the dissociation volume of the complexes that have penetrated into the resin, while the complex concentration profile has not yet reached full dissociation in the resin domain. When full dissociation is reached, a further increase of δ^r has no effect neither on the lability degree nor on the accumulation. Thus, the lability degree is not an intrinsic property of a complex, since it also depends on the geometrical characteristic of the sensor, among other factors, as Eq (4.6) indicates.

Table 4.4 Experimental and predicted lability degrees obtained for conditions of Exp A and B from Table 4.1., for each type of DGT device. Parameters used for the rigorous simulations and analytical calculations as in Figure. 4.2

	$c_{T,NTA}$=5.5×10^{-2} mmol L^{-1} (Exp A)				$c_{T,NTA}$=1.15 mmol L^{-1} (Exp B)			
Geometrical configuration	1R1G	2R1G	1R2G	1R1G3F	1R1G	2R1G	1R2G	1R1G3F
n_{Ni} (µmol)	0.26	0.28	0.24	0.16	0.18	0.23	0.13	0.15
Standard Deviation (n_{Ni} (µmol))	0.04	0.05	-	0.02	0.03	0.05	-	0.05
ExperimentaL ξ	0.46	0.55	0.72	0.49	0.35	0.46	0.56	0.49
Standard Deviation (Experimental ξ)	0.08	0.09	-	0.06	0.06	0.09	-	0.15
Predicted ξ (simulation)	0.44	0.53	0.63	0.55	0.38	0.48	0.57	0.49
Predicted ξ (Analytical Eq. (eq16(4.6)))	0.45	0.55	0.60	0.57				
Predicted ξ (Analytical Eqs.(eq16(4.6)),(eq11(4.11))-eq15(4.15))					0.39	0.50	0.59	0.51

Experimental ξ values measured with DGT devices of different geometrical characteristics for the Ni complexes in the solutions described in Table 4.1. are reported in Table 4.4 . These values corroborate the increase of ξ as either δ^r or δ^g increase. Table 4.4 also gathers the theoretical prediction of ξ–values obtained with numerical simulations as indicated in Section "Numerical simulation of concentrations profiles and accumulations.". Notice the agreement between experimental measurements and numerical simulation predictions, indicating that, despite its simplicity, the model contains an essentially correct description of the main physicochemical phenomena in DGT devices.

We aim at checking whether Eq. (4.6) is useful in the prediction of the lability degree for different thicknesses of the diffusive or resin gels. Eq. (4.6) can only be directly applied to the system with $c_{T,NTA}$=5.5×10^{-2}mmol L^{-1}, since in this solution, NiNTA is the only one relevant Ni complex and the simple scheme $M + L \rightleftharpoons ML$ linked to Eq. (4.6) applies. The predicted ξ values for all the DGT configurations used in Exp A are close to the experimental measurements and to the numerical simulation values.

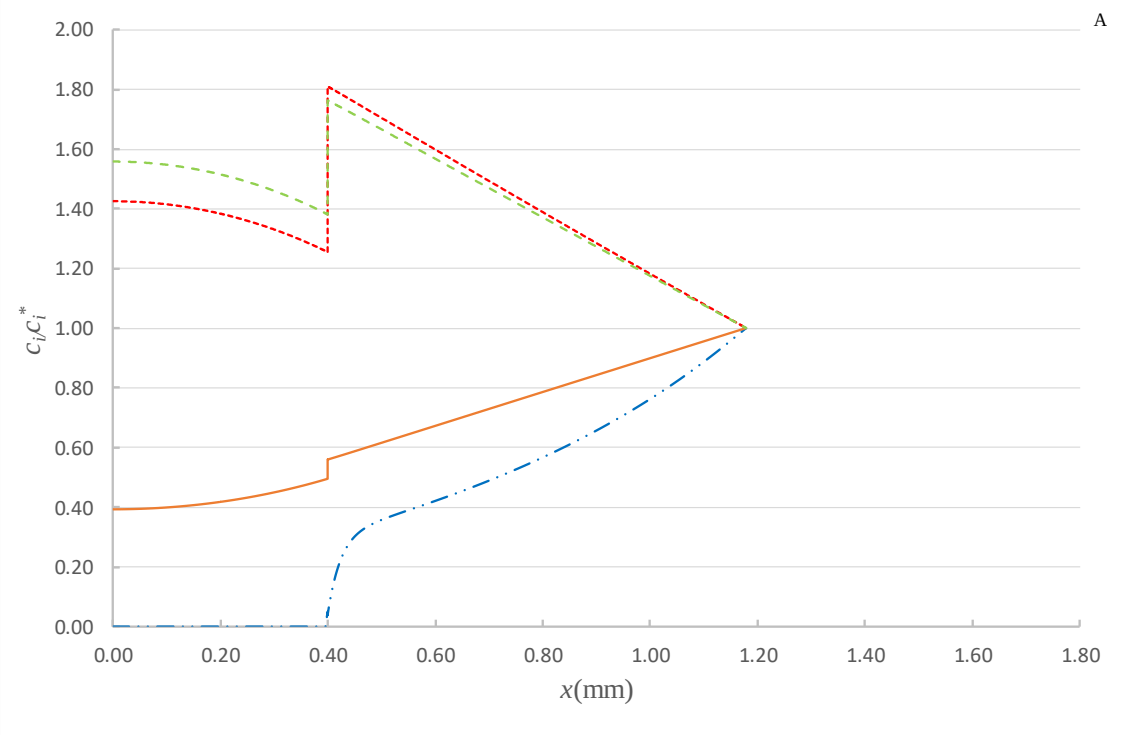

B

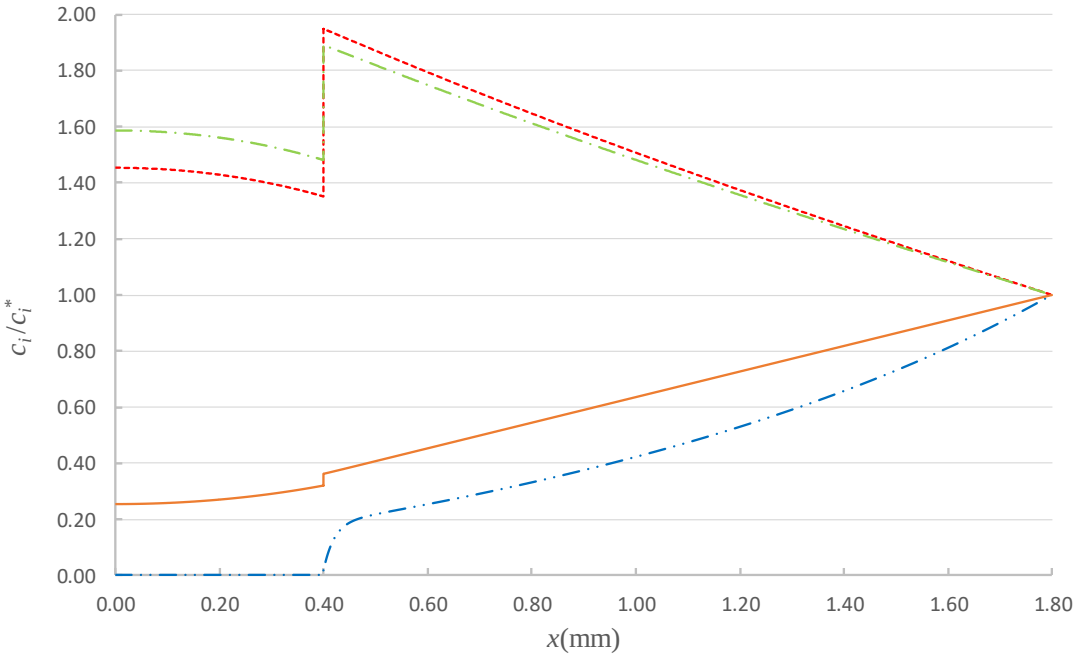
2.00
1.80
1.60
1.40
1.20
1.00
0.80
0.60
0.40
0.20
0.00
c_i/c_i^*
0.00
0.20
0.40
0.60
0.80
1.00
1.20
1.40
1.60
1.80
x(mm)

C

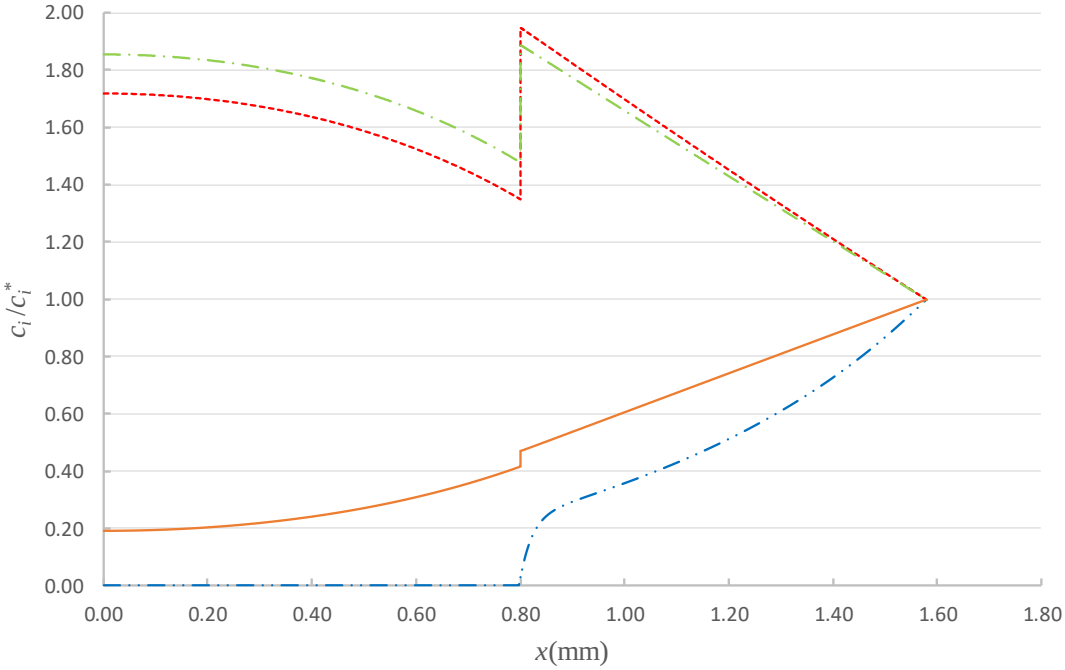
2.00
1.80
1.60
1.40
1.20
1.00
0.80
0.60
0.40
0.20
0.00
c_i/c_i^*
0.00
0.20
0.40
0.60
0.80
1.00
1.20
1.40
1.60
1.80
x(mm)

Figure. 4.2 Normalized concentrations profiles c_i/c_i^* for $c_{T,NTA}=5.5\times10^{-2}$ mmol L^{-1} and $c_{T,Ni}=3.5\times10^{-2}$ mmol L^{-1} obtained by numerical simulation. Dashed line with two points represents $\frac{c_{Ni}}{c_{Ni}^*}$, dashed line represents $\frac{c_{NTA}}{c_{NTA}^*}$, solid line represents $\frac{c_{NiNTA}}{c_{NiNTA}^*}$ and dotted-dashed line $\frac{c_{HNTA}}{c_{HNTA}^*}$. Total concentrations used for this simulation are in columns 2 to 4 of Table . Diffusion coefficients, $D_{Ni}=5.77\times10^{-10}$, $D_{NiNTA}=4.75\times10^{-10}$, $D_{Ni(NTA)_2}=2.25\times10^{-10}$ m^2s^{-1}, except for 1R2G devices, where all values of diffusion coefficients are reduced by a factor 0.8.The kinetic constants are $k_{d,1}=1.48\times10^{-3}$ s^{-1}, $k_{d,Ni(NTA)_2}=0.148$ s^{-1}, $k_{d,HNTA}=1\times10^{2}$ s^{-1}, $k_{a,1}=4.68\times10^{5}$ L $mmol^{-1}s^{-1}$, $k_{a,Ni(NTA)_2}=9.635$ L $mmol^{-1}s^{-1}$, $k_{a,HNTA}=4.46\times10^{8}$ L $mmol^{-1}s^{-1}$ and $\Pi=1.13$

Eq.(4.6) was obtained as an analytical solution of the reaction diffusion problem assuming excess of ligand. In this approximation, the concentration profile of the ligand is expected to be flat. Figure. 4.2 depicts the simulated concentration profiles in DGT devices of the Ni complexes of the solution described in column 1 of Table 4.1. (Exp A). The discontinuities of electrically charged species at $x=\delta^r$ are due to the Donnan partitioning, so that the size of the discontinuity depends on $(\Pi)^{z_i}$ where z_i labels the electrical charge of the species. However, besides the discontinuity, Figure. 4.2 shows that $c_L(x)$ increases as x decreases, indicating that the ligand produced by dissociation of the complex at the resin domain is not negligible with respect to the ligand in the bulk solution. Thus, ligand excess conditions are not strictly fulfilled and accordingly, we are not in the best situation for using Eq.(4.6) However, even in this case, its predictions of ξ are quite accurate, since the NTA concentration is buffered by the presence of HNTA as the main NTA species and most of the NTA produced by dissociation is transformed into HNTA to diffuse back to the bulk solution.

Furthermore, in Figure. 4.2 Ni and NiNTA are in equilibrium along most of the diffusive gel (for instance for x>0.47mm in Figure. 4.2A). However, close to the resin interface, the metal concentration drops to zero while the complex cannot reach equilibrium, since dissociation is not fast enough. This is the so-called reaction layer, which extends also to

all the resin domain, where a negligible concentration of Ni coexists with a non-negligible NiNTA concentration. It is in the reaction layer where net dissociation occurs, while just net diffusion takes place in the rest of the diffusion domain.

Figure. 4.2 also offers an overview of how steady-state concentration profiles of the species in the DGT device evolve with the thickness of the diffusive or the resin gels. This overview is useful to understand the dependence of the lability degree on these geometrical characteristics. Indeed, according to Eq.(4.5), ζ_{NiNTA} is just the distance from the normalized NiNTA profile at $x=\delta^r$ up to 1. The effect of δ^g can be assessed by comparing Figure. 4.2A with Figure. 4.2B. In steady state, the flux of the complex dissociation in the resin domain should equal the flux of the complex entering into the resin domain, i.e., the flux of complex crossing the resin/diffusive gel interface. As a first approximation, we can assume that the profile of NiNTA is approximately flat inside the resin and linear in the diffusive gel domain, with slope ζ/δ^g as seen in the figure. For a given δ^r, an increase of δ^g implies a decrease of the slope of the NiNTA in the diffusive gel. Accordingly, the flux of NiNTA entering into the resin domain will decrease, and to keep steady state, the amount of NiNTA dissociated in the resin domain must also decrease by decreasing the concentration of NiNTA in the resin domain. Likewise, an increase of δ^r increases the capacity of dissociation in the resin domain requiring an increased flux supply of NiNTA to reach steady state and a lower value of the normalized concentration profile at the resin-diffusive gel interface (compare Figure. 4.2A with Figure. 4.2C).

The prediction of the lability degree in Exp B goes parallel to the discussion of the influence of the NTA concentration on the lability degree and it is reported in the next section.

4.6.3 Dependence of the lability degree on the NTA concentration

The dependence of the lability degree of a complex on the ligand concentration is relevant to assess the influence of the composition on the availability of toxic or nutritive elements in natural media. It has been reported that increasing the ligand concentration, the lability degree of a complex decreases, since the dissociation equilibrium is shifted towards association. However, the availability of a metal in DGT devices under ligand excess

conditions is mainly due to the complex dissociation in the resin domain [34]. As the concentration of free metal in the resin domain is negligible, in the typical case where the metal is strongly and quickly bound to the resin, the complexation equilibria cannot be shifted by an increase of the ligand concentration and the availability of the metal becomes almost independent of the ligand concentration in the DGT devices. This result facilitates the determination (or estimation) of the lability degree of a complex in DGT devices, since it allows the use of any ligand concentration in the measurement system just with the proviso of being under ligand excess conditions. When the free ligand concentration is below that of the free metal, a decrease of the ligand concentration also decreases the lability degree against the expected general trend commented above [36].

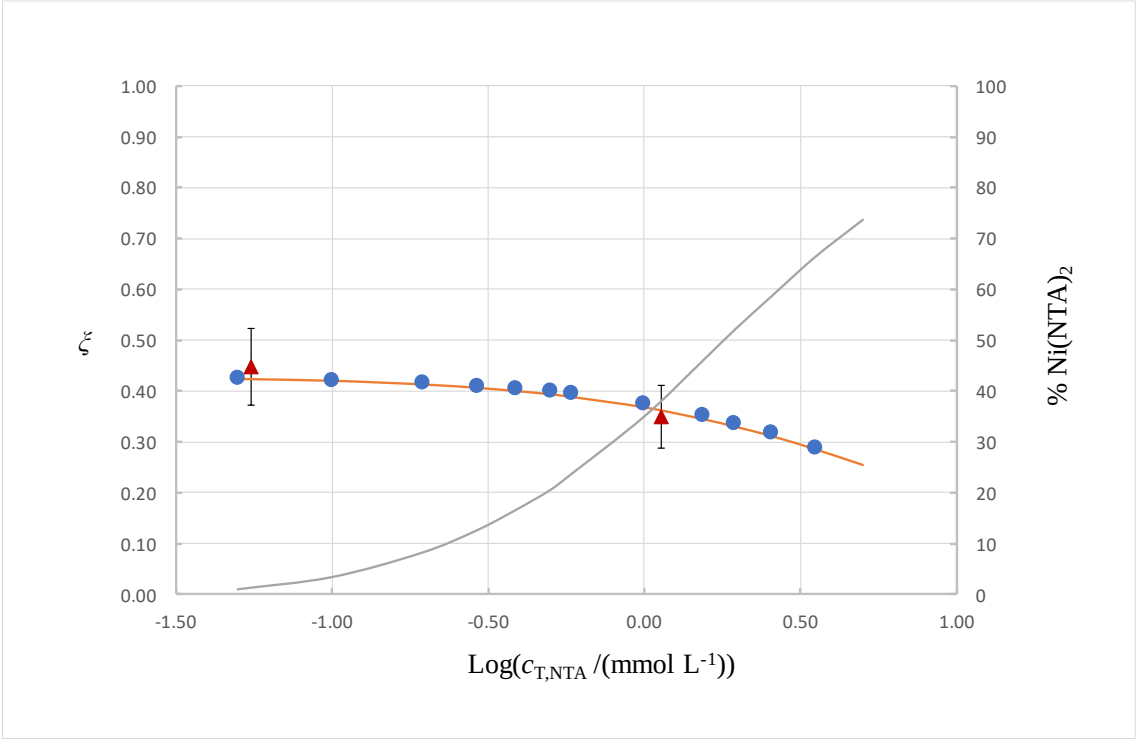

Figure 4.3 Impact of the total NTA concentration on the lability degree of Ni (referred to left ordinate axis) in a solution with Ni and NTA measured with a 1R1G DGT device. Blue circles correspond to numerical simulation results of the DGT processes, orange line stands for the calculated values with Eqs. ((4.6))-((4.9)), (4.11)-(4.15), red triangles indicate the results of experiments A i B in Table (Ionic strength 100 mmol L^{-1}, pH= 7.7; T=25ºC). The gray line depicts the percentage of Ni(NTA)$_2$ (referred to the right ordinate axis) present in the solution. Total Ni concentration and all the parameters as in Figure. 4.2

However, other changes associated to an increase of the ligand concentration can concomitantly take place. Indeed, as seen in Table 4.2. and in Figure 4.3, when the total

NTA concentration increases (Exp B), the bulk speciation indicates a very relevant increase of $Ni(NTA)_2$.

Table 4.4 shows the experimental lability degree of the Ni complexes. Decreasing values of ξ are obtained when $c_{T,NTA}$ increases, as noticed by comparing the values corresponding to Exp B ($c_{T,NTA}$=1.14 mmol L^{-1}) with those of Exp A ($c_{T,NTA}=5.50\times10^{-2}$ mmol L^{-1}) for a fixed configuration of the DGT devices. Theoretical expectations for ξ obtained with numerical simulations (described in Section "Numerical simulation of concentrations profiles and accumulations.") are also gathered in Table 4.4 . Notice that the value $k_{d,(NiNTA)}$ fitted for the 1R1G device deployed at $c_{T,NTA}=5.50\times10^{-2}$ mmol L^{-1} for the system with $c_{T,NTA}$=1.14 mmol L^{-1} has been used, since the rate dissociation constant is a physicochemical parameter independent of the ligand concentration. Equilibrium between $Ni(NTA)_2$ and NiNTA was assumed as explained in Section "Determination of kinetic constants.". The remarkable agreement between experimental and theoretical predictions lends support to the developed model. Moreover, the fitting of only one experimental parameter -the dissociation rate constant of the NiNTA complex- was enough for the interpretation of all the data reported in the manuscript, i. e., the data corresponding to the different DGT configurations (4) and to the different NTA concentrations (2) either with the formation of only NiNTA or the formation of both NiNTA and $Ni(NTA)_2$. This result lends support to the robustness of the model developed.

A simple analytical relationship between the lability degree and the physicochemical parameters in a system like the one with NiNTA and $Ni(NTA)_2$ can be helpful. The simple model $M+L \rightleftharpoons ML$ does not account for this phenomenon, so a general theory for ML_n complexes would be useful.

As quoted above, in a set of successive complexes, the dissociation of ML into M and L is usually the rate limiting step [42-43]. Accordingly, it is reasonable to assume that ML_2, ML_3, and successive complexes are in equilibrium with ML, but not with M if they are partially labile. These equilibrium relationships allow to reformulate the reaction-diffusion set of equations corresponding to the DGT processes in a scheme formally analogous to the case of only one complex of 1:1 metal-to-ligand stoichiometry (see SI).

Labelling as ML_{eff} the effective (formal) complex, the reformulation of a system that only contains ML and ML_2 is reached by defining

$$c^*_{\mathrm{ML,eff}} = c^*_{\mathrm{ML}} + c^*_{\mathrm{ML_2}} \tag{4.11}$$

$$D_{\mathrm{ML,eff}} = \frac{D_{\mathrm{ML}} + K_2^{'} D_{\mathrm{ML_2}}}{1+K_2^{'}} \tag{4.12}$$

$$k^{'}_{\mathrm{a,eff}} = k^{'}_{\mathrm{a},1} \tag{4.13}$$

$$k_{\mathrm{d,eff}} = k_{\mathrm{d},1} \frac{1}{1+K_2^{'}} \tag{4.14}$$

$$K^{'}_{\mathrm{eff}} = K^{'}_1 \left(1+K^{'}_2\right) \tag{4.15}$$

$$\Pi_{\mathrm{eff}} = \frac{c^{\mathrm{r}^-}_{\mathrm{ML,eff}}}{c^{\mathrm{r}^+}_{\mathrm{ML,eff}}} = \frac{\Pi^{z_{\mathrm{ML}}} + K_2^{'} \Pi^{z_{\mathrm{ML_2}}}}{1+K_2^{'}} \tag{4.16}$$

where $K_i = \frac{k_{\mathrm{a},i}}{k_{\mathrm{d},i}}$ stands for the stability constant of the process $\mathrm{ML}_{i-1} + \mathrm{L} \rightleftharpoons \mathrm{ML}_i$, $k_{\mathrm{a},i}$ and $k_{\mathrm{d},i}$ are the association and dissociation rate constants and $K_i^{'} = \frac{k_{\mathrm{a},i} c^*_{\mathrm{L}}}{k_{\mathrm{d},i}} = \frac{c^*_{\mathrm{ML}_i}}{c^*_{\mathrm{ML}_{i-1}}}$.

Eqs (4.12), (4.14) and (4.15) have to be understood as "local" expressions, in the sense that the computation of the effective diffusion coefficient, dissociation rate constant and stability constant of this formal complex should use the corresponding values at the domain of interest (e.g the diffusive gel or the resin). For instance, since the free ligand is electrically charged, the ligand concentration profile in excess of ligand conditions exhibits a discontinuity at the resin/diffusive gel interface ($x = \delta^{\mathrm{r}}$). For $x > \delta^{\mathrm{r}}$, $c_{\mathrm{L}}(x) = c^*_{\mathrm{L}}$, while for $x < \delta^{\mathrm{r}}$, $c_{\mathrm{L}}(x) = c^{*\mathrm{R}}_{\mathrm{L}} = \Pi^{z_{\mathrm{L}}} c^*_{\mathrm{L}}$. Thus, K_i' takes different values in the diffusive gel or in the resin gel and accordingly, K'_{eff} given in (4.15) becomes

$$K^{'}_{\mathrm{eff}} = \begin{cases} K_1^{'\mathrm{R}} \left(1+K_2^{'\mathrm{R}}\right) = \Pi^{z_{\mathrm{L}}} K^{'}_1 \left(1+\Pi^{z_{\mathrm{L}}} K^{'}_2\right) & x < \delta^{\mathrm{r}} \\ K^{'}_1 \left(1+K^{'}_2\right) & x > \delta^{\mathrm{r}} \end{cases} \tag{4.17}$$

According to Eq (4.14), in a system with ML and ML_2, an increase of the ligand concentration not only shifts the equilibrium towards complexation, but also modifies the

effective dissociation rate constant. Indeed, as Eq (4.14) indicates, the effective dissociation rate constant decreases as the ligand concentration increases whenever

$$K_2' = K_2 c_L^* = \frac{c_{ML_2}^*}{c_{ML}^*} > 1 \quad (4.18)$$

indicating that when $c_{ML_2}^* > c_{ML}^*$, i.e., when ML_2 is the relevant species in the system, an increase in the ligand concentration reduces the lability degree of the system. This is a noticeable result in DGT, since it is a particular trait of ML_n complexes that contrasts with the almost negligible influence of the ligand concentration on the lability when only ML complexes arise [34].

The dissociation rate constant of the formal complex defined in Eq (4.14) can be calculated in the diffusive gel domain from K_2' and $k_{d,1}$. For Exp B in (Table 4.1), it becomes $k_{d,eff} = 9.08\times10^{-4}$ s^{-1}, so that $k_{d,eff} < k_{d,1}$. It has to be highlighted that $k_{d,eff}$ is not fitted from the experimental results, but derived from Eq (4.14), so that all the experiments are interpreted with only one fitted parameter, $k_{d,1}$ as quoted above.

Using $k_{d,eff}$, Exp B can be interpreted as if there was a solution with only one complex instead of the two complexes NiNTA and $Ni(NTA)_2$. Thus, the lability degree in each DGT device in Exp B is calculated using expression ((4.6)) and the effective parameters given by Eqs.(4.11)-(4.15). The resulting ξ values, reported in the last row of Table 4.4 and as orange line in Figure 4.3, indicate that the analytical expression ((4.6)) is consistent with experimental and simulated values (see red and blue markers in Figure 4.3 respectively), paving the way to the use of a DGT device with different configurations to obtain information about dynamic speciation in natural systems.

Given the increase of the total NTA concentration, close to a factor of 100, one could expect a stronger decrease. However, we have to notice that the decrease of the effective rate constant depends on $1+K_2 c_{NTA^{3-}}$ as Eq (4.14) indicates. Taking into account the speciation of the system, as given by VMinteq, $K_2 c_{NTA^{3-}}$ keeps being smaller than 1, so that there is only a mild decrease in $k_{d,eff}$. Actually, speciation of NTA is mainly dominated by HNTA at the pH of the experiment. Accordingly, only a mild decrease of the lability degree is observed in Table 4.4 when the NTA concentration increases and $Ni(NTA)_2$ starts to be relevant as also seen in Figure 4.3.

Additional insight on the effect of the total NTA concentration on the lability degree of the Ni complexes can be obtained looking at the concentration profiles. The concentration profile of $Ni(NTA)_2$ is now included in Figure 4.4 , given the non-negligible concentration of this complex. Unlike the concentration profiles depicted in Figure. 4.2, the NTA concentration profile in Figure 4.4 is almost flat indicating fulfilment of excess of ligand conditions, as expected from the increase of the total NTA by a factor of 50. Discontinuities of the concentration profiles at $x=\delta^{r}$ are in agreement with the electrostatic partitioning and, for each type of DGT device, the NiNTA concentration at $x=\delta^{r^+}$ is in Figure 4.4 higher than in Figure. 4.2, consistent with the lower lability degree in the conditions of Figure 4.4 .

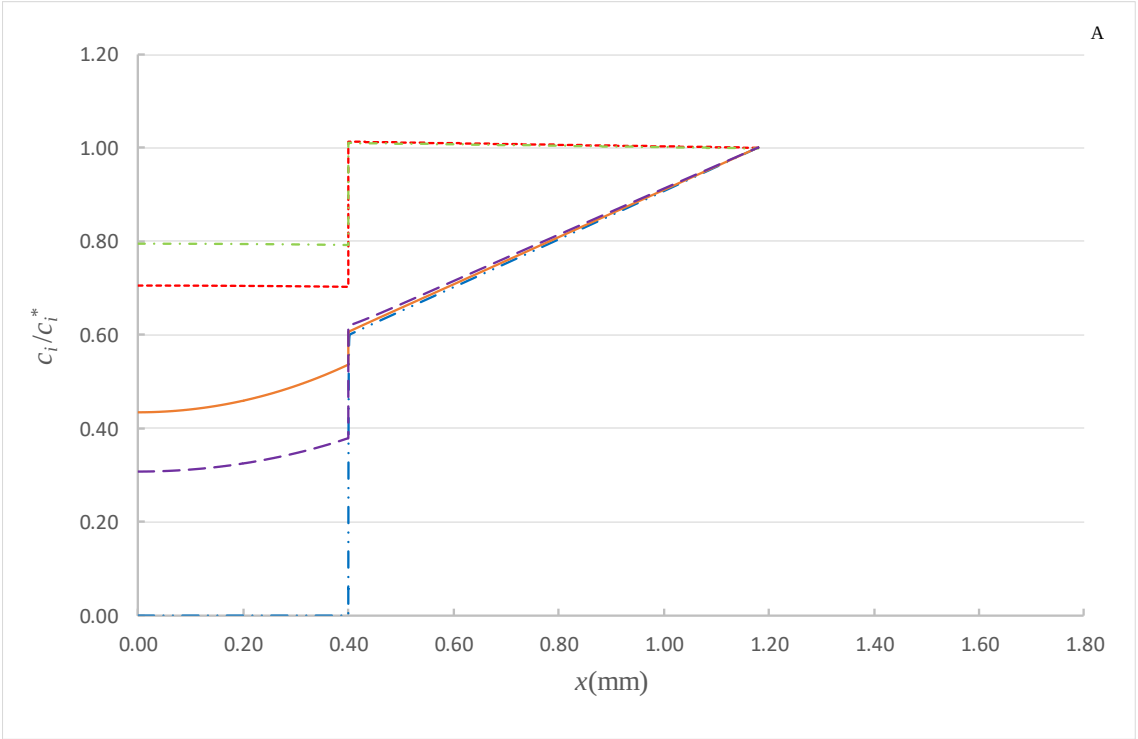

B

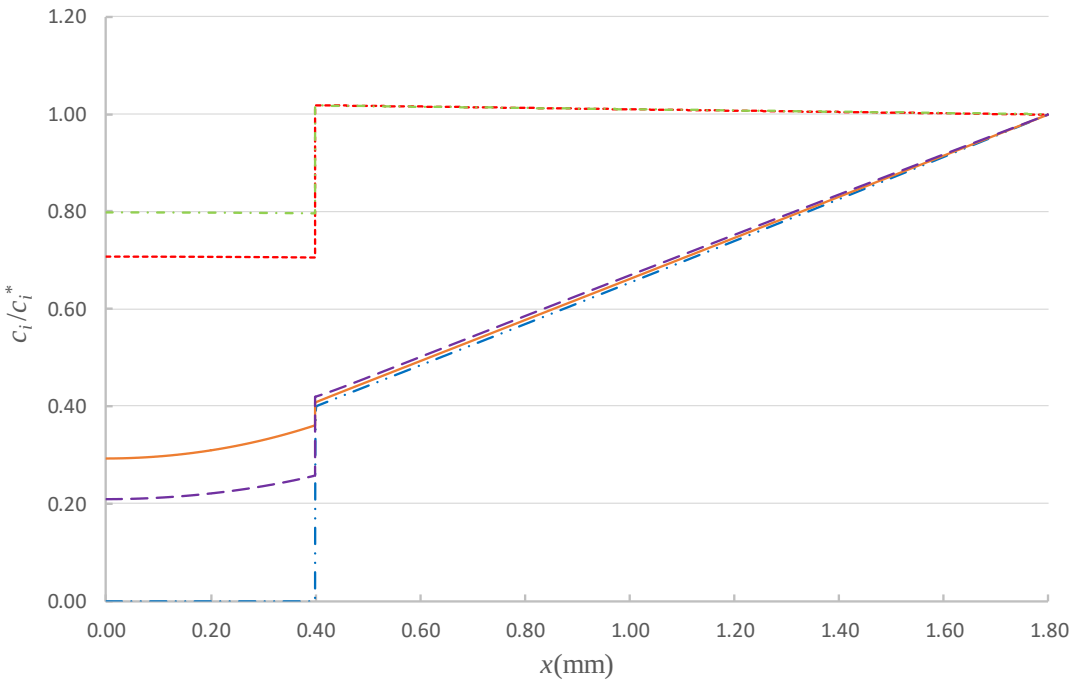
1.20
1.00
0.80
0.60
0.40
0.20
0.00
c_i/c_i^*
0.00
0.20
0.40
0.60
0.80
1.00
1.20
1.40
1.60
1.80
x(mm)

C

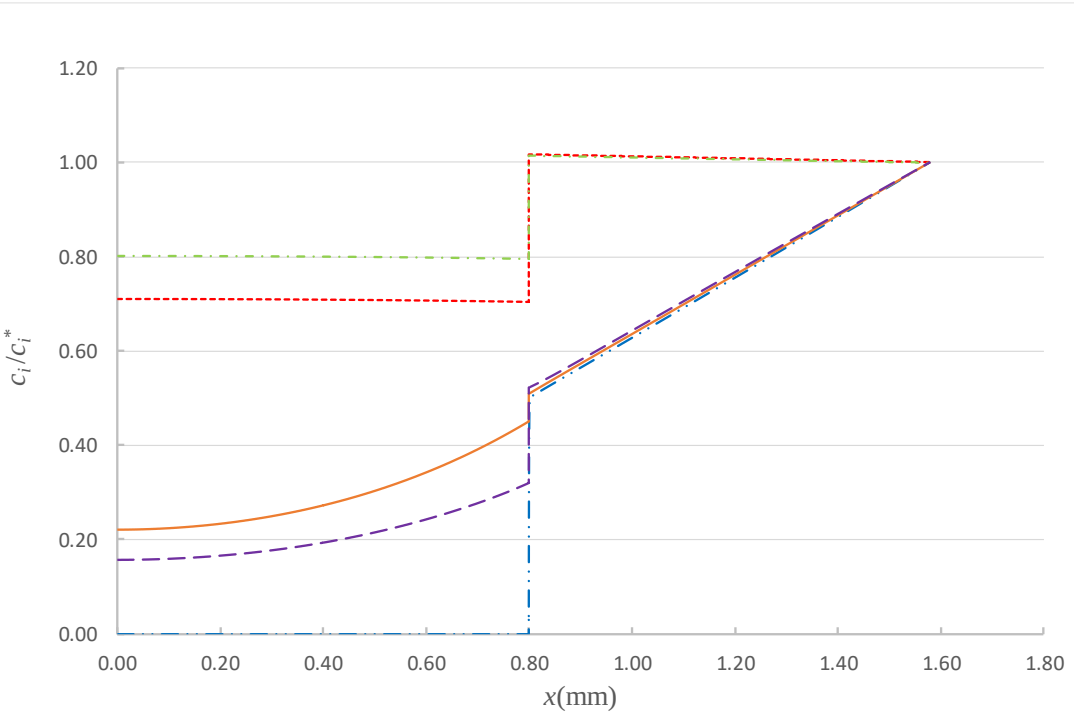
1.20
1.00
0.80
0.60
0.40
0.20
0.00
c_i/c_i^*
0.00
0.20
0.40
0.60
0.80
1.00
1.20
1.40
1.60
1.80
x(mm)

Figure 4.4 Normalized concentration profiles c_i/c_i^* for $c_{T,NTA}$=1.136 mmol L^{-1} and $c_{T,Ni}$=3.5×10^{-2} mmol L^{-1}. Dashed line with two points represents $\frac{C_{Ni}}{C^*_{Ni}}$, short dashed line $\frac{C_{NTA}}{C^*_{NTA}}$, solid line $\frac{C_{NiNTA}}{C^*_{NiNTA}}$, dashed line with one point $\frac{C_{HNTA}}{C^*_{HNTA}}$ and long dashed line $\frac{C_{Ni(NTA)_2}}{C^*_{Ni(NTA)_2}}$. Rest of parameters as in Figure. 4.2.

A main difference between the concentration profiles in Figure. 4.2 and Figure 4.4 is the overlapping of normalized concentration profiles of Ni and NiNTA along most of the diffusion gel domain. In excess ligand conditions this overlapping indicates equilibrium [29, 46-48]. The diverging of both normalized profiles defines the reaction layer, where net dissociation takes place. Moreover, the normalized NiNTA concentration profile converges with that of $Ni(NTA)_2$ in all the diffusive gel domain, indicating that both complexes are in equilibrium, as expected from assuming that the dissociation of NiNTA is the rate limiting dissociation step. Thus, according to Eq (4.4), the particular lability degrees of both complexes coincide and also coincide with the lability degree of the full system, since it can be shown (see Eq (8) in reference [30]) that the last one is a weighted average of the particular lability degrees of the present complexes. The particular lability degree of a complex is not usually measurable. However, in excess of ligand conditions, the lability degree of successive complexes in equilibrium with ML_1 can be measured, since all these complexes have a common lability degree which coincides with that of the system.

In Figure. 4.2, the existing equilibrium between some Ni species (in some regions) does not show up as a collapse of the concentration profiles (of the species in equilibrium), due to the system not being under ligand excess conditions.

The dependence of the lability degree on the thickness of the diffusive gel or of the resin follows the same trend commented in the above section and for the same reasons.

Almost all transition metals yield ML_n complexes with simple ligands due to the high number of possible bonds in the coordination sphere and almost all of these ligands are involved in acid-base equilibria. Thus, the effects commented above are of a broad applicability to most of the trace metal complexes. As general conclusion, the model here

developed suggests that lability decreases as the ligand-to-metal ratio increases, i.e., as the ligand-to-metal stoichiometry (*n*) of the dominant species increases.

4.7 CONCLUSIONS

Speciation in natural systems is challenging since many measurements involve the contribution of multiple species through several physicochemical parameters. Accordingly, a set of independent measurements and a suitable theoretical framework is required to solve the speciation unless more selective analytical techniques were developed. Based on using a set of DGT devices with different resin or diffusive gel thicknesses, this work paves the way to optimize the correlation between chemical composition and bioavailability, as well as it lays out a framework to solve the speciation and labilities of complexes present in natural samples.

It is shown that the lability degree increases as the thickness of either the diffusive gel or the resin disc of the DGT device increases. A simple analytical expression is shown to reproduce accurately this dependence in excess of ligand condition as usually met in trace metal analysis. Defining effective concentrations and parameters, this expression can be extended to systems with sequential complexation. In this case, an increase of the ligand concentration tends to decrease the lability degree of the system due to a decrease of the effective dissociation rate constant. The decrease of the lability degree is more evident when, following the increase of the ligand concentration, the main complex present in the solution moves from ML to ML_n. Only the fitting of the dissociation constant of ML is required for the interpretation of the lability of the ML_n system with any DGT configuration.

4.8 Acknowledgements

Support from the Spanish Minister of Science and Innovation is gratefully acknowledged (Project PID2019-107033GB-C21). JSD acknowledges the University of Lleida for a fellowship PhD contract.

4.9 References

1. Bakker, E.; Pretsch, E., Modern Potentiometry. *Angewandte Chemie-International Edition* **2007,** *46* (30), 5660-5668.
2. Temminghoff, E. J. M.; Plette, A. C. C.; van Eck, R.; van Riemsdijk, W. H., Determination of the chemical speciation of trace metals in aqueous systems by the Wageningen Donnan Membrane Technique. *Analytica Chimica Acta* **2000,** *417* (2), 149-157.
3. Parat, C.; Pinheiro, J. P., ISIDORE, a probe for in situ trace metal speciation based on Donnan membrane technique with related electrochemical detection part 1: Equilibrium measurements. *Analytica Chimica Acta* **2015,** *896*, 1-10.
4. Lao, M.; Companys, E.; Weng, L.; Puy, J.; Galceran, J., Speciation of Zn, Fe, Ca and Mg in wine with the Donnan Membrane Technique. *Food Chemistry* **2018,** *239*, 1143-1150.
5. Companys, E.; Galceran, J.; Puy, J.; Sedo, M.; Vera, R.; Antico, E.; Fontas, C., Comparison of different speciation techniques to measure Zn availability in hydroponic media. *Analytica Chimica Acta* **2018,** *1035*, 32-43.
6. Noel, S.; Tercier-Waeber, M. L.; Lin, L.; Buffle, J., Complexing gel integrated microelectrode arrays for direct detection of free metal ion concentrations in natural waters. *Journal de Physique Iv* **2003,** *107*, 965-968.
7. Mikkelsen, O.; van den Berg, C. M. G.; Schroder, K. H., Determination of labile iron at low nmol L-1 levels in estuarine and coastal waters by anodic stripping voltammetry. *Electroanalysis* **2006,** *18* (1), 35-43.
8. Cindric, A. M.; Marcinek, S.; Garnier, C.; Salaun, P.; Cukrov, N.; Oursel, B.; Lenoble, V.; Omanovic, D., Evaluation of diffusive gradients in thin films (DGT) technique for speciation of trace metals in estuarine waters - A multimethodological approach. *Science of the Total Environment* **2020,** *721*.
9. Parthasarathy, N.; Pelletier, M.; Buffle, J., The use of Permeation Liquid Membrane (PLM) as an analytical tool for trace metal speciation studies in natural waters. *Journal de Physique Iv* **2003,** *107*, 1021-1024.
10. Gramlich, A.; Tandy, S.; Slaveykova, V. I.; Duffner, A.; Schulin, R., The use of permeation liquid membranes for free zinc measurements in aqueous solution. *Environmental Chemistry* **2012,** *9* (5), 429-437.
11. Vera, R.; Fontas, C.; Galceran, J.; Serra, O.; Antico, E., Polymer inclusion membrane to access Zn speciation: Comparison with root uptake. *Science of the Total Environment* **2018,** *622*, 316-324.
12. van Leeuwen, H. P.; Town, R. M.; Buffle, J.; Cleven, R.; Davison, W.; Puy, J.; van Riemsdijk, W. H.; Sigg, L., Dynamic speciation analysis and bioavailability of metals in Aquatic Systems. *Environmental Science and Technology* **2005,** *39*, 8545-8585.
13. Worms, I.; Simon, D. F.; Hassler, C. S.; Wilkinson, K. J., Bioavailability of trace metals to aquatic microorganisms: importance of chemical, biological and physical processes on biouptake. *Biochimie* **2006,** *88* (11), 1721-1731.
14. Davison, W.; Zhang, H., In-situ speciation measurements of trace components in natural- waters using thin-film gels. *Nature* **1994,** *367* (6463), 546-548.
15. Galceran, J.; Puy, J., Interpretation of diffusion gradients in thin films (DGT) measurements: a systematic approach. *Environmental Chemistry* **2015,** *12* (2), 112-122.

16. Menegario, A. A.; Yabuki, L. N. M.; Luko, K. S.; Williams, P. N.; Blackburn, D. M., Use of diffusive gradient in thin films for in situ measurements: A review on the progress in chemical fractionation, speciation and bioavailability of metals in waters. *Analytica Chimica Acta* **2017,** *983*, 54-66.
17. Canovas, C. R.; Basallote, M. D.; Borrego, P.; Milian-Becerro, R.; Perez-Lopez, R., Metal partitioning and speciation in a mining-impacted estuary by traditional and passive sampling methods. *Science of the Total Environment* **2020,** *722*.
18. Levy, J. L.; Zhang, H.; Davison, W.; Puy, J.; Galceran, J., Assessment of trace metal binding kinetics in the resin phase of diffusive gradients in thin films. *Analytica Chimica Acta* **2012,** *717*, 143-150.
19. Huang, J. Y.; Bennett, W. W.; Welsh, D. T.; Li, T. L.; Teasdale, P. R., "Diffusive Gradients in Thin Films" Techniques Provide Representative Time-Weighted Average Measurements of Inorganic Nutrients in Dynamic Freshwater Systems. *Environmental Science and Technology* **2016,** *50* (24), 13446-13454.
20. Altier, A.; Jimenez-Piedrahita, M.; Rey-Castro, C.; Cecilia, J.; Galceran, J.; Puy, J., Accumulation of Mg to diffusive gradients in thin films (DGT) devices: kinetic and thermodynamic effects of the ionic strength. *Analytical Chemistry* **2016,** *88* (20), 10245-10251.
21. Galceran, J.; Puy, J.; Salvador, J.; Cecília, J.; van Leeuwen, H. P., Voltammetric lability of metal complexes at spherical microelectrodes with various radii. *Journal of Electroanalytical Chemistry* **2001,** *505* (1-2), 85-94.
22. Puy, J.; Galceran, J., Theoretical aspects of dynamic metal speciation with electrochemical techniques. *Curr.Opin.Electrochem.* **2017,** *1* (1), 80-87.
23. Mongin, S.; Uribe, R.; Puy, J.; Cecilia, J.; Galceran, J.; Zhang, H.; Davison, W., Key role of the resin layer thickness in the lability of complexes measured by DGT. *Environ.Sci.Technol.* **2011,** *45* (11), 4869-4875.
24. Uribe, R.; Mongin, S.; Puy, J.; Cecilia, J.; Galceran, J.; Zhang, H.; Davison, W., Contribution of partially labile complexes to the DGT metal flux. *Environmental Science and Technology* **2011,** *45* (12), 5317-5322.
25. Levy, J. L.; Zhang, H.; Davison, W.; Galceran, J.; Puy, J., Kinetic Signatures of Metals in the Presence of Suwannee River Fulvic Acid. *Environmental Science and Technology* **2012,** *46* (6), 3335-3342.
26. Warnken, K. W.; Davison, W.; Zhang, H., Interpretation of in situ speciation measurements of inorganic and organically complexed trace metals in freshwater by DGT. *Environmental Science and Technology* **2008,** *42* (18), 6903-6909.
27. Baeyens, W.; Gao, Y.; Davison, W.; Galceran, J.; Leermakers, M.; Puy, J.; Superville, P. J.; Beguery, L., In situ measurements of micronutrient dynamics in open seawater show that complex dissociation rates may limit diatom growth. *Scientific Reports* **2018,** *8*.
28. Gao, Y.; Zhou, C. Y.; Gaulier, C.; Bratkic, A.; Galceran, J.; Puy, J.; Zhang, H.; Leermakers, M.; Baeyens, W., Labile trace metal concentration measurements in marine environments: From coastal to open ocean areas. *Trac-Trends in Analytical Chemistry* **2019,** *116*, 92-101.
29. Salvador, J.; Puy, J.; Cecilia, J.; Galceran, J., Lability of complexes in steady state finite planar diffusion. *Journal of Electroanalytical Chemistry* **2006,** *588*, 303-313.
30. Uribe, R.; Puy, J.; Cecilia, J.; Galceran, J., Kinetic Mixture Effects in Diffusion Gradients in Thin Films (DGT). *Phys.Chem.Chem.Phys.* **2013,** *15* (27), 11349-11355.

31. Zhao, J. J.; Cornett, R. J.; Chakrabarti, C. L., Assessing the uranium DGT-available fraction in model solutions. *Journal of Hazardous Materials* **2020,** *384*.
32. Puy, J.; Galceran, J.; Cruz-Gonzalez, S.; David, C. A.; Uribe, R.; Lin, C.; Zhang, H.; Davison, W., Metal accumulation in DGT: Impact of ionic strength and kinetics of dissociation of complexes in the resin domain. *Anal. Chem.* **2014,** *86*, 7740-7748.
33. Pommier, A. L.; Buzier, R.; Simon, S.; Guibaud, G., Impact of low ionic strength on DGT sampling with standard APA gels: Effect of pH and analyte. *Talanta* **2021,** *222*, 121413.
34. Puy, J.; Uribe, R.; Mongin, S.; Galceran, J.; Cecilia, J.; Levy, J.; Zhang, H.; Davison, W., Lability Criteria in Diffusive Gradients in Thin Films. *Journal of Physical Chemistry A* **2012,** *116* (25), 6564-6573.
35. Puy, J.; Galceran, J.; Rey-Castro, C., Interpreting the DGT measurement: speciation and dynamics. In *Diffusive Gradients in Thin-Films for environmental measurements*, Davison, W., Ed. Cambridge University Press: Cambridge, 2016; pp 93-122.
36. Altier, A.; Jimenez-Piedrahita, M.; Uribe, R.; Rey-Castro, C.; Cecilia, J.; Galceran, J.; Puy, J., Effects of a mixture of ligands on metal accumulation in diffusive gradients in thin films (DGT). *Environmental Chemistry* **2018,** *15* (3), 183-193.
37. Altier, A. Diffusive Gradients in Thin-Films (DGT) beyond perfect sink conditions, PhD thesis. http://hdl.handle.net/10803/585874. Universitat de Lleida, 2018.
38. Mohan, C., Buffers. A guide for the preparation and use of buffers in biological systems. Merck., C., Ed. Darmstadt (D), 2003.
39. Scally, S.; Davison, W.; Zhang, H., Diffusion coefficients of metals and metal complexes in hydrogels used in diffusive gradients in thin films. *Analytica Chimica Acta* **2006,** *558* (1-2), 222-229.
40. Shiva, A. H.; Teasdale, P. R.; Bennett, W. W.; Welsh, D. T., A systematic determination of diffusion coefficients of trace elements in open and restricted diffusive layers used by the diffusive gradients in a thin film technique. *Analytica Chimica Acta* **2015,** *888*, 146-154.
41. Gustafsson, J. P. *Visual MINTEQ version 3.1.*, 2016.
42. Puy, J.; Cecília, J.; Galceran, J.; Town, R. M.; van Leeuwen, H. P., Voltammetric lability of multiligand complexes. The case of ML_2. *Journal of Electroanalytical Chemistry* **2004,** *571* (2), 121-132.
43. Morel, F. M. M.; Hering, J. G., Complexation. In *Principles and Applications of Aquatic Chemistry*, John Wiley: New York, 1993; Vol. 197, pp 319-420.
44. Jimenez-Piedrahita, M.; Altier, A.; Cecilia, J.; Rey-Castro, C.; Galceran, J.; Puy, J., Influence of the settling of the resin beads on Diffusion Gradients in Thin films measurements. *Analytica Chimica Acta* **2015,** *885*, 148-155.
45. Yezek, L. P.; van Leeuwen, H. P., Donnan effects in the steady-state diffusion of metal ions through charged thin films. *Langmuir* **2005,** *21* (23), 10342-10347.
46. Salvador, J.; Garcés, J. L.; Galceran, J.; Puy, J., Lability of a mixture of metal complexes under steady-state planar diffusion in a finite domain. *Journal of Physical Chemistry B* **2006,** *110* (27), 13661-13669.
47. Zhang, Z. S.; Alemani, D.; Buffle, J.; Town, R. M.; Wilkinson, K. J., Metal flux through consuming interfaces in ligand mixtures: boundary conditions do not influence the lability and relative contributions of metal species. *Physical Chemistry Chemical Physics* **2011,** *13* (39), 17606-17614.

48. Zhang, Z. S.; Buffle, J., Interfacial Metal Flux in Ligand Mixtures. 1. The Revisited Reaction Layer Approximation: Theory and Examples of Applications. *Journal of Physical Chemistry A* **2009,** *113* (24), 6562-6571.

4.10 Supporting Information: Availability of metals to DGT devices with different configurations. The case of sequential Ni complexation.

Jordi Sans-Duñó[a], Joan Cecilia[b], Josep Galceran[a], Jaume Puy[a]*

[a]*Departament de Química,* [b]*Departament de Matemàtica, Universitat de Lleida and AGROTECNIO, Rovira Roure 191, 25198, Lleida, Spain*

* Corresponding author. E-mail address: jpuy@quimica.udl.cat, Phone 34 973 702529, Fax 34 973 702924

Citation: Sans-Duñó J, Cecilia J, Galceran J, Puy J. *Availability of metals to DGT devices with different configurations. The case of sequential Ni complexation*. Sci Total Environ. **779** (2021) 146277.

4.10.1 Formulation of continuity equations in a DGT device when a metal M forms successive metal complexes with a ligand L

Let us consider a system with a metal M and a ligand L which react to yield successive metal complexes. Let us restrict ourselves to the case where only two complexes of stoichiometry ML and ML_2 are formed. Let $K_1 = \frac{k_{a,1}}{k_{d,1}}$ and $K_2 = \frac{k_{a,2}}{k_{d,2}}$ be the equilibrium constants of the successive processes and $k_{a,1}$, $k_{a,2}$, $k_{d,1}$ and $k_{d,2}$ the respective association and dissociation rate constants.

We model the DGT accumulation by considering that the total diffusion thickness consists of the resin layer thickness, δ^r, plus the aggregate thickness of the diffusive gel, filter and diffusive boundary layer (DBL) which we represent just as δ^g (See Figure S 4.1) . This aggregation of diffusion regions is useful whenever the diffusing species have a common diffusion coefficient in all these regions. We are assuming that the diffusion coefficient for the metal D_M is the same, not only in the diffusive gel, in the filter and in the DBL (Diffusive Boundary Layer), but also in the resin. The same is assumed for D_L , D_{ML} and D_{ML_2} [1]. We label the diffusion axis as *x*.

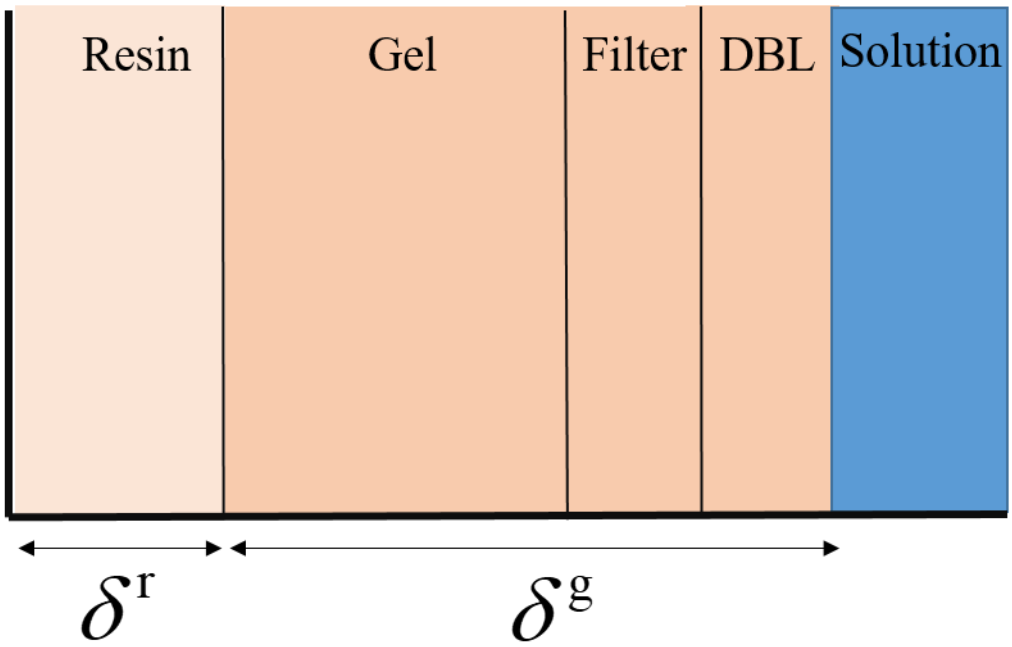

Figure S 4.1 Schematic representation of a DGT device. In this work, the DBL, filter and gel layers are lumped together as a unique diffusion domain whose thickness is labelled as δ^g.

The diffusion-reaction equations can be written as

$$\frac{\partial c_M}{\partial t} = D_M \frac{\partial^2 c_M}{\partial x^2} + k_{d,1} c_{ML} - k_{a,1} c_M c_L \quad \text{(S4.1)}$$

$$\frac{\partial c_{ML}}{\partial t} = D_{ML} \frac{\partial^2 c_{ML}}{\partial x^2} - k_{d,1} c_{ML} - k_{a,2} c_{ML} c_L + k_{d,2} c_{ML_2} + k_{a,1} c_M c_L \quad \text{(S4.2)}$$

$$\frac{\partial c_{ML_2}}{\partial t} = D_{ML_2} \frac{\partial^2 c_{ML_2}}{\partial x^2} - k_{d,2} c_{ML_2} + k_{a,2} c_{ML} c_L \quad \text{(S4.3)}$$

$$\frac{\partial c_L}{\partial t} = D_L \frac{\partial^2 c_L}{\partial x^2} + k_{d,1} c_{ML} - k_{a,1} c_M c_L + k_{d,2} c_{ML_2} - k_{a,2} c_{ML} c_L + k_{da,1} c_{HL} - k_{aa,1} c_H^{*(R)} c_L \quad \text{(S4.4)}$$

$$\frac{\partial c_{HL}}{\partial t} = D_{HL} \frac{\partial^2 c_{HL}}{\partial x^2} - k_{da,1} c_{HL} + k_{aa,1} c_H^{*(R)} c_L \quad \text{(S4.5)}$$

We assume that the pH is fixed with the use of a buffer so that $c_H = c_H^*$ for $x > \delta^r$ while $c_H = \Pi c_H^*$ for $x < \delta^r$. We are then assuming that a discontinuity in the proton concentration profile can arise at $x = \delta^r$ as commented below. We have labelled the

proton concentration in Eq (S4.5) as $c_{\mathrm{H}}^{*(R)}$ to recall this discontinuity so that in the resin domain the proton concentration is different than in the diffusive gel domain and we have used $k_{\mathrm{aa},1}$ and $k_{\mathrm{da},1}$ to denote the first association and dissociation rate constant of the proton to the NTA, respectively.

The boundary value problem, at $x = \delta^{\mathrm{r}} + \delta^{\mathrm{g}}$ (where we assume that bulk concentrations are restored due to the natural or artificial stirring) can be written as

$$\begin{aligned} c_{\mathrm{M}} &= c_{\mathrm{M}}^{*} \\ c_{\mathrm{L}} &= c_{\mathrm{L}}^{*} \\ c_{\mathrm{ML}} &= c_{\mathrm{ML}}^{*} \\ c_{\mathrm{ML_2}} &= c_{\mathrm{ML_2}}^{*} \\ c_{\mathrm{HL}} &= c_{\mathrm{HL}}^{*} \end{aligned} \tag{S4.6}$$

At x=0, the boundary conditions can be written as

$$\begin{aligned} \left.\frac{\partial c_{\mathrm{M}}}{\partial x}\right|_{x=0} &= 0 \\ \left.\frac{\partial c_{\mathrm{ML}}}{\partial x}\right|_{x=0} &= 0 \\ \left.\frac{\partial c_{\mathrm{ML_2}}}{\partial x}\right|_{x=0} &= 0 \\ \left.\frac{\partial c_{\mathrm{L}}}{\partial x}\right|_{x=0} &= 0 \\ \left.\frac{\partial c_{\mathrm{HL}}}{\partial x}\right|_{x=0} &= 0 \end{aligned} \tag{S4.7}$$

indicating that no flux is crossing the plane x=0. Assuming (as said before) that the species share a common diffusion coefficient in the diffusive gel and the resin layer, continuity equations at the gel-resin interface (x=r) become:

$$\left.\frac{\partial c_{\mathrm{M}}}{\partial x}\right|_{r-} = \left.\frac{\partial c_{\mathrm{M}}}{\partial x}\right|_{r+} \tag{S4.8}$$

$$\left.\frac{\partial c_{\mathrm{L}}}{\partial x}\right|_{r-} = \left.\frac{\partial c_{\mathrm{L}}}{\partial x}\right|_{r+} \tag{S4.9}$$

$$\left.\frac{\partial c_{\mathrm{ML}}}{\partial x}\right|_{r-} = \left.\frac{\partial c_{\mathrm{ML}}}{\partial x}\right|_{r+} \tag{S4.10}$$

$$\left.\frac{\partial c_{\mathrm{ML_2}}}{\partial x}\right|_{r-} = \left.\frac{\partial c_{\mathrm{ML_2}}}{\partial x}\right|_{r+} \tag{S4.11}$$

$$\left.\frac{\partial c_{\mathrm{HL}}}{\partial x}\right|_{r-} = \left.\frac{\partial c_{\mathrm{HL}}}{\partial x}\right|_{r+} \tag{S4.12}$$

Additionally, the negative charge of the resin can induce a migration flux and a gradient of the electrical potential at the resin-gel interphase. As the gradient of the electrical potential is located in a thin layer (of the order of the Debye length which at I =100 mM is of the order of 10^{-9} m) close to the resin-diffusive gel interface, while resin and diffusive gel layers have a thickness of the order of 10^{-3} m, the electrostatic effects are modelled using the Donnan partition model which considers the electrical potential as a step function located at the resin-gel interphase. Accordingly, concentrations at x=r are related [2-4]through:

$$\frac{c_i^{\mathrm{r^-}}}{c_i^{\mathrm{r^+}}} = \exp\left(\frac{z_i F \Psi_{\mathrm{D}}}{RT}\right) = \Pi^{z_i} \tag{S4.13}$$

where F is the Faraday constant, R the gas constant, and T the absolute temperature. Ψ_{D} is the electric potential difference between both phases, and $c_i^{\mathrm{r^-}}$ and $c_i^{\mathrm{r+}}$ are the concentrations of species i at the resin and diffusive gel sides, respectively, z_i is the electrical charge of the species i, and Π is the so-called Boltzmann factor for a species of charge 1. As described in the main manuscript, Π is experimentally measured by adding Rb in the solution and dividing the Rb concentration at the bulk solution by the concentration of rubidium in the resin disk.

Eqs.(S4.1)-(S4.4) with the boundary conditions Eqs (S4.6)-(S4.13) have been numerically solved using the Finite Element Method. Details of the application of this method to this system are reported elsewhere [5]

4.10.1.1 Formulation when excess of ligand conditions applies. Transformation of the formulation of the diffusion-reaction processes for a system with ML and ML2 into a system with only one formal complex

In excess of ligand conditions ($c^*_{T,L} >> c^*_{T,M}$), instead of Eq (S4.4) one can consider

$$c_L\left(0 \le x \le \delta^{r^-}\right) = \Pi^{z_L} c^*_L \tag{S4.14}$$

$$c_L\left(\delta^{r^+} \le x \le \delta^r + \delta^g\right) = c^*_L \tag{S4.15}$$

The ligand concentration profile is flat except at the resin-diffusive gel interface where a discontinuity arises. When the ligand is negatively charged, $\Pi^{z_L} < 1$ and the ligand concentration in the resin domain is $\Pi^{z_L} c^*_L < c^*_L$.

Indeed, the equilibrium constants K_1 and K_2 hold everywhere, but $K_1^{'} = K_1 c_L$ and $K_2^{'} = K_2 c_L$ take discontinuous values whenever the ligand is a charged species in agreement with the discontinuous c_L .

The relationship between $K_i^{'}$ inside the resin (denoted as $K_i^{'R}$) and inside the diffusive gel domains (denoted just as $K_i^{'}$) can be written as:

$$K_i^{'R} = K_i^{'} \Pi^{z_L} \tag{S4.16}$$

In general, in a set of successive complexes, the dissociation of ML into M and L is usually the rate limiting step [6-7]. Accordingly, it is reasonable to assume that ML_2, ML_3, and successive complexes are in equilibrium with ML, but not with M if they are partially labile. Below it is shown that these equilibrium relationships allow to reformulate the reaction-diffusion set of equations corresponding to the DGT processes in a scheme formally analogous to the case of only one complex of 1:1 metal-to-ligand stoichiometry.

Let us label ML_{eff} to a formal complex whose concentration is given by

$$c_{ML,eff} = c_{ML} + c_{ML_2} \tag{S4.17}$$

Using the equilibrium constant K_2, both c_{ML} and c_{ML_2} can be written in terms of $c_{ML,eff}$.

$$c_{\mathrm{ML}} = \frac{c_{\mathrm{ML,eff}}}{1+K_2^{'}} \tag{S4.18}$$

$$c_{\mathrm{ML_2}} = \frac{K_2^{'} c_{\mathrm{ML,eff}}}{1+K_2^{'}} \tag{S4.19}$$

Adding up the diffusion-reaction equations for both complexes, Eq (S4.2) and Eq (S4.3), and replacing both c_{ML} and $c_{\mathrm{ML_2}}$ in terms of $c_{\mathrm{ML,eff}}$, we have:

$$0 = D_{\mathrm{ML,eff}} \frac{\partial^2 c_{\mathrm{ML,eff}}}{\partial x^2} + k_{\mathrm{a}} c_{\mathrm{M}} c_{\mathrm{L}}^{*} - k_{\mathrm{d,eff}} c_{\mathrm{ML,eff}} \tag{S4.20}$$

where,

$$D_{\mathrm{ML,eff}} = \frac{D_{\mathrm{ML}} + D_{\mathrm{ML_2}} K_2^{'}}{1+K_2^{'}} \tag{S4.21}$$

and

$$k_{\mathrm{d,eff}} = \frac{k_{\mathrm{d,1}}}{1+K_2^{'}} \tag{S4.22}$$

Eq (S4.20) is formally identical to the reaction-diffusion equation for a system $\mathrm{M+L} \rightleftharpoons \mathrm{ML}$, so that the formulation of the transport phenomena in a DGT device for a system with a metal and two successive complexes is formally analogous to the formulation of a simple $\mathrm{M+L} \rightleftharpoons \mathrm{ML}$ system whenever dissociation of ML into M and L is the rate limiting in the dissociation process and effective concentrations, rate constants and diffusion coefficients given by Eqs (S4.17), (S4.21) and (S4.22) are considered.

The diffusion coefficient, effective stability relationship, effective dissociation rate constant as well as other related parameters of the effective complex take different values depending on the diffusion phase considered. Thus, according to equations (S4.21) and (S4.22) for the gel layer these parameters become:

$$K_{\mathrm{eff}}^{'} = K_1^{'}\left(1+K_2^{'}\right) \tag{S4.23}$$

$$D_{\mathrm{ML,eff}} = \frac{D_{\mathrm{ML}} + D_{\mathrm{ML}_2} K_2^{'}}{1 + K_2^{'}} \quad \text{(S4.24)}$$

$$k_{\mathrm{d,eff}} = \frac{k_{\mathrm{d},1}}{1 + K_2^{'}} \quad \text{(S4.25)}$$

$$\mu = \sqrt{\frac{D_{\mathrm{M}}}{k_{\mathrm{a},1} c_{\mathrm{L}}^{*}}} \quad \text{(S4.26)}$$

$$\varepsilon_{\mathrm{eff}} = \frac{D_{\mathrm{ML,eff}}}{D_{\mathrm{M}}} \quad \text{(S4.27)}$$

$$m_{\mathrm{eff}} = \mu \sqrt{\frac{\varepsilon_{\mathrm{eff}} K_{\mathrm{eff}}^{'}}{1 + \varepsilon_{\mathrm{eff}} K_{\mathrm{eff}}^{'}}} \quad \text{(S4.28)}$$

while for the resin layer:

$$D_{\mathrm{ML,eff}}^{\mathrm{R}} = \frac{D_{\mathrm{ML}} + D_{\mathrm{ML}_2} \Pi^{z_{\mathrm{L}}} K_2^{'}}{1 + \Pi^{z_{\mathrm{L}}} K_2^{'}} \quad \text{(S4.29)}$$

$$k_{\mathrm{d,eff}}^{\mathrm{R}} = \frac{k_{\mathrm{d}}}{1 + \Pi^{z_{\mathrm{L}}} K_2^{'}} \quad \text{(S4.30)}$$

$$K_{\mathrm{eff}}^{'\mathrm{R}} = K_1^{'} \left(1 + \Pi^{z_{\mathrm{L}}} K_2^{'}\right) \quad \text{(S4.31)}$$

$$\lambda_{\mathrm{ML,eff}}^{\mathrm{R}} = \sqrt{\frac{D_{\mathrm{ML,eff}}^{\mathrm{R}}}{k_{\mathrm{d,eff}}^{\mathrm{R}}}} \quad \text{(S4.32)}$$

$$\varepsilon_{\mathrm{eff}}^{\mathrm{R}} = \frac{D_{\mathrm{ML,eff}}^{\mathrm{R}}}{D_{\mathrm{M}}} \quad \text{(S4.33)}$$

4.10.2 Boltzmann factor for the formal complex

The formal complex, see Eq.(S4.17) ,is composed of two species (c_{ML} and c_{ML_2}) that have different electrical charge (z_{ML} and z_{ML_2}). The partition of these species at the resin-diffusive gel interface is given by the respective Boltzmann factors.

$$\frac{c_{ML}^{r^-}}{c_{ML}^{r^+}} = \Pi^{z_{ML}} \tag{S4.34}$$

$$\frac{c_{ML_2}^{r^-}}{c_{ML_2}^{r^+}} = \Pi^{z_{ML_2}} \tag{S4.35}$$

To derive an expression for the Boltzmann factor of the effective complex concentration, it is necessary to relate $c_{ML,eff}^{r^+}$ with $c_{ML,eff}^{r^-}$. Recalling that

$$c_{ML,eff}^{r^-} = c_{ML}^{r^-} + c_{ML_2}^{r^-} \tag{S4.36}$$

and replacing $c_{ML}^{r^-} = c_{ML}^{r^+}\Pi^{z_{ML}}$ and $c_{ML_2}^{r^-} = c_{ML_2}^{r^+}\Pi^{z_{ML_2}}$ into (S4.36),

$$c_{ML,eff}^{r^-} = c_{ML}^{r^+}\Pi^{z_{ML}} + c_{ML_2}^{r^+}\Pi^{z_{ML_2}} \tag{S4.37}$$

Equilibrium relationships, Eqs. (S4.18) and (S4.19), allow to relate $c_{ML}^{r^+}$ and $c_{ML_2}^{r^+}$ with $c_{ML,eff}^{r^+}$ so that:

$$\Pi_{eff} = \frac{c_{ML,eff}^{r^-}}{c_{ML,eff}^{r^+}} = \frac{\Pi^{z_{ML}} + K_2 c_L^* \Pi^{z_{ML_2}}}{1 + K_2 c_L^*} \tag{S4.38}$$

which can also be written as

$$\Pi_{eff} = \frac{c_{ML,eff}^{r^-}}{c_{ML,eff}^{r^+}} = \Pi^{z_{ML}} \frac{c_{ML}^*}{c_{ML}^* + c_{ML_2}^*} + \Pi^{z_{ML_2}} \frac{c_{ML_2}^*}{c_{ML}^* + c_{ML_2}^*} \tag{S4.39}$$

Eq. (S4.39) indicates that Π_{eff} is the weighted average of the Boltzmann factors of both species ML and ML_2.

4.10.2.1 The lability degree for the formal complex

According to Eq (S4.20), the lability degree in a system with successive complexes ML and ML_2 is given by the lability degree of a system $M+L \rightleftharpoons ML$, given in Eq (10) of a previously published work [8], once the parameters of the formal complex, Eqs (S4.23)-(S4.33) are used. Accordingly,

$$\xi = 1 - \frac{\left(1+\varepsilon_{\text{eff}} K'_{\text{eff}}\right)}{\varepsilon_{\text{eff}} K'_{\text{eff}} + \frac{\delta^{\text{g}}}{m_{\text{eff}}} \coth\left(\frac{\delta^{\text{g}}}{m_{\text{eff}}}\right) + \frac{\delta^{\text{g}} \Pi_{\text{eff}} \left(1+\varepsilon_{\text{eff}} K'_{\text{eff}}\right)}{\lambda^{\text{R}}_{\text{ML,eff}}} \frac{D^{\text{R}}_{\text{ML,eff}}}{D_{\text{ML,eff}}} \tanh\left(\frac{\delta^{\text{r}}}{\lambda^{\text{R}}_{\text{ML,eff}}}\right)} \quad \text{(S4.40)}$$

4.10.2.2 Fitting chart-flow to estimate the dissociation rate constant from the lability degree of a complex in a system $M+L \rightleftharpoons ML$.

The following chart-flow summarizes an algorithm to obtain k_d of a complex in a system with the scheme $M+L \rightleftharpoons ML$ from Eq (12) in reference [8]:

$$\xi = 1 - \frac{\left(1+\varepsilon K'\right)}{\varepsilon K' + \frac{\delta^{\text{g}}\sqrt{1+\varepsilon K'}}{\mu\sqrt{\varepsilon K'}} \coth\left(\frac{\delta^{\text{g}}\sqrt{1+\varepsilon K'}}{\mu\sqrt{\varepsilon K'}}\right) + \frac{\delta^{\text{g}} \Pi^{z_{\text{ML}}} \left(1+\varepsilon K'\right)}{\mu\sqrt{\varepsilon K'}} \tanh\left(\frac{\delta^{\text{r}}}{\mu\sqrt{\varepsilon K'}}\right)} \quad \text{(S4.41)}$$

The meaning of the physical parameters, $m = \frac{\mu\sqrt{\varepsilon K'}}{\sqrt{1+\varepsilon K'}}$ and $\lambda_{\text{ML}} = \mu\sqrt{\varepsilon K'}$ can be found elsewhere [8].

The algorithm requires an educated guess of the initial value for μ, usually of the order of 10^{-6} m. When the difference between the previous and the new value of μ is less than a given tolerance (e.g. 10^{-9} m), self-consistence is reached and the kinetic dissociation constant is obtained.

For the sake of simplicity, the expressions $\coth\left(\frac{\delta^{\text{g}}\sqrt{1+\varepsilon K'}}{\mu\sqrt{\varepsilon K'}}\right)$ and $\tanh\left(\frac{\delta^{\text{r}}}{\mu\sqrt{\varepsilon K'}}\right)$ are substituted for *a* and *b* in the following flow chart.

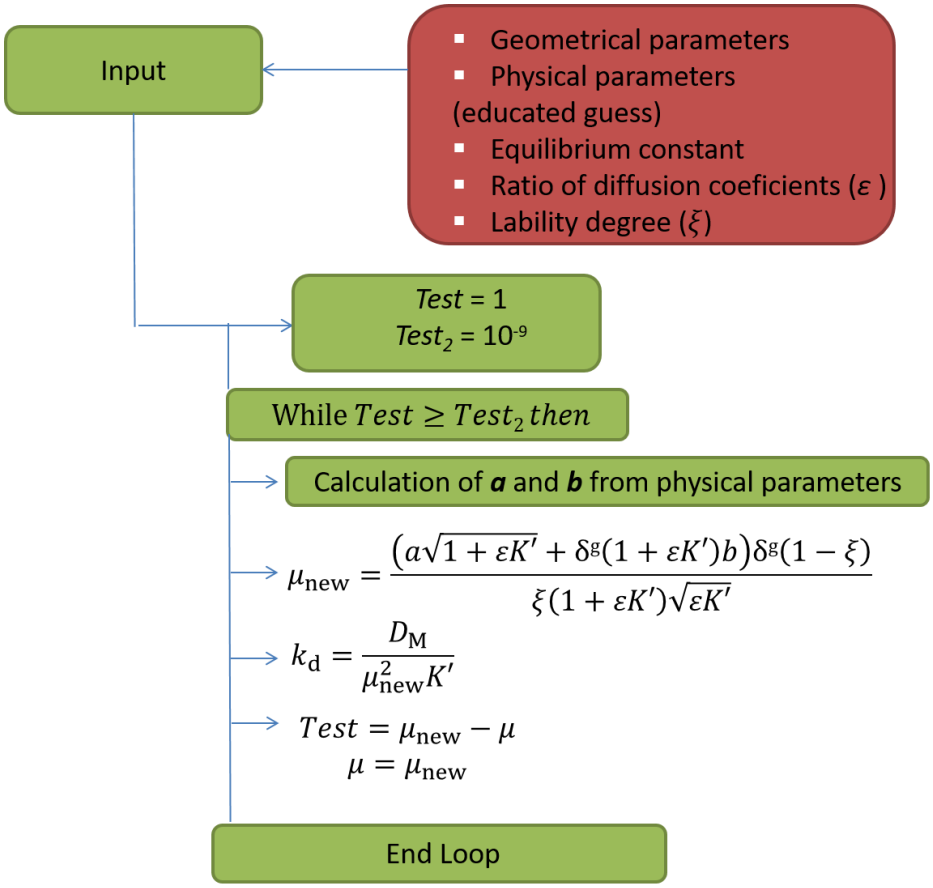

Figure S 4.2 Flow chart algorithm designed to calculate the kinetic dissociation constant, where a and b stand for $\coth\left(\frac{\delta^{g}\sqrt{1+\varepsilon K'}}{\mu\sqrt{\varepsilon K'}}\right)$ *and* $\tanh\left(\frac{\delta^{r}}{\mu\sqrt{\varepsilon K'}}\right)$*, respectively.*

4.10.3 Experimental set-up for DGT measurements.

Plastic holders (or caps), resins and diffusive gels have been received from DGT research. DGT devices have been prepared in a laminar flux hood fume on a high density polyethylene (HDPE) opaque sheet. Tweezers have been used for assembling resin, gel discs and a filter on a piston base, then a plastic holder is added on the top. Previously, plastic caps and pistons have been washed 3 times with HNO_3 10% during 24 hours and rinsed with Ultrapure water with a resistivity higher than 18 $\mu\Omega$ cm $^{-1}$ [9].

4.10.4 Speciation of Ni and NTA solutions.

Speciation of solutions of Table 1 of the main manuscript is obtained with VMINTEQ and reported in Table S 4.1 and Table S 4.2

Table S 4.1 Percentage of Ni species calculated using VMINTEQ based on experimental working conditions corresponding to Exp A ($c_{T,Ni}$=0.035 mmol L^{-1}, $c_{T,NTA}$=0.055 mmol L^{-1}) and Exp B ($c_{T,Ni}$=0.035 mmol L^{-1}, $c_{T,NTA}$=1.14 mmol L^{-1}) of Table 1 from the main manuscript.

% Ni speciation	Exp A	Exp B
Ni	0.0018	$2.03x10^{-5}$
NiNTA	98.84	61.53
$Ni(NTA)_2$	1.010	38.44

Table S 4.2 Percentage of NTA species calculated using VMINTEQ based on experimental working conditions as in Table S 4.1 .

% NTA Speciation	Exp A	Exp B
H_2NTA^-	$2.987x10^{-4}$	$8.061 x10^{-4}$
$H_3NTA_{(aq)}$	$4.548x10^{-10}$	$1.227 x10^{-9}$
H_4NTA^+	$1.189x10^{-16}$	$3.209 x10^{-16}$
$HNTA^{-2}$	35.60	96.08
$Ni(NTA)_2^{-4}$	0.7047	1.184
$NiNTA^-$	63.35	1.895
$NiOHNTA^{-2}$	$3.341x10^{-2}$	$9.994 x10^{-4}$
NTA^{-3}	0.3123	0.8426

4.10.5 Experimental details for the set-up procedure in the diffusion-cell

Before the experiment, acceptor and donor compartments, two plastic tweezers and a plastic spacer have been washed with Ultrapure MQ water. Afterwards, they have been rinsed in a closed compartment with HNO_3 10% during 24 hours. This procedure is repeated 3 times.

The set-up of the diffusion cell consisted in mounting the donor and acceptor compartments. In the mounting process, before introducing an APA gel, it is necessary to put (on the top of the surface of one of the tilt compartments) a plastic spacer with a similar thickness to that of the gel. This spacer presents a hole with a diameter slightly larger than the gel, thus the gel can perfectly fit in it. The APA gel has been introduced with clean tweezers on the surface of the hole. Both cells are clamped by a compressing tool. Once the set-up is completed, it can be introduced into a thermostatic bath (Polyscience Thermostat) to keep the temperature constant [10].

During the experiment, both cells are submitted to a controlled agitation using plastic mechanical stirrers. Every 20 min three samples from each compartment are taken and pH is measured using Orion™ Dual Star with double channel. Each channel is connected to an electrode (previously calibrated with three standard solutions of pH 7, 4 and 10) which is exclusively used for one of the compartments. The experiment is finished approximately within 3 hours.

In experiments 2 to 4, donor and acceptor solutions have been preconditioned. They have been stirred during 24 hours at the experimental temperature (24.9°C) using Labnet 211DS .This procedure is extremely important when the solution is composed by a metal and a ligand. For experiment 1, the donor solution has been stirred using a Mini Digital Vortex Mixer VXMNDG for at least 1 minute in order to ensure a homogenized concentration.

4.10.6 Experimental results: accumulation vs time in acceptor diffusion-cell compartment.

The time-accumulation plots recorded for experiments 1 to 4 (reported in Table 2 of the main manuscript) are included below.

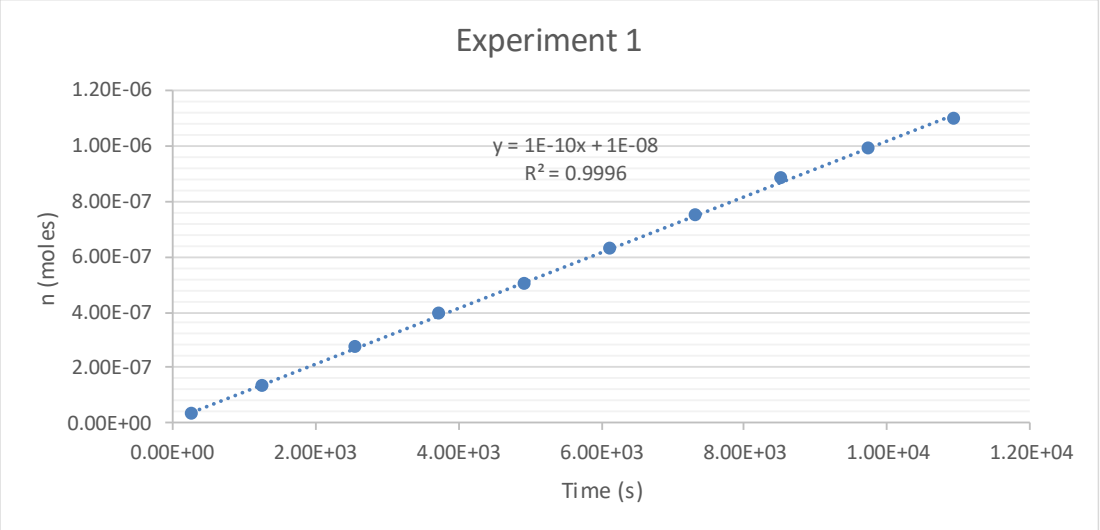

Figure S 4.3 Moles of Ni^{+2} accumulated in the acceptor diffusion cell over time using an APA gel of thickness 0.629 mm for experimental conditions of Exp 1 of Table 2 from the main manuscript

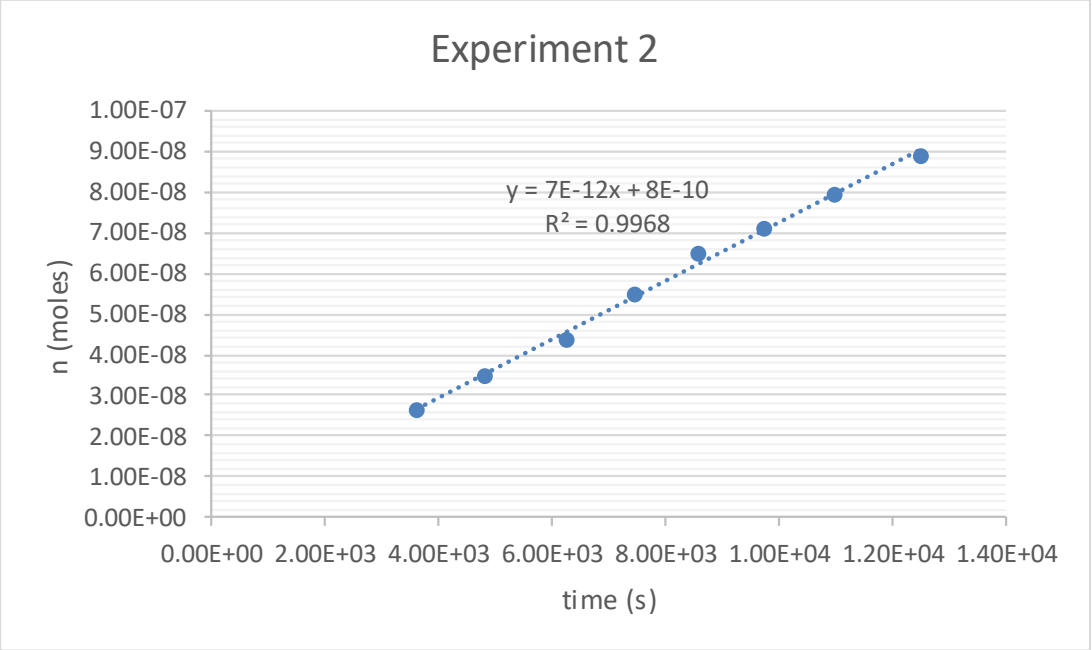

Figure S 4.4 Moles of Ni^{+2} accumulated in the acceptor diffusion cell over time using an APA gel of thickness 0.629 mm for experimental conditions of Exp 2 of Table 2 from the main manuscript.

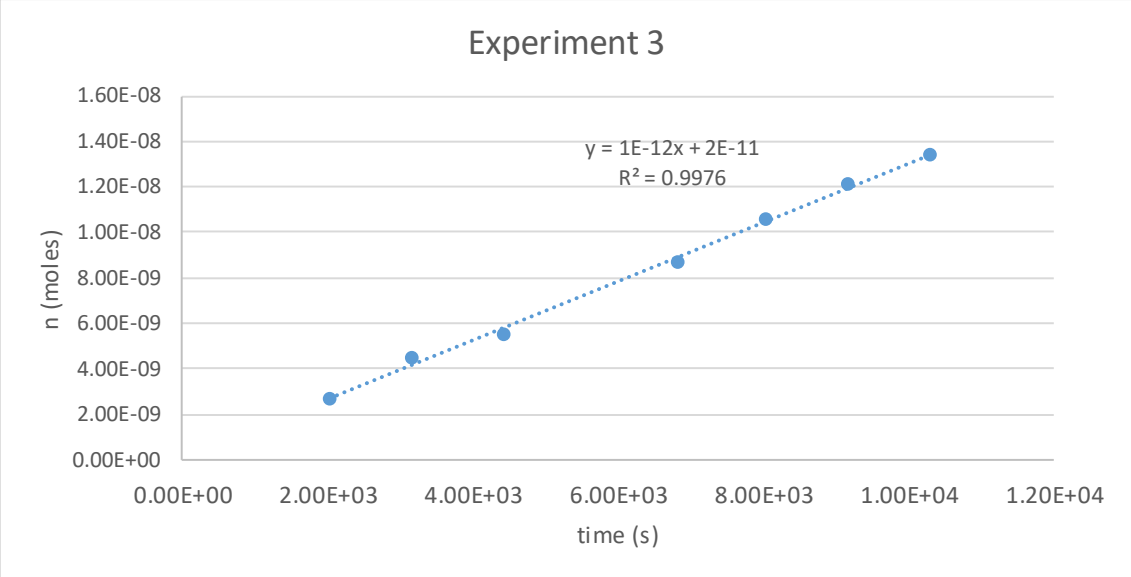

Figure S 4.5 Moles of Ni^{+2} accumulated in the acceptor diffusion cell over time using an APA gel of thickness 0.629 mm for experimental conditions of Exp 3 of Table 2 from the main manuscript.

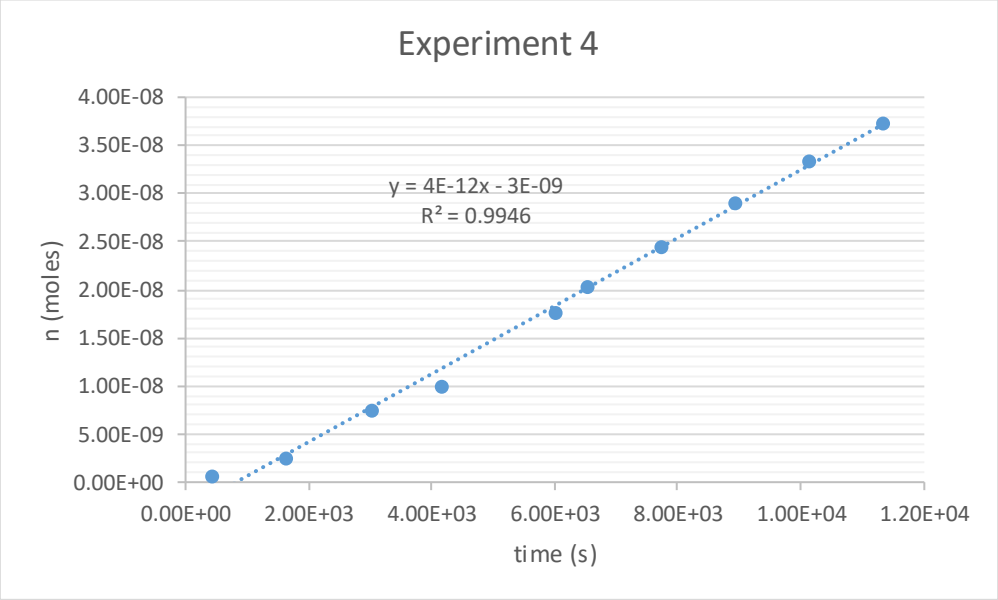

Figure S 4.6 Moles of Ni^{+2} accumulated in the acceptor diffusion cell over time using two APA gels of thicknesses 0.629 mm for experimental conditions of Exp 4 of Table 2 from the main manuscript.

4.10.7 References

1. Puy, J.; Galceran, J.; Rey-Castro, C., Interpreting the DGT measurement: speciation and dynamics. In *Diffusive Gradients in Thin-Films for environmental measurements*, Davison, W., Ed. Cambridge University Press: Cambridge, 2016; pp 93-122.
2. Altier, A.; Jimenez-Piedrahita, M.; Rey-Castro, C.; Cecilia, J.; Galceran, J.; Puy, J., Accumulation of Mg to diffusive gradients in thin films (DGT) devices: kinetic and thermodynamic effects of the ionic strength. *Analytical Chemistry* **2016,** *88* (20), 10245-10251.
3. Ohshima, H.; Ohki, S., Donnan potential and surface-potential of a charged membrane. *BIOPHYSICAL JOURNAL* **1985,** *47* (5), 673-678.
4. Puy, J.; Galceran, J.; Cruz-Gonzalez, S.; David, C. A.; Uribe, R.; Lin, C.; Zhang, H.; Davison, W., Metal accumulation in DGT: Impact of ionic strength and kinetics of dissociation of complexes in the resin domain. *Anal. Chem.* **2014,** *86*, 7740-7748.
5. Jimenez-Piedrahita, M.; Altier, A.; Cecilia, J.; Rey-Castro, C.; Galceran, J.; Puy, J., Influence of the settling of the resin beads on Diffusion Gradients in Thin films measurements. *Analytica Chimica Acta* **2015,** *885*, 148-155.
6. Morel, F. M. M., *Principles and applications of aquatic chemistry*. Wiley: New York, 1983.
7. Puy, J.; Cecília, J.; Galceran, J.; Town, R. M.; van Leeuwen, H. P., Voltammetric lability of multiligand complexes. The case of ML_2. *Journal of Electroanalytical Chemistry* **2004,** *571* (2), 121-132.
8. Uribe, R.; Mongin, S.; Puy, J.; Cecilia, J.; Galceran, J.; Zhang, H.; Davison, W., Contribution of partially labile complexes to the DGT metal flux. *Environmental Science and Technology* **2011,** *45* (12), 5317-5322.
9. Altier, A. Diffusive Gradients in Thin-Films (DGT) beyond perfect sink conditions, PhD thesis. http://hdl.handle.net/10803/585874. Universitat de Lleida, 2018.
10. Quattrini, F. Emerging techniques for inorganic metal speciation and bioavailability. Universitat de Lleida, 2018.

5 Back accumulation of Diffusive Gradients in Thin films (DGT) devices with a stack of resin discs to assess availability of metal cations to biota in natural waters

Jordi Sans-Duñó[1,2], Joan Cecilia[3], Josep Galceran[1], Jaume Puy[1]*, Willy Baeyens[2] and Yue Gao[2]

1. Departament de Química. Universitat de Lleida, and AGROTECNIO-CERCA, Rovira Roure 191, 25198 Lleida, Catalonia, Spain

2. Analytical, Environmental & Geochemical (AMGC), Vrije Universiteit Brussel (VUB), Pleinlaan 2, B-1050 Brussels, Belgium

3. Departament de Matemàtica. Universitat de Lleida, and AGROTECNIO-CERCA, Rovira Roure 191, 25198 Lleida, Catalonia, Spain

*Corresponding author. E-mail address: jpuy@quimica.udl.cat, Phone 34 973 702529, Fax 34 973 702924

5.1 Abstract

Determining species, concentrations and physicochemical parameters in natural waters is key to improve our understanding of the functioning of these ecosystems. Diffusive Gradients in Thin-films (DGT) devices with different thicknesses of the resin or of the diffusive disc can be used to collect independent information on relevant parameters. In particular, DGT devices with a stack of two resin discs offer a simple way to determine dissociation rate constants of metal complexes from the accumulation of the target metal in the back resin disc. In this work, simple approximate expressions for the determination of the dissociation rate constant are reported and applied to a model Ni nitrilotriacetic complex as well as to Zn complexes in the Mediterranean Osor stream. Once the physicochemical parameters are known, one can plot the labile fraction of the metal complexes in terms of the thickness of the diffusion domain. These plots reveal a strong dependence on the nature of complexes as well as on the characteristics of the diffusion domain and they are of high interest as predictors of availability to biota whose uptake is limited by diffusion.

5.2 Short synopsis statement

A method to determine dissociate rate constants of metal complexes and to estimate metal bioavailability in environmental waters is reported.

5.3 Introduction

Micronutrients such as Fe, Co, Zn or Mn are governing and limiting autotrophic productivity in High Nutrient Low Chlorophyll (HNLC) areas in the ocean. However, the very complex cellular machinery of phytoplankton species for resource acquisition and for growth makes it necessary to dwell on the concept of "nutrient availability", because trace metals can exist in different forms in the ocean (free ion, weak and strong inorganic and organic complexes and colloids) and they are not all bioavailable. The same reasoning as for the micronutrients can be held for toxic trace metals. Knowledge of trace metal availability is thus of crucial importance to understand key processes such as phytoplankton growth or intoxication of organisms in natural aquatic systems. Availability of metal cations to microorganisms or chemical sensors results from a set of physicochemical and biological phenomena that include at least the mobility and kinetics of dissociation of the species present in the aquatic medium and the internalization of the metal ion, whenever the free metal ion is the only one chemical species able to be internalized, i.e., transported through the cell membrane.[1-4]

The consumption of the metal cation by internalization leads to the development of a free metal concentration profile. All equilibrium processes involving the metal cation are, then, shifted to buffer the metal consumption and both, the kinetics of dissociation and the transport determine the contribution of each species to the accumulation. For trace metals in natural waters, total metal concentrations are well below those of simple or macromolecular ligands and, then, the accumulation is mainly dependent on the properties of the complexes.[5] When transport is the rate-limiting step in the uptake process, the system is called labile, while when dissociation is the rate-limiting step, the accumulation is under kinetic control.[6] Only when the internalization is the rate-limiting step, the concentration profile of all metal species is almost flat, and availability is given by the free metal concentration as predicted by the Biotic Ligand Model (BLM).[7]

In laminar conditions, sufficiently close to the consuming surface of the living organism or of the chemical sensor ($x=\delta^{r}$, in Figure 5.1), the arrival of the metal species takes place by diffusion. Beyond the diffusion domain (i.e. $x>\delta^{r}+\delta^{g}$), bulk concentrations of

free metal and complexes are usually assumed as fulfilling equilibrium conditions, unless experimental measurements lead to other considerations.

The thickness of the diffusion domain defines a timescale window that needs to fit the dissociation of the complex to contribute to its availability.[8] Thus, availability is sensor dependent, so that the metal flux, measured by different analytical techniques such as Diffusive Gradients in Thin-films (DGT), Anodic Stripping Voltammetry or by several measurements of only one technique with configurations where the thickness of the diffusion domain varies, can be used to obtain a labile concentration signature that characterizes the natural water.[9-10]

The contribution of complexes to the metal flux either individually or collectively (the global set of complexes) can be quantified with the so-called lability degree.[11-13]

The lability degree indicates the ratio of the current contribution of a complex (or of all the complexes present in the system, when the global lability degree is considered) to the metal flux over the maximum contribution of this(these) complex(es) that could be reached if dissociation was so fast that complexes were in equilibrium with the free metal at all times and relevant spatial positions.[6,14-16]

DGT devices with a stack of resin discs allow to access the metal accumulation in each resin disc of the stack by separate elution of each one (see Figure 5.1). [17-18] In this work DGT devices with a stack of two resin discs will be used. The top or front resin disc is in contact with the gel disc and it accumulates the free metal arriving by diffusion from the gel disc plus the metal released by dissociation of complexes in this front resin disc.[19] Further away from the sampled solution, we find the bottom or back resin disc where the whole metal accumulated comes from the dissociation of partially labile complexes provided that the front resin disc is far from saturation, the binding agent is well dispersed in the front resin disc (i.e. the free metal cannot diffuse and cross any resin disc without getting bound) and the formation of ternary complexes with the resin sites is negligible. Indeed, since both, the diffusive and resin gels, share common pore sizes, complexes able to diffuse through the diffusive gel disc can also penetrate the front resin disc and the back one, where they will dissociate. A non-negligible presence of mass of a target metal in the back resin disc indicates, then, the presence of partially labile complexes. The use of DGT devices with a stack of resin discs is, then, relevant

to reveal the presence of partially labile complexes, as well as to obtain the dissociation characteristics of these complexes in an easy way.

In this work, a more general expression for the back accumulation is reported without neglecting the accumulation in the front resin disc due to the flux of free metal as done previously.[20] Simple criteria are discussed to decide in which cases the simplified formula yields accurate values of the dissociation rate constant. This discussion suggests that the settling of the resin beads could also be relevant in the back accumulation. Accordingly, an analytical expression for the percentage of back accumulation that takes into account the heterogeneity of the resin beads distribution (due to the settling process during casting) in the DGT resin discs is reported. The procedure is applied to determine the dissociation rate constant of the well-defined Ni nitrilotriacetic acid (NTA) complex, NiNTA. The back accumulation in DGT devices deployed in a Mediterranean river is also used to determine an effective dissociation rate constant for a pool of inorganic zinc complexes in this freshwater. In both cases, dissociation rate constants obtained from the back resin accumulation are compared with values that can be obtained from the total accumulation, since accumulation is also impacted by the lability of complexes.

In this framework, once the dissociation rate constant is known, the “effective” metal concentration seen by biota in the media can be predicted as a function of the thickness of the diffusion domain developed around the surface of the biota driven by the uptake process.

5.4 Theoretical framework: dissociation rate constant and accumulation in DGT devices

5.4.1 Assuming perfect dispersion of the resin beads in the resin disc

DGT is a dynamic technique that measures, for a certain deployment time, the metal accumulation in a resin disc. On top of the resin disc, a diffusive gel is used to define a diffusive domain where the metal species, coming from the aqueous sample, travel by diffusion towards the resin disc. When the binding to the resin is fast and strong, after a short time, the accumulation takes place in a quasi-steady-state regime. The flux in the DGT device can be computed as the accumulation per unit of time and surface, and it depends on speciation, mobilities, labilities and other factors such as pH and ionic strength, among others. For a metal M which only forms a complex, ML, in a given media, the total accumulation can be written as [21]

$$n_{\mathrm{M}} = At\left(\frac{D_{\mathrm{M}}c_{\mathrm{M}}^{*}}{\delta^{\mathrm{g}}} + \frac{D_{\mathrm{ML}}c_{\mathrm{ML}}^{*}}{\delta^{\mathrm{g}}}\xi\right) \tag{5.1}$$

where n_{M} is the accumulation (moles) of M at a certain deployment time t, c_{M}^{*} and c_{ML}^{*} are the bulk equilibrium concentrations of the free metal and complex in the sample solution, D_{M} and D_{ML}, the respective diffusion coefficients, δ^{g} is the thickness of the diffusive gel disc plus that of the Diffusive Boundary Layer (DBL, the extension of the diffusion domain into the solution, omitted in Figure 5.1 for the sake of clarity), A labels the area of the DGT device and ξ is the lability degree of the complex. The lability degree in terms of the physico-chemical parameters, for one complex in excess ligand conditions can be written as: [21-22]

$$\xi = \frac{\varepsilon K'}{\varepsilon K' + \frac{\delta^{\mathrm{g}}}{m}\coth\left(\frac{\delta^{\mathrm{g}}}{m}\right) + \frac{\delta^{\mathrm{g}}(1+\varepsilon K')}{\lambda_{\mathrm{ML}}}\tanh\left(\frac{\delta^{\mathrm{r}}}{\lambda_{\mathrm{ML}}}\right)} \tag{5.2}$$

where $\varepsilon = \frac{D_{\mathrm{ML}}}{D_{\mathrm{M}}}$ describes the ratio of diffusivities, $K' = \frac{c_{\mathrm{ML}}^{*}}{c_{\mathrm{M}}^{*}}$ is the excess-ligand conditional stability constant, δ^{r} is the thickness of the resin layer, λ_{ML} is related to the thickness of complex penetration into the resin layer before full dissociation,

$$\lambda_{ML} = \sqrt{\frac{D_{ML}}{k_d}} \quad (5.3)$$

and *m* is related to the reaction layer thickness in the diffusive gel disc:

$$m = \sqrt{\frac{D_{ML}}{k_d (1+\varepsilon K')}} \quad (5.4)$$

and k_d is the dissociation rate constant.

The lability of complexes in DGT devices tends to be higher than in other sensors due to the (relatively high) thickness of the diffusive gel, of the order of 10^{-3} m, and to the penetration of complexes in the resin disc.[8] Indeed, the reaction layer, where there is net dissociation of the complexes, starts at the neighbourhood of the resin-gel interface and penetrates into the resin domain where free metal concentration is negligible, due to the typical fast and strong binding of the metal to the resin (perfect sink conditions).[21]

In a laboratory experiment, when the speciation and diffusion coefficients are known, Eq (5.1) can be used to determine the lability degree and, in a further step, by solving Eq (5.2) to determine the dissociation rate constant of the complex.

The calculation of the dissociation rate constant from the accumulation can be extended to systems with a mixture of complexes like those in natural media. In presence of a set of complexes, the second term of the r.h.s. of Eq (5.1) would contain a summation for all the complexes. The knowledge of relationships between lability degrees, sensor characteristics and physicochemical parameters of the chemical species [21-22] opens the way to use the measurements of a set of sensors (equal or larger than the number of unknowns) to determine physicochemical parameters of the system as well as to predict the availability to microorganisms. In this case, there is a set of unknown kinetic dissociation constants and, accordingly, a set of DGT devices with different configurations in terms of thickness of the diffusive or the resin discs are required to write a set of equations determining the set of dissociation rate constants. [17-18, 23-25] Mobilities can also be included in the set of unknowns. Nonetheless, the detailed application of this procedure to natural waters is still unapproachable, unless a reduced number of pools of complexes sharing similar mobilities and labilities could be defined

to simplify the system. In any case, this method allows a step further in the understanding of the behaviour of metal complexes in natural systems.

In this work, another independent strategy to obtain the dissociation rate constants of complexes is proposed.

When DGT devices with a stack of two resin discs are used (see Figure 5.1 for a scheme), the metal concentration drops to zero at the resin-diffusive gel interface (perfect sink) and remains negligible along all the resin discs whenever we are far from saturation. Thus, when there is only metal in the solution (Panel A of Figure 5.1) the metal does not reach the back resin disc. However, in presence of complexes (Panel B of Figure 5.1), the decreasing concentration of the complex towards the bottom of the DGT device indicates a flux of complex in this direction that, in steady state, needs to dissociate to avoid complex accumulation. Since there is no free metal in both resin discs (the M profile is flat (no diffusion) and equal to zero), all the metal released by dissociation of the partially labile complex ML is retained in the corresponding resin disc where dissociation takes place. Thus, in the back resin disc, only metal from the local dissociation of partially labile complexes is expected to be found whenever ternary complexes are negligible. Once these discs are eluted separately, the mass in the back resin disc informs on the presence of partially labile complexes as well as on their dissociation rate constants.

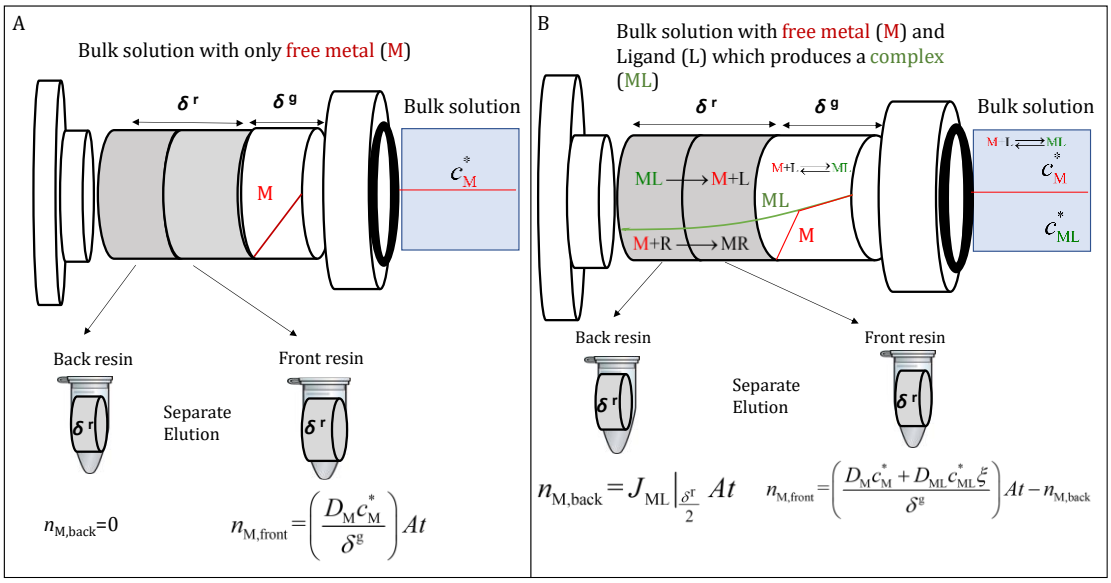

Figure 5.1: Schematic representation of a DGT device with a diffusive gel (of thickness δ^g) and two resin discs (each one of thickness $\delta^r/2$) deployed in a solution with only free metal (M) at a concentration C_M^* (panel A) or in a solution that also contains M, a ligand (L) and a partially labile complex (ML) (panel B) with concentrations C_M^*, C_L^* and C_{ML}^*, respectively. The figure also depicts schematic concentration profiles of M (red line) and ML (green line) in excess of ligand conditions and steady-state.

Let us define the percentage of back accumulation, *B*, as the moles of metal accumulated in the back resin divided by the total moles accumulated in all resin layers of the DGT.

In steady state, the accumulation in a back resin per unit of time can be computed as the total metal flux crossing the plane $x= \delta^r/2$ (which is just due to the complex ML), while the total accumulation per unit of time (in both resins) equals to the total metal flux crossing $x= \delta^r$. Accordingly,

$$B = \frac{n_{M.back}}{n_{M.back} + n_{M.front}} = \frac{J_{ML}\left|_{x=\delta^r/2}\right.}{J_{ML}\left|_{x=\delta^r}\right. + J_M\left|_{x=\delta^r}\right.} \quad (5.5)$$

Assuming perfect sink conditions, excess of ligand and steady-state concentrations, *B* can be written as: [20]

$$B = \frac{\varepsilon K' \operatorname{sech}\left(\frac{\delta^r}{\lambda_{ML}}\right)\sinh\left(\frac{\delta^r}{2\lambda_{ML}}\right)}{\lambda_{ML}\coth\left(\frac{\delta^g}{m}\right) + (1+\varepsilon K')\, m \tanh\left(\frac{\delta^r}{\lambda_{ML}}\right)} \quad (5.6)$$

as derived also in section 5.9.4, Eq S5.89 of the supporting information (SI).

Equation (5.6) relates B with the dissociation rate constant of a complex allowing the determination of k_d by numerical solution of this equation (see SI, Section 5.9.5) once B is experimentally known.

Additionally, when $\varepsilon K' >> 1$ the transport of the metal towards the resin mainly takes place through the complex. In these conditions, it has been shown that most of the metal accumulated comes from the dissociation of complexes inside the resin domain, [19] i.e., $J_M\big|_{x=\delta^r} << J_{ML}\big|_{x=\delta^r}$. With this approximation, Eq (5.6) becomes:

$$B = \frac{1}{2}\operatorname{sech}\left(\frac{\delta^r}{2\lambda_{ML}}\right) \tag{5.7}$$

and, accordingly,

$$k_d = \frac{D_{ML}}{\left(\frac{\delta^r}{2}\right)^2}\ln\left(\frac{1+\sqrt{1-(2B_{exp})^2}}{2B_{exp}}\right)^2 \tag{5.8}$$

Equation (5.8) leads to the determination of k_d from an experimental value of B (B_{exp}) provided that D_{ML} is known.

Figure 5.2A plots B computed with Eqs (5.6) and (5.7) *vs.* the dissociation rate constant (k_d) for a case with $\varepsilon K' = 2.54\times10^4$. According to the figure, for $k_d > 10^{-3}$ s^{-1}, there is a good agreement between (5.6) and (5.7). However, as k_d decreases both Eqs. diverge and, while (5.7) tends to B=0.5 regardless of the k_d-value, B decreases according to Eq (5.6) without reaching the value 0.5. This is a fundamental difference between both expressions that comes from neglecting the flux entering to the resin as free metal in the derivation of Eq (5.7). Indeed, for any $\varepsilon K'$ value, a low enough lability of the complex will render negligible the dissociation inside the resin compared to the flux entering to the resin as free metal, so the use of Eq (5.6) would be required.

As $\varepsilon K'$ decreases, see Figure 5.2B where $\varepsilon K' = 4.70$ in contrast to $\varepsilon K' = 2.54\times10^4$ of panel A, the agreement between eqs (5.6) and (5.7) is restricted to higher k_d-values ($k_d > 10^{-1}$ s^{-1} in Figure 5.2B), because of the increase of the metal flux $J_M\big|_{x=\delta^r}$.

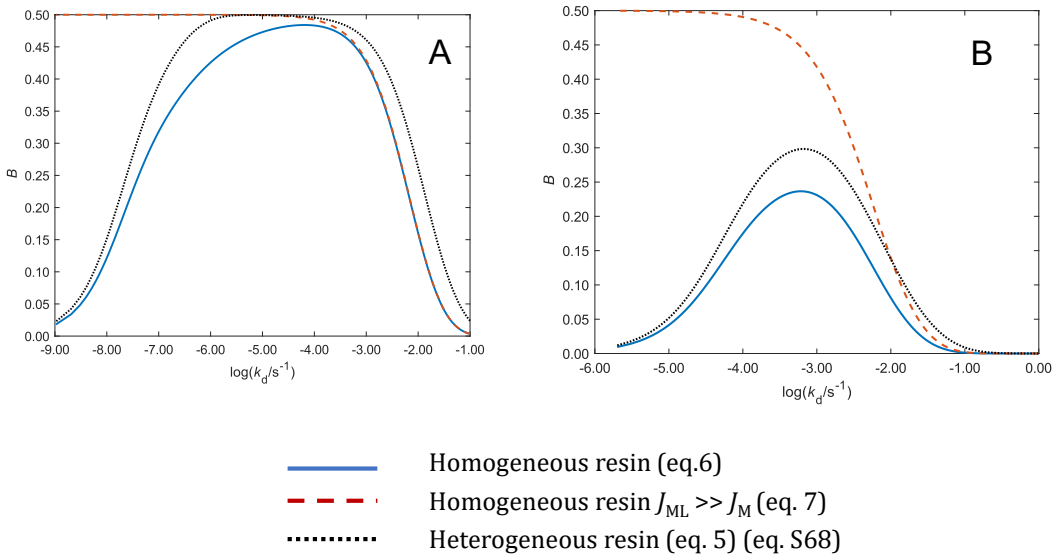

Figure 5.2: Percentage of back accumulation against the dissociation rate constant (k_d) while keeping the ratio k_a/k_d constant. Panel A) $K'=3.63\times10^4$, $D_{Ni}=7.07\times10^{-10}$ m s^{-2}, $\varepsilon=0.7$, $\delta^g=8.54\times10^{-4}$ m, $\delta^r=8\times10^{-4}$ m, and $k_{d,E}=7.7\times10^{-6}$ s^{-1}, Panel B) $K'=4.70$, $D_{Zn}=4.20\times10^{-10}$ m s^{-2}, $\varepsilon=1.0$, $\delta^g=1.079\times10^{-3}$ m and $\delta^r=8\times10^{-4}$ m. The blue line stands for Eq (5.6) that considers a homogeneous distribution of beads in the resin disc. The dashed red line is given by Eq (5.7) and the dotted black line is given by Eq S5.78 in SI assuming a heterogeneous distribution of the resin beads.

5.4.2 Influence of the settling of the resin beads in *B*

As it is well documented, the resin beads settle during casting, so that both large surfaces of the resin disc are not equal. [26] Schemes illustrating this heterogeneity are included for instance in references. [27-28]

A small roughness indicates the side of the resin disc that should be placed in contact with the diffusive gel when the DGT device is mounted. The settling of the resin beads can be clearly appreciated in Figure S5.1, a picture obtained with a microscope of the resin gel. The influence of this heterogeneity on the accumulation has been studied in reference. [20]

The settling influences accumulations when a DGT device with a stack of resin discs is used, especially in the presence of partially labile complexes. In the supplementary information, we provide details on the calculation of *B* considering this effect with Eq S5.78, to which we are going to refer as the heterogeneous model.

Figure 5.2 (both panels) also plot *B* computed with Eq S5.78 considering that only half of the volume of each resin disc contains resin beads as suggested by the picture of the

resin reported as Figure S5.1. This is a reasonable assumption given the size of the beads (100 μm) and the thickness of the disc. Notice that for a fixed k_d, the value of B computed with Eq S5.78 is greater than the value resulting from Eq (5.6) which corresponds to a homogeneous distribution of the resin beads. This difference can be understood from the observation of the concentration profiles of free metal and complex in a heterogeneous resin depicted in Figure S5.4. The percentage of metal accumulation in the front resin disc is higher in the homogeneous resin since the front resin disc collects all the metal released in its volume, while in the heterogeneous resin, part of the metal released in the front resin disc volume is collected in the back resin disc.

As discussed in reference [20], maximum discrepancies in the accumulation between the homogeneous and the heterogeneous models appear for lability degrees close to 0.25. Regarding back accumulation, Figure 5.2 indicates that differences between Eq (5.6) and Eq S5.78 are negligible for small B values, since the system is either very inert or very labile and there is practically no dissociation of the complex in the resin domain. For intermediate B values, the difference, according to Figure 5.2, is quite independent of K' and close to 0.3 log units especially at the right side of the maximum that corresponds to systems where complexes are more labile and relevant for the accumulation. Thus, k_d calculated with the heterogeneous model is close to a factor of 2 higher than the k_d calculated with the homogeneous model when we are on the right side of the maximum (or half of the k_d calculated with the homogeneous model when we are on the left of the maximum) as expected from the argument that a reduction of one-half in the volume of dissociation requires a double kinetic dissociation constant to release a given amount of free metal. For B values close to the maximum, the differences in k_d recovered from both models increase and the homogeneous model may even be unable to justify B_{exp}. A plot of the maximum B value calculated with the homogeneous model vs K' can be seen in Figure S5.5. B_{exp} values higher or close to the maximum B of the homogeneous model require the use of the heterogeneous model to recover k_d-values.

In the following sections, we are going to apply Eqs (5.5), (5.6) and (5.7) for the determination of the kinetic dissociation rate of NiNTA complexes as well as to Zn

complexes in the freshwater Osor, a small tributary of the Fluvià river in the northeast of Spain.

5.5 Methodology

5.5.1 Experimental section

5.5.1.1 Laboratory experiments: Ni accumulation in DGT devices in presence of NTA at pH=7.5

Experimental details are described elsewhere.[22] Briefly, DGT holders (piston type, 2 cm diameter window), polyacrylamide gel discs (diffusive disc, 0.8 mm thick, Chelex resin disc, 0.4 mm thick) from DGT Research Ltd. were used. The 5L polyethylene exposure chamber was kept at 25 °C by using a thermostat and stirred at 240 rpm. DGT devices were deployed per triplicate in solutions of 0.5 M $NaNO_3$ (Merck, Suprapur) and 10^{-5} mol L^{-1} Cd and Co and 2.5×10^{-5} mol L^{-1} of Ni (prepared from 10^{-2} mol L^{-1} stock solutions of nitrate salts $Cd(NO_3)_2$ $3H_2O$, $Co(NO_3)_2{\cdot}6H_2O$, $Zn(NO_3)_2{\cdot}6H_2O$ and $Ni(NO_3)_2{\cdot}6H_2O$) and 8×10^{-5} mol L^{-1} of NTA (Fluka, analytical grade) during 24 hours at pH=7.5 (Sigma-Aldrich). In addition to standard DGT devices composed of 1 resin layer and 1 gel layer, DGT devices with 2 resins layers (labelled as 2R1G devices) were also used. The front and the back resin discs were eluted separately.

5.5.2 DGT accumulation in the Osor stream

The Osor stream is a small tributary of the Fluvià river located in Girona province (Catalonia) in the Northeast of Spain whose surface waters are impacted by former mining activities of F-Ba-Pb-Zn ore. [29-30]

Our sampling strategy was mainly designed to assess the speciation of Zn by deploying DGT devices in this freshwater as described elsewhere.[10] At the sampling site, coordinates 41° 57′ 14” N, 2° 35′ 58″ E, a set of parallelepiped structures were fixed with the purpose of holding the DGT devices parallel to the river flow. During 10th and 11th March 2020, in situ measurements of a set of physical parameters were taken with an Orion Star A329 pH/ISE/Conductivity/RDO/DO Meter and samples were collected and prepared in situ by filtering 9.98 mL of stream water though a 0.45 µM syringe filter and mixing it with 20 µL of HNO_3 70%. These samples were analysed for total Zn using an inductively coupled plasma mass spectrometer (ICP-MS, 7700x, Agilent Technologies, Inc.). The electroanalytical technique Absence of Gradients and Nernstian Equilibrium Stripping (AGNES) was applied to the last grab sample from

11th March 2020 [10] to determine the free Zn concentration in the water. Main anions and cations were measured with IC (ion chromatography), alkalinity of this last grab sample was analysed in the Scientific and Technical Services of the Catalan Institute for Water Research (ICRA) and Dissolved Organic Carbon (DOC) was analysed at "serveis científico tècnics" of the Universitat de Lleida.

5.5.3 Determination of *K'*

For the well-defined NiNTA complex, the speciation code VMINTEQ allows a detailed prediction of the species and concentrations in solution under conditions reported in "Experimental section" so that K'_{NiNTA} can be computed by just dividing the equilibrium concentration of the complex (c^*_{NiNTA}) by the free Ni (c^*_{Ni}) resulting in $K'=3.63\times10^4$.

In the Osor stream, $c_{T,Zn}$ measured with ICP-MS was 6.33×10^{-7} mol L^{-1} and c^*_{Zn}, obtained from AGNES, was 1.11×10^{-7} nmol L^{-1} [10]. All measured concentrations are $c_{T,Na}=6.25\times10^{-4}$ mol L^{-1}, $c_{T,K}=3.07\times10^{-5}$ mol L^{-1}, $c_{T,Mg}=2.03\times10^{-4}$ mol L^{-1}, $c_{T,Ca}=4.32\times10^{-4}$ mol L^{-1}, $c_{T,Li}=8.64\times10^{-7}$ mol L^{-1}, $c_{T,NO2}=2.17\times10^{-7}$ mol L^{-1}, $c_{T,NO3}=1.29\times10^{-6}$ mol L^{-1}, $c_{T,Cl^-}=3.42\times10^{-4}$ mol L^{-1}, $c_{T,SO4^{-2}}=1.55\times10^{-4}$ mol L^{-1}, $c_{T,F}=1.47\times10^{-5}$ mol L^{-1}, $c_{T,CO3}=7.32\times10^{-4}$ mol L^{-1}, $c_{T,Zn}= 6.33\times10^{-7}$ mol L^{-1}, $c_{TPb}=4.64\times10^{-9}$ mol L^{-1}, $c_{T,Mn}=3.13\times10^{-7}$ mol L^{-1}, $c_{T,Fe}=1.46\times10^{-7}$ mol L^{-1}

Speciation of Zn in the Osor stream can also be estimated by using VMINTEQ. The prediction is that zinc is mainly present in the freshwater as free zinc (c^*_{Zn}) 192 nmol L^{-1} (in agreement with the concentration obtained by AGNES result) and a set of inorganic complexes ($ZnCO_{3(aq)}$, $ZnOH_2$, $ZnOH^+$, etc) with concentrations of 78.6 nmol L^{-1}, 287 nmol L^{-1} and 22.5 nmol L^{-1} respectively. Complexes of Zn with Dissolved Organic Matter, computed with default parameters of NICA-DONNAN [31] have a concentration of 8.21 nmol L^{-1} which represents around 1% of $c_{T,Zn}$, so that from now on, we are going to neglect the Zn bound to Dissolved Organic Matter.

Assuming that the inorganic complexes could be treated as a pool with a common diffusion coefficient, $D_{ZnL}=D_{Zn}$, the concentration of this pool can be estimated as

$c^*_{\mathrm{ZnL}} = c_{\mathrm{T,Zn}} - c^*_{\mathrm{Zn}}$ and a *K'* (*K'*=4.70 of this pool was straightforwardly obtained by dividing c^*_{ZnL} by c^*_{Zn} (111 nmol L^{-1}).

5.5.4 Determination of k_d from *B*

The use of the limiting expression Eq (5.8), when applicable, allows a straightforward determination of k_d, while, when Eq (5.6) needs to be used, an iterative procedure can be applied.

In order to have a simple criterion for the plausibility of the application of Eq (5.8), we need to explore the fulfilment of the approximation:

$$J_{\mathrm{M}}\Big|_{x=\delta^{\mathrm{r}}} << J_{\mathrm{ML}}\Big|_{x=\delta^{\mathrm{r}}} \tag{5.9}$$

on which the limiting expression Eq (5.8) relies. The reaction layer concept[32] applied to the DGT devices can provide approximate expressions for $J_{\mathrm{M}}\Big|_{x=\delta^{\mathrm{r}}}$ and $J_{\mathrm{ML}}\Big|_{x=\delta^{\mathrm{r}}}$.[19] As detailed in the SI (see Eq S5.93), with these expressions, the inequality $J_{\mathrm{M}}\Big|_{x=\delta^{\mathrm{r}}} << J_{\mathrm{ML}}\Big|_{x=\delta^{\mathrm{r}}}$ reduces to

$$\sqrt{\frac{1}{1+\varepsilon K'}}\tanh\left(\frac{\delta^{\mathrm{g}}}{m}\right)\tanh\left(\frac{\delta^{\mathrm{r}}}{\lambda_{\mathrm{ML}}}\right) << \frac{1}{2} \tag{5.10}$$

whose fulfillment validates the k_d-value obtained with the limiting expression (Eq (5.8)). Conversely, if Eq (5.10) is not satisfied, a better approximation for k_d should be sought using Eq (5.6) instead of (5.8).

In order to check whether the heterogeneity of the resin beads distribution is relevant for the determination of k_d, we can examine the inequality $B_{\mathrm{exp}}<B_{\mathrm{max}}$. A plot of B_{max} *vs*. *K*' for the homogeneous resin and typical values of the rest of parameters is given in Fig. S5.5 of the SI. When B_{exp} is close to or greater than B_{max}, then Eq S5.78 is needed to recover accurate k_d values as discussed in section "

When Eq. (5.6) or S5.78 have to be used, we notice that according to Figure 5.2 two k_d-values are obtained, corresponding to a more inert or a more labile system. Both k_d-values can be used to compute accumulations (with Eqs. (5.1)- (5.4)) to be compared with the experimental one in order to select the one leading to the closest agreement. See details in section 5.9.5 of the SI.

An Excel file ready to generate the solutions of Eq. (5.8), Eq (5.6) and Eq S5.78 is provided as SI. See section 5.9.9 in the SI for further instructions. According to the results of the inequalities (5.10) and $B_{exp}<B_{max}$, the selected value of k_d appears in a cell with green background.

5.6 Results and discussion

5.6.1 Determination of k_d for the NiNTA complex using 2R1G DGT devices.

A previous work[22] showed that, while the dissociation in the diffusive gel follows Eigen principles based on a dissociative mechanism, the dissociation reaction of the NiNTA complex (the rest of Ni complexes in solution are fully labile) in the resin layer follows a faster ligand-assisted mechanism. Thus, a dissociation rate constant, $k_{d,E}$ (7.7×10^{-6} s^{-1}) [22], was assumed in the diffusive gel, where subindex E indicates Eigen mechanism, while a dissociation rate constant, $k_{d,R}$, was considered for the dissociation within the resin disc which corresponds to a ligand-assisted exchange mechanism. Actually, both mechanisms compete inside the resin disc, but the higher rate of the ligand-assisted one renders negligible the presence of the Eigen mechanism in the resin domain.

Accordingly, λ_{ML} involves $k_{d,R}$, while m uses $k_{d,E}$ in Eq (5.2) when the determination of k_d is done from the lability degree or when it is determined from B using Eq (5.6).

Table 1 Dissociation rate constants values determined from the back accumulation (with either the homogeneous or the heterogeneous resin model). The parameters needed to calculate $k_{d,R}$ (for NiNTA) or k_d (for Zn in Osor) are specified in section "Determination of K"" and in Figurefig 5.2 caption.

Model	Laboratory Experiments	Osor stream
	k_d NiNTA (s^{-1})	k_d $ZnL_{Inorganic}$ (s^{-1})
Homogeneous resin and eq (5.8)	$4.0(\pm0.9)\times10^{-3}$	$3(\pm1)\times10^{-3}$
Homogeneous resin and eq (5.6)	$4.1(\pm0.9)\times10^{-3}$	Undetermined
Heterogeneous resin and eq S78 in SI	$8(\pm2)\times10^{-3}$	$1.2(\pm0.6)\times10^{-3}$
Lability degree (ξ), found from Eq (5.1)	0.67(±0.01)	0.76(±0.03)
k_d from lability degree (ξ) and Eq (5.2)	$2.8(\pm0.3)\times10^{-3}$	$2.8(\pm0.7)\times10^{-3}$

As seen in Table , using Eq (5.8) and $k_{d,E}$ $=7.7\times10^{-6}$ s^{-1}, a dissociation rate constant $k_{d,R}$ of 4×10^{-3} s^{-1} has been obtained for the partially labile complex NiNTA. When Eq (5.10) is checked, we obtain $3.88\times10^{-3}<<1/2$, indicating that the condition is satisfied. Therefore, the k_d value computed with Eq (5.8) can be accepted as can be confirmed by comparing this value with that obtained from the complete Eq (5.6), also reported in

Table , 4.1×10^{-3} s^{-1} . These values are in good agreement between them and with the result obtained from the lability degree 2.8×10^{-3} s^{-1}. [33]

As the B_{exp} value (0.29±0.03 for NiNTA) is well below the corresponding B_{max} value obtained from Fig. S5.5 of the SI for $\varepsilon K'=2.54\times10^{4}$, we expected that the simplified expression (Eq (5.8))would yield an accurate value (i.e. within the order of magnitude) of the rate dissociation constant of this complex. Indeed, applying the expression for B reported as Eq S5.78), $k_{d,R}$ results in 8×10^{-3} s^{-1} , a value just twofold higher than the homogeneous estimation of $k_{d,R}$ as expected from Figure 5.2.

5.6.2 Determination of k_d for inorganic Zn complexes in the stream Osor.

The same procedure (except that a single k_d is assumed everywhere), applied to the availability of Zn in the stream Osor, leads to a different outcome. The simplified expression (Eq (5.8)) produces $k_d= 3\times10^{-3}$ s^{-1}. This value of k_d in Eq (5.10) yields 0.25, a value smaller than 1/2, but not at the level of orders of magnitude. Nevertheless, this k_d-value cannot be compared with the one obtained from the more complete expression (5.6), because this equation does not yield any k_d value with a B=0.29±0.06 for the set of used parameters, indicating that B_{exp} value is higher than B_{max}=0.22 reported in Fig. S5.5 of the SI for K'=4.70. Therefore, in this case, we need to apply the heterogeneous model for the resin layer to obtain a solution for k_d.

As seen in Figure 5.2, a B equal to 0.29±0.06 yields two solutions of eq S5.78: $k_d=1.2\times10^{-3}$ s^{-1} and $k_d=3.4\times10^{-4}$ s^{-1}. For the Osor stream, the selected solution is $k_d=1.2\times10^{-3}s^{-1}$, according to the agreement of the Zn accumulation predicted by eqns. with eqns. (5.1)- (5.4) with the experimental measurement.

The difference between this value ($k_d=1.2\times10^{-3}s^{-1}$) and the one obtained from the lability degree assuming a homogeneous resin, $k_d=2.8\times10^{-3}$ s^{-1}, reflects the differences between models as well as the corresponding experimental uncertainties associated to the back and to the total accumulation, respectively.

In conclusion, DGT devices with two resin discs provide complementary information of the system that can be used, at least, to double-check the determination of reaction-rate constants from the lability degree.

5.6.3 Environmental implications

When internalization is not the rate-limiting step, the free metal develops a concentration profile supported by the dissociation of complexes that depends on the respective diffusion coefficients and the thickness of the diffusion domain. Dynamic analytical techniques can mimic, in this case, the uptake process of some biota becoming suitable for predicting bioavailability. It should be noticed that different dynamic techniques such as DGT, Permeation Liquid Membrane[34-35] or stripping voltammetry (including Scanned Stripping ChronoPotentiometry, SSCP) yield different availability measurements in a common sample reflecting different contributions of complexes in agreement to the different diffusion layer thickness of each technique. [8] Likewise, different microorganisms, algae, or biological consumers face different available concentrations in a common sample since they exhibit different diffusion domains. These different domains induce different dissociation degrees of metal complexes, which are a signature of the lability of the pool of complexes in the sample.

While the diffusion domain extends out of the biota membrane, in DGT, complexes can penetrate in the resin disc, so that the diffusion domain encompasses both the diffusive and the resin disc. For a closer resemblance with the biouptake process of biota, once k_d is determined as explained in this work, we can compute the expected accumulation (n_M) in a DGT device without penetration of complexes by setting $\delta^r=0$ in Eqs (5.1) - (5.2), as done in reference.[10] Defining as usual $c_{DGT} = \frac{1}{At}\frac{n_M \delta^g}{D_M}$, a plot of c_{DGT} *vs.* δ^g computed with $\delta^r=0$ and a given total concentration of a target metal can be understood as the potential maximum "effective" concentration that a microorganism can uptake in the studied solution according to its thickness of the diffusion domain. Notice how this concentration increases as the thickness of the diffusion domain of the organism increases, due to a higher contribution of partially labile complexes to the accumulation reaching the total concentration of the metal when all the complexes are labile and with a common diffusion coefficient with the free metal. [36]

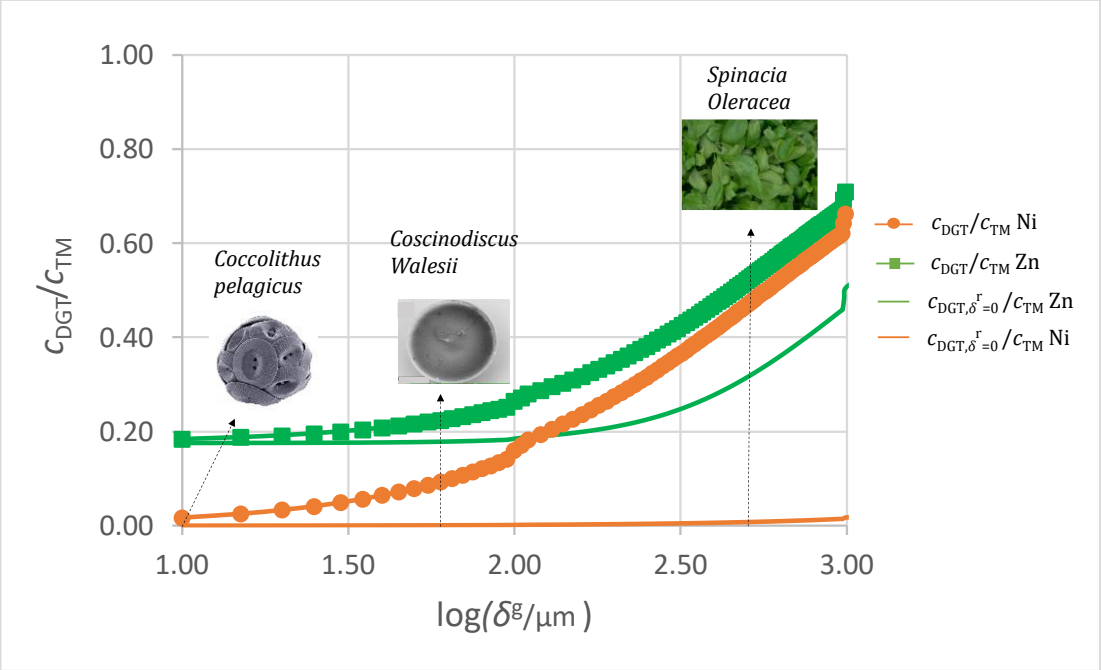

Figure 5.3: Available DGT concentration as a function of the diffusion thickness for two types of DGT (δ^r=4×10^{-4} m and δ^r=0 m) devices and two types of metal complexes (ZnL_{Inorg} of Osor water and NiNTA) for a $c_{T,Zn}$=6.33×10^{-4} mol m^{-3} and $c_{T,Ni}$=2.5×10^{-2} mol m^{-3}.

Figure 5.3 depicts c_{DGT} (normalized with respect to the total metal concentration) for Ni in our laboratory solution with NTA as well as c_{DGT} for Zn in the Osor stream expected for any biota whose diffusion domain thickness ranges from 10 µm to 1 mm. In any case, an important decrease of the Ni and Zn availability is seen in the figure from the standard DGT device to a DGT without penetration of complexes in the resin disc.

For the case of Zn, the minimum availability is close to 20% of the total Zn, in agreement with the free Zn concentration (111 nM) in this freshwater, but it reaches a value close to 50% for biota with diffusion domain thickness close to 1mm (see continuous green line). For example, diatom species such as *Coccolithus pelagicus* or *Coscinodiscus wailesii* are expected to show an availability of 20% of the total concentration because their radius is between 2-10 µm and 50 µm, respectively, which is also the size of their diffusion domain. [37-39] . Reference [40] used a diffusion layer length of 400 µm to determine the flux available to *Spinacia oleracea* grown in hydroponic

media. According to Figure 5.3, it would face an availability of 30% of the total Zn concentration of the Osor water.

For the case of Ni, as complexes with NTA are strong, biota with a diffusion domain thickness from 10 µm to 1000 µm would face an effective Ni concentration lower than 1% of the total Ni (see continuous orange line). Thus, *Spinacia oleracea* in the same solution would face the same "effective" concentration of Ni as *Coccolithus pelagicus* or *Coscinodiscus wailesii* even though its diffusion thickness is 40 times greater than the one of *Coccolithus pelagicus.*

The building of figures similar to Figure 5.3 can be of high environmental interest for any target element in natural waters. In the present case, this process has been facilitated by the determination of the dissociation kinetic constants of the complexes. Obviously, limitations in this task come from the measurement of the low free metal concentrations in some waters, the identification of the ligands, the determination of the physicochemical parameters and the fact that we lack knowledge about the presence of functional ligands on the outer membrane of the organisms. The use of DGT devices with different thicknesses of the diffusive and resin discs, as well as devices with a stack of resin discs, can be helpful to improve our understanding of the lability and availability of metal complexes in natural waters.

5.7 Acknowledgements

Support from the Ministry of Science and Innovation under projects PID2019-107033GB-C21 and PID2020-117910GB-C21 is acknowledged. JSD acknowledges support from University of Lleida and VUB. We also thank C. David for the help in the picture of the resin disc included in the SI.

5.8 References

1. Buffle, J.; Wilkinson, K. J.; van Leeuwen, H. P., Chemodynamics and Bioavailability in Natural Waters. *Environmental Science and Technology* **2009,** *43* (19), 7170-7174.
2. Campbell PGC, F. C., Biotic Ligand Model In *Encyclopia of Aquatic Ecotoxicology*, C.Blaise, J. F. F. a., Ed. Springer-Verlag, Heildeberg: 2013; pp 237-245.
3. Errecalde, O.; Campbell, P. G. C., Cadmium and zinc bioavailability to Selenastrum capricornutum (Chlorophyceae): accidental metal uptake and toxicity in the presence of citrate. *Journal of Phycology* **2000,** *36* (3), 473-483.
4. Fortin, C.; Campbell, P. G. C., Thiosulfate enhances silver uptake by a green alga: Role of anion transporters in metal uptake. *Environmental Science and Technology* **2001,** *35* (11), 2214-2218.
5. Buffle, J.; Zhang, Z.; Startchev, K., Metal flux and dynamic speciation at (Bio)interfaces. part 1: Critical evaluation and compilation of physicochemical parameters for complexes with simple Ligands and Fulvic/Humic substances. *Environmental Science and Technology* **2007,** *41* (22), 7609-7620.
6. Salvador, J.; Puy, J.; Cecilia, J.; Galceran, J., Lability of complexes in steady state finite planar diffusion. *Journal of Electroanalytical Chemistry* **2006,** *588*, 303-313.
7. Galceran, J.; Monné, J.; Puy, J.; van Leeuwen, H. P., The impact of the transient uptake flux on biouptake accumulation. Linear adsorption and first-order internalisation coupled with spherical semi-infinite mass transport. *Mar.Chem.* **2004,** *85* (1-2), 89-102.
8. van Leeuwen, H. P.; Town, R. M.; Buffle, J.; Cleven, R.; Davison, W.; Puy, J.; van Riemsdijk, W. H.; Sigg, L., Dynamic speciation analysis and bioavailability of metals in Aquatic Systems. *Environmental Science and Technology* **2005,** *39*, 8545-8585.
9. Unsworth, E. R.; Warnken, K. W.; Zhang, H.; Davison, W.; Black, F.; Buffle, J.; Cao, J.; Cleven, R.; Galceran, J.; Gunkel, P.; Kalis, E.; Kistler, D.; van Leeuwen, H. P.; Martin, M.; Noel, S.; Nur, Y.; Odzak, N.; Puy, J.; Van Riemsdijk, W.; Sigg, L.; Temminghoff, E.; Tercier-Waeber, M. L.; Toepperwien, S.; Town, R. M.; Weng, L. P.; Xue, H. B., Model predictions of metal speciation in freshwaters compared to measurements by in situ techniques. *Environmental Science and Technology* **2006,** *40* (6), 1942-1949.
10. Rosales-Segovia, K.; Sans-Duñó, J.; Companys, E.; Puy, J.; Alcalde, B.; Antico, E.; Fontas, C.; Galceran, J., Effective concentration signature of Zn in a natural water derived from various speciation techniques. *Science of the Total Environment* **2022,** *806* (3), 151201.
11. Galceran, J.; Puy, J., Interpretation of diffusion gradients in thin films (DGT) measurements: a systematic approach. *Environmental Chemistry* **2015,** *12* (2), 112-122.
12. Galceran, J.; Puy, J.; Salvador, J.; Cecília, J.; van Leeuwen, H. P., Voltammetric lability of metal complexes at spherical microelectrodes with various radii. *Journal of Electroanalytical Chemistry* **2001,** *505* (1-2), 85-94.

13. Puy, J.; Galceran, J., Theoretical aspects of dynamic metal speciation with electrochemical techniques. *Curr.Opin.Electrochem.* **2017,** *1* (1), 80-87.
14. Salvador, J.; Garcés, J. L.; Galceran, J.; Puy, J., Lability of a mixture of metal complexes under steady-state planar diffusion in a finite domain. *Journal of Physical Chemistry B* **2006,** *110* (27), 13661-13669.
15. Molina, A.; Martinez-Ortiz, F.; Laborda, E.; Puy, J., Lability of metal complexes at spherical sensors. Dynamic voltammetric measurements. *Physical Chemistry Chemical Physics* **2010,** *12* (20), 5396-5404.
16. Mongin, S.; Uribe, R.; Puy, J.; Cecilia, J.; Galceran, J.; Zhang, H.; Davison, W., Key role of the resin layer thickness in the lability of complexes measured by DGT. *Environ.Sci.Technol.* **2011,** *45* (11), 4869-4875.
17. Levy, J. L.; Zhang, H.; Davison, W.; Puy, J.; Galceran, J., Assessment of trace metal binding kinetics in the resin phase of diffusive gradients in thin films. *Analytica Chimica Acta* **2012,** *717*, 143-150.
18. Levy, J. L.; Zhang, H.; Davison, W.; Galceran, J.; Puy, J., Kinetic Signatures of Metals in the Presence of Suwannee River Fulvic Acid. *Environmental Science and Technology* **2012,** *46* (6), 3335-3342.
19. Puy, J.; Uribe, R.; Mongin, S.; Galceran, J.; Cecilia, J.; Levy, J.; Zhang, H.; Davison, W., Lability Criteria in Diffusive Gradients in Thin Films. *Journal of Physical Chemistry A* **2012,** *116* (25), 6564-6573.
20. Jimenez-Piedrahita, M.; Altier, A.; Cecilia, J.; Rey-Castro, C.; Galceran, J.; Puy, J., Influence of the settling of the resin beads on Diffusion Gradients in Thin films measurements. *Analytica Chimica Acta* **2015,** *885*, 148-155.
21. Uribe, R.; Mongin, S.; Puy, J.; Cecilia, J.; Galceran, J.; Zhang, H.; Davison, W., Contribution of partially labile complexes to the DGT metal flux. *Environmental Science and Technology* **2011,** *45* (12), 5317-5322.
22. Puy, J.; Galceran, J.; Cruz-Gonzalez, S.; David, C. A.; Uribe, R.; Lin, C.; Zhang, H.; Davison, W., Metal accumulation in DGT: Impact of ionic strength and kinetics of dissociation of complexes in the resin domain. *Anal. Chem.* **2014,** *86*, 7740-7748.
23. Baeyens, W.; Gao, Y.; Davison, W.; Galceran, J.; Leermakers, M.; Puy, J.; Superville, P. J.; Beguery, L., In situ measurements of micronutrient dynamics in open seawater show that complex dissociation rates may limit diatom growth. *Scientific Reports* **2018,** *8*.
24. Gao, Y.; Zhou, C. Y.; Gaulier, C.; Bratkic, A.; Galceran, J.; Puy, J.; Zhang, H.; Leermakers, M.; Baeyens, W., Labile trace metal concentration measurements in marine environments: From coastal to open ocean areas. *Trac-Trends in Analytical Chemistry* **2019,** *116*, 92-101.
25. Companys, E.; Galceran, J.; Puy, J.; Sedo, M.; Vera, R.; Antico, E.; Fontas, C., Comparison of different speciation techniques to measure Zn availability in hydroponic media. *Analytica Chimica Acta* **2018,** *1035*, 32-43.
26. Dianne F.Jolley, S. M., Yue Gao and Hao Zhang, Practicalities of working with DGT. In *Diffusive Gradients in Thin-Films for environmental measurements*, Davison, W., Ed. 2016.

27. Zhang, H.; Davison, W., Performance characteristics of diffusion gradients in thin films for the insitu measurement of trace metals in aqueous solution. *Analytical Chemistry* **1995,** *67* (19), 3391-3400.
28. Dahlqvist, R.; Zhang, H.; Ingri, J.; Davison, W., Performance of the diffusive gradients in thin films technique for measuring Ca and Mg in freshwater. *Analytica Chimica Acta* **2002,** *460* (2), 247-256.
29. Navarro, A.; Font, X.; Viladevall, M., Metal Mobilization and Zinc-Rich Circumneutral Mine Drainage from the Abandoned Mining Area of Osor (Girona, NE Spain). *Mine Water and the Environment* **2015,** *34* (3), 329-342.
30. Morin, S.; Corcoll, N.; Bonet, B.; Tlili, A.; Guasch, H., Diatom responses to zinc contamination along a Mediterranean river. *Plant Ecology and Evolution* **2014,** *147* (3), 325-332.
31. Milne, C. J.; Kinniburgh, D. G.; van Riemsdijk, W. H.; Tipping, E., Generic NICA-Donnan model parameters for metal-ion binding by humic substances. *Environmental Science and Technology* **2003,** *37* (5), 958-971.
32. van Leeuwen, H. P.; Puy, J.; Galceran, J.; Cecília, J., Evaluation of the Koutecky-Koryta approximation for voltammetric currents generated by metal complex systems with various labilities. *Journal of Electroanalytical Chemistry* **2002,** *526* (1-2), 10-18.
33. Sans-Duñó, J.; Cecilia, J.; Galceran, J.; Puy, J., Availability of metals to DGT devices with different configurations. The case of sequential Ni complexation. *Science of The Total Environment* **2021,** *779*, 146277.
34. Buffle, J.; Parthasarathy, N.; Djane, N. K.; Matthiasson, L., Permeation liquid membranes for field analysis and speciation of trace compounds in waters. In *In situ monitoring of aquatic systems*, Buffle, J.; Horvai, G., Eds. John Wiley: Chichester, UK, 2000; pp 407-493.
35. Tomaszewski, L.; Buffle, J.; Galceran, J., Theoretical and analytical characterisation of a flow-through permeation liquid membrane with well-controlled flux for metal speciation measurements. *Analytical Chemistry* **2003,** *75*, 893-900.
36. Altier, A.; Jimenez-Piedrahita, M.; Uribe, R.; Rey-Castro, C.; Galceran, J.; Puy, J., Time weighted average concentrations measured with Diffusive Gradients in Thin films (DGT). *Analytica Chimica Acta* **2019,** *1060*, 114-124.
37. R.Moheimani, J. P. W., M.A. Borowitzka, Bioremediation and other potential applications of coccolithophorid algae: A review. *Algal Research* **2012,** *1*, 120-133.
38. De Tommasi, E. C., R.; Dardano, P.; De Luca, A.; Managò, S.; Rea,I. and De Stefano,M., UV-shielding and wavelength conversion by centric diatom nanopatterned frustules. *Scientific Reports* **2018,** *8*.
39. Ecolink, Canada *Characterization of Laurentian Fulvic Acid*; 1994.
40. Degryse, F.; Smolders, E.; Merckx, R., Labile Cd complexes increase Cd availability to plants. *Environmental Science and Technology* **2006,** *40* (3), 830-836.

5.9 Supporting Information for: Back accumulation of DGT (Diffusive Gradients in Thin films) devices with a stack of resin discs to assess availability of metal cations to biota in natural waters

Jordi Sans-Duñó[1,2], Joan Cecilia[3], Josep Galceran[1], Jaume Puy[1]*, Willy Baeyens[2], Yue Gao [2]

1.Departament de Química. Universitat de Lleida, and AGROTECNIO-CERCA, Rovira Roure 191, 25198 Lleida, Catalonia, Spain

2. Analytical, Environmental & Geochemical (AMGC), Vrije Universiteit Brussel (VUB), Pleinlaan 2, B-1050 Brussels, Belgium

3. Departament de Matemàtica. Universitat de Lleida, and AGROTECNIO-CERCA, Rovira Roure 191, 25198 Lleida, Catalonia, Spain

*Corresponding author. E-mail address: jpuy@quimica.udl.cat, Phone 34 973 702529, Fax 34 973 702924

5.9.1 Homogeneous and heterogeneous resin models

During the preparation of the Chelex resin discs, while the resin gels are becoming solid, the settling of the beads generates a heterogeneous distribution of the beads in the resin disc which concentrates the binding sites close to the bottom surface. We have used an optic microscope to show the heterogeneous distribution of the resin beads from the profile.

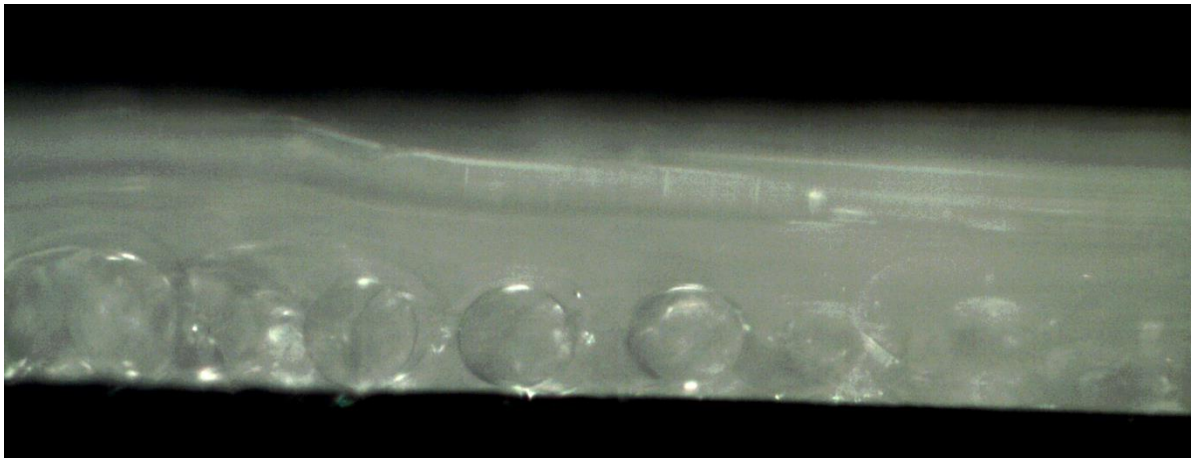

Figure S5.1 Photograph with an optic microscope of a Chelex resin. At the bottom of the picture we can see round shapes that correspond to Chelex 100 beads. On the bottom left of the picture there are different beads at different planes and that is why they become more blurry.

Therefore, it could be convenient to develop a model that takes into account this heterogeneous distribution of the resin beads in the binding disc of a DGT device.
Let us consider a DGT device with a stack of two resin discs, whose resin beads have settled just in the front part of each resin disc (See Figure S5.1). In order to assess for the relevance of the settling, we will use the homogeneous model as reference. In contrast to the heterogeneous model, in the homogeneous model, the binding sites are uniformly distributed within the whole resin disc (See Figure S5.2B).
Figure S5.2 is a schematic representation of the stack of the two resin discs. The x-axis is perpendicular to the interface between the resin disc and the diffuse disc. The resins are in the range $0<\underline{x}<\delta$.

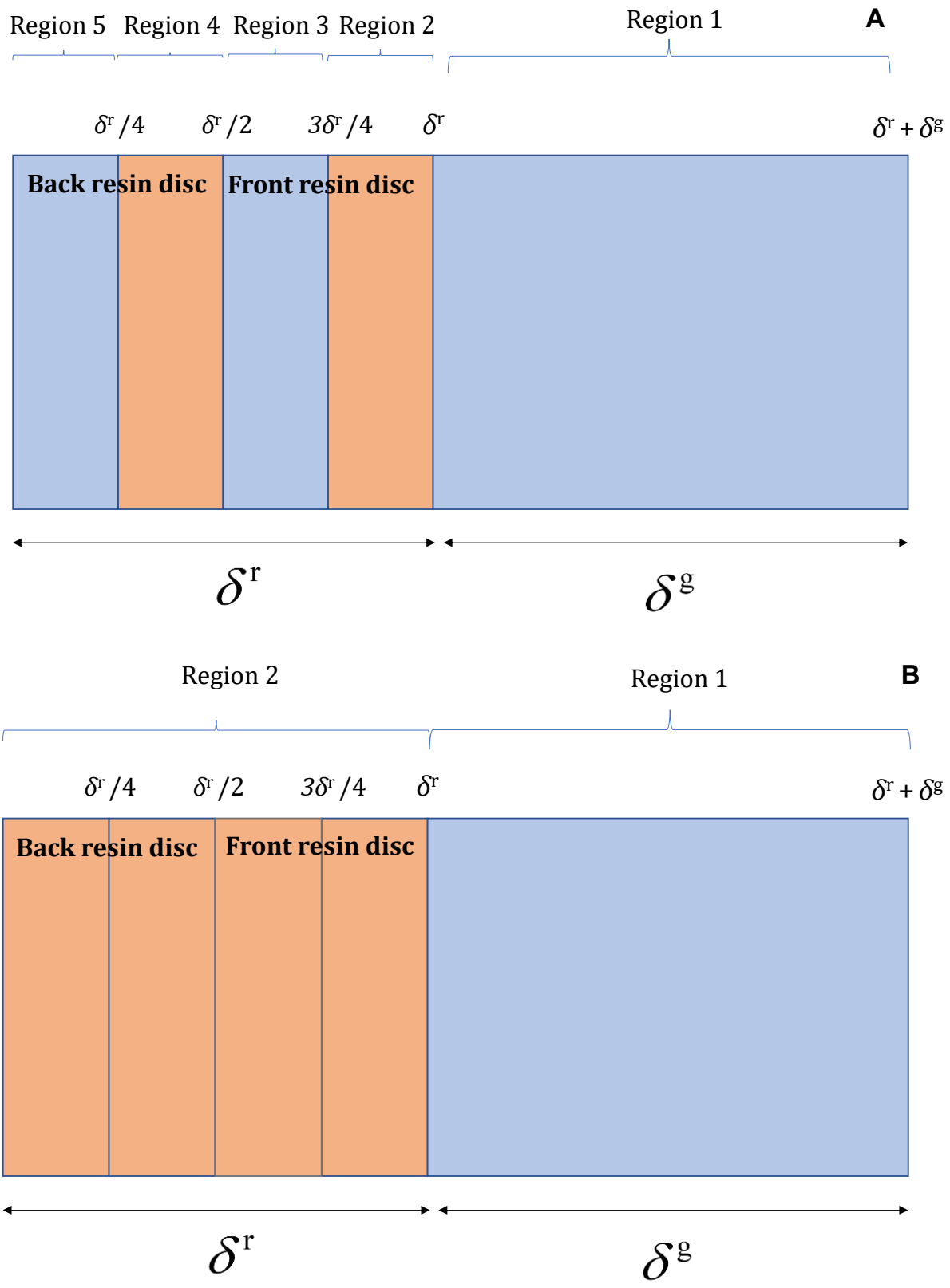
Region 5
Region 4
Region 3
Region 2
Region 1
A
$\delta^r/4$
$\delta^r/2$
$3\delta^r/4$
δ^r
$\delta^r + \delta^g$
Back resin disc
Front resin disc
δ^r
δ^g
Region 2
Region 1
B
$\delta^r/4$
$\delta^r/2$
$3\delta^r/4$
δ^r
$\delta^r + \delta^g$
Back resin disc
Front resin disc
δ^r
δ^g

Figure S5.2 Domains considered in a heterogeneous distribution (panel A) and a homogeneous distribution of the resin beads (panel B) in a stack of two resin discs (front resin, $\delta_r/2<x<\delta_r$ and back resin $0<x<\delta_r/2$). Orange background indicates the presence of resin sites, while they are absent in the blue background shading. δ_g is the aggregate thickness of the diffusive disc plus that of the Diffusive Boundary Layer (DBL). δ_r is the aggregate thickness of the two resin discs.

In the next section, an analytical solution for the diffusion-reaction equations involving heterogeneous resin discs is reported.

5.9.2 Derivation of a solution for c_M and c_{ML} for a heterogeneous resin of a DGT device

We have developed a model that solves the diffusion-reaction equations for the boundary conditions of a DGT device considering a heterogeneous distribution of the beads of the resin in the resin discs.

Let us consider the simple case of a free metal (M) that reacts with a ligand (L) to produce a complex (ML).

$$\mathrm{M} + \mathrm{L} \underset{k_d}{\overset{k_a}{\rightleftharpoons}} \mathrm{ML}$$

The association reaction of M with L is considered a second order reaction rate with a constant (k_a) with units $\frac{\mathrm{m}^3}{\mathrm{mol\ s}}$ and the dissociation reaction is considered a first order rate with a constant (k_d) with units s^{-1}.

The equilibrium constant of this reaction process is defined as:

$$K = \frac{k_a}{k_d} \qquad \text{(S5.1)}$$

We assume excess of ligand conditions, which imply that the concentration of L (c_L) is much larger than the concentration of M (c_M), so that it stays approximately constant everywhere in the DGT spatial domain. Therefore, a conditional equilibrium constant can be defined as:

$$K' = \frac{k_a'}{k_d} = \frac{k_a c_L^*}{k_d} \qquad \text{(S5.2)}$$

Along the heterogeneous distribution presented in Figure S5.2A, the following assumptions are going to be considered to solve the diffusion-reaction equations:

- The resin domain is $\delta^r > x > 0$, but only in the subdomains $\delta^r \geq x \geq \frac{3\delta^r}{4}$ and $\frac{\delta^r}{2} \geq x \geq \frac{\delta^r}{4}$ there is a constant concentration of resin beads (c_R^*). In the intervals $\frac{3\delta^r}{4} \geq x \geq \frac{\delta^r}{2}$ and $\frac{\delta^r}{4} \geq x \geq 0$, c_R=0.
- The association of M with the resin beads is considered fast and strong, so perfect sink conditions for M are applied.
- The system is in steady-state conditions, so $\frac{\partial c_M}{\partial t} = \frac{\partial c_{ML}}{\partial t} = 0$.

- In the bulk solution ($x>\delta^r+\delta^g$), the concentration of free metal (c_M) and the concentration of complex (c_{ML}) are considered constant ($c_M = c_M^*$ and $c_{ML} = c_{ML}^*$) and in equilibrium conditions, so $c_{ML}^* = K' c_M^*$.

Considering the previous assumptions and the schematic representation shown in Figure S5.2A , the steady state diffusion-reaction equations to be solved are

Mathematical formulation

Regions 1 $\left(\delta^r + \delta^g \geq x > \delta^r\right)$, **3** $\left(\frac{3\delta^r}{4} \geq x > \frac{\delta^r}{2}\right)$, **and 5** ($0 < x < \delta^r/4$):

$$D_M \frac{\partial^2 c_M}{\partial x^2} + k_d c_{ML} - k_a' c_M = 0 \quad \text{(S5.3)}$$

$$D_{ML} \frac{\partial^2 c_{ML}}{\partial x^2} - k_d c_{ML} + k_a' c_M = 0 \quad \text{(S5.4)}$$

Regions 2 ($\delta^r \geq x > \frac{3\delta^r}{4}$), **and 4** ($\frac{\delta^r}{2} \geq x > \frac{\delta^r}{4}$):

$$c_M(x)=0 \quad \text{(S5.5)}$$

$$D_{ML} \frac{\partial^2 c_{ML}}{\partial x^2} - k_d c_{ML} = 0 \quad \text{(S5.6)}$$

Boundary conditions:

$$x = \delta^r + \delta^g \quad c_M(x = \delta^r + \delta^g) = c_M^*;\ c_{ML}(x = \delta^r + \delta^g) = c_{ML}^* \quad \text{(S5.7)}$$

$$x = \delta^r \quad c_M\left(x = \delta^r\right) = 0\ ;\ c_{ML}(x = \delta^{r^-}) = c_{ML}(x = \delta^{r^+});\ \left.\frac{\partial c_{ML}}{\partial x}\right|_{x=\delta^{r^-}} = \left.\frac{\partial c_{ML}}{\partial x}\right|_{x=\delta^{r^+}} \quad \text{(S5.8)}$$

$$x = \frac{3\delta^r}{4} \quad c_M\left(x = \frac{3\delta^r}{4}\right) = 0\ ;\ c_{ML}(x = \frac{3\delta^{r^-}}{4}) = c_{ML}(x = \frac{3\delta^{r^+}}{4});\ \left.\frac{\partial c_{ML}}{\partial x}\right|_{x=\frac{3\delta^{r^-}}{4}} = \left.\frac{\partial c_{ML}}{\partial x}\right|_{x=\frac{3\delta^{r^+}}{4}} \quad \text{(S5.9)}$$

$$x = \frac{\delta^r}{2} \quad c_M\left(x = \frac{\delta^r}{2}\right) = 0\ ;\ c_{ML}(x = \frac{\delta^{r^-}}{2}) = c_{ML}(x = \frac{\delta^{r^+}}{2});\ \left.\frac{\partial c_{ML}}{\partial x}\right|_{x=\frac{\delta^{r^-}}{2}} = \left.\frac{\partial c_{ML}}{\partial x}\right|_{x=\frac{\delta^{r^+}}{2}} \quad \text{(S5.10)}$$

$$x = \frac{\delta^r}{4} \quad c_M\left(x = \frac{\delta^r}{4}\right) = 0\ ;\ c_{ML}(x = \frac{\delta^{r^-}}{4}) = c_{ML}(x = \frac{\delta^{r^+}}{4});\ \left.\frac{\partial c_{ML}}{\partial x}\right|_{x=\frac{\delta^{r^-}}{4}} = \left.\frac{\partial c_{ML}}{\partial x}\right|_{x=\frac{\delta^{r^+}}{4}} \quad \text{(S5.11)}$$

$$x = 0 \qquad \left.\frac{\partial c_{\mathrm{M}}}{\partial x}\right|_{x=0} = 0 \; ; \quad \left.\frac{\partial c_{\mathrm{ML}}}{\partial x}\right|_{x=0} = 0 \tag{S5.12}$$

Solution

In the gel layer ($\delta^{\mathrm{r}} + \delta^{\mathrm{g}} \geq x > \delta^{\mathrm{r}}$), which, according to the Figure S5.2A is referred as region 1, the transport equations are:

$$D_{\mathrm{M}} \frac{\partial^2 c_{\mathrm{M}}}{\partial x^2} + k_{\mathrm{d}} c_{\mathrm{ML}} - k_{\mathrm{a}}^{'} c_{\mathrm{M}} = 0 \tag{S5.13}$$

$$D_{\mathrm{ML}} \frac{\partial^2 c_{\mathrm{ML}}}{\partial x^2} - k_{\mathrm{d}} c_{\mathrm{ML}} + k_{\mathrm{a}}^{'} c_{\mathrm{M}} = 0 \tag{S5.14}$$

An equivalent system of equations that is uncoupled can be found by searching linear combinations of Eqs (S5.13) and (S5.14). By addition, we obtain:

$$\frac{\partial^2 (D_{\mathrm{M}} c_{\mathrm{M}} + D_{\mathrm{ML}} c_{\mathrm{ML}})}{\partial x^2} = 0 \tag{S5.15}$$

After solving a homogeneous second order differential equation, the general solution for Eq (S5.15) is:

$$D_{\mathrm{M}} c_{\mathrm{M}} + D_{\mathrm{ML}} c_{\mathrm{ML}} = A_0 x + A_1 \tag{S5.16}$$

A second independent uncoupled equation can be found for $\phi = c_{\mathrm{ML}} - K' c_{\mathrm{M}}$. Using Eqs (S5.13) and (S5.14), after some rearrangements we obtain:

$$\frac{\partial^2 \phi}{\partial x^2} = \left(\frac{k_{\mathrm{a}}^{'}}{D_{\mathrm{M}}} + \frac{k_{\mathrm{d}}}{D_{\mathrm{ML}}} \right) \phi \tag{S5.17}$$

The general solution for Eq (S5.17) is

$$\phi = Q \exp\left(\frac{x}{m} \right) + P \exp\left(-\frac{x}{m} \right) \tag{S5.18}$$

where $\frac{1}{m} = \sqrt{\frac{k_{\mathrm{a}}^{'}}{D_{\mathrm{M}}} + \frac{k_{\mathrm{d}}}{D_{\mathrm{ML}}}}$. Q and P can be redefined in terms of a new couple of constants A' and B' in order to obtain simplified expressions. In the case of the first region, these parameters are set equal to:

$$Q = \left(\frac{A' - B'}{2} \right) \exp\left(\frac{-(\delta^{\mathrm{r}} + \delta^{\mathrm{g}})}{m} \right) \tag{S5.19}$$

$$P = \left(\frac{A'+B'}{2}\right)\exp\left(\frac{\delta^{r}+\delta^{g}}{m}\right) \quad \text{(S5.20)}$$

Then ϕ in the first region has the following expression:

$$\phi = A'\cosh\left(\frac{\delta^{r}+\delta^{g}-x}{m}\right)+B'\sinh\left(\frac{\delta^{r}+\delta^{g}-x}{m}\right) \quad \text{(S5.21)}$$

Now, to obtain a particular solution for the free metal concentration and complex concentration, we need to apply the boundary conditions (from the first region) to find the particular solutions for Eq (S5.16) and (S5.21). These conditions correspond to:

$$c_{M}(x=\delta^{r}+\delta^{g}) = c_{M}^{*} \quad \text{(S5.22)}$$

$$c_{M}\left(x=\delta^{r}\right) = 0 \quad \text{(S5.23)}$$

$$c_{ML}(x=\delta^{r}+\delta^{g}) = c_{ML}^{*} \quad \text{(S5.24)}$$

$$c_{ML}\left(x=\delta^{r}\right) = c_{ML}^{r} \quad \text{(S5.25)}$$

where the superscript "r" indicates value of a concentration at $x=\delta^{r}$. These values $\left(c_{M}^{r} \text{ and } c_{ML}^{r}\right)$, will be found later on (e.g. see Eq (S5.63))

Once applied the boundary conditions (S5.22)-(S5.25), we obtain the solution for the integration constants:

$$A_0 = \frac{D_M c_M^{*} + D_{ML}(c_{ML}^{*}-c_{ML}^{r})}{\delta^{g}},\ A_1 = D_{ML}c_{ML}^{r} - \frac{D_M c_M^{*} + D_{ML}(c_{ML}^{*}-c_{ML}^{r})}{\delta^{g}} \quad \text{(S5.26)}$$

and

$$A' = 0,\ B' = \frac{c_{ML}^{r}}{\sinh\left(\frac{\delta^{g}}{m}\right)} \quad \text{(S5.27)}$$

With the integration constants, we can obtain the concentration profiles in region 1 for c_M and c_{ML} as:

$$c_{\mathrm{M}}(x)=\frac{c_{\mathrm{M}}^{*}+\varepsilon(c_{\mathrm{ML}}^{*}-c_{\mathrm{ML}}^{\mathrm{r}})}{\delta^{\mathrm{g}}(1+\varepsilon K')}x-\frac{\varepsilon c_{\mathrm{ML}}^{\mathrm{r}}\sinh\left(\dfrac{\delta^{\mathrm{r}}+\delta^{\mathrm{g}}-x}{m}\right)}{(1+\varepsilon K')\sinh\left(\dfrac{\delta^{\mathrm{g}}}{m}\right)}+\frac{\delta^{\mathrm{g}}\varepsilon c_{\mathrm{ML}}^{\mathrm{r}}-(c_{\mathrm{M}}^{*}+\varepsilon(c_{\mathrm{ML}}^{*}-c_{\mathrm{ML}}^{\mathrm{r}}))\delta^{\mathrm{r}}}{\delta^{\mathrm{g}}(1+\varepsilon K')} \tag{S5.28}$$

and

$$c_{\mathrm{ML}}(x)=\frac{c_{\mathrm{ML}}^{*}+\varepsilon K'(c_{\mathrm{ML}}^{*}-c_{\mathrm{ML}}^{\mathrm{r}})}{\delta^{\mathrm{g}}(1+\varepsilon K')}x+\frac{c_{\mathrm{ML}}^{\mathrm{r}}\sinh\left(\dfrac{\delta^{\mathrm{r}}+\delta^{\mathrm{g}}-x}{m}\right)}{(1+\varepsilon K')\sinh\left(\dfrac{\delta^{\mathrm{g}}}{m}\right)}+\frac{\delta^{\mathrm{g}}\varepsilon K' c_{\mathrm{ML}}^{\mathrm{r}}-(c_{\mathrm{ML}}^{*}+\varepsilon K'(c_{\mathrm{ML}}^{*}-c_{\mathrm{ML}}^{\mathrm{r}}))\delta^{\mathrm{r}}}{\delta^{\mathrm{g}}(1+\varepsilon K')} \tag{S5.29}$$

where $\varepsilon=\dfrac{D_{\mathrm{ML}}}{D_{\mathrm{M}}}$, is the ratio of the diffusion coefficient of the metal complex and the free metal.

It is interesting to calculate $\left.\dfrac{\partial c_{\mathrm{ML}}}{\partial x}\right|_{x=\delta^{\mathrm{r}^{-}}}$ for the boundary condition involving the flux. From eq (S5.29), we obtain:

$$\left.\frac{\partial c_{\mathrm{ML}}}{\partial x}\right|_{x=\delta^{\mathrm{r}^{+}}}=\frac{c_{\mathrm{ML}}^{*}}{\delta^{\mathrm{g}}}-\frac{c_{\mathrm{ML}}^{\mathrm{r}}}{\delta^{\mathrm{g}}\left(1+\varepsilon K'\right)}\left(\varepsilon K'-\frac{\delta^{\mathrm{g}}\coth\left(\dfrac{\delta^{\mathrm{g}}}{m}\right)}{m}\right) \tag{S5.30}$$

This expression is of the interest to apply a boundary condition involving the flux at the right side of the resin-gel interface (eq (S5.30)) which will allow one to find an expression for $c_{\mathrm{ML}}^{\mathrm{r}}$ in terms of the physical parameters.

In region 2 ($\delta^{\mathrm{r}}\geq x\geq\dfrac{3\delta^{\mathrm{r}}}{4}$), c_{M}=0. The system of differential equations (S5.13)-(S5.14) is then reduced to:

$$D_{\mathrm{ML}}\frac{\partial^{2}c_{\mathrm{ML}}}{\partial x^{2}}-k_{\mathrm{d}}c_{\mathrm{ML}}=0 \tag{S5.31}$$

A general solution for eq (S5.31) is :

$$c_{\mathrm{ML}}(x) = A_0 \sinh\left(\frac{\delta^{\mathrm{r}} - x}{\lambda_{\mathrm{ML}}}\right) + A_1 \cosh\left(\frac{\delta^{\mathrm{r}} - x}{\lambda_{\mathrm{ML}}}\right) \tag{S5.32}$$

where $\lambda_{\mathrm{ML}} = \sqrt{\frac{D_{\mathrm{ML}}}{k_{\mathrm{d}}}}$.

Now to obtain a particular solution for Eq (S5.31), we need to apply the boundary conditions (S5.25) together with

$$c_{\mathrm{ML}}\left(x = \frac{3\delta^{\mathrm{r}}}{4}\right) = c_{\mathrm{ML}}^{\frac{3\mathrm{r}}{4}} \tag{S5.33}$$

where the superscript "3r/4" indicates that the value of the concentration is taken at x=3δ/4.

The solutions for the integration constants are:

$$A_0 = \frac{c_{\mathrm{ML}}^{\frac{3\mathrm{r}}{4}} - c_{\mathrm{ML}}^{\mathrm{r}} \cosh\left(\frac{\delta^{\mathrm{r}}}{4\lambda_{\mathrm{ML}}}\right)}{\sinh\left(\frac{\delta^{\mathrm{r}}}{4\lambda_{\mathrm{ML}}}\right)}, \quad A_1 = c_{\mathrm{ML}}^{\mathrm{r}} \tag{S5.34}$$

Substituting these integration constants, we obtain the concentration profile for the complex inside region 2, as a function of the boundary conditions and the physicochemical parameters.

$$c_{\mathrm{ML}}(x) = \frac{c_{\mathrm{ML}}^{\frac{3\mathrm{r}}{4}} - c_{\mathrm{ML}}^{\mathrm{r}} \cosh\left(\frac{\delta^{\mathrm{r}}}{4\lambda_{\mathrm{ML}}}\right)}{\sinh\left(\frac{\delta^{\mathrm{r}}}{4\lambda_{\mathrm{ML}}}\right)} \sinh\left(\frac{\delta^{\mathrm{r}} - x}{\lambda_{\mathrm{ML}}}\right) + c_{\mathrm{ML}}^{\mathrm{r}} \cosh\left(\frac{\delta^{\mathrm{r}} - x}{\lambda_{\mathrm{ML}}}\right) \tag{S5.35}$$

We can also calculate $\left.\frac{\partial c_{\mathrm{ML}}}{\partial x}\right|_{x=\delta^{\mathrm{r}-}}$ and $\left.\frac{\partial c_{\mathrm{ML}}}{\partial x}\right|_{x=\frac{3\delta^{\mathrm{r}-}}{4}}$, which will be useful to find an expression for

$c_{\mathrm{ML}}^{\mathrm{r}}$ and $c_{\mathrm{ML}}^{\frac{3\mathrm{r}}{4}}$ in terms of the physicochemical parameters:

$$\left.\frac{\partial c_{\mathrm{ML}}}{\partial x}\right|_{x=\delta^{\mathrm{r}-}} = \frac{c_{\mathrm{ML}}^{\mathrm{r}} \cosh\left(\frac{\delta^{\mathrm{r}}}{4\lambda_{\mathrm{ML}}}\right) - c_{\mathrm{ML}}^{\frac{3}{4}\mathrm{r}}}{\lambda_{\mathrm{ML}} \sinh\left(\frac{\delta^{\mathrm{r}}}{4\lambda_{\mathrm{ML}}}\right)} \tag{S5.36}$$

$$\left.\frac{\partial c_{\mathrm{ML}}}{\partial x}\right|_{x=\frac{3\delta^{r+}}{4}} = c_{\mathrm{ML}}^{\mathrm{r}}\left(\coth\left(\frac{\delta^{\mathrm{r}}}{4\lambda_{\mathrm{ML}}}\right)\cosh\left(\frac{\delta^{\mathrm{r}}}{4\lambda_{\mathrm{ML}}}\right)-\sinh\left(\frac{\delta^{\mathrm{r}}}{4\lambda_{\mathrm{ML}}}\right)\right)-\frac{c_{\mathrm{ML}}^{\frac{3}{4}\mathrm{r}}\coth\left(\frac{\delta^{\mathrm{r}}}{4\lambda_{\mathrm{ML}}}\right)}{\lambda_{\mathrm{ML}}} \quad \text{(S5.37)}$$

Let us, now, consider the region 3 ($\frac{3\delta^{\mathrm{r}}}{4} \geq x \geq \frac{\delta^{\mathrm{r}}}{2}$) where Eq (S5.15) and Eq (S5.14) have to be solved. The general solutions for c_{M} and c_{ML} are Eqs (S5.16) and (S5.21).

In region 3, we have to apply Eq (S5.33) and the following boundary conditions for the free metal and complex:

$$c_{\mathrm{M}}(x) = 0 \quad \text{for } x = \frac{3\delta^{\mathrm{r}}}{4} \text{ and } x = \frac{\delta^{\mathrm{r}}}{2} \quad \text{(S5.38)}$$

$$c_{\mathrm{ML}}\left(x = \frac{\delta^{\mathrm{r}}}{2}\right) = c_{\mathrm{ML}}^{\frac{\mathrm{r}}{2}} \quad \text{and} \quad c_{\mathrm{ML}}\left(x = \frac{3\delta^{\mathrm{r}}}{4}\right) = c_{\mathrm{ML}}^{\frac{3\mathrm{r}}{4}} \quad \text{(S5.39)}$$

The integration constants are:

$$A_0 = \frac{4D_{\mathrm{ML}}\left(c_{\mathrm{ML}}^{\frac{3\mathrm{r}}{4}} - c_{\mathrm{ML}}^{\frac{\mathrm{r}}{2}}\right)}{\delta^{\mathrm{r}}}, A_1 = D_{\mathrm{ML}}c_{\mathrm{ML}}^{\frac{\mathrm{r}}{2}} + 2D_{\mathrm{ML}}\left(c_{\mathrm{ML}}^{\frac{\mathrm{r}}{2}} - c_{\mathrm{ML}}^{\frac{3\mathrm{r}}{4}}\right) \quad \text{(S5.40)}$$

$$A' = \frac{c_{\mathrm{ML}}^{\frac{\mathrm{r}}{2}} - c_{\mathrm{ML}}^{\frac{3\mathrm{r}}{4}}\cosh\left(\frac{\delta^{\mathrm{r}}}{4m}\right)}{\sinh\left(\frac{\delta^{\mathrm{r}}}{4m}\right)}, B' = c_{\mathrm{ML}}^{\frac{3\mathrm{r}}{4}} \quad \text{(S5.41)}$$

With the integration constants, we can write the concentration profiles in region 3 for c_{M} and c_{ML} in terms of the boundary values (e.g. $c_{\mathrm{ML}}^{\frac{\mathrm{r}}{2}}$) and the physicochemical parameters as:

$$c_{\mathrm{M}}(x) = \frac{\varepsilon\left(3c_{\mathrm{ML}}^{\frac{\mathrm{r}}{2}} - 2c_{\mathrm{ML}}^{\frac{3\mathrm{r}}{4}}\right)}{(1+\varepsilon K')} + \frac{4\varepsilon\left(c_{\mathrm{ML}}^{\frac{3\mathrm{r}}{4}} - c_{\mathrm{ML}}^{\frac{\mathrm{r}}{2}}\right)}{\delta^{\mathrm{r}}(1+\varepsilon K')}x - \frac{c_{\mathrm{ML}}^{\frac{\mathrm{r}}{2}} - c_{\mathrm{ML}}^{\frac{3\mathrm{r}}{4}}\cosh\left(\frac{\delta^{\mathrm{r}}}{4m}\right)}{(1+\varepsilon K')\sinh\left(\frac{\delta^{\mathrm{r}}}{4m}\right)}\varepsilon\sinh\left(\frac{\frac{3}{4}\delta^{\mathrm{r}} - x}{m}\right) - \frac{\varepsilon c_{\mathrm{ML}}^{\frac{3\mathrm{r}}{4}}\cosh\left(\frac{\frac{3}{4}\delta^{\mathrm{r}} - x}{m}\right)}{(1+\varepsilon K')} \quad \text{(S5.42)}$$

and

$$c_{\mathrm{ML}}(x)=\frac{\varepsilon K'\left(3c_{\mathrm{ML}}^{\frac{\mathrm{r}}{2}}-2c_{\mathrm{ML}}^{\frac{3\mathrm{r}}{4}}\right)}{(1+\varepsilon K')}+\frac{4\varepsilon K'\left(c_{\mathrm{ML}}^{\frac{3\mathrm{r}}{4}}-c_{\mathrm{ML}}^{\frac{\mathrm{r}}{2}}\right)}{\delta^{\mathrm{r}}(1+\varepsilon K')}x+\frac{c_{\mathrm{ML}}^{\frac{\mathrm{r}}{2}}-c_{\mathrm{ML}}^{\frac{3\mathrm{r}}{4}}\cosh\left(\frac{\delta^{\mathrm{r}}}{4m}\right)}{(1+\varepsilon K')\sinh\left(\frac{\delta^{\mathrm{r}}}{4m}\right)}\sinh\left(\frac{\frac{3}{4}\delta^{\mathrm{r}}-x}{m}\right)+\frac{c_{\mathrm{ML}}^{\frac{3\mathrm{r}}{4}}\cosh\left(\frac{\frac{3}{4}\delta^{\mathrm{r}}-x}{m}\right)}{(1+\varepsilon K')} \quad \text{(S5.43)}$$

Now we can calculate $\left.\frac{\partial c_{\mathrm{ML}}}{\partial x}\right|_{x=\frac{3\delta^{\mathrm{r}-}}{4}}$ and $\left.\frac{\partial c_{\mathrm{ML}}}{\partial x}\right|_{x=\frac{\delta^{\mathrm{r}+}}{2}}$. We obtain:

$$\left.\frac{\partial c_{\mathrm{ML}}}{\partial x}\right|_{x=\frac{3\delta^{\mathrm{r}-}}{4}}=c_{\mathrm{ML}}^{\frac{3\mathrm{r}}{4}}\left(\frac{4\varepsilon K'}{\delta^{\mathrm{r}}\left(1+\varepsilon K'\right)}+\frac{\coth\left(\frac{\delta^{\mathrm{r}}}{4m}\right)}{m\left(1+\varepsilon K'\right)}\right)-c_{\mathrm{ML}}^{\frac{\mathrm{r}}{2}}\left(\frac{\operatorname{csch}\left(\frac{\delta^{\mathrm{r}}}{4m}\right)}{m\left(1+\varepsilon K'\right)}+\frac{4\varepsilon K'}{\delta^{\mathrm{r}}\left(1+\varepsilon K'\right)}\right) \quad \text{(S5.44)}$$

$$\left.\frac{\partial c_{\mathrm{ML}}}{\partial x}\right|_{x=\frac{\delta^{\mathrm{r}+}}{2}}=\frac{c_{\mathrm{ML}}^{\frac{3\mathrm{r}}{4}}\left(\frac{\cosh\left(\frac{\delta^{\mathrm{r}}}{4m}\right)\coth\left(\frac{\delta^{\mathrm{r}}}{4m}\right)-\sinh\left(\frac{\delta^{\mathrm{r}}}{4m}\right)}{m}+\frac{4\varepsilon K'}{\delta^{\mathrm{r}}}\right)}{\left(1+\varepsilon K'\right)}-\frac{c_{\mathrm{ML}}^{\frac{\mathrm{r}}{2}}\left(\frac{\coth\left(\frac{\delta^{\mathrm{r}}}{4m}\right)}{m}+\frac{4\varepsilon K'}{\delta^{\mathrm{r}}}\right)}{\left(1+\varepsilon K'\right)} \quad \text{(S5.45)}$$

From these expressions, later on, we are going to find $c_{\mathrm{ML}}^{\frac{3}{4}\mathrm{r}}$ and $c_{\mathrm{ML}}^{\frac{\mathrm{r}}{2}}$ in terms of the physicochemical parameters.

In region 4, ($\frac{\delta^{\mathrm{r}}}{2}\geq x\geq\frac{\delta^{\mathrm{r}}}{4}$), the same differential equation as in region 2 has to be solved, (Eq (S5.31)) whose general solution is:

$$c_{\mathrm{ML}}(x)=A_0\sinh\left(\frac{\frac{\delta^{\mathrm{r}}}{2}-x}{\lambda_{\mathrm{ML}}}\right)+A_1\cosh\left(\frac{\frac{\delta^{\mathrm{r}}}{2}-x}{\lambda_{\mathrm{ML}}}\right) \quad \text{(S5.46)}$$

In this region 4, the boundary conditions to obtain the particular solution of the differential equation are (S5.39) together with

$$c_{\mathrm{ML}}\left(x=\frac{\delta^{\mathrm{r}}}{4}\right)=c_{\mathrm{ML}}^{\frac{\mathrm{r}}{4}} \quad \text{and} \quad c_{\mathrm{ML}}\left(x=\frac{\delta^{\mathrm{r}}}{2}\right)=c_{\mathrm{ML}}^{\frac{\mathrm{r}}{2}} \quad \text{(S5.47)}$$

The solutions for the integration constants are:

$$A_0 = \frac{c_{ML}^{\frac{r}{4}} - c_{ML}^{\frac{r}{2}} \cosh\left(\frac{\delta^r}{4\lambda_{ML}}\right)}{\sinh\left(\frac{\delta^r}{4\lambda_{ML}}\right)},\ A_1 = c_{ML}^{\frac{r}{2}} \qquad \text{(S5.48)}$$

After obtaining the integration constants, the concentration profile for c_{ML} in region 4 becomes:

$$c_{ML}(x) = \frac{c_{ML}^{\frac{r}{4}} - c_{ML}^{\frac{r}{2}} \cosh\left(\frac{\delta^r}{4\lambda_{ML}}\right)}{\sinh\left(\frac{\delta^r}{4\lambda_{ML}}\right)} \sinh\left(\frac{\delta^r - x}{\lambda_{ML}}\right) + c_{ML}^{\frac{r}{2}} \cosh\left(\frac{\delta^r - x}{\lambda_{ML}}\right) \qquad \text{(S5.49)}$$

Now we can obtain $\left.\frac{\partial c_{ML}}{\partial x}\right|_{x=\frac{\delta^{r-}}{2}}$ and $\left.\frac{\partial c_{ML}}{\partial x}\right|_{x=\frac{\delta^{r+}}{4}}$ as:

$$\left.\frac{\partial c_{ML}}{\partial x}\right|_{x=\frac{\delta^{r-}}{2}} = \frac{c_{ML}^{\frac{r}{2}} \cosh\left(\frac{\delta^r}{4\lambda_{ML}}\right) - c_{ML}^{\frac{r}{4}}}{\lambda_{ML} \sinh\left(\frac{\delta^r}{4\lambda_{ML}}\right)} \qquad \text{(S5.50)}$$

and

$$\left.\frac{\partial c_{ML}}{\partial x}\right|_{x=\frac{\delta^{r+}}{4}} = \frac{\left(c_{ML}^{\frac{r}{2}} \cosh\left(\frac{\delta^r}{4\lambda_{ML}}\right) - c_{ML}^{\frac{r}{4}}\right)\cosh\left(\frac{\delta^r}{4\lambda_{ML}}\right)}{\lambda_{ML} \sinh\left(\frac{\delta^r}{4\lambda_{ML}}\right)} - \frac{c_{ML}^{\frac{r}{2}} \sinh\left(\frac{\delta^r}{4\lambda_{ML}}\right)}{\lambda_{ML}} \qquad \text{(S5.51)}$$

From these expressions we will find an expression for $c_{ML}^{\frac{r}{2}}$ and $c_{ML}^{\frac{r}{4}}$ in terms of the physicochemical parameters.

In region 5, ($0 < x < \delta^r/4$), the same system of uncoupled differential equations as in region 1 and 3 has to be solved (eqs (S5.15) and (S5.17). Their general solutions are eq (S5.16) and an equation similar to eq (S5.21) :

$$\phi = A'\cosh\left(\frac{\frac{1}{4}\delta^r - x}{m}\right) + B'\sinh\left(\frac{\frac{1}{4}\delta^r - x}{m}\right) \qquad \text{(S5.52)}$$

Now to obtain a particular solution for the free metal concentration and complex concentration in region 5, we need to apply the boundary conditions.

$$c_{\mathrm{M}}\left(x=\frac{\delta^{\mathrm{r}}}{4}\right)=0 \tag{S5.53}$$

$$\left.\frac{\partial c_{\mathrm{M}}}{\partial x}\right|_{x=0}=0 \tag{S5.54}$$

$$c_{\mathrm{ML}}\left(x=\frac{\delta^{\mathrm{r}}}{4}\right)=\overline{c}^{\frac{\mathrm{r}}{4}}_{\mathrm{ML}} \tag{S5.55}$$

$$\left.\frac{\partial c_{\mathrm{ML}}}{\partial x}\right|_{x=0}=0 \tag{S5.56}$$

The solutions for the integration constants are:

$$A_0=0, A_1=D_{\mathrm{ML}}\overline{c}^{\frac{\mathrm{r}}{4}}_{\mathrm{ML}} \tag{S5.57}$$

$$A'=-\overline{c}^{\frac{\mathrm{r}}{4}}_{\mathrm{ML}}\tanh\left(\frac{\delta^{\mathrm{r}}}{4m}\right), B'=\overline{c}^{\frac{\mathrm{r}}{4}}_{\mathrm{ML}} \tag{S5.58}$$

-With the integration constants, we obtain the concentration profiles for c_{ML} and c_{M} in region 5 as:

$$c_{\mathrm{M}}(x)=\frac{\varepsilon\overline{c}^{\frac{\mathrm{r}}{4}}_{\mathrm{ML}}}{1+\varepsilon K'}\left(1+\tanh\left(\frac{\delta^{\mathrm{r}}}{4m}\right)\sinh\left(\frac{\frac{\delta^{\mathrm{r}}}{4}-x}{m}\right)-\cosh\left(\frac{\frac{\delta^{\mathrm{r}}}{4}-x}{m}\right)\right) \tag{S5.59}$$

and

$$c_{\mathrm{ML}}(x)=\frac{\overline{c}^{\frac{\mathrm{r}}{4}}_{\mathrm{ML}}}{1+\varepsilon K'}\left(K'\varepsilon+\tanh\left(\frac{\delta^{\mathrm{r}}}{4m}\right)\sinh\left(\frac{\frac{\delta^{\mathrm{r}}}{4}-x}{m}\right)-\cosh\left(\frac{\frac{\delta^{\mathrm{r}}}{4}-x}{m}\right)\right) \tag{S5.60}$$

while $\left.\frac{\partial c_{\mathrm{ML}}}{\partial x}\right|_{x=\frac{\delta^{\mathrm{r}^+}}{4}}$ becomes:

$$\left.\frac{\partial c_{\mathrm{ML}}}{\partial x}\right|_{x=\frac{\delta^{\mathrm{r}^+}}{4}}=\frac{\overline{c}^{\frac{\mathrm{r}}{4}}_{\mathrm{ML}}\tanh\left(\frac{\delta^{\mathrm{r}}}{4m}\right)}{m\left(1+\varepsilon K'\right)} \tag{S5.61}$$

Now that we have an expression for each region of our piecewise function, we can obtain the constants $c^{\mathrm{r}}_{\mathrm{ML}}, c^{\frac{3\mathrm{r}}{4}}_{\mathrm{ML}}, c^{\frac{\mathrm{r}}{2}}_{\mathrm{ML}}, c^{\frac{\mathrm{r}}{4}}_{\mathrm{ML}}$ in terms of the physical parameters by applying conditions of flux continuity.

In order to obtain $c^{\mathrm{r}}_{\mathrm{ML}}$, we can write:

$$D_{\mathrm{ML}} \left.\frac{\partial c_{\mathrm{ML}}}{\partial x}\right|_{x=\delta^{\mathrm{r}+}} = D_{\mathrm{ML}} \left.\frac{\partial c_{\mathrm{ML}}}{\partial x}\right|_{x=\delta^{\mathrm{r}-}} \tag{S5.62}$$

Using Eqs (S5.30) and (S5.36) and solving for $c^{\mathrm{r}}_{\mathrm{ML}}$, a solution is found in terms of $c^{\frac{3\mathrm{r}}{4}}_{\mathrm{ML}}$ and some physical parameters:

$$c^{\mathrm{r}}_{\mathrm{ML}} = \frac{c^{*}_{\mathrm{ML}}(1+\varepsilon K')\lambda_{\mathrm{ML}} + c^{\frac{3\mathrm{r}}{4}}_{\mathrm{ML}}\delta^{\mathrm{g}}(1+\varepsilon K')\operatorname{csch}\left(\frac{\delta^{\mathrm{r}}}{4\lambda_{\mathrm{ML}}}\right)}{\varepsilon K'\lambda_{\mathrm{ML}} + \frac{\delta^{\mathrm{g}}\lambda_{\mathrm{ML}}}{m}\coth\left(\frac{\delta^{\mathrm{g}}}{m}\right) + \delta^{\mathrm{g}}(1+\varepsilon K')\coth\left(\frac{\delta^{\mathrm{r}}}{4\lambda_{\mathrm{ML}}}\right)} \tag{S5.63}$$

In order to obtain $c^{\frac{3\mathrm{r}}{4}}_{\mathrm{ML}}$, we apply:

$$D_{\mathrm{ML}} \left.\frac{\partial c_{\mathrm{ML}}}{\partial x}\right|_{x=\frac{3\delta^{\mathrm{r}+}}{4}} = D_{\mathrm{ML}} \left.\frac{\partial c_{\mathrm{ML}}}{\partial x}\right|_{x=\frac{3\delta^{\mathrm{r}-}}{4}} \tag{S5.64}$$

from which, using Eqs (S5.37) and (S5.44) and solving for $c^{\frac{3\mathrm{r}}{4}}_{\mathrm{ML}}$, we find a solution in terms of $c^{\frac{\mathrm{r}}{2}}_{\mathrm{ML}}$ and some physical parameters. To write the solution for $c^{\frac{3\mathrm{r}}{4}}_{\mathrm{ML}}$ in a compact way, we define the variables *a*, *b* and *z* :

$$a = \left(\varepsilon K'\lambda_{\mathrm{ML}} + \frac{\delta^{\mathrm{g}}\lambda_{\mathrm{ML}}}{m}\coth\left(\frac{\delta^{\mathrm{g}}}{m}\right) + \delta^{\mathrm{g}}(1+\varepsilon K')\coth\left(\frac{\delta^{\mathrm{r}}}{4\lambda_{\mathrm{ML}}}\right)\right) \tag{S5.65}$$

$$b = a\left(\frac{4\varepsilon K'}{\delta^{\mathrm{r}}(1+\varepsilon K')} + \frac{\coth\left(\frac{\delta^{\mathrm{r}}}{4m}\right)}{m(1+\varepsilon K')} + \frac{\coth\left(\frac{\delta^{\mathrm{r}}}{4\lambda_{\mathrm{ML}}}\right)}{\lambda_{\mathrm{ML}}}\right) - \frac{\left(\left(\coth\left(\frac{\delta^{\mathrm{r}}}{4\lambda_{\mathrm{ML}}}\right)\cosh\left(\frac{\delta^{\mathrm{r}}}{4\lambda_{\mathrm{ML}}}\right) - \sinh\left(\frac{\delta^{\mathrm{r}}}{4\lambda_{\mathrm{ML}}}\right)\right)\mathrm{csch}\left(\frac{\delta^{\mathrm{r}}}{4\lambda_{\mathrm{ML}}}\right)\delta^{\mathrm{g}}(1+\varepsilon K')\right)}{\lambda_{\mathrm{ML}}} \quad \text{(S5.66)}$$

and

$$z = a\left(\frac{\mathrm{csch}\left(\frac{\delta^{\mathrm{r}}}{4m}\right)}{m(1+\varepsilon K')} + \frac{4\varepsilon K'}{\delta^{\mathrm{r}}(1+\varepsilon K')}\right) \quad \text{(S5.67)}$$

With these definitions,

$$c_{\mathrm{ML}}^{\frac{3\mathrm{r}}{4}} = \frac{c_{\mathrm{ML}}^{*}(1+\varepsilon K')\left(\coth\left(\frac{\delta^{\mathrm{r}}}{4\lambda_{\mathrm{ML}}}\right)\cosh\left(\frac{\delta^{\mathrm{r}}}{4\lambda_{\mathrm{ML}}}\right) - \sinh\left(\frac{\delta^{\mathrm{r}}}{4\lambda_{\mathrm{ML}}}\right)\right) + c_{\mathrm{ML}}^{\frac{\mathrm{r}}{2}} z}{b} \quad \text{(S5.68)}$$

Then, to obtain $c_{\mathrm{ML}}^{\frac{\mathrm{r}}{2}}$, we apply:

$$D_{\mathrm{ML}}\left.\frac{\partial c_{\mathrm{ML}}}{\partial x}\right|_{x=\frac{\delta^{\mathrm{r}^+}}{2}} = D_{\mathrm{ML}}\left.\frac{\partial c_{\mathrm{ML}}}{\partial x}\right|_{x=\frac{\delta^{\mathrm{r}^-}}{2}} \quad \text{(S5.69)}$$

which, using Eqs (S5.45) and (S5.50) and solving for $c_{\mathrm{ML}}^{\frac{\mathrm{r}}{2}}$, has a solution in terms of $c_{\mathrm{ML}}^{\frac{\mathrm{r}}{4}}$ and some physical parameters. To be able to display the solution for $c_{\mathrm{ML}}^{\frac{\mathrm{r}}{2}}$, we use the previous variables b (Eq (S5.66)), z (Eq (S5.67)) and the following variables:

$$h = \frac{c_{\mathrm{ML}}^{*}(1+\varepsilon K')\left(\coth\left(\frac{\delta^{\mathrm{r}}}{4\lambda_{\mathrm{ML}}}\right)\cosh\left(\frac{\delta^{\mathrm{r}}}{4\lambda_{\mathrm{ML}}}\right) - \sinh\left(\frac{\delta^{\mathrm{r}}}{4\lambda_{\mathrm{ML}}}\right)\right)}{b}\left(\frac{\left(\coth\left(\frac{\delta^{\mathrm{r}}}{4m}\right)\cosh\left(\frac{\delta^{\mathrm{r}}}{4m}\right) - \sinh\left(\frac{\delta^{\mathrm{r}}}{4m}\right)\right)}{m(1+\varepsilon K')} + \frac{4\varepsilon K'}{\delta^{\mathrm{r}}(1+\varepsilon K')}\right) \quad \text{(S5.70)}$$

and

$$f = \frac{-z}{b}\left(\frac{\left(\coth\left(\frac{\delta^{\mathrm{r}}}{4m}\right)\cosh\left(\frac{\delta^{\mathrm{r}}}{4m}\right) - \sinh\left(\frac{\delta^{\mathrm{r}}}{4m}\right)\right)}{m(1+\varepsilon K')} + \frac{4\varepsilon K'}{\delta^{\mathrm{r}}(1+\varepsilon K')} \right) + \frac{\coth\left(\frac{\delta^{\mathrm{r}}}{4\lambda_{\mathrm{ML}}}\right)}{\lambda_{\mathrm{ML}}} + \frac{\coth\left(\frac{\delta^{\mathrm{r}}}{4m}\right)}{m(1+\varepsilon K')} + \frac{4\varepsilon K'}{\delta^{\mathrm{r}}(1+\varepsilon K')} \tag{S5.71}$$

With these definitions,

$$c_{\mathrm{ML}}^{\frac{\mathrm{r}}{2}} = \frac{c_{\mathrm{ML}}^{\frac{\mathrm{r}}{4}}\operatorname{csch}\left(\frac{\delta^{\mathrm{r}}}{4\lambda_{\mathrm{ML}}}\right) + h\lambda_{\mathrm{ML}}}{f\lambda_{\mathrm{ML}}} \tag{S5.72}$$

Then, to obtain $c_{\mathrm{ML}}^{\frac{\mathrm{r}}{4}}$, we apply:

$$D_{\mathrm{ML}}\left.\frac{\partial c_{\mathrm{ML}}}{\partial x}\right|_{x=\frac{\delta^{\mathrm{r}+}}{4}} = D_{\mathrm{ML}}\left.\frac{\partial c_{\mathrm{ML}}}{\partial x}\right|_{x=\frac{\delta^{\mathrm{r}-}}{4}} \tag{S5.73}$$

which, using Eqs (S5.51) and (S5.61), has a solution only in terms of some physical parameters. To be able to show the solution for $c_{\mathrm{ML}}^{\frac{\mathrm{r}}{4}}$, we use the previous variables *f* (Eq (S5.71)) and *h* (Eq (S5.70)) and define the variable *p*:

$$p = \frac{\left(\coth\left(\frac{\delta^{\mathrm{r}}}{4\lambda_{\mathrm{ML}}}\right)\cosh\left(\frac{\delta^{\mathrm{r}}}{4\lambda_{\mathrm{ML}}}\right) - \sinh\left(\frac{\delta^{\mathrm{r}}}{4\lambda_{\mathrm{ML}}}\right)\right)}{f\lambda_{\mathrm{ML}}^2}\operatorname{csch}\left(\frac{\delta^{\mathrm{r}}}{4\lambda_{\mathrm{ML}}}\right) + \frac{\coth\left(\frac{\delta^{\mathrm{r}}}{4\lambda_{\mathrm{ML}}}\right)}{\lambda_{\mathrm{ML}}} + \frac{\tanh\left(\frac{\delta^{\mathrm{r}}}{4m}\right)}{m(1+\varepsilon K')} \tag{S5.74}$$

With these definitions,

$$c_{\mathrm{ML}}^{\frac{\mathrm{r}}{4}} = \frac{\left(\coth\left(\frac{\delta^{\mathrm{r}}}{4\lambda_{\mathrm{ML}}}\right)\cosh\left(\frac{\delta^{\mathrm{r}}}{4\lambda_{\mathrm{ML}}}\right) - \sinh\left(\frac{\delta^{\mathrm{r}}}{4\lambda_{\mathrm{ML}}}\right)\right)h}{fp\lambda_{\mathrm{ML}}} \tag{S5.75}$$

The ML concentration profile in the whole resin domain is a piecewise function defined by equations (S5.29), (S5.35), (S5.43) and (S5.49) which contain the boundary values given in Eqs (S5.63), (S5.68), (S5.72) and (S5.75).

5.9.3 Deriving the back percentage *B* for a heterogeneous resin

To derive an expression to determine the percentage of back accumulation, B , one needs to calculate the ratio of accumulated moles of metal from x=0 to $x=\delta^r/2$ over the accumulated moles of metal from x=0 to $x=\delta^r$.

In order to derive this expression, first, one needs to add the differential equations for the free metal and complex (Eq (S5.13) and Eq (S5.14)). Second, one needs to integrate twice the resulting differential equation (S5.15). After obtaining the general solution (S5.16) and applying the boundary conditions (S5.22)-(S5.25), we obtain:

$$J\Big|_{x=\delta^r} = \frac{D_M c_M^*}{\delta^g} + D_{ML}\frac{c_{ML}^* - c_{ML}^r}{\delta^g} \qquad \text{(S5.76)}$$

A similar procedure leads to obtain the flux at x= $\delta^{r/2}$, but one needs to apply the boundary conditions of the region 3 (Eqs (S5.33), (S5.38) and (S5.39)).

$$J\Big|_{x=\delta^{\frac{r}{2}}} = 4D_{ML}\left(\frac{c_{ML}^{\frac{3r}{4}} - c_{ML}^{\frac{r}{2}}}{\delta^r}\right) \qquad \text{(S5.77)}$$

Then, to obtain B in a heterogeneous resin, one needs to divide the flux in the back resin (Eq (S5.77)) by the total flux (Eq (S5.76)):

$$B_{het} = \frac{4D_{ML}\left(\frac{c_{ML}^{\frac{3r}{4}} - c_{ML}^{\frac{r}{2}}}{\delta^r}\right)}{\frac{D_M c_M^*}{\delta^g} + \frac{D_{ML}\left(c_{ML}^* - c_{ML}^r\right)}{\delta^g}} \qquad \text{(S5.78)}$$

5.9.4 Deriving *B* for a homogeneous resin

As above, to derive an expression for *B* in a homogenous resin, one needs to calculate the ratio of accumulated moles of metal from x=0 to $x=\delta^r/2$ over the accumulated moles of metal from x=0 to $x=\delta^r$.

In steady-state and ligand excess conditions, the accumulation when a metal (M) reacts with a ligand (L) to produce a complex (ML) can be written as:

$$n_M = At\left(D_{ML}\left.\frac{\partial\, c_{ML}}{\partial x}\right|_{x=\delta^r} + D_M\left.\frac{\partial\, c_M}{\partial x}\right|_{x=\delta^r}\right) \quad \text{(S5.79)}$$

The flux is

$$J = D_{ML}\left.\frac{\partial\, c_{ML}}{\partial x}\right|_{x=\delta^r} + D_M\left.\frac{\partial\, c_M}{\partial x}\right|_{x=\delta^r} \quad \text{(S5.80)}$$

In the back resin (i.e $x<\delta^r/2$) the accumulation is:

$$n_M = At\, D_M\left.\frac{\partial c_{ML}}{\partial x}\right|_{x=\frac{\delta^r}{2}} \quad \text{(S5.81)}$$

With the same procedure used in the heterogenous resin, but using c_M =0 for the whole resin domain $0 < x < \delta^r$, the flux at $x=\delta^r$ can be written as,

$$J\big|_{x=\delta^r} = \frac{D_M c_M^*}{\delta^g} + D_{ML}\,\frac{c_{ML}^* - c_{ML}^r}{\delta^g} \quad \text{(S5.82)}$$

The main difference in the flux calculation respect to the heterogeneous resin is found in the calculation of the flux of complex at $x=\delta^r/2$.

Eq (S5.31) describes the diffusion-reaction equation for ML in a region with resin beads. This equation holds now for the complex in region 2 of the homogenous resin. The general solution of Eq (S5.31) can be written as:

$$c_{ML}(x) = A_2 \exp\left(\frac{x}{\lambda_{ML}}\right) + B_2 \exp\left(\frac{-x}{\lambda_{ML}}\right) \quad \text{(S5.83)}$$

A particular solution can be found by applying the following boundary conditions:

$$c_{\mathrm{ML}}(x=\delta^{\mathrm{r-}}) = c^{\mathrm{r}}_{\mathrm{ML}} = c_{\mathrm{ML}}(x=\delta^{\mathrm{r+}})\,;\ \left.\frac{\partial c_{\mathrm{ML}}}{\partial x}\right|_{x=\delta^{r-}} = \left.\frac{\partial c_{\mathrm{ML}}}{\partial x}\right|_{x=\delta^{r+}} \tag{S5.84}$$

and

$$\left.\frac{\partial c_{\mathrm{ML}}}{\partial x}\right|_{x=0} = 0 \tag{S5.85}$$

The result for the integration constants A_2 and B_2 after applying the boundary conditions is :

$$A_2 = B_2 = \frac{c^{\mathrm{r}}_{\mathrm{ML}}}{2\cosh\left(\dfrac{\delta^{\mathrm{r}}}{\lambda_{\mathrm{ML}}}\right)}\,;\ c^{\mathrm{r}}_{\mathrm{ML}} = c^{*}_{\mathrm{ML}}\left(\frac{\dfrac{\delta^{\mathrm{g}}}{m}\coth\left(\dfrac{\delta^{\mathrm{g}}}{m}\right)+\dfrac{\delta^{\mathrm{g}}(1+\varepsilon K')}{\lambda_{\mathrm{ML}}}\tanh\left(\dfrac{\delta^{\mathrm{r}}}{\lambda_{\mathrm{ML}}}\right)}{\varepsilon K'+\dfrac{\delta^{\mathrm{g}}}{m}\coth\left(\dfrac{\delta^{\mathrm{g}}}{m}\right)+\dfrac{\delta^{\mathrm{g}}(1+\varepsilon K')}{\lambda_{\mathrm{ML}}}\tanh\left(\dfrac{\delta^{\mathrm{r}}}{\lambda_{\mathrm{ML}}}\right)}\right) \tag{S5.86}$$

and the concentration profile after substituting the integration constants is:

$$c_{\mathrm{ML}}(x) = \frac{c^{\mathrm{r}}_{\mathrm{ML}}\cosh\left(\dfrac{x}{\lambda_{\mathrm{ML}}}\right)}{\cosh\left(\dfrac{\delta^{\mathrm{r}}}{\lambda_{\mathrm{ML}}}\right)} \tag{S5.87}$$

Applying $\left.\dfrac{\partial c_{\mathrm{ML}}}{\partial x}\right|_{x=\frac{\delta^{\mathrm{r}}}{2}}$ to the previous equation, the flux at x=δ^{r}/2 can be found as:

$$J_{\mathrm{ML}}\Big|_{x=\frac{\delta^{\mathrm{r}}}{2}} = D_{\mathrm{ML}}c^{\mathrm{r}}_{\mathrm{ML}}\frac{\sinh\left(\dfrac{\delta^{\mathrm{r}}}{2\lambda_{\mathrm{ML}}}\right)}{\lambda_{\mathrm{ML}}\cosh\left(\dfrac{\delta^{\mathrm{r}}}{\lambda_{\mathrm{ML}}}\right)} \tag{S5.88}$$

The expression for *B* in the homogeneous case results from dividing *J* at $x=\delta^{\mathrm{r}}$ (Eq S5.87) by *J* at $x=\delta^{\mathrm{r}}/2$ (Eq (S5.88)):

$$B = \frac{\varepsilon K'\,\mathrm{sech}\left(\dfrac{\delta^{\mathrm{r}}}{\lambda_{\mathrm{ML}}}\right)\sinh\left(\dfrac{\delta^{\mathrm{r}}}{2\lambda_{\mathrm{ML}}}\right)}{\lambda_{\mathrm{ML}}\coth\left(\dfrac{\delta^{\mathrm{g}}}{m}\right)+(1+\varepsilon K')m\tanh\left(\dfrac{\delta^{\mathrm{r}}}{\lambda_{\mathrm{ML}}}\right)} \tag{S5.89}$$

5.9.5 Determination of k_d from B

Sections 5.4 and 5.5 outline the determination of B from the limiting expression (5.8) of the main manuscript, from Eq (S5.89) or from Eq (S5.78). A short discussion on the validity conditions for using each one of these expression follows. Complementary to these Sections, an additional Excel file is included in the SI ready to estimate k_d value using to all these equations once input data from the user is introduced. The most accurate value of k_d appears in a green cell.

5.9.5.1 Algorithm to obtain k_d using the complete expression for B corresponding to a homogeneous resins

The use of the limiting expression Eq (5.8) of the main manuscript, when applicable, allows a straightforward determination of k_d, while, when Eq (S5.89) (Eq (5.6) of the main manuscript) needs to be used, an iterative procedure can be applied.

In order to have a simple criterion for the plausibility of the application of Eq (5.8), we explore the fulfilment of the approximation:

$$J_M\big|_{x=\delta^r} << J_{ML}\big|_{x=\delta^r} \qquad \text{(S5.90)}$$

on which the limiting expression Eq (5.8) relies. The reaction layer concept[30] applied to the DGT devices can provide approximate expressions for $J_M\big|_{x=\delta^r}$ and $J_{ML}\big|_{x=\delta^r}$.[23] Indeed, since almost all the metal arriving as free metal at $x=\delta^r$ comes from the dissociation of complex in the reaction layer located inside the diffusive disc,

$$J_M\big|_{x=\delta^r} \approx k_d c^*_{ML}\left(1-\xi\right) m \tanh\left(\frac{\delta^g}{m}\right) \qquad \text{(S5.91)}$$

where $c^*_{ML}\left(1-\xi\right)$ stands for the complex concentration at the interface resin-diffusive disc, i.e., estimates the complex concentration taken as constant along the reaction layer inside the diffusive disc whose thickness is estimated by $m\tanh\left(\frac{\delta^g}{m}\right)$.[17]

On the other hand, due to steady state, one can assume that the flux of arriving ML at $x=\delta^r$ is also the amount of ML that is dissociating along an effective thickness of the complex

penetration into the resin disc given by $\lambda_{ML}\coth\left(\frac{\delta^r}{\lambda_{ML}}\right)$(see figure 1 in reference [17]) with average concentration $\frac{1}{2}c^*_{ML}(1-\xi)$. Then,

$$J_{ML}\big|_{x=\delta^r} \approx \frac{1}{2}k_d c^*_{ML}(1-\xi)\lambda_{ML}\coth\left(\frac{\delta^r}{\lambda_{ML}}\right) \qquad \text{(S5.92)}$$

According to eqs (S5.91) and (S5.92), the inequality $J_M\big|_{x=\delta^r} << J_{ML}\big|_{x=\delta^r}$ reduces to $m\tanh\left(\frac{\delta^g}{m}\right) << \frac{1}{2}\lambda_{ML}\coth\left(\frac{\delta^r}{\lambda_{ML}}\right)$ which considering the definitions of *m* and λ_{ML} given in Eqs (4) and (3) of the main manuscript, can be written as

$$\sqrt{\frac{1}{1+\varepsilon K^{'}}}\tanh\left(\frac{\delta^g}{m}\right)\tanh\left(\frac{\delta^r}{\lambda_{ML}}\right) << \frac{1}{2} \qquad \text{(S5.93)}$$

as reported in the main manuscript.

The fulfillment of Eq (5.10) allows one to use the limiting expression (5.8) for the determination of k_d. Since both, *m* and λ_{ML} depend on k_d, we cannot verify Eq (5.10) until a provisional k_d-value was obtained from Eq (5.8). The fulfilment of Eq (5.10) with this provisional value ensures that the k_d obtained is a good approximation for the dissociation rate constant of the complex. Conversely, if Eq (5.10) is not satisfied, a better approximation for k_d should be sought using eq (S5.89) instead of (5.8).

A simple, but effective, algorithm to calculate k_d using Eq (S5.89) is explained as a flowchart in Figure S5.3.

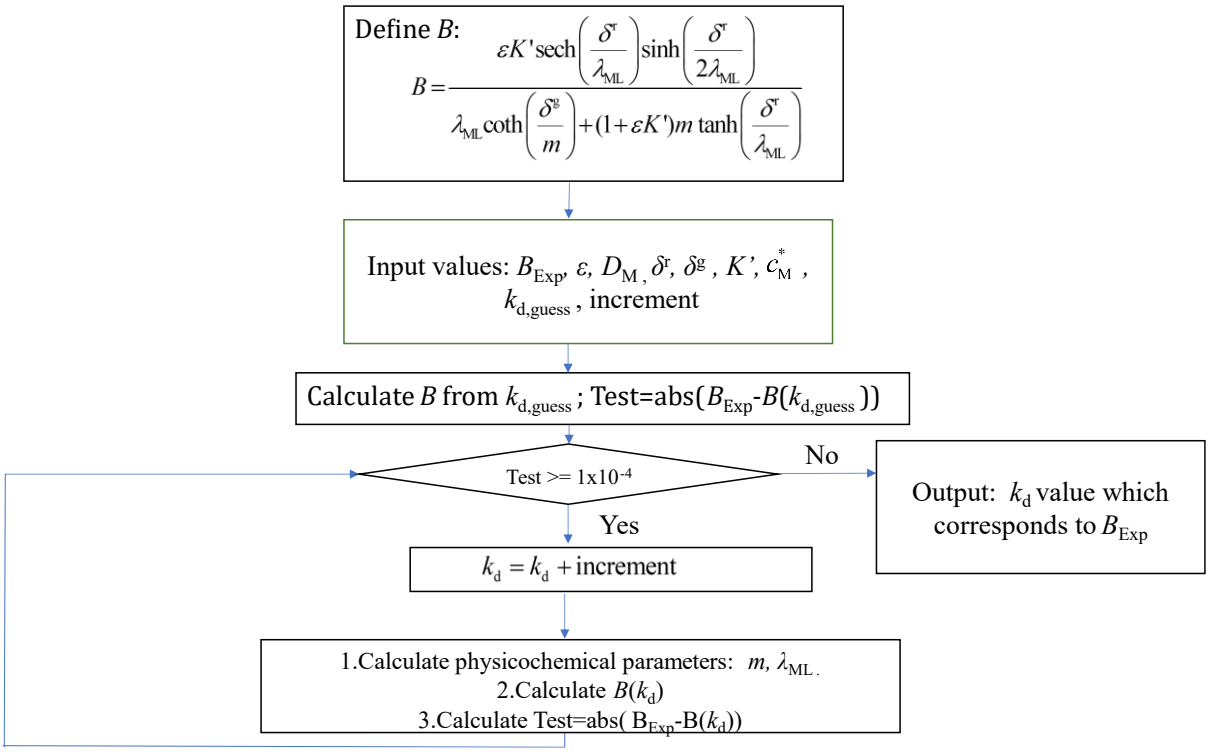

Figure S5.3 Algorithm applied to determine k_d from an experimental measurement of B_{exp} measured in Osor stream for a homogeneous resin.

The algorithm follows an iterative procedure that allows to obtain a value for k_d from an experimental B (in our work B_{Exp}=0.29 in the case of stream Osor). The algorithm searches the k_d result that satisfies the B_{exp} for a given tolerance (Test=1×10^{-4}) within a span of k_d values (1×10^{-1} s^{-1} to 1×10^{-6} s^{-1}). This iterative procedure needs an educated guess as an initial value for k_d which should be taken as a k_d=1×10^{-6} s^{-1} or k_d=1×10^{-1} s^{-1}. This educated guess can be assessed depending on the lability degree (ξ) of the complex. For ξ close to 0.7, k_d should be close to 1×10^{-2} s^{-1} (as it is expected for a quite labile complex), but for cases where ξ is close to 0.3, k_d will be close to 1×10^{-4} s^{-1} (as the behaviour of the complex should be quite inert). Therefore, in the first case a good educated guess would be 1×10^{-1} s^{-1} while for the second case a good educated guess would be 1×10^{-6} s^{-1}. Moreover, for the first case in this algorithm it has to be chosen a negative increment (e.g increment=-1×10^{-6} s^{-1}), so the k_d value decreases and we search for a solution for partially labile complexes. While in the second case a positive increment is needed so the k_d increases and then we start searching for a solution of k_d for rather inert complexes. Solutions for k_d either for very labile or very inert complexes are not feasible with these method as transport is limited by diffusion and the kinetic reaction process does not have an impact on the accumulation.

Alternatively, a value for k_d can be obtained from high-level coding programs. For example, Mathematica has a subroutine called Findroot that helps to find a solution for a given equation or system of equations.

Then, we need to check whether the heterogeneity of the resin beads distribution is relevant for the determination of k_d. To do so, we need to check that $B_{exp}<B_{max}$, where B_{max} is the maximum back percentage that can be reached in a stack of two homogeneous resin discs. When B_{exp} is close to B_{max}, an accurate computation of k_d requires the use of the heterogeneous resin model, by means of Eq (S5.78), as outlined in the following Section.

5.9.5.2 Algorithm to obtain k_d for a heterogeneous resin

According to Figure (5.2) in the main manuscript, Eq (S5.89) for the homogeneous model plotted against $k_{d,}$ has a maximum, that can be labelled as B_{max}. B_{max} is then, the maximum back percentage that can be reached by a stack of two homogeneous resin discs. Section "Derivation of maximum B for a homogeneous model" gives some details on the calculation of B_{max}.

When B_{exp} is close or greater than B_{max}, Eq (S5.78) is needed to recover accurate k_d values. In this task, we can use essentially the same algorithm as in section "Derivation of a solution for c_M and c_{ML} for a heterogeneous resin of a DGT device ".

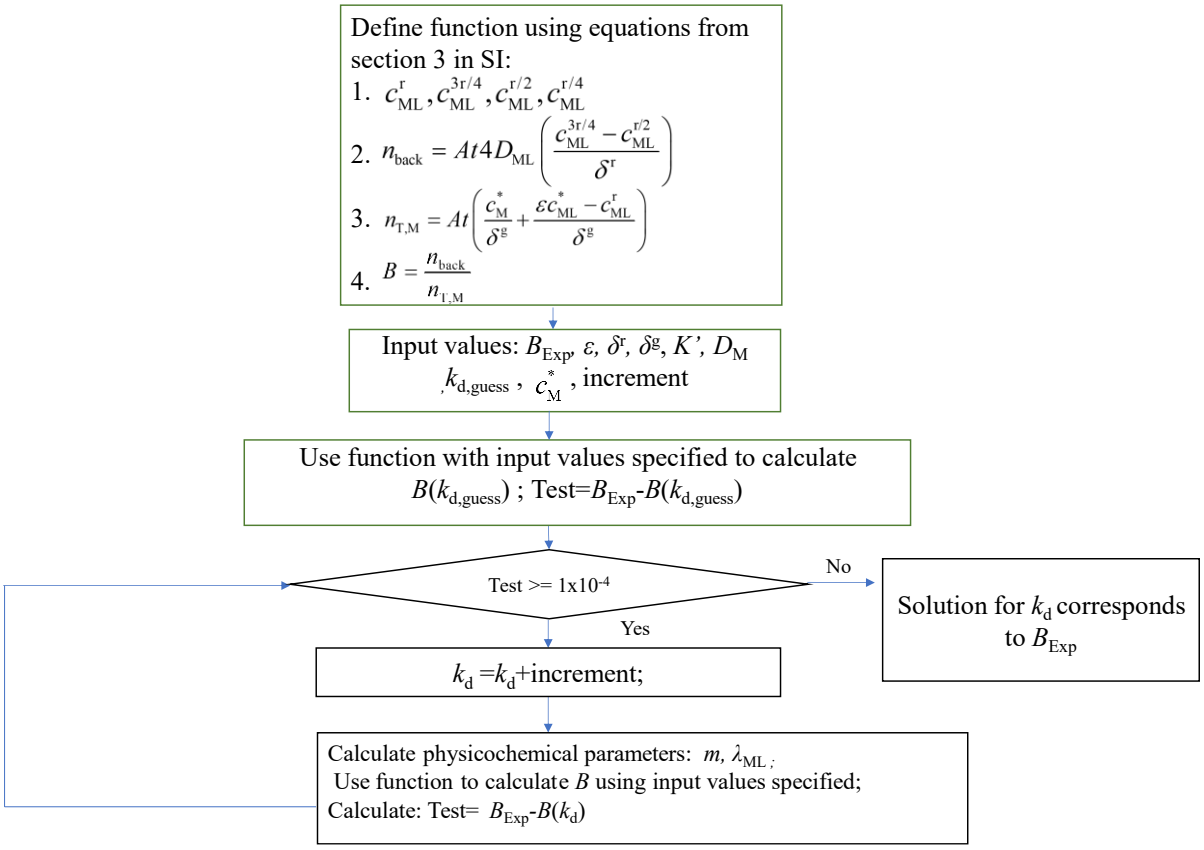

Figure S5.4 Algorithm applied to determine k_d from a B measured in Osor stream for a heterogeneous resin.

In the flowchart shown in Figure S5.4, c_{ML}^{r}, $c_{ML}^{3r/4}$ and $c_{ML}^{r/2}$ and $c_{ML}^{r/4}$ can be computed with Eqs (S5.63), (S5.68), (S5.72) and (S5.75), respectively.

Once they are written down in the program, B can be computed as prescribed in Eq (S5.78). Once again, notice that this procedure is the algorithm that has been used in this work, nevertheless other programs can be applied to iteratively solve the equation and find a solution for k_d that satisfies the B_{exp}.

5.9.6 Concentration profiles of Zn^{+2} and pool of inorganic Zn complexes for an heterogeneous resin model

Using the equations derived in section "Derivation of a solution for c_M and c_{ML} for a heterogeneous resin of a DGT device " and the data from Osor stream (regarding equilibrium concentrations, kinetic dissociation constant and diffusion coefficients), one can compute the concentration profiles for the free metal and the complex with the boundary conditions of the DGT device equipped with a stack of two resin discs. For the standard thickness of the resin disc, 0.4 mm, the back disc occupies the abscissas axis in the range $0< x< 0.4$ mm, while the front resin disc is located in the abscissa range $0.4 \text{ mm} < x <0.8$ mm.

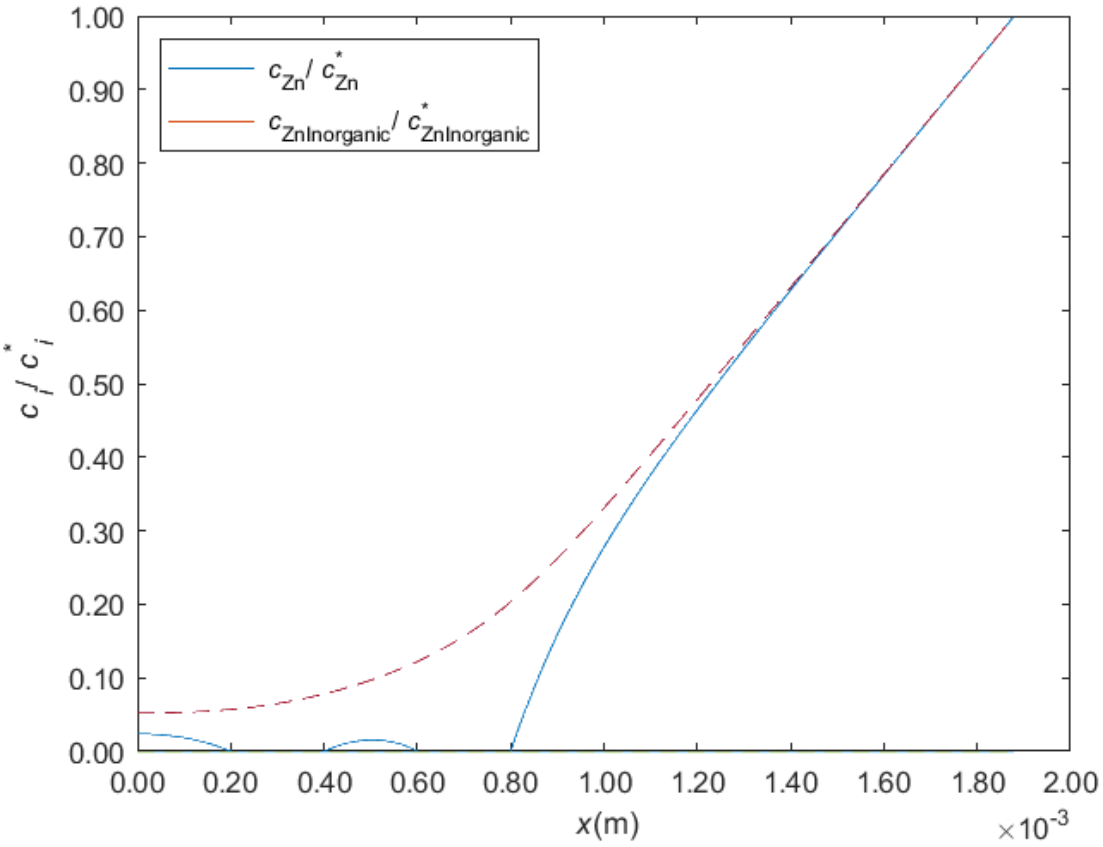

Figure S5.5 The continuous blue line shows the concentration profile for free zinc, the dashed red line shows the concentration profile for a pool of inorganic complexes ZnL_{Inor}. The thickness of the resin layer and gel layer are $\delta^r=8\times10^{-4}$ m and $\delta^g=1.079\times10^{-4}$ m, respectively. The diffusion coefficients of complex and free metal are $D_{ZnLinor}=D_{Zn}=4.21\times10^{-10}$ m^2 s^{-1}. The kinetic dissociation constant is $k_d=3.35\times10^{-3}$ s^{-1} and the condiditional stability constant is $K'=4.70$ mol m^{-3}.

Figure S5.5 depicts the concentration profiles of free metal and complex in a stack of two heterogeneous resin discs (as illustrated in Figure S5.2). This figure is quite useful to understand that the percentage of back accumulation, when using heterogeneous resin discs, is higher than the back accumulation when the resin discs are homogeneous. Dissociation of the complex in the volume 0 < x < 0.4 mm leads to back accumulation when the resins are homogeneous. Instead, dissociation in the volume 0 < x <0.5 mm leads to back accumulation when the resins are heterogeneous. Notice in Figure S5.5 that in the volume 0<x<0.2 mm where there is no resin beads, a profile of free metal resulting from the complex dissociation appears. The decreasing c_M concentration as x increases indicates that the free metal produced in this volume diffuses towards increasing x values and gets bound to the back resin at x=0.2 mm. Likewise, a free metal concentration appears in the volume 0.4 mm < x <0.6 mm. The profile

of the free metal (continuous blue line in Figure S5.5) indicates that the metal produced between 0.4 mm < x< 0.5 mm diffuses also towards the back resin disc and binds to it (at *x*=0.4 mm) increasing the back accumulation with respect to what takes place when the resin discs are homogeneous.

5.9.7 Derivation of maximum *B* for a homogeneous model

Back accumulation in a DGT device is negligible for a fully labile system as well as for a completely inert one. In both cases there is no dissociation of complexes in the resin domain, which is the phenomenon responsible for the back accumulation assuming that the resin beads are homogeneously distributed in the resin disc with a concentration enough to bind all the metals that diffuse in this domain (i.e. no saturation effects).

The accumulation in the back resin disc depends on the physicochemical parameters of the metal species (D_M, D_{ML}, K', k_d), as well on the characteristics of a DGT device (δ^g and δ^r). In this Section, we are going to derive a condition to determine the dissociation rate constant of the complex that yields to the maximum percentage of back accumulation, assuming fixed values of the rest of parameters.

The partial derivative of *B* respect to k_d on Eq (S5.89) becomes

$$\frac{\partial B}{\partial k_d}=\frac{\lambda_{ML}K'\operatorname{sech}\left(\frac{\delta^r}{\lambda_{ML}}\right)\left(\delta^r\cosh\left(\frac{\delta^r}{2\lambda_{ML}}\right)\alpha+2\sinh\left(\frac{\delta^r}{2\lambda_{ML}}\right)\left(\left(\delta^g\sqrt{1+\varepsilon K'}\right)\operatorname{csch}\left(\frac{\delta^g\sqrt{1+\varepsilon K'}}{\lambda_{ML}}\right)^2-\delta^r\beta\right)\right)}{4D_M\sqrt{1+\varepsilon K'}\alpha^2} \quad \text{(S5.94)}$$

where $\lambda_{ML}=\sqrt{\frac{D_{ML}}{k_d}}$ and

$$\alpha=\coth\left(\frac{\delta^g\sqrt{1+\varepsilon K'}}{\lambda_{ML}}\right)+\sqrt{1+\varepsilon K'}\tanh\left(\frac{\delta^r}{\lambda_{ML}}\right) \quad \text{(S5.95)}$$

and

$$\beta=\sqrt{1+\varepsilon K'}+\coth\left(\frac{\delta^g\sqrt{1+\varepsilon K'}}{\lambda_{ML}}\right)\tanh\left(\frac{\delta^r}{\lambda_{ML}}\right) \quad \text{(S5.96)}$$

The condition of maximum requires that this derivative is equal 0. Unfortunately, there is not an explicit solution of Eq (S5.94) for k_d. Therefore, the Bolzano method has been applied to find the k_d value ($k_{d,max}$) which produces a 0 in Eq (S5.94), where $B(k_{d,max})= B_{max}$ .The initial points that define the starting section are selected as $k_{d,a}=0.1$ s^{-1} and $k_{d,b}=1\times10^{-9}$ s^{-1} . To calculate a middle point $k_{d,c}$ between $k_{d,a}$ and $k_{d,b}$, we have used $\log(k_{d,c})=(\log(k_{d,a})+\log(k_{d,b}))/2$. The solution for k_d is found once the condition $(k_{d,a}-k_{d,b})/2<$tolerance is satisfied, where tolerance=1×10^{-9} s^{-1}.

The Bolzano method can be applied iteratively for a range of K' values, so that we can plot a figure of B_{max} vs K'. We have computed this relationship for the following parameters $\delta^g = 1.079\times10^{-3}$ m, $\delta^r = 8\times10^{-4}$ m, $D_{ML}=D_M=4.20\times10^{-10}$ and the result is shown in Figure S5.6 .

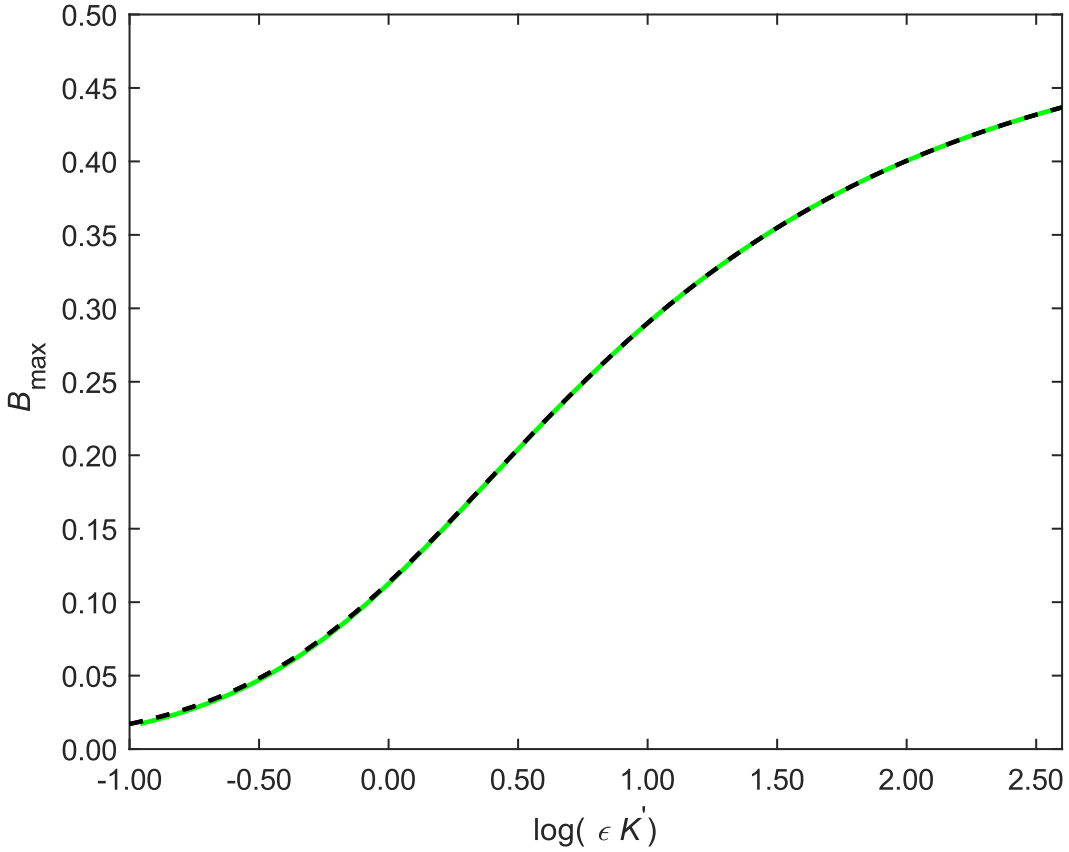

Figure S5.6 : The dashed black line shows the behaviour of B_{max} (computed with the homogeneous model) against log ($\varepsilon K'$) for the parameters of $\delta^g = 1.079x10^{-3}$ m, $\delta^r = 8x10^{-4}$ m, $DM=4.20x10^{-10}$ m^2 s^{-1} and $\varepsilon=0.1$. The solid green line is calculated with the same parameters as the dashed black line but using $\varepsilon=1$.

This figure is of high interest to assess whether the homogenous model of the resin disc is accurate for determining k_d or the heterogeneous model of the resin disc is required. As seen in Fig. 5.2 of the main text, when the percentage of back accumulation (B_{exp}) approaches the maximum value of the homogeneous model (B_{max}), an accurate value of k_d will require the use of Eq (S5.IS78). Figure S5.6 allows one to check whether B_{exp} is close to the maximum B (B_{max}) for a given K' and standard $\delta^g = 1.079\times10^{-3}$ m and $\delta^r = 8\times10^{-4}$ m values. Figure S5.6 also shows that a change of ε from 1 (solid green line) to 0.1 (dashed black line) leads to just small discrepancies in B_{max} , when $\varepsilon K'$ is smaller than 1. Thus this plot can be used for the typical values in standard DGT devices.

Just as an example, we can consider the case of Zn in the Osor stream. We have K'=4.70 and ε=1 so log(εK')=0.67. From Figure S5.6 we know that the maximum value that can be achieved for B is near to 0.22. As in our case we have B_{exp}=0.29 , it is not possible to find a solution for k_d using the homogeneous model. Then, instead of applying Eq (S5.89) we will need to apply Eq (S5.78). In the case that $B_{exp}<B_{max}$, then we can find a solution for k_d applying the homogeneous model (Eq (S5.89)) and from our computations we know -for these data- that the k_d retrieved by the heterogeneous model will be just 0.3 log units greater than the result retrieved by the homogeneous model which corresponds to a k_d value 2 times greater.

5.9.8 List of symbols

M: free metal ion

ML: complex

L: Ligand

k_a: association rate constant of the complexation reaction of the free metal ion with the ligand

k_d: dissociation rate constant of the complexation reaction of the free metal ion with the ligand

K: Equilibrium constant

K': Conditional equilibrium constant

c_M^* : Concentration of free metal ion in the bulk solution

c_{ML}^* : Concentration of the complex in the bulk solution

c_L^* : Concentration of the ligand in the bulk solution

D_M : diffusion coefficient of the free metal ion

D_{ML} : diffusion coefficient of the complex

δ^g: Thickness diffusive gel layer + thickness of DBL

δ^r: Thickness resin layer

A : Area

t: time

ε: ratio diffusion coefficient of the complex divided the diffusion coefficient of the free metal ion

J: total metal flux at the resin-gel interface

J_{ML}: Flux of complex at the resin interface

J_M: Flux of free metal at the resin interface

n_M : total metal accumulation at the resin interface

B_{exp}: Experimental value %back

B_{max}: maximum value %back for homogeneous model

B: theoretical value %back homogeneous

B_{het}: theoretical value %back heterogeneous model

$\lambda_{ML:}$ penetration distance of the complex in the resin layer

$m_{:}$ reaction layer

ξ: lability degree

c_{ML}^{r} : concentration of complex at x=r

$c_{ML}^{3r/4}$: concentration of complex at x=3r/4

$c_{ML}^{r/2}$: concentration of complex at x=r/2

$c_{ML}^{r/4}$: concentration of complex at x=r/4

c_R : concentration of resin beads

5.9.9 Use of Excel file

5.9.9.1 How to enable Macros

The use of the Excel file requires that Macros were enabled. Usually Microsoft displays a yellow warning which reads: “Security Warning: Macros has been disabled”. This message has a button that enables the Macros in your excel file.

If this message does not appear in your screen look at internet for how to enable macros for excel taking into account your excel version and your operative system.

5.9.9.2 Structure of the excel file

The excel file contains 3 sheets: “Input”, “Intermediary calculations” and “Output”.

In the Input sheet, you can find the list of Input values that are needed to calculate “k_d”. By default, the list of entries are filled with the values from the measurements in natural waters in the Osor stream:

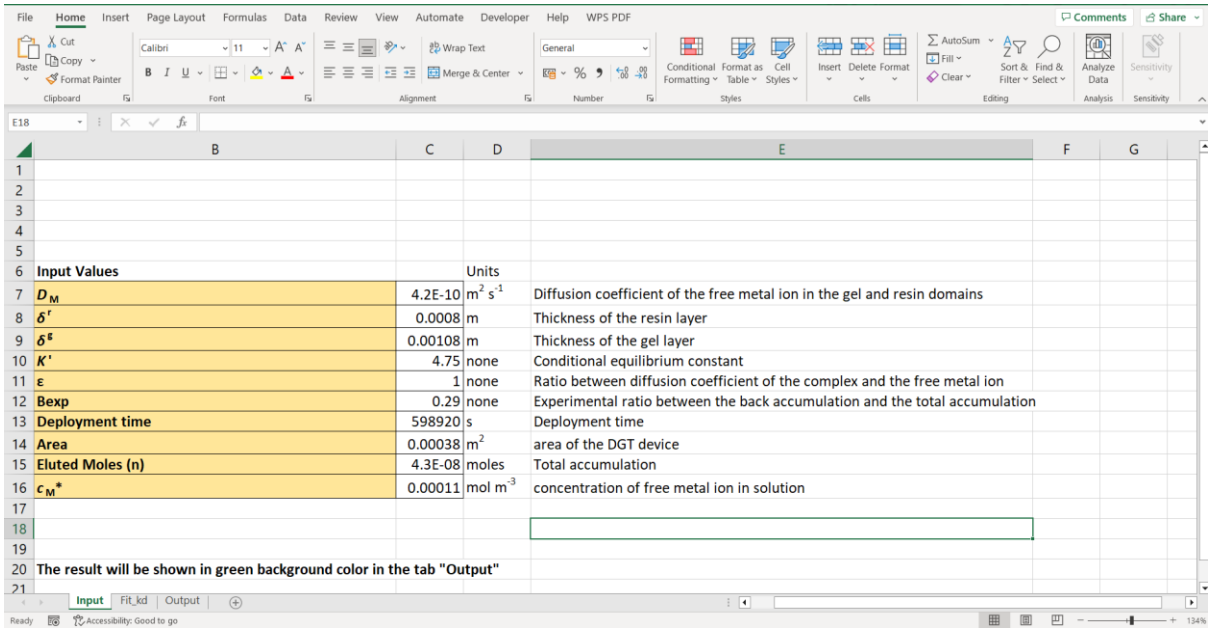

	B	C	D	E	F	G
6	**Input Values**		Units			
7	**D_M**	4.2E-10	$m^2 s^{-1}$	Diffusion coefficient of the free metal ion in the gel and resin domains		
8	**δ^r**	0.0008	m	Thickness of the resin layer		
9	**δ^g**	0.00108	m	Thickness of the gel layer		
10	**K'**	4.75	none	Conditional equilibrium constant		
11	**ε**	1	none	Ratio between diffusion coefficient of the complex and the free metal ion		
12	**Bexp**	0.29	none	Experimental ratio between the back accumulation and the total accumulation		
13	**Deployment time**	598920	s	Deployment time		
14	**Area**	0.00038	m^2	area of the DGT device		
15	**Eluted Moles (n)**	4.3E-08	moles	Total accumulation		
16	**c_M^***	0.00011	$mol\ m^{-3}$	concentration of free metal ion in solution		
20	**The result will be shown in green background color in the tab "Output"**					

Figure S 5.7 List of Input values from the measurements in Osor stream with the units that use the program to compute k_d (s^{-1}).

Figure S 5.7 displays the list of Input values to be provided by the user in order to fit a k_d value from $B_{exp.}$

The second sheet, named “Intermediary calculations”, is used for the automatic computation of k_d according to the homogenous resin model, when $B_{exp} < B_{max}$, or to the heterogeneous model when $B_{exp} > B_{max}$. As 2 solutions can be obtained, the excel file uses the accumulation in the DGT device to select the correct solution

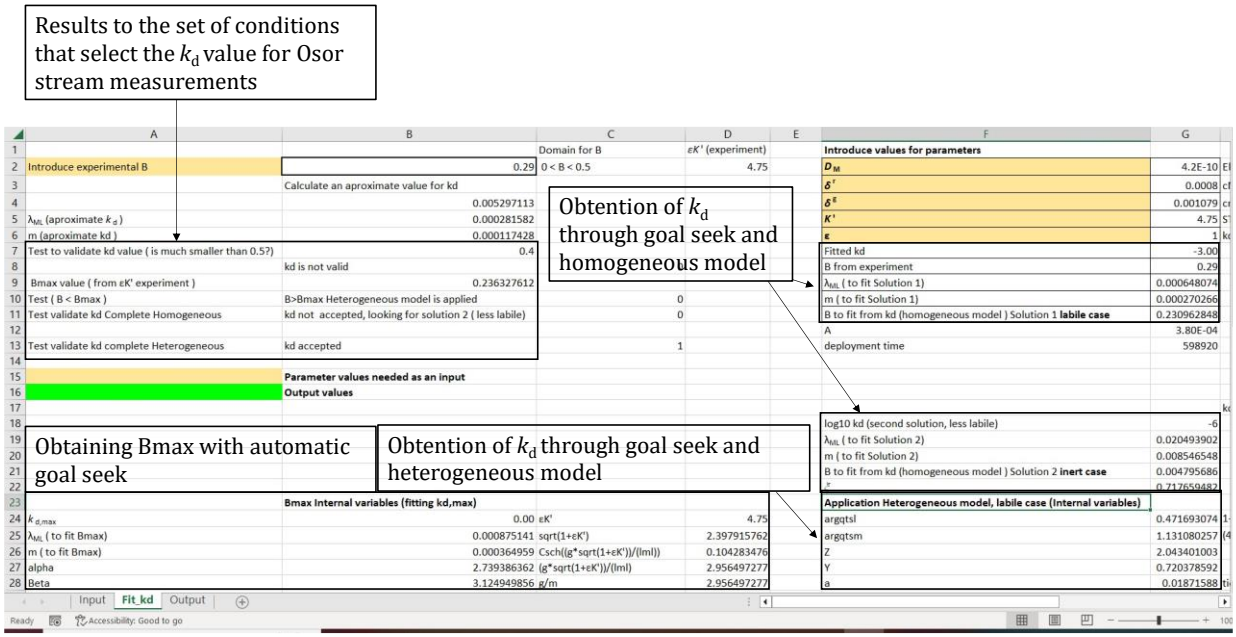

Figure S 5.8 Screenshot of sheet "Intermediary calculations" with a short explanation of the functioning of each section.

Figure S 5.8 displays the main calculations that the program does in order to fit k_d from $B_{exp.}$ On the Top left of the figure, there are conditions that need to be fulfilled in order to select k_d .On the Top right, it is shown the calculation of k_d with Eq (5.6) of the main manuscript. The computation is done twice with a different seed for the labile case (k_d=1x10^{-3} s^{-1}) and k_d=1x10^{-6} s^{-1} for the inert case. The right value is selected based on the accumulation in the DGT device. The bottom left is used to obtain the maximum *B* value with Eq (S5.94). On the bottom right, the fitting of k_d is done by using Eq (S5.78) and the set of equations that are needed to calculate B_{het} explained in the previous sections. The fitting procedures are done by using the tool goal seek.

The sheet "Output" displays the model and the result for k_d that is obtained. The correct solution is highlighted in green.

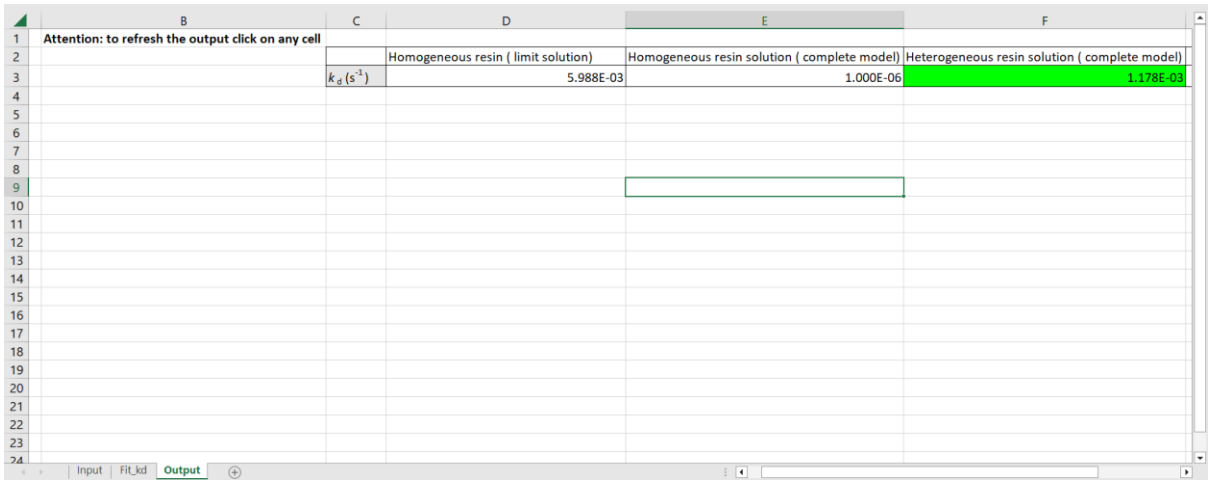

	B	C	D	E	F
1	Attention: to refresh the output click on any cell				
2			Homogeneous resin (limit solution)	Homogeneous resin solution (complete model)	Heterogeneous resin solution (complete model)
3		k_d (s^{-1})	5.988E-03	1.000E-06	1.178E-03

Input | Fit_kd | Output

Figure S 5.9 Output sheet of the excel file displaying in green background the correct result for k_d.

6 Hg availability to DGT devices in the presence of dissolved organic matter: an experimental and numerical approach

6.1 Introduction

Despite Hg concentration in natural waters is generally in the order of picomolar (pM) levels, its concentration sharply increases along the food chain [1]. The mechanisms behind these bioaccumulation and biomagnification processes are multiple and complex, with a lot of them still far from being understood. The fact that Hg is a highly toxic element coupled to this biomagnification problem results to an important issue related to human health. Thus, the availability of Hg species to biota is a topic of main concern on the scientific community. Speciation of Hg in the natural waters has a great influence on its availability and toxicity in a given media. In particular, the knowledge of the free metal concentration is a key factor when the internalization step is slow in comparison to the transport of the trace-metals to the membrane surface. In these conditions, the biouptake of trace-metals is directly proportional to the free concentration as FIAM or BLM models prescribe [2]. However, when concentration gradients arise close to the membrane, the diffusive properties of the Hg species coupled with their labilities are key variables that allow to understand the availability of Hg for biota such as phytoplankton or plants[3]. Therefore, the development of dynamic analytical techniques that measure fluxes in diffusive-controlled conditions is of great help for a better understanding of the uptake of Hg species by biota.

DGT is a dynamic speciation technique that allows to quantitatively monitor the fluxes of diverse trace-metals in all types of natural waters [4]. On top of a resin disc that acts as a sink for the target metal, DGT devices have a diffusive gel disc to define a diffusion domain that reduces the influence on the mass of the metal accumulated in the resin disc by the convective transport of the water out of the diffusive gel. The strong binding of the free metal by the binding agent dispersed in the resin disc leads to a metal concentration profile and to a shift of all the metal complexes towards dissociation in order to buffer the metal consumption. Thus the total metal flux in DGT devices is related to the free Hg plus the Hg-complexes that are able to dissociate in the spatio-temporal window of the DGT device (i.e labile Hg-complexes). Accordingly, DGT measurements allow us to define a labile Hg-

concentration in the solution that is expected to be in close correlation with the Hg uptake by biota. Due to these characteristics, the use of DGT to understand the availability of Hg-species in natural waters has been widely extended [5-8].

In addition to the labile Hg fraction based on DGT measurements other Hg fractions can be recognized. Some Hg species are able to be reduced to elemental Hg by $SnCl_2$. This fraction is known as "reducible" or "reactive" Hg, which encompasses small inorganic Hg complexes ($HgCl_x^{2-x}$, $HgOH_2$, HgOHCl, …) ,as well as, some Hg complexed with dissolved organic matter (DOM). It has been shown that the type of DOM and the ratio Hg/DOM in solution greatly influence the fraction of reducible Hg [9-11], so that the measurement of this fraction gives information on the Hg speciation in a natural water and can be used to investigate the role of Hg complexation in solution on Hg bioavailability via passive diffusion.

In general, natural waters contain dissolved organic matter (DOM) that give rise to complexation with Hg ions [12] Mercury speciation in presence of DOM is complex due to the DOM heterogeneity and polyelectrolytic effects. Heterogeneity means that DOM molecules (usually of macromolecular nature) are mixture of particles with size diversity which have a large number of sites that show different affinity for the metal ions due to the presence of different functional groups or different electronic environments. Also, these functional groups can interact with many metal cations so that there are important competitive effects. Depending on pH and ionic strength, these functional groups can be electrically charged so that part of the binding energy with the cations comes from an electrostatic origin. The NICA-Donnan model, developed by L K Koopal, W van Riemsdijk and coworkers [13] has been successfully used in describing the competitive metal binding to DOM. It allows to describe non-ideal competitive binding of a set of cations to DOM with an explicit description of the electrostatic effects through the Donnan model. A set of generic proton and metal parameters to describe this binding has been reported [14 15] and included in the speciation software VMINTEQ so that a complete speciation including simple ligands and DOM can be obtained with this software. Since the acid-base titration of DOM usually shows a shape of a double wave, the NICA-Donnan model for the generic description of metals and protons includes a bimodal description of affinities, that are labelled as a carboxylic and phenolic distributions. In general, the affinity of the phenolic sites for the proton and the rest of cations is higher than the affinity of the carboxylic sites in the naked ligand.

It could then be interesting to study the distribution of Hg ions in these fractions: free mercury, inorganic Hg complexes with simple ligands, Hg complexed to the carboxylic sites and Hg complexed to the phenolic sites of the DOM.

In this work, we have performed a set of experiments increasing the DOM/Hg ratio by increasing the concentration of Suwannee river fulvic acid (SRFA) or Suwannee river humic acid (SRHA) in simulated seawater controlled experimental solutions (pH=8, I=0.5, T=20°C) where DGT devices were deployed.

In each solution, we have determined the reducible Hg fraction (via Cold Vapor Atomic Fluorescence Spectrometry) and the labile Hg fraction, from the mass of Hg accumulated in DGT resin gels analysed with Atomic Absorption Spectrometry. The Hg complexed to carboxylic sites and phenolic sites of the DOM have been assessed using Visual Minteq speciation modelling software using as input values the total Hg concentration, the total metal concentration coming from the impurities of the background salt and the DOC measured in solution (via TOC analyzer). These data allow us to discuss the relationship between the different fractions. Finally, a visualization of the occupied sites in terms of the site affinity allows an overview of these relationships.

6.2 Methodology

6.2.1 Fractionation and speciation of Hg in solution

6.2.1.1 Reducible, non-reducible and total Hg in solution

Different fractions of Hg can be recognized based on the reactivity of Hg complexes in the solution. Following the strategy of Lamborg et al.[9], modified by Miller et al.[10], the reducible Hg concentration in solution is identified with the Hg fraction able to be reduced to elemental Hg by using $SnCl_2$. Elemental Hg can then be measured with CV-AFS as mentioned in the section "Measurement of Hg in solution ".

Lamborg[9] suggested that free Hg ions (Hg^{2+}), inorganic Hg complexes (HgL) and organic Hg complexes (Hg-DOM) that are weakly bound, i.e., with low stability constant, are reducible by $SnCl_2$ and accordingly they give rise to the reducible Hg. However, in the same publication it is reported that Hg complexed with small inorganic ligands such as $HgCl_2$ and $Hg(OH)_2$, which have high equilibrium constants (log K=19 – 22), are encompassed in this pool. In the work of Miller 2009, it is proved that other organic forms of Hg with low molecular weight and formula Hg-S-R, like Hg-Cysteine with log K=37.5 [16], Hg-thiosalicylic acid or Hg-thioglycolic, can also be reduced by using $SnCl_2$ even though they have greater stability constants than $HgCl_2$ and $Hg(OH)_2$. Therefore, they state that $c_{red,Hg}$ cannot only be a function of the bond strength.

Other experiments made by Miller (2009) with Suwannee River NOM (SRNOM) show that not all Hg species in solution are reducible. Moreover, this reducible fraction further decreases when the ratio of SRNOM/Hg increases as well as when the equilibration time between SRNOM and Hg increases. However, this all suggest that the ability of Hg to be reduced cannot only be related to the stability of its complexes but also to kinetic effects so that non-reducible Hg-complexes may be kinetically limited.

6.2.1.2 Labile and non-labile Hg concentration

The mass of Hg accumulated in the resin disc of a DGT device along the deployment depends on the mobility and kinetics of metal complexes. Thus, another fraction of Hg species in a solution can be associated to the outcome of a DGT measurement. In a DGT device, the fast and strong binding agent dispersed in the resin disc (in our case 3-mercaptopropyl functionalized silica) acts as a sink for the Hg ions. Neglecting the formation of ternary complexes, labile species in DGT are those that can dissociate within the time scale of the

DGT measurement, related to the diffusion time spent in crossing the diffusive gel, plus the resin disc. The accumulation of Hg in the resin disc allows us to define a DGT labile concentration as:

$$c_{\text{labile}} = \frac{n\delta^g}{D_L A t} \qquad (6.1)$$

where n (moles) is the accumulation in the DGT device, δ^g (m) is the thickness of the gel layer plus the thickness of the DBL, A (m^2) is the geometric area and t (s) is the deployment time.

This definition comes parallel to the usual c_{DGT} definition and relies on Fick first law of diffusion, but we would like to highlight that instead of using the diffusion coefficient of the free metal as done in the definition of c_{DGT}, we will use the diffusion coefficient of the SRFA or SRHA (D_L (m^2 s^{-1})) in the solutions that contain these ligands. Actually, for the concentrations of our experiments in presence of SRHA or SRFA, we will assume that all the metal is bound to the SRHA or SRFA and, accordingly, the diffusion coefficient of the complex Hg-SRHA is expected to be very close to the diffusion coefficient of the SRHA due to the high volume of this macromolecular species. A similar argument applies when Hg-SRFA complexes are formed in solution.

The diffusion coefficient of SRFA (D_{SRFA}) and SRHA (D_{SRHA}) were determined by Lead et al. with fluorescence correlation spectroscopy. [17] The choice of the diffusion coefficient has been done according to Lead's results considering the pH of our experiment and the medium where the species diffuse (i.e a gel of agarose). Thus, the values of the diffusion coefficients for SRHA and SRFA used in this work for pH=8 in agarose gel are $D_{SRHA} = 2.3 \cdot 10^{-10}$ $m^2 s^{-1}$ and $D_{SRFA} = 2.5 \cdot 10^{-10}$ $m^2 s^{-1}$, respectively. However, D_{SRHA} and D_{SRFA} were also determined by other authors using different experimental techniques leading to a variety of results. Therefore in the subsection "Labile Hg concentrations measured with DGT" values of the diffusion coefficients in best agreement with our experimental results are reported. In the SI, the calculations (c_{labile}, ξ, k_d ,*%back*) done with different D_{SRHA} and D_{SRFA} values are reported together with a discussion related to the choice of the result that is in best agreement with the results of our model.

Obviously, the chemical reactions involved in the binding of Hg to the resin sites are different from those involved in the measurement of the reducible fraction. But we would like to assess whether there is a relationship or not between the reducible and the labile fraction. To this

aim, we will determine c_{labile} through Eq (6.1) using in this equation the experimental data and the diffusion coefficient of the ligand (D_L) (SRHA or SRFA).

6.2.1.3 Lability degree (ξ)

From the ratio between c_{labile} (Eq (6.1)) and the total Hg concentration in solution ($c_{T,Hg}$) a lability degree (ξ) of the system can be calculated as:

$$\xi = \frac{c_{labile}}{c_{T,Hg}} \qquad (6.2)$$

The experimental measurement of the lability degree of the system as done in Eq (6.2) provides an estimation of the extent at which the Hg-SRHA complexes contribute to the accumulation in the DGT devices. The complexes that achieve complete dissociation at the interface between the resin-gel layer are fully labile ξ =1. Whereas the complexes that do not contribute at all are called inert and ξ =0. The complexes with a behaviour between these two cases are partially labile and ($0<\xi<1$).

In the section "Determination of k_d from ξ for Hg-SRHA or Hg-SRFA complexes" the procedure to recover an effective dissociation rate constant for the pool of Hg complexes from the value obtained for ξ will be explained.

6.2.1.4 Complementary information about lability of Hg-DOM complexes (%back measured)

The experimental measurement of the back accumulation from the DGT device with a stack of 2 resins provides complementary information of the lability of Hg-SRHA or Hg-SRFA complexes, more specifically informs whether the complexes are partially labile or not. When complexes are partially labile, they are kinetically limited and do not achieve complete dissociation in the front resin disc. Therefore, the complex will diffuse to the back resin layer, which dissociation will give rise to some Hg accumulation.

Conversely, fully labile complexes achieve complete dissociation at the interface of the resin-diffusive gel, thus they only contribute to the accumulation in the front resin disc. Whereas, inert complexes do not dissociate at all, and accordingly they should not contribute to the accumulation in the front resin disc nor in the back resin disc [18].

6.2.1.5 Hg speciation according to the NICA-Donnan model

Speciation software can also be used to estimate the equilibrium concentrations of the Hg species present in solution. These calculations rely on the database of thermodynamic magnitudes for the working temperature as well as on the consideration of all the reactions

taking place in the solution. In particular, VMINTEQ uses, by default, a database derived from MINTEQA2 but values from NIST, based on the data gathered on [19] can also be used if necessary.

We are interested in the speciation derived from the presence of SRFA and SRHA. VMINTEQ includes for the speciation with natural organic matter the model NICA-Donnan [13] with a set of constants derived for generic fulvic or humic acids [14].The binding properties of the SRFA or SRHA are described with distributions of sites with different affinities that take into account the heterogeneity of these macromolecular ligands and use a Donnan model to describe the electrostatic interaction of the binding.

As proton titration of these ligands show a double wave, a bimodal NICA is used in this model, one distribution to describe the so-called carboxylic distribution and another one to describe the phenolic distribution. Notice that the binding affinities of these distributions not only take into account carboxylic and phenolic groups which are dominant, but other type of groups are implicitly included in the phenolic and carboxylic distributions (e.g thiols in the phenolic distribution). In addition to the Hg bound to these distributions, there is also some Hg ions territorially bound by electrostatic attraction close to the ligands within the so-called Donnan volume.

To visualize the distribution of sites behind the NICA isotherm and the site occupation at different ratios of Hg-DOM, the conditional affinity spectrum (CAS) associated to the NICA-Donnan model has been applied [20-22]

Since the solutions contain high concentrations of background salts, to perform the speciation calculations with VMINTEQ and to visualize the distribution of sites behind the NICA isotherm with CAS, it has been included the presence of competing metal cations coming from the impurities of the background salt.

6.2.2 Experimental section

6.2.2.1 Measurement of Hg in solution

The measurement of the concentration of Hg in solution has been done by Cold Vapor Absorption Fluorescence Spectrometry (CV-AFS), which uses on-line reduction of ionic Hg^{2+} species in solution via $SnCl_2$, gold-trap amalgamation, pyrolysis and AFS detection via Ar and N_2 gas flow. Solution samples (10 mL) were periodically retrieved from the experimental media throughout the DGT deployment times and acidified to 1%HCl

(suprapur) and stored at 4 °C in 15mL clean container. This step was mandatory since it was not possible to analyse each sample after each sampling time .The solution samples are divided in 2 aliquots. In the first aliquot, only the reducible Hg fraction is analysed via direct reduction with $SnCl_2$ in CV-AFS. The concentration of these species is called $c_{red,\,Hg}$.
In the second aliquot, a 0.5% BrCl solution is added for 12h, so all the Hg species will be oxidized to Hg^{+2} before reduction with $SnCl_2$ in CV-AFS. From this procedure, total Hg concentration in solution ($c_{T,\,Hg}$) is measured. The difference between the total and the reducible concentration is called the non-reducible Hg concentration ($c_{nr,Hg}$).
Notice that the fraction of reducible Hg measured also depends on sample storage, which in our case involved acidification to 1% Hg to prevent loss of Hg onto walls. This acidification step might influence the measurement of the reducible Hg fraction. In this sense, our results could overestimate the direct analysis of the reducible fraction (i.e. without 1% HCl acidification step)

6.2.3 Measurement of Hg in the resin disc of DGT devices

The Hg bound in the resin layer is analysed by using an Advanced Mercury Analyzer (AMA-254). The instrument combusts the sample to produce gaseous Hg which is amalgamized in a gold trap and measured by Atomic Absorption Spectrometer (AAS). After removing from DGT, the resin gel was thoroughly washed (3 times) with MQ water to remove excess salt that would interfere with the analysis by AMA-254. Before introduction in the instrument, the resin was weighted on a microbalance.

6.2.4 Humic and fulvic acid composition and preparation

Suwannee River Humic Acid (SRHA) and Suwannee River Fulvic Acid (SRFA) have been bought from the International Humic Substances Society (IHSS). The quantity of carbon in SRHA and SRFA is about 50% its mass. Nevertheless it is considered that not all the functional groups are reactive to Hg, thus, DOM=1.65 DOC a ratio assessed in the publication of Sjostedt et al [23]
The solution of humic acid and fulvic acid were prepared by dissolving 80 mg of humic acid in 80 mL of MilliQ (MQ) water and 100 mg of fulvic acid in 100 mL of MQ water respectively. These solutions, covered with aluminium foil, were stirred for 24h. After that, NaOH was added in these solutions until reaching pH=8, then, the solution was filtered by using a syringe filter of 0.22 µm. Assuming that the resulting stock solutions had 1g/L of

fulvic acid and humic acid, we calculated the volumes needed to be added to the solutions of 2.6L to achieve the concentrations in solution from Table 6.1 and Table 6.2 for experiment SRHA and SRFA respectively.

6.2.4.1 DGT manufacturing

12 DGT devices divided in 4 configurations have been prepared to perform a set of experiments. 3 devices are equipped with a resin disc of 0.5 mm thickness and different diffusive gel thickness 0.25 mm (1R1G), 0.5 mm (1R2G) and 0.75 mm (1R3G) respectively and 1 device was equipped with a diffusive gel thickness of 0.25 mm and two resin discs of 0.5 mm (2R1G). For this last configuration, the front and back resin disc are analysed separately. A PVDF filter of 0.125 mm thickness and 0.45 µm pore size is added on top of each diffusive gel layer.

The composition of the diffusive and resin gels were made of 1.5% of agarose. For a hydrogels made of a 2% of agarose has been reported a pore size of few hundreds of nm [17, 24]. Moreover, the resin discs contain a 10% of 3-mercaptopropyl functionalized silica (3-MFS) resins, which is commercially available from Sigma-Aldrich. This type of resin layer has been proven to bind efficiently with Hg due to presence of thiol binding groups (RSH charge = 1.18 µmol g^{-1} of raw 3-MFS) [6, 25].

6.2.4.2 Experimental conditions

The experiments are grouped in 2 sets related to the system composition: SRHA solution (Experiment SRHA), SRFA solution (Experiment SRFA).

In experiments SRHA and SRFA, the goal is to make a series of SRHA or SRFA solutions with a constant $c_{T,Hg}$ concentration of 0.2 ppb and with the concentrations of $NaNO_3$ and $NaHCO_3$ reported in Table 6.1 and Table 6.2 respectively. In the case of SRFA, a solution with Hg at $c_{T,Hg}$=0.2 ppb was poured in the container in order to saturate the walls and avoid Hg adsorption to the walls during the experiment. This solution was removed after 24h. Once this procedure was done, the experimental solution for the experiment with SRFA was prepared with very similar experimental conditions detailed in Table 6.2 .

For the case of experiment with SRHA, a stock solution of 1g/L SRHA was diluted to make the concentration levels of SRHA mentioned in Table 6.1 according to the procedure described in “Humic and fulvic acid composition and preparation”. For the case of experiment with SRFA, the same procedure was followed and the c_{SRFA} in solution 2, 3 and 4

are proportional, regarding the global charge, to the humic acid concentration in solution 2, 3 and 4 respectively.

Before deploying the DGT devices (4 configurations with 3 replicates) 4 days of equilibration time were used in order to ensure the equilibration of Hg-DOM complexes [10]. Before and during the deployment of DGT devices, the solutions were stirred with magnetic stirrers at 300rpm. The pH≈8 was measured by using a visual indicator at the beginning and at the end of the experiment.

Table 6.1 Total concentration of reagents in DGT experiments SRHA with Hg. All solutions had a pH≈8 and V=2.6 L

Solution	1	2	3	4
c_{NaNO3} (M)	0.5			
c_{NaHCO3} (M)	$3.2x10^{-3}$			
$c_{T,Hg}$ (ppb)	0.2			
c_{SRHA} (mg/L)	0	0.68	5.43	23
Deployment time (h)	116			

Table 6.2 Total concentration of reagents in the experiments SRFA with Hg. All solutions had a pH≈8 and V=2.6 L.

Solution	1	2	3	4
c_{NaNO3} (M)	0.5			
c_{NaHCO3} (M)	$3.2x10^{-3}$			
$c_{T,Hg}$ (ppb)	0.2			
c_{SRFA} (mg/L)	0	0.5	4	17
Deployment time (h)	114.6			

6.2.5 Determination of k_d from ξ for Hg-SRHA or Hg-SRFA complexes

Considering the SRHA as a pool of ligands for the Hg ions, we would like to characterise the fraction of sites of this pool occupied with Hg ions by an "effective" dissociation rate constant (k_d). To this aim, a lability degree of the system can be determined from the

accumulation of Hg in the resin as indicated in Eq (6.2). Assuming that the lability degree can be related with the physicochemical parameters of the complex as in the case of only one complex in excess of ligand conditions [26],

$$\xi = \frac{\varepsilon K'}{\varepsilon K' + \frac{\delta^g}{m}\coth\left(\frac{\delta^g}{m}\right) + \frac{\delta^g(1+\varepsilon K')}{\lambda_{ML}}\tanh\left(\frac{\delta^r}{\lambda_{ML}}\right)} \quad (6.3)$$

In Eq (6.3), *K*' is the conditional stability constant which labels the ratio of bound versus free metal, δ^g is the thickness of the diffusive layer plus the thickness of the DBL, δ^r is the thickness of the resin layer, ε is the ratio between the diffusion coefficient of the free metal ion and the complex, $\lambda_{ML} = \sqrt{\frac{D_{ML}}{k_d}}$ and $m = \sqrt{\frac{D_{ML}}{k_d(1+\varepsilon K')}}$ .The parameter λ_{ML} is the distance that the complex has travelled by diffusion along the resin layer until full dissociation, whereas *m* is related to the thickness of the reaction layer in the gel layer, i. e., the layer where there is no equilibrium between the complex and the free metal ion.

To recover a value for k_d, Eq (6.3) needs a value for the conditional stability constant of the Hg-SRHA complexes. In order to estimate a value for the stability constant for the pool of Hg bound to the SRHA, speciation data from VMINTEQ have been used to calculate the concentration of Hg bound to carboxylic and phenolic sites, as well as the free Hg concentration. From this data, $K' = (c_{Hg,phenolic} + c_{Hg,carboxilic})/c_{Hg,free}$ is defined for the global pool of Hg complexes with the organic matter.

The diffusion coefficient for the complexes is expected to be close to the diffusion coefficient of the ligand due to the size of the ligand. Accordingly, we will assume hat ligand and complex share a common diffusion coefficient, an assumption that is already made when calculating the value for c_{labile} in Eq (6.1). Values D_{SRHA}=2.30x10^{-10} m^2 s^{-1} and D_{Hg}=8.44x10^{-10} m^2 s^{-1} have been used. The value for D_{Hg} is related to the diffusion coefficient of free Hg in agarose gels reported in [6, 25].

Following the procedure to determine the conditional stability constant outlined above, and the mentioned values for the rest of parameters, the subroutine Findroot from Mathematica has been applied to determine k_d [27]. The subroutine needs as input parameters ξ, *K'*, $\varepsilon = D_{HgSRHA}/D_{Hg}$, δ^g and δ^r and an educated guess value for k_d=1x10^{-3} s^{-1}. With this information the subroutine uses the Newton-Raphson method to find a new value for k_d which applied to Eq (6.3) gives a value for ξ closer to the experimental measurement. This process is repeated

until the solution of the value for k_d satisfies the experimental value for ξ within a certain tolerance.

Notice that the use of Eq (6.3) in order to determine the effective dissociation rate constant (k_d) requires ($0<\xi<1$). If the system is labile, i. e., $\xi=1$ the accumulation is only dependent on the transport by diffusion without any dependence on k_d. In the opposite case ($\xi=0$), the pool of Hg complexes would not contribute at all to the accumulation and therefore, a determination of k_d from the experimental data would not be representative of the physical process.

Finally, the determination of the physical parameters (K' and k_d) from our experimental data together with the diffusion coefficient gathered from literature are going to be useful for a numerical simulation of the reaction-diffusion processes of the system of Hg-SRHA or Hg-SRFA in the DGT devices. The simulations are going to be done with the numerical tool presented in the chapter 2 of the thesis.

6.3 Results and discussion

6.3.1 Time evolution of $c_{T,Hg}$ and $c_{red,Hg}$

Hg is a heavy metal that is known to be highly reactive and presents several chemical attributes that discern it from the rest of heavy metal elements (e.g Pb, Cd, Zn, Ni). For example, in its neutral state belongs to the gas phase, which some materials have shown to present some permeability when contained in a closed compartment (e.g Polyethylene (PE))[28] for glass containers no permeability has been observed. Hg has a great affinity for plastic material which leads to endure adsorption reactions with wall containers [28]. For the reasons stated above and since the flux of Hg in the DGT devices at the resin-gel interface is related to the total Hg concentration in solution, it is of high importance to track the evolution of $c_{T,Hg}$ and $c_{red,Hg}$ with time because it is expected that a significant fraction of Hg will bind to the container walls during the time-course of the experiment at the pH of our working conditions.

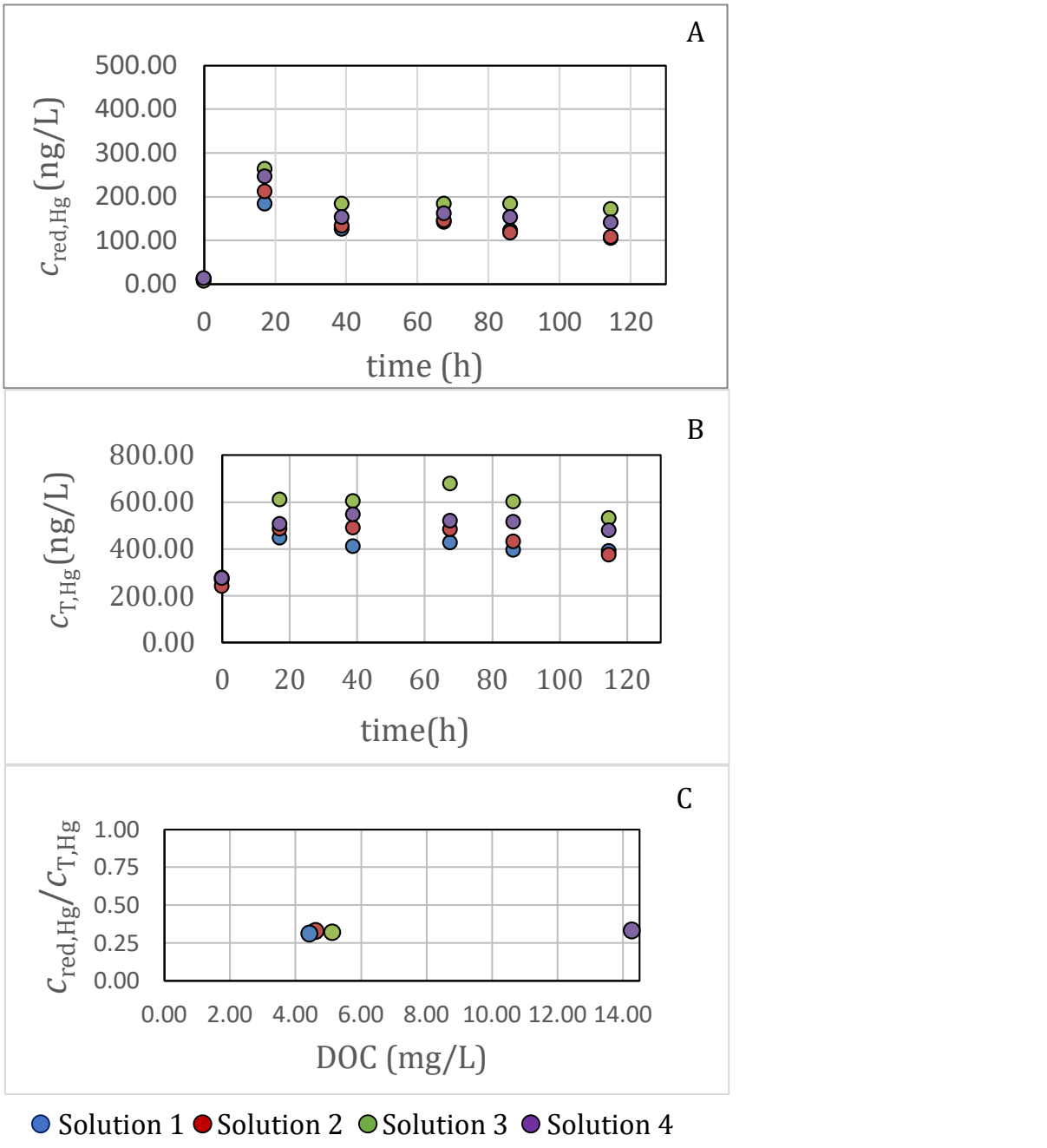

Figure 6.1 Evolution of $c_{red,Hg}$ (Panel A), $c_{T,Hg}$ (Panel B) within the deployment time of the DGT devices. The time reference belongs to the deployment of DGT devices . Panel C shows the fraction of reducible Hg vs DOC in solution when the experiment was finished. Solution 1 (blue dots) is composed by the reagents shown in Table 6.2 where no SRFA was present, but has a source of residual DOC of 4.6 mg/L, solution 2 (red dots) is composed by c_{SRFA} = 0.66 mg/L (DOC=0.4 mg/L), solution 3 (green dots) is composed by c_{SRFA} =1.98 mg/L (DOC=1.2 mg/L), and solution 4 (purple dots) is composed by c_{SRFA} =14.2 mg/L (DOC=8.6mg/L). The concentration of the other reagents added in each solution is described in Table 6.2 .

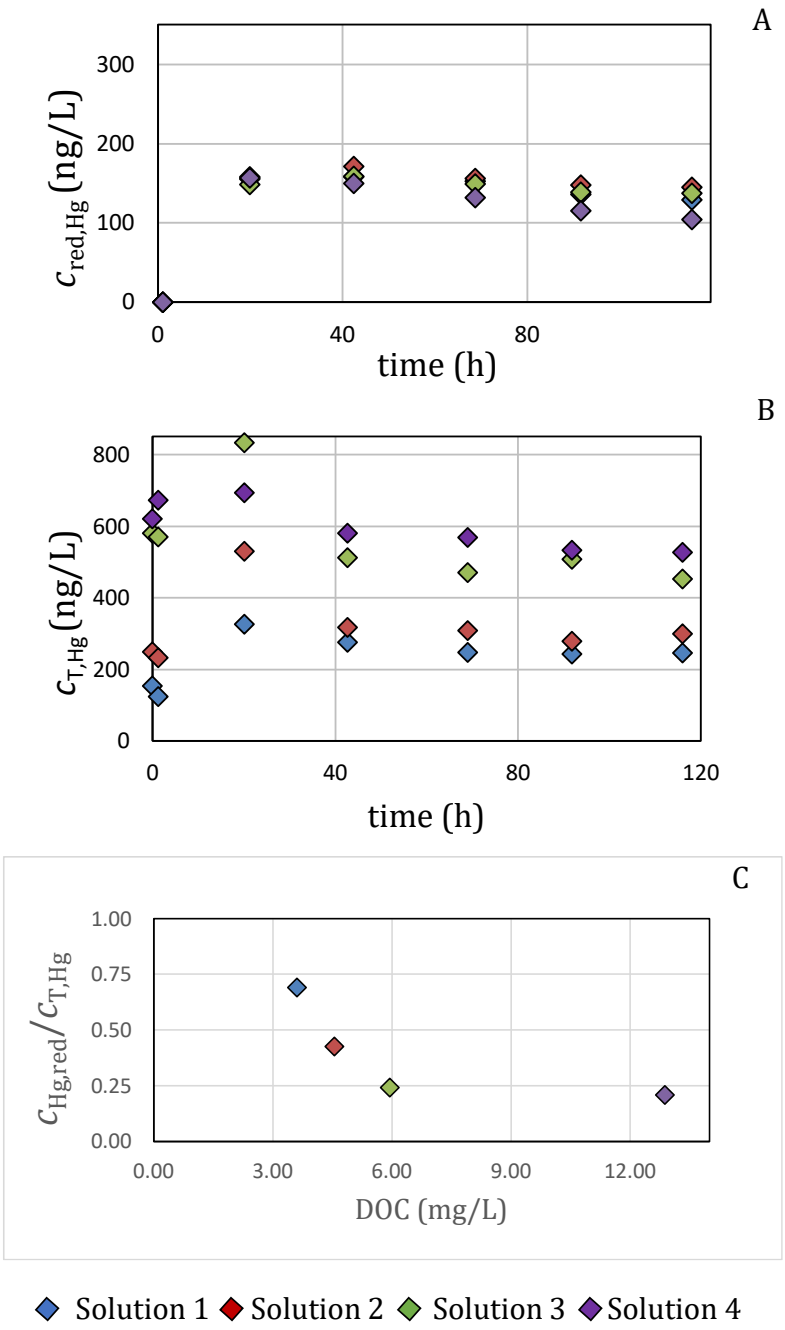

Figure 6.2 Evolution of $c_{red,Hg}$ (Panel A), $c_{T,Hg}$ (Panel B) within the deployment time of the DGT devices. The time reference belongs to the deployment of DGT devices. Panel C shows the fraction of reducible Hg vs DOC in solution. In Solution 1 (blue diamonds) no SRHA was added, however, a significant concentration of DOC is observed (3.6mg/L). In solution 2 (red diamonds) was added c_{SRHA} = 1.49 mg/L (DOC=0.9 mg/L). In solution 3 (green diamonds) was added c_{SRHA} = 3.96 mg/L (DOC=2.4 mg/L) and solution 4 (purple diamonds) was added c_{SRHA} = 15.3 mg/L (DOC=9.3 mg/L).

First of all, it is worth noting that even though we have worked at very low $c_{T,Hg}$ in experiments B and C, these concentrations are still a few orders of magnitude higher than those in natural waters [1, 28-29].

In Figure 6.1, Panel B, at the beginning of the deployment the measured $c_{T,Hg}$ is quite close to the expected value added in every solution (see Table 6.2). After DGT devices are deployed $c_{T,Hg}$ increases and after that, it reaches equilibrium. This phenomenon seems to be related with the increase of $c_{red,Hg}$ in every solution (see Figure 6.1 Panel A). Thus, the source of Hg contamination may come from residual Hg adsorbed in the walls (from walls saturation step) that is desorbed to the solution.

In Figure 6.1, Panel C , it can be seen that the fraction of reducible Hg stays constant when c_{SRFA} increases in solution. In our working hypotheses, we assume that 1) all Hg is bound to SRFA according to VMINTEQ calculations and 2) increasing the concentration of SRFA in solution while keeping Hg concentration constant should increase the fraction of Hg that is bound to stronger sites. Hence, it could be expected a decrease of the fraction of reducible Hg when c_{SRFA} increases in solution. However, this is not what we observe suggesting that the increase of the stability is not high enough to be relevant for a decrease of the reducible concentration

In Figure 6.2, we can observe that $c_{T,Hg}$ measured is higher for every solution than the value reported at Table 6.1. Nevertheless, in this case, the increase of $c_{T,Hg}$ is correlated to the increase of c_{SRHA} in solution, thus SRHA may have had traces of Hg that contaminated the solutions (remember that we are working at ng/L level). After deploying the DGT devices there is a disequilibrium period where $c_{red,Hg}$ increases, after that it reaches an equilibrium value that is maintained until the end of the experiment. A second difference is obtained in relation with the ratio of reducible Hg vs DOC (see Figure 6.2, panel C) where it is observed that an increase of SRHA in solution produces a lower ratio $c_{red,Hg}/c_{T,Hg}$. A very similar trend is observed, when comparing the fraction of reducible Hg vs time for 3 concentrations of SRNOM (c_{SRNOM} =1mg/L, c_{SRNOM} = 4 mg/L and c_{SRNOM}=16 mg/L) vs time obtained in a publication by [10] . In contrast, no correlation is observed between the fraction of $c_{red,Hg}/c_{T,Hg}$ and c_{SRFA}..

Since molar ratios, rather than mass ratios, between Hg and DOM (and its functional groups) are better variables to discuss Hg affinity towards DOM, from now on in this manuscript we will use the units (mol /m^3) for c_{redHg} and $c_{T,Hg}$.

6.3.2 NICA-Donnan speciation results

The set of input values regarding DOC (mg/L), $c_{T,Hg}$ (M), c_{NaNO3} (M) and the concentration of impurities in the salt background are reported in section 6.6.1 of the supporting information for the case of SRFA and SRHA. In order to simplify the Hg speciation calculations, residual DOM has not been considered (neither in the case of SRFA nor in the case of SRHA) as input value of DOC in VMINTEQ reported at section 6.6.1 of the supporting information.
Given the above information on the input parameters, the outcome of VMINTEQ for the Hg speciation in presence of SRFA is reported below :

Table 6.3 Hg distribution among the species in solution in experiment with SRFA. Where $\%Hg^{+2}$ is percentage of free Hg in solution, $\%Hg_D^{+2}$ is the percentage of Hg in the Donnan volume, %Hg carboxylic labels the percentage of Hg bound to the carboxylic sites and % Hg phenolic labels the percentage of Hg bound to phenolic sites.

Experiment SRFA	Solution 2	Solution 3	Solution 4
	NICA-Donnan		
% Hg^{+2}	3.23E-19	9.14E-21	1.91E-24
% Hg_D^{+2}	5.84E-23	4.96E-24	7.45E-27
% Hg carboxylic	0.06	0.05	0.03
% Hg phenolic	99.94	99.95	99.97

According to Table 6.3, the results of the speciation in the SRFA solutions by using NICA-Donnan show that all the Hg is bound to organic matter.
In the experiment with SRFA, for the NICA-Donnan model we notice that almost all the Hg is bound to the phenolic sites. Moreover, the percentage of Hg bound to phenolic sites increases very slightly from solution 2 to solution 4 because Hg/SRFA in solution decreases. The free Hg (% Hg^{+2}), inorganic Hg species, Hg bound to carboxylic sites (% Hg carboxylic) or Hg territorially bound (% Hg_D^{+2}) are negligible. Notice that the carboxylic and phenolic distributions represent a pool of binding sites that are related to different functional groups. Therefore, this result indicates that if Hg is bound to thiol groups, these groups are represented in the phenolic pool.
In presence of SRHA, the outcome of VMINTEQ allows to build Table 6.4

Table 6.4 Hg distribution among the species in solution in experiment SRHA. The meaning of the labels is defined in the caption of Table 6.3.

Experiment SRHA	Solution 2	Solution 3	Solution 4
	NICA-Donnan		
% Hg^{+2}	7.47E-14	1.50E-15	1.02E-17
% Hg_D^{+2}	9.31E-18	8.97E-19	2.31E-20
% Hg carboxylic	7.00	5.89	4.31
% Hg phenolic	92.99	94.11	95.69

The Hg speciation predicted by VMINTEQ in presence of SRHA also points to almost all the Hg being bound to the phenolic pool of sites and a little fraction in all cases, less than 10%, is bound to carboxylic sites. The fraction of Hg bound to phenolic sites increases from solution 2 to solution 4 because the Hg/SRHA ratio in solution decreases. The fraction of Hg bound to inorganic species or to the Donnan volume is negligible.

6.3.3 Relationship between reducible, total and labile Hg

6.3.3.1 Labile Hg concentrations measured with DGT

The moles of Hg accumulated in the DGT devices deployed in the solution 2-4 from experiment SRHA and SRFA (reported in SI section 2 Table S6.1 and Table S6.2 respectively) have been used to determine the labile Hg concentrations (c_{labile}) in the solutions according to Eq.(6.1). The results c_{labile} for experiments SRFA are gathered in Table 6.5.

Table 6.5 Values of c_{labile} (mol m^{-3}), $c_{T,Hg}$(mol m^{-3}), $c_{red,Hg}$ (mol m^{-3}) and *DOC* (mg/L)for experiment SRFA for solutions 2,3,4. The value of the diffusion coefficient for fulvic acid to calculate c_{labile} (mol m^{-3}) is D_{SRFA}=2.5x10^{-10} m^2 s^{-1} respectively. The values for *DOC* mg/L presented in this table are the difference between the value measured in each solution with the value measured in solution 1.

	Experiment SRFA					
Units: mol m^{-3}	c_{labile} 1R1G	c_{labile} 1R2G	c_{labile} 1R3G	$c_{T,Hg}$	$c_{red,Hg}$	*DOC* (mg/L)
Solution 2	3.00(±0.7) x10^{-6}	2.6 (±0.3) x10^{-6}	2.57(±0.04)x10^{-6}	2.2(±0.3) x10^{-6}	7(±2)x10^{-7}	0.4
Solution 3	3.6(±0.1)x 10^{-6}	3.5(±0.2)x 10^{-6}	3.4(±0.1)x 10^{-6}	3.0(±0.4)x 10^{-6}	9(±3) x10^{-7}	0.5(±0.5)
Solution 4	4.61(±0.08) x10^{-6}	3.1(±0.2)x 10^{-6}	2.7(±0.2)x 10^{-6}	2.5(±0.3)x 10^{-6}	8(±3) x10^{-7}	9.7(±0.9)

In experiment SRFA (Table 6.5), the comparison of the values of c_{labile} (mol m^{-3}) with $c_{T,Hg}$ (mol m^{-3}) indicate that all the Hg species in the solution are labile given the lower values of $c_{T,Hg}$ versus c_{labile} for all the concentrations of SRFA considered (solutions 2, 3, and 4). The fact c_{labile} is around a 10-20% higher than $c_{T,Hg}$ for every solution and DGT configuration suggests that SRFA diffuses faster in our experiment than the value for D_{SRFA} used from [17] in agarose gels. Notice also that the labile concentration does not increase when we compare the values of DGT devices with increasing thickness of the diffusive gel. This result reinforces the interpretation that all the species are labile, because even at the thinner thickness of gel layer (1R1G device) the labile concentration coincides with the total and no additional increase is possible.

Obviously, the labile concentrations measured rely on the diffusion coefficient used in Eq.(6.1) for the Hg species, and we would like to highlight that the value of the diffusion coefficient has been gathered from a publication that uses a fully independent measurement with a different technique [17]. Other values of diffusion coefficients have been tested in the section 6.6.2 (Tables S6.9-S6.11) of the supporting information.

The results $c_{labile} > c_{T,Hg}$ suggest that the diffusion coefficient chosen is too low and a better estimation according to the present results while imposing $c_{labile} \leq c_{T,Hg}$ is D_{SRFA}=2.8x10^{-10}.

Conversely, values for the reducible Hg concentration are clearly smaller than both the total Hg and the labile concentrations indicating that only part of the Hg in the SRFA solution is reducible.

The data obtained does not support a clear relationship between the reducible Hg and the strength of the binding since the fraction of reducible Hg stays constant as the c_{SRFA} in solution increases (See Panel C in Figure 6.1). This trend is perhaps unexpected looking at the strength of binding because, when c_{SRFA} increases, the concentration of strong sites also increases but the reducible fraction stays constant. In addition to the strength of binding other effects play a role. While the lability of a the Hg complexes depend on their reactivity with the functional groups of the resin (strength of binding and kinetics of dissociation of the complex), the reducibility of the same complexes depend on the reactivity of Hg(II) with the reducing agent (Sn(II)), which is a different reaction.

In summary, the current results suggest that the complexes Hg-SRFA reach full-dissociation at the resin-gel interface.

The results for c_{labile} for experiment SRHA are gathered in Table 6.6 .

Table 6.6 Values of c_{labile} (mol m^{-3}), $c_{T,Hg}$ (mol m^{-3}), $c_{red,Hg}$ (mol m^{-3}) and DOC mg/L for experiment SRHA for solutions 1,2,3,4. The values of the diffusion coefficients for humic acid to calculate c_{labile} (mol m^{-3}) is D_{SRHA}=2.3x10^{-10} m^2 s^{-1}. The values for DOC mg/L presented in this table are the difference between the value measured in each solution with the value measured in solution 1.

(mol m^{-3})	Experiment SRHA					
Units: mol m^{-3}	c_{labile} 1R1G	c_{labile} 1R2G	c_{labile} 1R3G	$c_{T,Hg}$	$c_{red,Hg}$	DOC (mg/L)
Solution 2	1.8(±0.1)x 10^{-6}	1.96(±0.3)x10^{-6}	1.95(±0.4)x10^{-6}	1.68(±0.3) x10^{-6}	7.12 x10^{-7}	0.9(±0.2)
Solution 3	1.43(±0.2) x10^{-6}	1.66(±0.5)x10^{-6}	1.73(±0.7) x10^{-6}	2.5(±0.4) x10^{-6}	6.76 x10^{-7}	2.3(±0.3)
Solution 4	1.44(±0.1) x10^{-6}	1.63(±0.1)x10^{-6}	1.74(±0.2) x10^{-6}	2.8(±0.3) x10^{-6}	6.14 x10^{-7}	9.3(±0.1)

In experiment SRHA (Table 6.6), the comparison of $c_{T,Hg}$, $c_{red,Hg}$ and c_{labile} indicates clear differences between these concentrations. Since $c_{T,Hg} > c_{labile} > c_{red,Hg}$, a fraction of the total

Hg-SRHA is non-labile in the DGT devices while all the reducible Hg might be labile which also encompass a fraction of the non-reducible Hg.

Increasing the SRHA concentration (moving row-wise in Table 6.6), the labile fraction decreases (although c_{labile} in solutions 3 and 4 are almost the same, the total Hg concentration increases as SRHA increases which decreases the lability degree of solution 4 as reported in Table 6.7). Indeed, an increase of c_{SRHA} implies an increase of strong sites in solution which decreases the dissociation rate constant in agreement with Eigen ideas. Moreover, considering Panel C in Figure 6.2, the fraction of reducible Hg also decreases as Hg binds to stronger SRHA sites.

The reducible Hg and the labile Hg are thus related to the stability of the binding, for the concentrations used in the experiment SRHA. Reducible Hg is also lower than labile Hg.

For solution 2 (experiment SRHA), c_{labile} is greater than $c_{T,Hg}$ for all the types of DGT devices which in principle points to experimental inaccuracies or inaccurate values as input parameters. However, the DOC measurements for each solution (See Figure 6.2 Panel C), indicate that there was a residual DOM in solution 1, where no humic acid was added. Thus, if we consider that not all the Hg is bound to SRHA and that the residual DOM diffuses with a diffusion coefficient similar to that of SRFA(which is supposed to be greater than SRHA). It is reasonable that c_{labile} appears overestimated due to the use of a too small diffusion coefficient.

It is also interesting to notice that for solutions 3 and 4 (in Table 6.6 moving column-wise), the labile concentration tends to increase as the thickness of the diffusive gel increases, in agreement to the increase of the time available for the dissociation of complexes. However, the comparison between c_{labile} and $c_{T,Hg}$ suggests that full lability of the SRHA complexes is not reached even in the 1R3G DGT devices, with the exception of solution 3, where the uncertainties in the measurement suggest that there are no significant differences between c_{labile} from 1R3G devices and $c_{T,Hg.}$ Thus, full dissociation would have been reached.

6.3.4 Estimation of a dissociation rate constant for the Hg-SRHA complexes

In the subsection “Labile Hg concentrations measured with DGT” we have observed that $c_{labile}=c_{T,Hg}$ (therefore, $\xi=1$) (when $D_{SRFA}=2.8\text{x}10^{-10}$ m^2 s^{-1}) for the experiment SRFA for each DGT device. This behaviour also occurred, when c_{SRFA} was increased (see SI section 6.6.2, Table S6.9 row-wise). Therefore, as stated in section “Determination of k_d from ξ for Hg-

SRHA or Hg-SRFA complexes" accumulation data cannot be used to estimate a dissociation reaction rate constant of Hg-SRFA complexes, because the accumulation is not dependent on dissociation but it is only limited by diffusion.

Conversely this is not the case for experiment SRHA, where a decrease of the Hg/SRHA ratio from solution 2 to solution 4 leads to a decrease in the labile concentration (see Table 6.6 row-wise)..

From the division of c_{labile} with $c_{T,Hg}$, it is possible to determine in which extent the pool of Hg-SRHA complexes is going to contribute to the accumulation (ξ) and a k_d can be determined from ξ (see Table 6.7).

The procedure employed to determine the values for k_d for solution 3 and 4 is described above in subsection "Determination of *kd* from ξ for Hg-SRHA or Hg-SRFA complexes".

The values obtained for k_d from 1R1G DGT device are 2.3×10^{-3} s^{-1} for solution 3 and 1.5×10^{-3} s^{-1} for solution 4. These k_d-values can be used to predict the ξ-values for the other configurations of DGT devices in the same solutions 3 and 4. All this set of predictions are gathered in Table 6.7 which also contain the experimental ξ-values resulting from Eq (6.3).

Table 6.7 Experimental and predicted ξ-values for experiment SRHA solution 3 and solution 4. The following parameter values have been used to predict ξ : $\Delta DBL = 8.05 \times 10^{-5}$ m, $\Delta g_1 = 3.75 \times 10^{-4}$ m, $\Delta g_2 = 6.25 \times 10^{-4}$ m, $\Delta g_3 = 8.75 \times 10^{-4}$ m, $D_{Hg} = 8.44 \times 10^{-10}$ m^2 s^{-1} , $D_{SRHA} = 2.3 \times 10^{-10}$ m^2 s^{-1}, $k_{d,solution\ 3} = 2.3 \times 10^{-3}$ s^{-1} , $k_{d,solution\ 4} = 1.7 \times 10^{-3}$ s^{-1}, $K'_{Hg,solution\ 3} = 2 \times 10^{16}$, $K'_{Hg,solution\ 4} = 2.4 \times 10^{18}$.

Experiment SRHA	DGT configuration	2R1G	1R2G	1R3G
Solution 3	ξ (experimental)	0.56	0.66	0.69
	ξ (predicted)	0.56	0.64	0.70
Solution 4	ξ (experimental)	0.49	0.57	0.60
	ξ (predicted)	0.50	0.57	0.60

As seen in Table 6.7, the predicted ξ-values are in very good agreement with the experimental ones. This indicates that the results for k_d from solutions 3 and 4 have been well-predicted applying the ligand excess model. This procedure has not been applied for

solution 2 because we have obtained a $c_{labile} > c_{T,Hg}$, from which it is deduced that all Hg in solution is labile and the transport is controlled by diffusion.

Notice that the agreement found in Table 6.7 indicates that the k_d-values hold for all the DGT configurations.

6.3.5 Lability assessment with the measurement of *%back*

As an additional result, the mass of Hg in the back resin disc from a DGT device with a stack of two resin discs informs about the lability of the Hg-SRFA or Hg-SRHA complexes in the DGT device. As can be seen in Table 6.8, the percentage of mass of Hg accumulated in the back resin disc (*%back*) are very low indicating that the Hg complexes behave as almost fully labile in the DGT devices with 2 resin discs for experiment SRHA and SRFA.

Table 6.8 Percentage between the back accumulation in the resin layer and the total accumulation, for experiments SRHA and SRFA.

Experiment / *%back*	SRHA	SRFA
(Solution 2)	0.5	5.0
(Solution 3)	0.4	1.1
(Solution 4)	1.4	0.92

For the case of SRFA , this result is in very good agreement with a labile Hg concentration being equal tot the total concentration (i.e ξ =1) for each DGT device. Moreover, by using a model of a single pool described in section "Determination of k_d from ξ for Hg-SRHA or Hg-SRFA complexes" we have been able to assess a *%back* by performing a set of simulations with a set of different diffusion coefficients reported in literature (results available in SI section 6.6.2 Table S6.15) . The comparison with our experimental *%back* suggest that a diffusion coefficient higher than $D_{SRFA}=2.8x10^{-10}$ m^2 s^{-1} is not in agreement with our experimental measurements.

For the case of SRHA, the partially labile character of the Hg complexes with SRHA shown in the previous section for 1R1G, 1R2G and 1R3G DGT devices is not incompatible with the results observed with the 2R1G DGT related to the *%back* because Hg-SRHA complexes

diffuse at a very slow rate and the thickness of the resin is 0.1 mm thicker than the standard DGT resin. Both circumstances coupled together seem to lead to a negligible presence of Hg in the back resin, as measured with AMA-254

To further analyse the congruence between the experimental results of *%back* and ξ for the SRHA solutions, a simulation of the concentration profiles for 2R1G DGT devices for solution 3 and 4 have been done by using a rigorous numerical code that solves the transport equations with the boundary conditions of the DGT device (see chapter 2 of this thesis).

To perform these simulations the values obtained for k_d and the conditional stability constants obtained from the speciation predicted by VM for solution 3 and 4 have been applied.

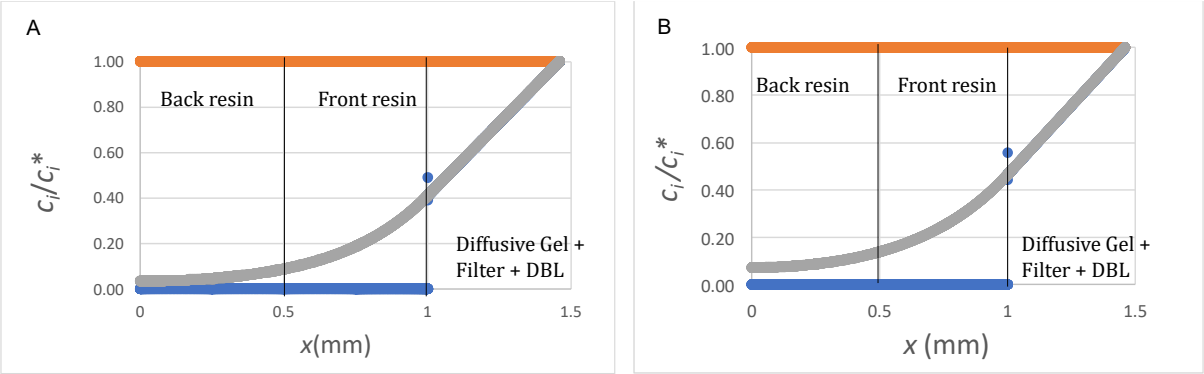

Figure 6.3 Normalized concentration profile of Hg^{+2} (Blue dots), Hg-SRHA complex (Gray dots), SRHA(Orange dots) in a 2R1G DGT device. Panel A is the simulation that represents the experimental data of solution 3 and Panel B is the simulation that represents the experimental data of solution 4. The following parameters has been used $D_{Hg^{+2}}=8.44x10^{-10}$ m^2 s^{-1} ,$D_{SRHA}=D_{Hg\text{-}SRHA}=2.3x10^{-10}$ m^2 s^{-1}, k_d (Hg-SRHA sol 3)$=1.5x10^{-3}$ s^{-1}, $K_{Hg\text{-}SRHA}=1.70x10^{23}$ m^3 mol^{-1} . For the simulation of solution 4, has been used the same diffusion coefficients as in the simulation of solution 3. k_d(Hg-SRHA, sol4)$=1.5x10^{-3}$ s^{-1}, $K_{Hg\text{-}SRHA}$, sol4$=9.98x10^{22}$ m^3 mol^{-1} .

In Figure 6.3 , the free metal and the complex are in equilibrium in the diffusive gel layer as noticed by the convergence of the respective normalized concentration profiles. At the interface of the resin-gel layer, the free metal profile drops to 0. The complex concentration at the interface resin/diffusive gel has a value close to $q^{r}_{ML}=\frac{c^{r}_{ML}}{c^{*}_{ML}}$=0.40 (Panel A) and close to $q^{r}_{ML}=\frac{c^{r}_{ML}}{c^{*}_{ML}}$=0.46 (Panel B), in well agreement with the value of ξ ($\xi=1-\frac{c^{r}_{ML}}{c^{*}_{ML}}=1-q^{r}_{ML}$) reported at Table 6.7.

In Figure 6.3 ,the SRHA complex has achieved almost complete dissociation at the front resin and achieves complete dissociation at the beginning of the back resin (For Panel A). As a

result, a *%back*=9 is obtained a value that is not in agreement with the experimental one (*%back*=0.4).

For Panel B the complex does not achieve complete dissociation at the back resin and its *%back*=12 is not in agreement with the experimental *%back*=1.5.

Both results of the *%back* obtained by simulation are not in agreement with the observed experimental *%back* but the differences could be considered as acceptable given the rough approximation that has been done and the experimental uncertainties of the DBL.

6.3.6 Relationship between labile and intrinsically bound Hg

The NICA-Donnan isotherm has been widely applied to describe the binding of trace-metals such as Pb, Cu or Cd to fulvic or humic matter [30-32]. For the binding of Hg, the generic NICA parameters have not been obtained from the fitting of experimental binding data but deduced from convenient extrapolations. It is then interesting to use these set of parameters to model the Hg binding to humic or fulvic substances and analyse whether the results make sense with the experimental data.

The results from Table 6.5 show that in presence of SRFA all the Hg complexes behave as labile. According to the speciation by VMINTEQ, the phenolic complexes are the only relevant Hg species. Thus, the phenolic species, independently of the affinity of the site are labile and dissociate fast enough in the DGT device to reach full dissociation along the gel disc. In contrast, only a fraction of the Hg is reducible indicating that part of the phenolic Hg complexes are non-reducible.

In presence of SRHA, only a fraction of the Hg is labile and a tendency to decrease the lability as the Hg binds to the strongest SRHA sites is observed (See Table 6.7). Accordingly, it could be interesting to depict the distribution of affinities of the occupied sites and to point out the affinity at which the lability is lost.

The distribution of affinities underlying the NICA isotherm can be displayed with the conditional affinity spectrum (CAS) [21]. It depicts the distribution of affinities for the binding of a given cation at a fixed concentration of the rest of competing cations, among which we have always the proton. The reference [22] includes an excel file ready to plot the CAS distributions for HA and FA. We have used this excel file to visualize the density of sites of each affinity seen by the Hg ions in the SRHA ligand at pH 8 and the corresponding density of occupied sites for the Hg concentrations in experiment SRHA.

For solution 3 of experiment SRHA, the CAS is depicted in the figure below

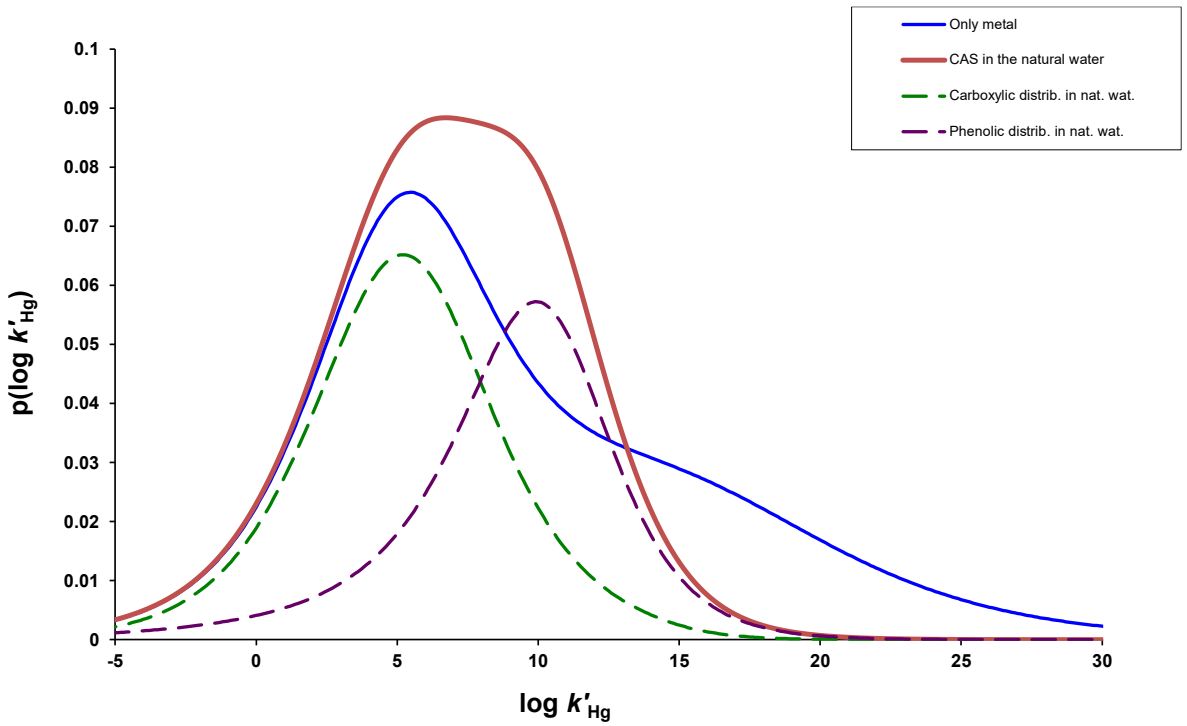

Figure 6.4 Conditional Affinity spectrum (CAS) (red line) of Hg in presence of competing cations coming from the impurities of the background salt (NaNO3). The dashed green line shows the carboxylic distribution and the dashed purple line shows the phenolic distribution in presence of competing ions. In blue line is depicted the affinity spectrum in absence of competing ions.

Figure 6.4 depicts the distribution of sites seen by the Hg ions in the SRHA. In blue is given the distribution in absence of competing ions (including the protons), which can be considered as the distribution in a solution at so high pH that there are no protons in the system. Continuous red line corresponds to the CAS in the solution at pH 8. When pH 8 is considered, some sites of the SRHA are occupied by protons so that the apparent affinity of the SRHA sites for Hg . shifts towards smaller affinities indicating that the effective affinity of the sites for Hg has decreased since part of the binding energy has to be spent in extracting the protons.

In Figure 6.4, the CAS corresponding to pH 8 is also split in the carboxylic distribution (in green discontinuous line) and the phenolic distribution in purple discontinuous line.

We are particularly interested in the distributions of occupied sites for solutions 3 and 4 for which we know that only a fraction of the occupied sites is labile.

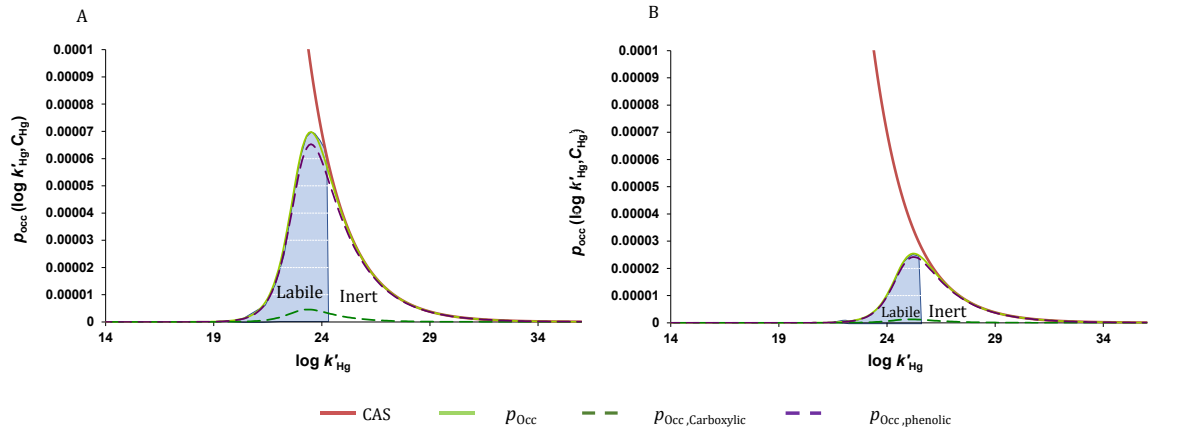

Figure 6.5 For the experiment of SRHA, panel A corresponds to the solution 3 and Panel B to solution 4 .The solid green line shows the global distribution of occupied sites. The phenolic and carboxylic distribution are represented by a dashed purple line and a dashed green line respectively. The shaded blue area represents the labile fraction.

Figure 6.5 reports the distribution of occupied sites for solutions 3 and 4 (see light green lines in Panel A and Panel B respectively). The density of occupied sites can be defined as:

$$p_{occ} = p\left(\log k^{'}\right)\frac{k^{'}c_{\mathrm{Hg,D}}}{1+k^{'}c_{\mathrm{Hg,D}}} \qquad (6.4)$$

Where *k'* is the affinity for a specific site, *p*(log*k*') is the density of sites with affinity log *k*' , and $c_{\mathrm{Hg,D}}$ is the Hg concentration in the Donnan phase. In Figure 6.5 Panel A, the red line stands for the density of sites. In the range of log*k*'>24, the green line approaches the red one indicating that almost all the sites of this range of affinities are fully occupied. The dashed purple line depicts the density of phenolic occupied sites which for each affinity is higher than the density of carboxylic occupied sites denoted by a dashed green line. The ratio of the areas below these dashed curves is the ratio between Hg bound to phenolic and Hg bound to carboxylic sites as reported by the VMINTEQ speciation output. From Panel A to Panel B in Figure 6.5, the ratio $c_{\mathrm{T,Hg}}$ /c_{SRHA} decreases, therefore the area below the thin green line has to decrease. When the ratio $c_{\mathrm{T,Hg}}$ /c_{SRHA} is lower (See Figure 6.5, Panel B) there is a shift to a higher range of affinities (compare in Figure 6.5 Panel A with Panel B) due to the increase of the concentration of strong sites that are preferred for occupation.

In Figure 6.5 Panel A, the shaded blue area corresponds to the concentration of bound Hg equal to c_{labile}. The affinity at which the lability is lost is located at log k'_{Hg} =24.5 in a DGT device 1R3G. In other words, Hg bound in the blue shaded area is labile while Hg bound at the right of this shaded area is inert in the DGT device 1R3G.

For DGT devices with 1R2G and 1R1G, the affinity at which the lability is lost decreases to log k'_{Hg} =24.3 and log k'_{Hg} =23.9, respectively, in agreement to a decrease of lability when the thickness of the diffusive gel of the DGT device decreases.

For solution 4, a similar discussion applies. Hg bound to sites with affinity smaller than log k'_{Hg} =26.1 are labile while for greater affinities, the lability is lost.

From solution 3 to solution 4 there is an increase of lability for sites with greater affinity. This increase is directly related to an increase of SRHA from solution 3 to solution 4 the indicating an increase on the concentration of the ligand sites. This increase in concentration makes sites with a given affinity more labile in agreement with the behaviour of the dependence of the lability on the ligand concentration in the range without ligand excess, as correspond to sites of a particular local affinity.

In the range without ligand excess, there is a back diffusion of the ligand from the resin to the solution in the DGT device which decreases the lability of the complexes. The back-diffusion process becomes negligible in excess of ligand since the ligand arising from the dissociation in the resin domain is negligible with respect to the free ligand in solution due to $c_{T,L}^{*} >> c_{T,M}^{*}$.

Although the commented results are obtained with the NICA-Donnan speciation model, we need to recall that the small concentrations involved in these calculation suggest to be cautious in purely quantitative interpretations.

6.4 Conclusions

A decrease of the reducible Hg concentration ($c_{red,Hg}$) in solution is found when the DOM/Hg ratio is increased. A similar result holds for the labile concentration which suggests a certain correlation between reducible and labile.

In the case of Hg-SRFA, $c_{labile} \approx c_{T,Hg}$ indicating that the Hg-SRFA complexes in solution were fully labile. For this case, the reducible Hg concentration is not a good predictor of the lability properties of the complex, as only a 30% of Hg-SRFA in the sample is found to be reducible in all the DOM/Hg ratio studied

Speciation calculated by VMINTEQ with the NICA-Donnan model suggests that for the concentrations of Hg and humic acids used in this work, almost all the Hg in solution is complexed to the humic substances. This speciation agree well with the reported high affinity of Hg for humic and fulvic substances. Nevertheless, the fitted affinity parameters are based on trends and not on actual Hg-binding data. Thus, there is a need to fit a new set of NICA-Donnan binding parameters based on experimental binding data of Hg to humic substances. Based on the current binding parameters, the conditional affinity spectrum (CAS) allows to visualize the range of affinities where the Hg bound to SRHA is labile as well as the range of affinities at which the lability is lost for a given concentration of SRHA.

6.5 References

1. Mason, R. P.; Fitzgerald, W. F.; Morel, F. M. M., The Biogeochemical Cycling OF Elemental Mercury - Anthropogenic Influences. *Geochimica Et Cosmochimica Acta* **1994,** *58* (15), 3191-3198.

2. Heijerick, D. G.; De Schamphelaere, K. A. C.; Janssen, C. R., Biotic ligand model development predicting Zn toxicity to the alga Pseudokirchneriella subcapitata: possibilities and limitations. *Comparative Biochemistry and Physiology C-Toxicology & Pharmacology* **2002,** *133* (1-2), 207-218.

3. Worms, I.; Simon, D. F.; Hassler, C. S.; Wilkinson, K. J., Bioavailability of trace metals to aquatic microorganisms: importance of chemical, biological and physical processes on biouptake. *Biochimie* **2006,** *88* (11), 1721-1731.

4. Davison, W.; Zhang, H., In-situ speciation measurements of trace components in natural- waters using thin-film gels. *Nature* **1994,** *367* (6463), 546-548.

5. Bratkic, A.; Klun, K.; Gao, Y., Mercury speciation in various aquatic systems using passive sampling technique of diffusive gradients in thin-film. *Science of the Total Environment* **2019,** *663*, 297-306.

6. Docekalova, H.; Divis, P., Application of diffusive gradient in thin films technique (DGT) to measurement of mercury in aquatic systems. *Talanta* **2005,** *65* (5), 1174-1178.

7. Fernández-Gómez, C.; Dimock, B.; Hintelmann, H.; Díez, S., Development of the DGT technique for Hg measurement in water: Comparison of three different types of samplers in laboratory assays. *Chemosphere* **2011,** *85* (9), 1452-1457.

8. Balch, J.; Gueguen, C., Effects of molecular weight on the diffusion coefficient of aquatic dissolved organic matter and humic substances. *Chemosphere* **2015,** *119*, 498-503.

9. Lamborg, C. T., Chung-Mao. et al., Determination of the Mercury Complexation Characteristics of Dissolved Organic Matter in Natural Waters with “Reducible Hg” Titrations. *Environ. Sci. Technol* **2003,** *37*, 3316-3322.

10. Miller, C. L., Southworth G. , Kinetic Controls on the Complexation between Mercury and Dissolved Organic Matter in a Contaminated Environment. *Environ. Sci. Technol.* **2009,** *43*, 8548–8553.

11. Miller, C. L., Liang L. and Gu B., Competitive ligand exchange reveals time dependant changes in the reactivity of Hg-dissolved organic matter complexes. *Environ. Chem* **2012,** *9*, 495-501.

12. Ravichandran, M., Interactions between mercury and dissolved organic matter-a review. *Chemosphere* **2004,** *55*, 319-331.

13. Kinniburgh, D. G.; van Riemsdijk, W. H.; Koopal, L. K.; Borkovec, M.; Benedetti, M. F.; Avena, M. J., Ion binding to natural organic matter: competition, heterogeneity, stoichiometry and thermodynamic consistency. *Colloids And Surfaces A-Physicochemical And Engineering Aspects* **1999,** *151* (1-2), 147-166.

14. Milne, C. J.; Kinniburgh, D. G.; van Riemsdijk, W. H.; Tipping, E., Generic NICA-Donnan model parameters for metal-ion binding by humic substances. *Environmental Science and Technology* **2003,** *37* (5), 958-971.

15. Milne, C. J.; Kinniburgh, D. G.; Tipping, E., Generic NICA-Donnan model parameters for proton binding by humic substances. *Environmental Science and Technology* **2001,** *35* (10), 2049-2059.

16. Song, Y., Jiang T., Thermodynamics of Hg(II) Bonding to Thiol Groups in Suwannee River Natural Organic Matter Resolved by Competitive Ligand Exchange, Hg LIII-Edge EXAFS and 1H NMR Spectroscopy. *Environ. Sci. Technol* **2018,** *52*, 8292-8301.

17. Lead, J. R.; Starchev, K.; Wilkinson, K. J., Diffusion coefficients of humic substances in agarose gel and in water. *Environmental Science and Technology* **2003,** *37* (3), 482-487.

18. van Leeuwen, H. P., Metal speciation dynamics and bioavailability: Inert and labile complexes. *Environmental Science and Technology* **1999,** *33* (21), 3743-3748.

19. Smith, R. M.; Martell, A. E.; Motekaitis, R. J.; Smith, R.; Motekaitis, R. J. In *NIST Critically Selected Stability Constants of Metal Complexes Database*, 2004.

20. Garcés, J. L.; Mas, F.; Puy, J., Conditional equilibrium constants in multicomponent heterogeneous adsorption: The conditional affinity spectrum. *Journal of Chemical Physics* **2006,** *124* (4), art num. 044710.

21. Puy, J.; Huidobro, C.; David, C.; Rey-Castro, C.; Salvador, J.; Companys, E.; Garces, J. L.; Galceran, J.; Cecilia, J.; Mas, F., Conditional affinity spectra underlying NICA isotherm. *Colloids And Surfaces A-Physicochemical And Engineering Aspects* **2009,** *347* (1-3), 156-166.

22. Rey-Castro, C.; Mongin, S.; Huidobro, C.; David, C.; Salvador, J.; Garces, J. L.; Galceran, J.; Mas, F.; Puy, J., Effective Affinity Distribution for the Binding of Metal Ions to a Generic Fulvic Acid in Natural Waters. *Environmental Science and Technology* **2009,** *43* (19), 7184-7191.

23. Sjostedt, C. S.; Gustafsson, J. P.; Kohler, S. J., Chemical Equilibrium Modeling of Organic Acids, pH, Aluminum, and Iron in Swedish Surface Waters. *Environmental Science & Technology* **2010,** *44* (22), 8587-8593.

24. Pluen, A., Netti, A., Jain,K., Diffusion of Macromolecules in Agarose gels: comparison of linear and globular configurations. *Biophysical Journal* **1999,** *77*, 542-552.

25. Gao, Y.; De Canck, E.; Leermakers, M.; Baeyens, W.; Van Der Voort, P., Synthesized mercaptopropyl nanoporous resins in DGT probes for determining dissolved mercury concentrations. *Talanta* **2011,** *87*, 262-267.

26. Mongin, S.; Uribe, R.; Puy, J.; Cecilia, J.; Galceran, J.; Zhang, H.; Davison, W., Key role of the resin layer thickness in the lability of complexes measured by DGT. *Environ.Sci.Technol.* **2011,** *45* (11), 4869-4875.

27. Research, W. Find Root. https://reference.wolfram.com/language/ref/FindRoot.html.

28. Li-Ping Yu, X.-P. Y., Factors affecting the stability of inorganic and methylmercury during sample storage. *Trends in Analytical Chemistry* **2003,** *22* (4).

29. Daniel Cossa, J. S., Jacques Cloud, Automated Technique for Mercury Determination at Sub-nanogram per Liter Levels in Natural Waters. *Journal of Analytical Atomic Spectrometry* **1995,** *10*, 287-291.

30. Pernet-Coudrier, B.; Companys, E.; Galceran, J.; Morey, M.; Mouchel, J. M.; Puy, J.; Ruiz, N.; Varrault, G., Pb-binding to various dissolved organic matter in urban aquatic systems: Key role of the most hydrophilic fraction. *Geochimica Et Cosmochimica Acta* **2011,** *75* (14), 4005-4019.

31. Pinheiro, J. P.; Mota, A. M.; Benedetti, M. F., Lead and calcium binding to fulvic acids: Salt effect and competition. *Environmental Science and Technology* **1999,** *33* (19), 3398-3404.

32. Meylan, S.; Odzak, N.; Behra, R.; Sigg, L., Speciation of copper and zinc in natural freshwater: comparison of voltammetric measurements, diffusive gradients in thin films (DGT) and chemical equilibrium models. *Analytica Chimica Acta* **2004,** *510* (1), 91-100

.

6.6 Supporting information for: Hg availability to DGT devices in the presence of dissolved organic matter: an experimental and numerical approach

6.6.1 Total concentrations of species for speciation calculation with Visual Minteq (VM)

In the main text, the NICA-Donnan model has been used for modelling Hg binding to organic matter. The list of input values for the total concentrations in the bulk solution used for the VM are the following:

Table S 6.1Total concentrations of Hg and DOC used in the speciation calculations for experiment SRHA .

Species VM (concentration)	Solution 2	Solution 3	Solution 4
$c_{T,Hg}$ (M)	1.68×10^{-9}	2.50×10^{-9}	2.8×10^{-9}
DOC (mg/L)	0.9	2.5	9.2

Table S 6.2 Total concentrations of Hg and DOC used in the speciation calculations for experiment SRFA.

Species VM (concentration)	Solution 2	Solution 3	Solution 4
$c_{T,Hg}$ (M)	2.25×10^{-9}	2.97×10^{-9}	2.52×10^{-9}
DOC (mg/L)	0.4	1.48	8.9

The ratio of active DOM is considered to be 1.65 times the value of DOC measured in solution in Table S 6.1 and Table S 6.2.

In Table S 6.3 are reported the total concentrations of the impurities of the background salt ($NaNO_3$ 0.5M).

Table S 6.3 Total concentrations of heavy metals coming from the impurities from the background salt and the concentration of background salt introduced as an input value. for each solution .

Species VM (concentration)	Concentration of impurities from back ground salt
H^+ (M)	$1.32x10^{-3}$
Na^+ (M)	0.5
NO_3^- (M)	0.5
Al^{+3} (M)	$7.85\ x10^{-8}$
Ca^{+2} (M)	$1.05\ x10^{-7}$
Co^{+2} (M)	$7.13\ x10^{-9}$
Mg^{+2} (M)	$1.72\ x10^{-8}$
Ni^{+2} (M)	$7.15\ x10^{-9}$
Pb^{+2} (M)	$2.03x10^{-9}$
$CO3^{-2}$ (M)	$1.32\ x10^{-3}$

6.6.2 Agreement between measured *%back* and predicted *%back* computed by rigorous simulation using fitted parameters from experimental data and diffusion coefficients of SRHA and SRFA in literature

In the main text the results obtained for c_{labile} (mol m^{-3}) ξ and k_d (s^{-1}) are based on a value of a diffusion coefficient for SRHA and SRFA measured in the medium (agarose gel) and pH of our experiment. We consider this a legitimate choice because it is representative of the characteristics of our system.

Nevertheless, diffusion coefficients for SRHA and SRFA have been reported in the literature in the ranges 2.0 $x10^{-10}$- 6.5 $x10^{-10}$ and 1.9$x10^{-10}$ -5.0$x10^{-10}$ m^2 s^{-1}, respectively.

Therefore, this section is dedicated to assess the change of $\xi = c_{labile}/c_{T,Hg}$ (i.e the contribution of the complexes to the accumulation) for the Hg complexes with SRHA and SRFA when other different diffusion coefficients reported in the literature for these complexes are considered [1-2]. En each case a value of the dissociation rate constant (k_d (s^{-1})) can be recovered, which will be used to compute the *%back* in experiments A and B by using a rigorous numerical simulation code. Calculated values of *%back* will be compared with our experimental *%back* to give us an idea about the significance of using this choice of the diffusion coefficient in our experiments. A non-negligible predicted *%back* suggests that the diffusion coefficient selected does not reproduce our experimental data.

The accumulations in our experiments SRHA and SRFA in solutions 2-4 are reported in the Table S 6.4 and Table S 6.5 from which c_{labile} and ξ for a set of diffusion coefficients:

Table S 6.4 Values of accumulation of Hg in the DGT devices 1R1G, 2R1G, 1R2G and 1R3G for experiment SRHA for solutions 2,3,4.

n_{Hg}	Experiment SRHA			
Units: moles	1R1G	2R1G	1R2G	1R3G
Solution 2	1.22(±0.09) x10^{-10}	1.06(±0.05)x 10^{-10}	8.4 (±0.5)x10^{-11}	6(±1) x10^{-11}
Solution 3	9(±1)x10^{-11}	9(±2) x10^{-11}	7(±1)x10^{-11}	5(±2)x10^{-11}
Solution 4	9.5(±0.9)x10^{-11}	9.2(±0.8) x10^{-11}	7.0(±0.2)x10^{-}	5.5(±0.5)x10^{-11}

Table S 6.5 Values of accumulation of Hg in the DGT devices 1R1G, 2R1G, 1R2G and 1R3G for experiment SRFA for solutions 2,3,4.

n_{Hg}	Experiment SRFA			
Units: moles	1R1G	2R1G	1R2G	1R3G
Solution 2	1.7(±0.5)x10^{-10}	1.5(±0.3) x10^{-10}	1.0(±0.2) x10^{-10}	7.90 (±0.1) x10^{-11}
Solution 3	2.08(±0.07) x10^{-10}	1.58(±0.06) x10^{-10}	1.4(±0.1) x10^{-10}	1.04 (±0.7)x10^{-10}
Solution 4	2.7(±0.1) x10^{-10}	1.7(±0.2) x10^{-10}	1.26(±0.08)x 10^{-10}	8.4(±0.4) x10^{-11}

From Table S 6.4 and Table S 6.5, c_{labile} is calculated for each DGT device and for each value of diffusion coefficient listed in the following Tables . Then ξ can be computed by dividing each value of c_{labile} in a by $c_{T,Hg}$ reported in Table S 6.1 and Table S 6.2 for experiment SRHA and SRFA respectively. Thus, the values for are reported in the following tables:

Table S 6.6 Experimental ξ-values in experiment SRHA for Solutions 2, 3 and 4 using D_{SRHA}=2.5x10^{-10} m^2 s^{-1}. Parameters: δ^{DBL}=8.05x10^{-5} m, Δg_1=3.75x10^{-4} m, Δg_2=6.25x10^{-4} m, Δg_3=8.75x10^{-4} m, D_{Hg}=8.44x10^{-10} m^2 s^{-1}. Deployment time=116.0h

D_{SRHA}=2.5x10^{-10} (m^2 s^{-1})	Experiment SRHA			
	ξ_{1R1G}	ξ_{2R1G}	ξ_{1R2G}	ξ_{1R3G}
Solution 2	1.2	1.0	1.3	1.3
Solution 3	0.53	0.52	0.61	0.63
Solution 4	0.46	0.45	0.52	0.56

Table S 6.7 Experimental ξ-values in experiment SRHA for Solutions 2, 3 and 4 using D_{SRHA}=4.95x10^{-10} m^2 s^{-1}. Parameters as in Table S 6.6.

D_{SRHA}=4.95x10^{-10} (m^2 s^{-1})	Experiment SRHA			
	ξ_{1R1G}	ξ_{2R1G}	ξ_{1R2G}	ξ_{1R3G}
Solution 2	0.60	0.52	0.63	0.63
Solution 3	0.27	0.26	0.31	0.32
Solution 4	0.23	0.23	0.26	0.28

Table S 6.8 Experimental ξ-values in experiment SRHA for Solutions 2, 3 and 4 using D_{SRHA}=6.05x10^{-10} m^2 s^{-1}. Parameters as in Table S 6.6.

D_{SRHA}=6.05x10^{-10} (m^2 s^{-1}) [1]	Experiment SRHA			
	ξ_{1R1G}	ξ_{2R1G}	ξ_{1R2G}	ξ_{1R3G}
Solution 2	0.49	0.43	0.52	0.52
Solution 3	0.22	0.21	0.25	0.26
Solution 4	0.19	0.18	0.22	0.23

Table S 6.9 Experimental ξ-values in experiment B for Solutions 2, 3 and 4 using D_{SRFA}=2.8x10^{-10} m^2 s^{-1} , Deployment time=114.6h. Rest of parameters as in Table S 6.6 except ΔDBL=1.64x10^{-4} m.

D_{SRFA}=2.8x10^{-10} (m^2 s^{-1})^2	Experiment SRFA			
	ξ_{1R1G}	ξ_{2R1G}	ξ_{1R2G}	ξ_{1R3G}
Solution 2	1.18	1.07	1.02	1.02
Solution 3	1.07	0.81	1.06	1.01
Solution 4	1.64	1.07	1.11	0.97

Table S 6.10 Experimental ξ-values in experiment SRFA for Solutions 2, 3 and 4 using D_{SRFA}=3.7x10^{-10} m^2 s^{-1}. Parameters as in Table S 6.6 except ΔDBL=1.64x10^{-4} m.

D_{SRFA}=3.7x10^{-10} (m^2 s^{-1})^2	Experiment SRFA			
	ξ_{1R1G}	ξ_{2R1G}	ξ_{1R2G}	ξ_{1R3G}
Solution 2	0.89	0.80	0.77	0.77
Solution 3	0.81	0.61	0.80	0.77
Solution 4	1.24	0.81	0.84	0.74

Table S 6.11 Experimental ξ-values in experiment SRFA for Solutions 2, 3 and 4 using D_{SRFA}=5.0x10^{-10} m^2 s^{-1}. Rest of parameters as in Table S 6.6 except ΔDBL=1.64x10^{-4} m

D_{SRFA}=5.0x10^{-10} (m^2 s^{-1}) [1]	Experiment SRFA			
	ξ_{1R1G}	ξ_{2R1G}	ξ_{1R2G}	ξ_{1R3G}
Solution 2	0.66	0.59	0.57	0.57
Solution 3	0.60	0.45	0.53	0.57
Solution 4	0.92	0.60	0.62	0.55

Values of ξ for experiment A coming out from the use of different diffusion coefficients of SRHA reported in the literature are gathered in Table S 6.6 to Table S 6.8. As can be observed, an increase of the diffusion coefficient leads to less labile complexes (i.e decreasing values of ξ). This is the expected trend because increasing the diffusion coefficient, the flux of metal in the resin layer increases and accordingly, to obtain a fixed

experimental value of the accumulation the complex has to become more inert. The same trend is observed for experiment B.

A column-wise comparison within Table S 6.6 to Table S 6.8 also indicates an increase of the lability as the length of the diffusion domain increases in experiment SRHA. This trend does not occur for experiment SRFA (Table S 6.9 - Table S 6.11) suggesting that the Hg complex with SRFA is already labile in the DGT with shortest diffusion domain.

From the experimental value of ξ determined for each solution and using the diffusion coefficients considered from Table S 6.6 to Table S 6.8 for experiment SRHA and Table S 6.9 - Table S 6.11 for experiment SRFA, plus the conditional constants obtained with VMINTEQ for these complexes, k_d (s^{-1})-values can be obtained with the use of Eq (6.3) of the main text. Because k_d (s^{-1}) is an intrinsic parameter that only depends on the ability of the complex to dissociate and in the main text it has been proven for SRHA that the value for k_d (s^{-1}) is able to reproduce the experimental lability degree for other DGT configurations. The results for the k_d (s^{-1}) values obtained in the following tables are only related to the DGT device configuration 2R1G.

Table S 6.12 Results of k_d (s^{-1}) for experiment A for solutions 2,3 and 4 for the list of different diffusion coefficients of SRHA reported in literature (shown in column 1).

k_d (s^{-1}) / D_{SRHA} ($m^2\ s^{-1}$)	Solution 2	Solution 3	Solution 4
$2.3x10^{-10}$	-	$2.3\ x10^{-3}$	$1.5x10^{-3}$
$2.5x10^{-10}$	-	$1.9x10^{-3}$	$1.3x10^{-3}$
$4.96x10^{-10}$	$6x10^{-3}$	$9.2x10^{-4}$	$7.2x10^{-4}$
$6.05x10^{-10}$	$3.7x10^{-3}$	$8.2x10^{-4}$	$5.6x10^{-4}$

Table S 6.13 Results of k_d (s^{-1}) for experiment B for solutions 2,3 and 4 for different diffusion coefficients of SRFA reported in literature.

k_d (s^{-1}) / D_{SRFA} ($m^2\ s^{-1}$)	Solution 2	Solution 3	Solution 4
$2.5x10^{-10}$	-	-	-
$2.8x10^{-10}$	-	-	-
$3.7x10^{-10}$	$6.9\ x10^{-3}$	$4.1\ x10^{-3}$	$6.0x10^{-3}$
$5.0x10^{-10}$	$2.2x10^{-3}$	$1.74x10^{-3}$	$4.1x10^{-3}$

In Table S 6.12 and Table S 6.13, the general trend (row-wise) for SRHA or SRFA is to obtain a lower k_d as the diffusion coefficient for SRFA or SRHA used as input value increases since an increase of the flux needs to be compensated with a decrease of dissociation for a given accumulation (i.e a lower k_d is obtained).

When Table S 6.12 and Table S 6.13 are observed column-wise (i.e adding more concentration of SRHA or SRFA to the sample respectively) different trends are observed. For the case of SRHA (Table S 6.12), the pool of complexes (Hg-SRHA) becomes more inert as the c_{SRHA} increases. This behaviour agrees with Hg ions being attached to increasingly strongest sites available as the concentration of SRHA increases. According to the Eigen

model, a common association reaction rate constant applies for the Hg binding to all the sites so that as the affinity of the site increases, the dissociation rate constant should decreases and accordingly, the complex becomes less labile.

In contrast, for the case of SRFA, the pool of complexes does not become more inert as c_{SRFA} increases. Instead, it seems to become more labile, a trend that that can hardly be understood

.

Table S 6.14 *%back* computed by rigorous numerical simulation by using the following parameters simulating experiment A. For solution 4 $K_{Hg\text{-}humic}$ =1.70x10^{20}, $c_{HgSRHA=}$1.2x10^{-6} mol m^{-3}, c_{SRHA} = 0.057 mol m^{-3} , $c_{Hg^{+2}}$ =2.37x10^{-25} mol m^{-3}. For solution 3 $K_{Hg\text{-}humic}$ =2.4x10^{18}, $c_{HgSRHA=}$2.13x10^{-6} mol m^{-3}, c_{SRHA} = 0.014 mol m^{-3} , $c_{Hg^{+2}}$ =5.92x10^{-23} mol m^{-3}. For solution 2, $K_{Hg\text{-}humic}$ =1.10x10^{18} , $c_{HgSRHA=}$1.27x10^{-6} mol m^{-3}, c_{SRHA} = 0.00577 mol m^{-3} , $c_{Hg^{+2}}$ =1.99x10^{-22} mol m^{-3} . Other parameters: δ^{g}=3.9x10^{-4} m, δ^{r}=1x10^{-4}m, δ^{DBL} =8.04x10^{-5}m, Δt=1x10^{-2} s, time=10 h

Predicted *%back* / D_{SRHA} ($m^2\ s^{-1}$)	Solution 2	Solution 3	Solution 4
2.3x10^{-10}	-	9%	12%
2.5x10^{-10}	-	12%	14%
4.96x10^{-10}	8%	20%	21%
6.05x10^{-10}	11%	21%	22%

Table S 6.15*%back* computed by rigorous numerical simulation by using the following parameters simulating experiment B. For each solution D_{SRFA} is specified in column 1 and k_d is specified in Table S 6.13 for the corresponding $D_{SRFA.}$ The association reaction constant in each solution is calculated from k_a=Kxk_d . For solution 4 $K_{Hg\text{-}SRFA}$ =6.26x10^{26}, , $c_{HgSRFA=}$1.2x10^{-6} mol m^{-3}, c_{SRFA} = 0.083 mol m^{-3} , $c_{Hg^{+2}}$ =4.79x10^{-32} mol m^{-3} For solution 3 $K_{Hg\text{-}SRFA}$ =1.46x10^{25}, $c_{HgSRFA=}$2.51x10^{-6} mol m^{-3}, c_{SRFA} = 0.054 mol m^{-3} , $c_{Hg^{+2}}$ =3.66x10^{-29} mol m^{-3}. For solution 2 $K_{Hg\text{-}SRFA}$ =7.92x10^{22}, $c_{HgSRFA=}$2.24x10^{-6} mol m^{-3}, c_{SRFA} = 0.039 mol m^{-3} , $c_{Hg^{+2}}$ =7.24x10^{-27} mol m^{-3} . Other parameters: δ^{g}=3.9x10^{-4} m, δ^{r}=1x10^{-4}m, δ^{DBL} =8.04x10^{-5}m, Δt=1x10^{-2} s, time=10 h

Predicted *%back* / D_{SRFA} ($m^2\ s^{-1}$)	Solution 2	Solution 3	Solution 4
2.5x10^{-10}	-	-	-
2.8x10^{-10}	-	-	-
3.7x10^{-10}	5.5%	13%	1%
5.00x10^{-10}	15.5%	17%	11%

6.6.3 Testing caps, pistons, diffusive gels and filters as possible sources of DOM

In the experiments SRHA and SRFA from the main text, in solution 1 no DOM was added. Nevertheless the measurement from the TOC analyzer has shown that there is a non-negligible quantity of DOM in those samples (approximately DOM≈4 mg/L).

The main hypotheses is that the residual DOM comes from one or more parts of the DGT devices. Therefore a side experiment has been made to check if there is any leaching of DOM from the DGT devices.

The experimental procedure consists on preparing a set of solutions with a background electrolyte NaNO3 with ionic strength (*I*=0.01M) containing the different parts of the DGT devices. The first solution contains the caps and pistons. The second solution contains the agarose gels. The third solution contains the filters.

The glass bottles have been cleaned with Milli-Q water for 3 times, then left with HCl 5% v/v 24 h and finally burned to 300 °C during 3 hours. Then, the bottles are weighted before and after adding MQ water to know the mass of the solution which is 1.4 L for the blank and 1.2 for the solution with caps and pistons.

Once the first solution is prepared, it is introduced into an incubator with an agitation frequency close to 90 rpm covered with a plastic bag and aluminium foil at a temperature of 20°C . A second glass bottle that contains a blank solution which is also covered by a plastic back and with aluminium foil is introduced to the incubator.

The bottles have left a total of 7 days inside the incubator. 3 replicate samples of 24 mL have been taken in day 1, 2, 3, 4 and 7.

After these 7 days, the second and third solution have been introduced to the incubator under the same conditions than the previous samples. 3 replicate samples of 20 mL have been taken in the days 2,3,4 and 7.

The samples have been stored in brown glass bottles covered with aluminium foil that have also been previously cleaned with the same procedure as the glass containers. These containers have been stored in the freezer until the day of analysis. NPOC determinations have been performed by “serveis cientifico-tècnics de la UdL”.

Table S 6.16 Average DOC measured in a blank bottle (column 1) and in a solution containing caps and pistons (column 2).

Days	DOC (mg/L) blank	DOC (mg/L) solution tith caps and pistons
1	0.30±0.06	0.21±0.06
2	0.28±0.02	0.36±0.06
3	0.33±0.01	0.31±0.02
4	2.58±0.07	0.89±0.08
7	4.1±0.1	4.73±0.03

In Table S 6.16 , from day 1 to day 3 the DOC in solution is rather low is clearly related to the concentration in MQ water. From the 3 onwards there is a source of contamination of DOC. An hypothesis is that the plastic tips, have polluted the solution of the blank bottle and the bottle with pistons and caps. Nevertheless, the important conclusion is that the pistons and caps are not a source of DOC in solution, as they show the same DOC as a blank bottle.

Table S 6.17 Average DOC measured in a blank bottle (column 1), in a solution containing filters (column 2), in a solution containing agarose gels (column 3).

Days	DOC (mg/L) blank	DOC (mg/L) filters	DOC (mg/L) agarose gels
2	0.18±0.02	0.71±0.04	0.75±0.07
3	0.34±0.03	1.76±0.04	1.33±0.04
4	0.77±0.03	2.10±0.09	1.33±0.09
7	1.14±0.06	4.9±0.2	1.6±0.1

In Table S 6.17we can see that from day 2 to day 7 the DOC in column 2 and 3 is significantly higher that in column 1 which is related to the blank bottle. Therefore it can be considered that the agarose gels and PVDF filters are a source of DOC in the solution.

6.6.4 References

1. Balch, J.; Gueguen, C., Effects of molecular weight on the diffusion coefficient of aquatic dissolved organic matter and humic substances. *Chemosphere* **2015,** *119,* 498-503.

2. Lead, J. R.; Wilkinson, K. J.; Balnois, E.; Cutak, B. J.; Larive, C. K.; Assemi, S.; Beckett, R., Diffusion coefficients and polydispersities of the Suwannee River fulvic acid: Comparison of fluorescence correlation spectroscopy, pulsed-field gradient nuclear magnetic resonance, and flow field-flow fractionation. *Environmental Science and Technology* **2000,** *34* (16), 3508-3513.

7 Zn DGT lability spectrum in natural waters

Part of the content of this chapter has been published in STOTEN: https://doi.org/10.1016/j.scitotenv.2021.151201

7.1 Introduction

Bioavailability of a toxic or nutrient element (e.g trace-metals) is characterized by a set of (bio)chemical steps that control the biouptake process such as internalization, diffusion of labile complexes or chemical kinetics [1]. The description of the trace-metal bioavailability to an organism can be approached by using a set of analytical techniques and models [2]. Equilibrium models such as FIAM (Free Ion activity model) or BLM (Biotic Ligand Model) have been used to predict the toxicity of a trace-metal when internalization is the limiting step to the uptake flux in the environment of analysis [3]. When these conditions apply, the biouptake flux is proportional to the free metal ion concentration and analytical techniques such as AGNES (Absence of Gradients and Nernstian Equilibrium Stripping) or DMT (Donnan Membrane techniques) are useful to measure the free metal ion concentration in equilibrium with other metals species in the media (e.g inorganic, organic complexes, colloids)[4-5]. Nevertheless, depending on the biota or the conditions of the media, the metal uptake is controlled by a diffusion process towards the membrane receptors, and then the magnitude of the diffusive flux is characterized by the thickness of the diffusion layer and the diffusion coefficient of the metal species[6-7].

Dynamic analytical techniques try to mimic the metal uptake by the cell membrane, typically under diffusion limiting conditions, where the thickness of the diffusion layer of the analytical technique determines the temporal scale of the diffusion process. When only the free metal ion is internalized, the contribution to the total flux of other metal species such as complexes depends on the rate of dissociation along the diffusion through the diffusion layer. The comparison of results between techniques that yield concentrations, such as AGNES, and dynamic techniques that provide metal fluxes, such as DGT or LASV (Linear scan Anodic stripping voltammetry), can represent a difficult task when it comes to recalculate the fluxes in terms of effective concentrations.

In this chapter of the thesis, we have combined the use of DGT along with other techniques such as AGNES, LASV (the experimental procedure and theory applied are explained in detail in Rosales et.al 2021) and ICP-MS to obtain complementary information to characterize the chemical availability of Zn in the stream Riera d'Osor localized in Girona. This chapter is focused on the application of DGT in the Osor stream and it will go through: a description of the sampling methodology, an analysis of the speciation using Visual Minteq (VM) together the experimental measurements, the interpretation of the effective DGT concentration in terms

of the concentration of the real species in the system (the free metal ion and a pool of inorganic complexes), the development of a methodology to calculate the lability degree of the pool of inorganic complexes and finally, the determination of an effective dissociation rate constant of this pool of complexes. The lability of inorganic zinc complexes in DGT devices of different configurations in a framework that considers the DGT resin disc as a perfect-sink surface it is going to be discussed in detail. Finally, the measurement of a spectrum of effective concentrations from dynamic techniques (DGT with different configuration and LASV) completed with the total and free metal concentration (AGNES and ICP-MS) can be applied to assess Zn bioavailability in diffusion controlled conditions.

7.2 Material and Methods

7.2.1 Sampling

Osor stream is a river located in Girona (Catalonia, Spain) whose surface waters have been contaminated by former mining activities of F-Ba-Pb-Zn ore 8. Our sampling strategy has been mainly designed to apply the DGT technique and produce and analysis in terms of the speciation of Zn concentration in water. To do so, in Figure 7.1 it can be seen that we deployed at the coordinates 41° 57′ 14” N, 2° 35′ 58″ E a set of parallelepiped structures with the purpose of holding the DGT devices parallel to the river flow.

Figure 7.1 Parallelepiped structure holding DGT devices parallel to the river flow to sample Osor stream.

During 10th and 11th March 2020 we made in situ measurements of a set of physical parameters with an Orion Star A329 pH/ISE/Conductivity/RDO/DO Meter and we collected samples and prepared them in situ by filtering 9.98 mL of stream water though a 0.45 µM syringe filter and mixing it with 20 µL of HNO_3 70%. These samples were analysed for total Zn using an inductively coupled plasma mass spectrometer (ICP-MS, 7700x, Agilent

Technologies, Inc.). AGNES and LASV experiments were conducted on the last grab sample from 11th March 2020 (last row in Table 7.2). Majority anions and cations were measured with IC (ion chromatography), alkalinity of this last grab sample was analysed in the Scientific and Technical Services of the Catalan Institute for Water Research (ICRA) and Dissolved Organic Carbon (DOC) was analysed at "serveis científico tècnics" of the Universitat de Lleida.

7.2.2 Speciation modelling with VM

The speciation of Zinc can be understood from a semi-quantitative point of view by using VM, a software that calculates equilibrium concentrations from a set of total concentration for a given Temperature (T) and ionic strength (calculated from the concentration of anions and cations). To perform the speciation calculation, we gathered the experimental data obtained from the results of the analysis described in the previous subsection.

These experimental data were used as an input for VM together with pH=8.584, the concentration of majority ions, DOC, T=12.3°C, alkalinity and the total metal concentration of Zn, Fe, Pb and Mn.

Table 7.1 Input concentrations used for the speciation program VM fixing pH=8.584, T=12.3 °C, DOC=2.03 mg C/L, Alkalinity=75.5 mg $CaCO_3$ L^{-1} in a closed system

	Concentration of Species in (mol L^{-1})	Source
Na^+	$6.25x10^{-4}$	IC
K^+	$3.07x10^{-5}$	IC
Mg^{+2}	$2.03x10^{-4}$	IC
Ca^{+2}	$4.32x10^{-4}$	IC
Li^+	$8.64x10^{-7}$	IC
NO_2-	$2.17x10^{-7}$	IC
NO_3-	$1.29x10^{-6}$	IC
Cl^-	$3.42x10^{-4}$	IC
SO_4^{2-}	$1.55x10^{-4}$	IC
F^-	$1.47x10^{-5}$	IC
CO_3^{2-}	$7.32x10^{-4}$	from Alkalinity
$c_{T,Zn}$	$6.33\ x10^{-7}$	ICP-MS
$c_{T,Pb}$	$4.64\ x10^{-9}$	ICP-MS
$c_{T,Mn}$	$3.13\ x10^{-7}$	ICP-MS
$c_{T,Fe}$	$1.46\ x10^{-7}$	ICP-MS

NICA-Donnan is the model that is used for calculating the concentration of Zn complexes bound to the organic matter. It is a non-ideal and competitive isotherm that considers that organic matter is composed of 2 distribution of sites: carboxylic and phenolic. When only one cation is present in the system, each distribution is given by a Sips distribution.. The free energy of the bound Zn-carboxilic or Zn-fenolic can be split in a chemical and an electrostatic contribution [9]. The main reason to use this model is that uses a data set of experimental measurements of H+ and metal titrations to fulvic and humic acids were used to derive the parameters of NICA-Donnan isotherm [10] .

Finally, we have considered a closed system (i.e the partial pressure of CO_2 is not fixed) and the total concentration of carbonates introduced as an input comes from the alkalinity measured in the Osor stream sample.

7.2.3 DGT

DGT devices contain a resin disc to immobilize the metal cations on top of which a diffusive disc defines a diffusion domain. The diffusive gel is a polyacrylamide cross-linked disc made of a commercial agarose derivative often designated as APA. The resin layer contains a powder (Chelex 100) incorporated into a gel matrix (APA gel). Other details on the preparation and handling of DGT devices can be found elsewhere [11].

Three DGT configurations of the DGT devices have been used in this work: i) one resin disc and one diffusive gel disc (code 1R1G); ii) two resin discs and one gel disc (2R1G) and iii) one resin disc and two gel discs (1R2G). Twelve DGTs containing 1R1G, seven DGT containing 2R1G and seven DGT containing 1R2G were deployed. Deployment times for different configurations were: 5 h 47 min (1R1G), 19 h 57 min (1R1G), 28 h 37 min (1R1G), 166 h 22 min (1R1G), 28 h (2R1G), 166 h 7 min (2R1G), 28 h 25 min (1R2G) and 165 h 52 min (1R2G). The longest time corresponded to a set of devices left until March 16th 2020.

DGT blanks (prepared as 1R1G, but not deployed) were transported from our laboratory to the field (and back) in a sealed plastic bag alongside DGT devices used for deployment. This blank accumulation is subtracted from the accumulated moles in DGT devices deployed in Osor stream.

The clamps used as support structure for DGT deployment were washed the day before deployment with ultra-purified water and nitric acid.

From the slope (s) of the linear regression of the plot accumulated moles vs. time (e.g. see Figure 7.), c_{DGT} is calculated as:

$$c_{DGT} = \frac{s\Delta g}{D_{Zn}^{g} A t} \qquad (7.1)$$

Where D_{Zn}^{g} is the diffusion coefficient of Zn across the gel disc (4.20×10^{-10} m^2 s^{-1}, reported by DGT Research), A is the exposed area (3.14 mm^2) and Δg is the aggregate thickness of the diffusive gel(s)

plus filter plus an estimated diffusive boundary layer (DBL) of 0.3 mm (Levy et al., 2012; Warnken et al., 2007). The thicknesses of an individual diffusive gel, resin and filter are δ^g = 0.629 mm, δ^r = 0.4 mm and δ^f = 0.150 mm, respectively.

7.3 Theory

7.3.1 The lability degree

The lability degree ξ is defined [12] as the fraction of the current contribution of the complexes to the flux with respect to the maximum possible contribution if all complexes were fully labile:

$$\xi \equiv \frac{J - J_{\text{inert}}}{J_{\text{labile}} - J_{\text{inert}}} \tag{7.2}$$

where J is the flux in the sampling measurement (where ξ is to be determined). J_{inert} indicates the flux that would be obtained if the complexes were fully inert (i.e. if the flux was only sustained by the free metal concentration, with no dissociation from the complex). J_{labile} indicates the flux that would be obtained if the complexes were fully labile (i.e. no kinetic limitation to reach equilibrium between the Zn species in solution at any place and time).

7.3.2 DGT model with penetration: expression for the lability degree

In excess of ligand conditions, with neutral complexes (i.e. there are no electrostatic effects because most Zn complexes are uncharged, see Table 7.2), ξ can be written in terms of physicochemical parameters as:

$$\xi = 1 - \frac{1 + \varepsilon K'}{\varepsilon K' + \frac{\Delta g}{m}\coth\left(\frac{\Delta g}{m}\right) + \frac{\Delta g(1+\varepsilon K')}{\lambda_{\text{ML}}}\tanh\left(\frac{\delta^{\text{r}}}{\lambda_{\text{ML}}}\right)} \tag{7.3}$$

where Δg stands here for the whole diffusion domain (except the resin), i.e. including diffusive gel, filter and DBL. Other parameters are:

$$m = \sqrt{\frac{D_{\text{ML}}}{k_{\text{d}}\left(1 + K'\right)}} \tag{7.4}$$

and

$$\lambda_{\text{ML}} = \sqrt{\frac{D_{\text{ML}}}{k_{\text{d}}}} \tag{7.5}$$

7.3.3 DGT model without complex penetration in the resin layer: expression for the lability degree

Although during the deployment time of a DGT device metal complexes can penetrate inside the resin layer, shifting the complexation reaction towards dissociation, a model without complex penetration would better mimic the surface reaction of the membrane receptors of an organism with the free metal ion. Then, if we make the same assumptions as the previous subsection and set $\delta^{r}=0$, the expression for the lability degree to a sensor that exhibits an impenetrable consuming surface becomes:

$$\xi = 1 - \frac{(1+K')}{K' + \frac{\Delta g}{m}\coth\left(\frac{\Delta g}{m}\right)} \tag{7.6}$$

As lability increases, the reaction layer, i.e., the layer where net dissociation takes place, decreases. For very labile complexes, their reaction layer (m) becomes at least 1/3 times smaller than the thickness of the diffusive gel ($m<\Delta g/3$). Therefore, the lability degree can be expressed as:

$$\xi = 1 - \left(\frac{1+K'}{K' + \Delta g\sqrt{\frac{k_{d}(1+K')}{D_{Zn}}}} \right) \tag{7.7}$$

7.3.4 c_{DGT} interpreted in terms of real species and lability degrees

As shown elsewhere [13-16], the operationally defined DGT concentration, c_{DGT}, can be expressed in terms of the contribution of the free metal plus those of the different complexes which are weighted by their normalized diffusion coefficients (ε_j) and their lability degrees (ξ_j). If there are h parallel complexes with the ligands ${}^{j}\mathrm{L}$,

$$c_{DGT} = [\mathrm{Zn}^{+2}] + \sum_{j=1}^{h} \xi_j \varepsilon_j [\mathrm{Zn}^{j}\mathrm{L}] \tag{7.8}$$

where the normalized diffusion coefficients are

$$\varepsilon_i = \frac{D_{\mathrm{M}^{i}\mathrm{L}}}{D_{\mathrm{M}}} \tag{7.9}$$

In Eq. (7.3) one assumes that the ratio of diffusion coefficients is the same in water (i.e. in the DBL) as in the gel phase or the filter.

7.3.5 Determination of the dissociation rate constant (k_d) from DGT with different configurations.

The dissociation rates of complexes have a huge impact on the DGT metal flux at the resin-gel interface. Such importance comes, in part, from the characteristics of the polymeric matrix of the resin layer that allow the penetration of complexes inside the resin layer. As shown in Eq.(7.8) the effective DGT concentration can be described in terms of the equilibrium concentration of the real species of the system, their diffusivities and lability degree. The lability degree of each zinc complex also depends on the thickness of the gel and the resin layer, as shown in Eq (7.3). Therefore, the c_{DGT} of devices with different configurations can be related to a system of equations. For example, in a case of a system composed of a metal that can react with two pools of ligands, an organic pool and an inorganic pool, the system of equations is :

$$\left.\begin{aligned} c_{DGT}^{1R1G} &= [Zn^{+2}] + \varepsilon_{Inorg}\xi_{ZnL_{Inorg}}^{1R1G}[ZnL_{Inorg}] + \varepsilon_{Org}\xi_{ZnL_{Org}}^{1R1G}[ZnL_{Org}] \\ c_{DGT}^{1R2G} &= [Zn^{+2}] + \varepsilon_{Inorg}\xi_{ZnL_{Inorg}}^{1R2G}[ZnL_{Inorg}] + \varepsilon_{Org}\xi_{ZnL_{Org}}^{1R2G}[ZnL_{Org}] \\ c_{DGT}^{2R1G} &= [Zn^{+2}] + \varepsilon_{Inorg}\xi_{ZnL_{Inorg}}^{2R1G}[ZnL_{Inorg}] + \varepsilon_{Org}\xi_{ZnL_{Org}}^{2R1G}[ZnL_{Org}] \end{aligned}\right\} \quad (7.10)$$

In the case that the concentration for the organic pool of complexes is negligible, the system of equations reduces to:

$$\left.\begin{aligned} c_{DGT}^{1R1G} &= [Zn^{+2}] + \varepsilon_{Inorg}\xi_{ZnL_{Inorg}}^{1R1G}[ZnL_{Inorg}] \\ c_{DGT}^{1R2G} &= [Zn^{+2}] + \varepsilon_{Inorg}\xi_{ZnL_{Inorg}}^{1R2G}[ZnL_{Inorg}] \\ c_{DGT}^{2R1G} &= [Zn^{+2}] + \varepsilon_{Inorg}\xi_{ZnL_{Inorg}}^{2R1G}[ZnL_{Inorg}] \end{aligned}\right\} \quad (7.11)$$

Now, to solve the latter system of equations, a 4th equation relating the parameter lability degree with the thickness of the resin gel layer or resin layer, such as Eq (7.3), is necessary.

In our case, the system of equations have the following unknowns: lability degrees (ξ^{1R1G}, ξ^{1R2G}, ξ^{2R1G}) and ε_{Inorg}. Nevertheless, as stated above, the lability degrees depend on the geometric characteristics of the DGT device, from them using the ligand excess formula (Eq (7.3)) a single value for the dissociation rate constant can be retrieved. Therefore, our system only has 2 unknowns (ε_{Inorg} and k_d), then from the system of equations displayed in Eq (7.11), only two equations are needed for example:

$$\left.\begin{aligned} c_{\mathrm{DGT}}^{\mathrm{1R1G}} &= [\mathrm{Zn}^{+2}] + \varepsilon_{\mathrm{Inorg}} \xi_{\mathrm{ZnL_{Inorg}}}^{\mathrm{1R1G}} [\mathrm{ZnL_{Inorg}}] \\ c_{\mathrm{DGT}}^{\mathrm{1R2G}} &= [\mathrm{Zn}^{+2}] + \varepsilon_{\mathrm{Inorg}} \xi_{\mathrm{ZnL_{Inorg}}}^{\mathrm{1R2G}} [\mathrm{ZnL_{Inorg}}] \end{aligned}\right\} \quad (7.12)$$

To solve Eq (7.12) a non-linear system of equations, we have selected a function called FindRoot from Wolfram Mathematica that uses a Newton-Raphson algorithm or a variant of the secant method in the case that two values are given as an input [17].

7.4 Results

7.4.1 Zinc species distribution in sampled water from Osor stream

The concentration of the majority ions measured by IC and the total concentrations measured by ICP-MS for Zn , Mn, Pb and Fe in Osor stream during the sampling campaign from 10th and 11th of March are displayed in Table 7.1. These concentrations have been used as an input value for VM to perform the calculation of the equilibrium concentrations in Osor stream.

Table 7.2 Predicted Zn speciation in Osor river water according to VM with input as defined in TableTauInputVM1 . The resulting charge imbalance was 14.7 %.

	Predicted concentration of Zn species in Osor stream (nmol L^{-1})	% Zn species
Zn^{+2}	192	32.6
$ZnCO_{3\ (aq)}$	78.6	13.3
$ZnHCO_3^+$	2.55	0.4
$Zn(OH)_{2\ (aq)}$	287	48.7
$ZnOH^+$	22.5	3.8
ZnOrg	8.21	1.1
$c_{T,Zn}$	633	100

The tiny fraction corresponding to a 1.1% that encompasses of Zn intrinsically bound to carboxylic or fenolic sites and the Zn territorially bound to the Donnan volume results derives from low equilibrium constants that describe the binding of Zinc with fulvic acid.

Apart from the results of the speciation program, we have measured the concentration of free zinc with AGNES yielding to [Zn^{+2}]=111 nM (The procedure followed is explained in detail at [Rosales et.al]). This result is also in quite agreement with [Zn^{+2}]=192 nM obtained from the equilibrium calculation done by VM. From now on, we are going to rely on the experimental result obtained by AGNES ([Zn^{+2}]=111 nM) to perform the calculations explained in the following sections.

7.4.2 Labile concentrations and lability degrees with DGT of different configurations

The accumulations in DGT devices increase linearly with time which indicates that mass transport is controlled by diffusion and steady state has been reached in the system.

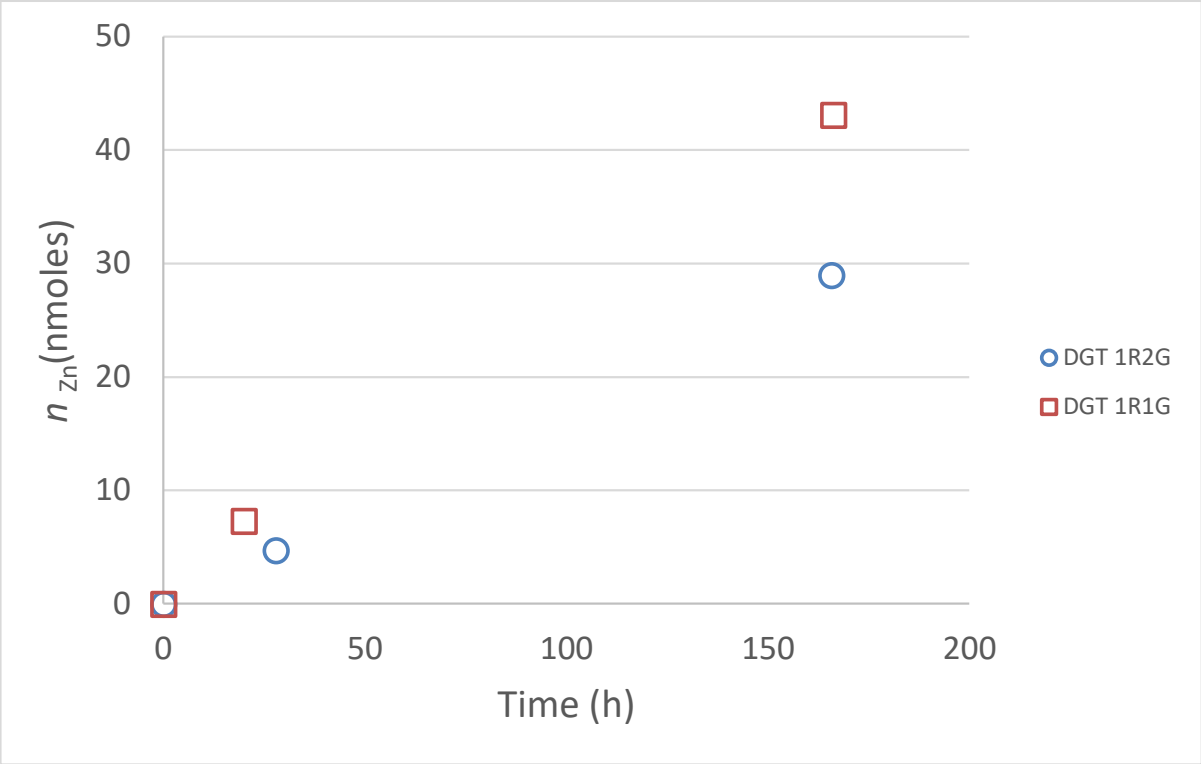

Figure 7.2 Zn accumulation against time in Osor stream for 1R1G devices (red squares) and 1R2G DGT (blue circles).

Hence, we applied first Fick law to compute c_{DGT} by using Eq (7.1) which led to 4.76(±0.23) × 10^{-7} mol L^{-1} (1R1G), 5.17(±0.03) × 10^{-7} mol L^{-1} (1R2G) and 5.68 (±0.06) × 10^{-7} mol L^{-1} (2R1G). In comparison with 1R1G device, when the thickness of the gel layer is increased (DGT 1R2G) the diffusion gradient decreases and, therefore, within the same deployment time, the accumulation is smaller. Conversely, an increase of the resin layer (DGT 2R1G) leads to a greater accumulation, because partially labile complexes have more time and volume to dissociate inside the resin layer. Moreover, this type of DGT devices provides us information on the ability of the complexes to achieve full dissociation at the resin-gel interface. For fully labile complexes the accumulation in the back resin is going to be negligible, because they will have achieved complete dissociation at the resin-gel interface. In contrast, for inert complexes, the kinetic dissociation rate constant is low enough so that their contribution to the total flux is negligible along the resin layer. But, when the equilibrium constant is large, the concentration of free metal is very low, and its contribution to the accumulation is negligible in comparison with the contribution of the complex, the *%back* will be close to 0 for fully labile complexes

and close to 0.5 for inert complexes. Nevertheless, in some cases it may happen that the contribution of the free metal is not negligible, then the *%back* is close to 0 for fully labile and inert complexes. Therefore, the result from our 2R1G DGT device elucidates that the complexes in our system are partially labile because the back ratio is around 0.29.

Once c_{DGT} values for each DGT configuration are obtained from the experimental accumulations, we would like to obtain the contribution of each complex by determining the corresponding lability degree. Due to the limited number of c_{DGT} values and the almost negligible presence of Zn complexes with the fulvic matter, as suggested by the VM prediction, we will restrict ourselves to a model that considers that the Zn speciation is composed by the the free Zn concentration and a pool of inorganic complexes for which we aim to compute effective values for the lability degree and dissociation rate constant. Considering the prediction of the equilibrium concentrations obtained by VM, we calculated a concentration for the inorganic pool of complexes by subtracting to the total metal concentration obtained by ICP-MS, the free metal concentration obtained by AGNES ($c_{ZnL_{Inorg}} = c_{T,Zn} - c_{Zn,free}$).

In order to apply the methodology presented at section "Determination of the dissociation rate constant (k_d) from DGT with different configurations." , we need to provide an initial guess of (i.e k_d=1x10^{-3} s^{-1}and ε=1) the value for the unknowns in our system (k_d, ε).Since inorganic Zn complexes have similar size than the free hydrated metal cation, we will consider ε=1 for the inorganic pool as an educated guess in Eq (7.11). By using this assumption, from Eq (7.8) we can calculate an experimental lability degree for the species ZnL_{inorg} for each DGT device configuration by assuming that ε=1. From these results, we set an educated guess in Eq (7.11) for ξ_{1R1G} and ξ_{1R2G} to calculate the dissociation rate constant applying the aforementioned methodology. The outcome of the system of equations gave an average value for k_d of 2.68 × 10^{-3} s^{-1} DGT 1R1G and 1R2G and the lability degrees (ξ_{DGT}) were 0.76 (1R1G), 0.84 (1R2G), and 0.94 (2R1G). Notice that these results are constrained by the assumption that ε=1, which is quite fair regarding that the inorganic complexes have a similar molecular size compared to the hydrated free metal ion. Furthermore, the experimental results of the back accumulation are in agreement with ξ_{DGT} being smaller than 1 for the pool of inorganic complexes.

Now, we would like to compare the ability to dissociate of this inorganic pool of complexes between DGT sensors with different configurations by using as a parameter for the comparison

a characteristic length. We will define this characteristic length (Δg^c (m)) as the thickness that would have the diffusive gel of a DGT device, in which there was no penetration of complexes in the resin layer but the accumulation coincides with that of the DGT device to which this effective length refers to. According to this definition, we can use Eq (7.7) to derive the characteristic length of each DGT device as:

$$\Delta g^c = \left(\frac{1+K'}{1-\xi} - K' \right) \sqrt{\frac{D_{Zn}}{k_d(1+K')}} \qquad (7.13)$$

Now, substituting the lability degree obtained for each DGT configuration into the last equation, we obtain 3.2 (1R1G), 5.2 (1R2G) and 16.6 (2R1G) mm. The last value obtained may be overestimated because the lability degree of the system is close to 1.

Moreover, we can use the result of the dissociation rate constant and apply it to a model without penetration (Eq (7.6)) to calculate a new lability degree for 1R1G and 1R2G DGT devices. This lability degree would be a better description of the contribution of complex to the biouptake, when the free metal ion reacts with the membrane receptors in diffusion limited conditions. The results of these lability degrees are 0.50 (1R1G) and 0.62 (1R2G) and applying Eq (7.13) we obtain the corresponding characteristic length 1.1 mm (1R1G) and 1.70 mm (1R2G).

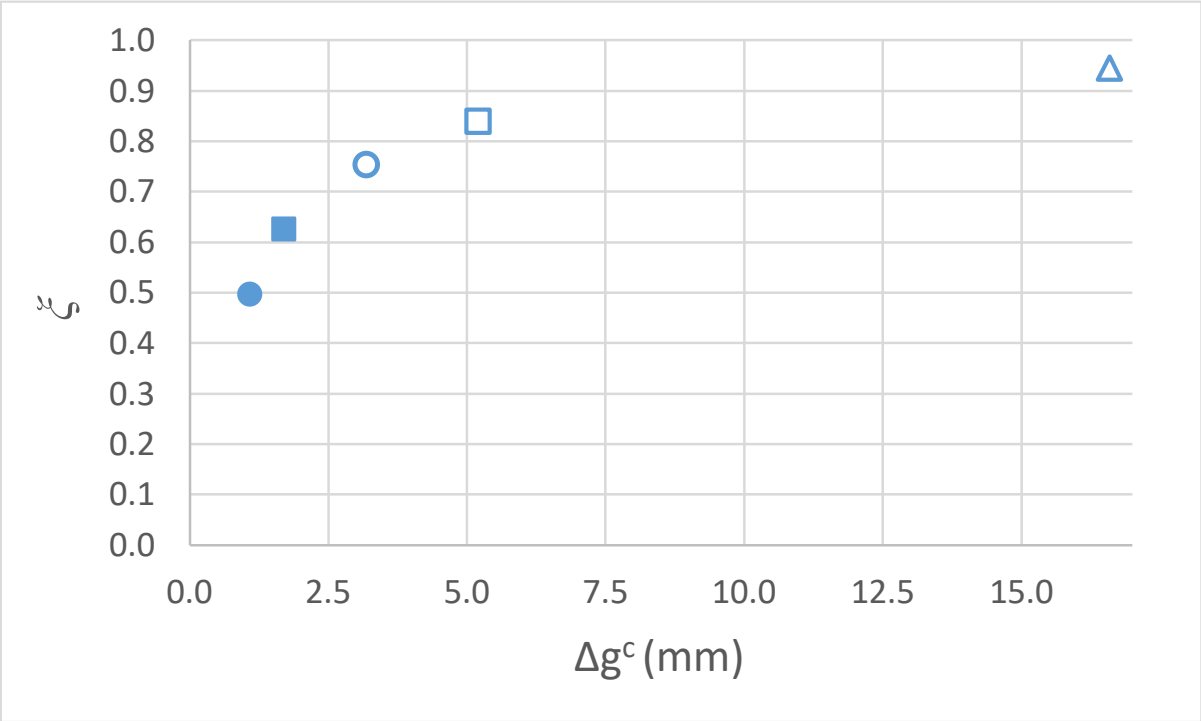

Figure 7.3 Graphical representation of the behaviour of the lability degree against the characteristic length of the DGT device. Blue solid circle and square represent the lability degree of DGT devices of 1R1G and 1R2G without considering penetration. Blue empty circle, square and triangle represent the lability degree of 1R1G,1R2G and 2R1G considering penetration.

Figure 7.3 shows the behaviour of the lability degree against the characteristic length of each DGT device which is in agreement with the statement that the longer the diffusion path of the analyte more time it has to reach complete dissociation [2]. Although it certainly seems that there is a positive correlation between the thickness of the diffusive layer and a higher lability of a complex, it needs to be pointed out that complexes only endure net dissociation when they are not in equilibrium, therefore the aforementioned statement may be a naive physical explanation of the phenomena that is occurring.

It is also worth to comment that although the lability degrees shown in Figure 7.3 are not in agreement with the Eigen mechanism which assesses that $Zn(OH)_2$ is fully labile, these results are supported by the experimental result of the back ratio=0.29 obtained by 2R1G DGT devices. In Price et al., 2021, they obtained a c_{DGT} for Zinc in pH=8.3 that was a 64% of the dissolved zinc concentration indicating that there are partially labile complexes, a case that cannot be explained by Eigen theory . Further work, is needed to fully understand the complexation mechanism of OH- with $[Zn(H_2O)_6]^{+2}$ that leads to a disagreement between experimental results and Eigen theory.

7.4.3 Chemical available concentrations as a proxy for Bioavailability

The available metal concentration for dynamic sensors as DGT or LASV depends on the metal flux arriving at the resin-gel interface or at the electrode surface. The contribution of metal complexes to the total metal flux depends on the characteristic length of the sensor which defines the diffusive time-scale of the dynamic technique. Dynamic sensors can achieve a maximum dynamic concentration when all the complexes that contribute to the total metal flux are fully labile (ξ=1). In the particular case that we are considering only one pool of complexes which share a common diffusion coefficient with the hydrated metal cation (ε=1), Eq (7.8), is equivalent to the maximum dynamic concentration which at the same time is equal to the total concentration of the system.

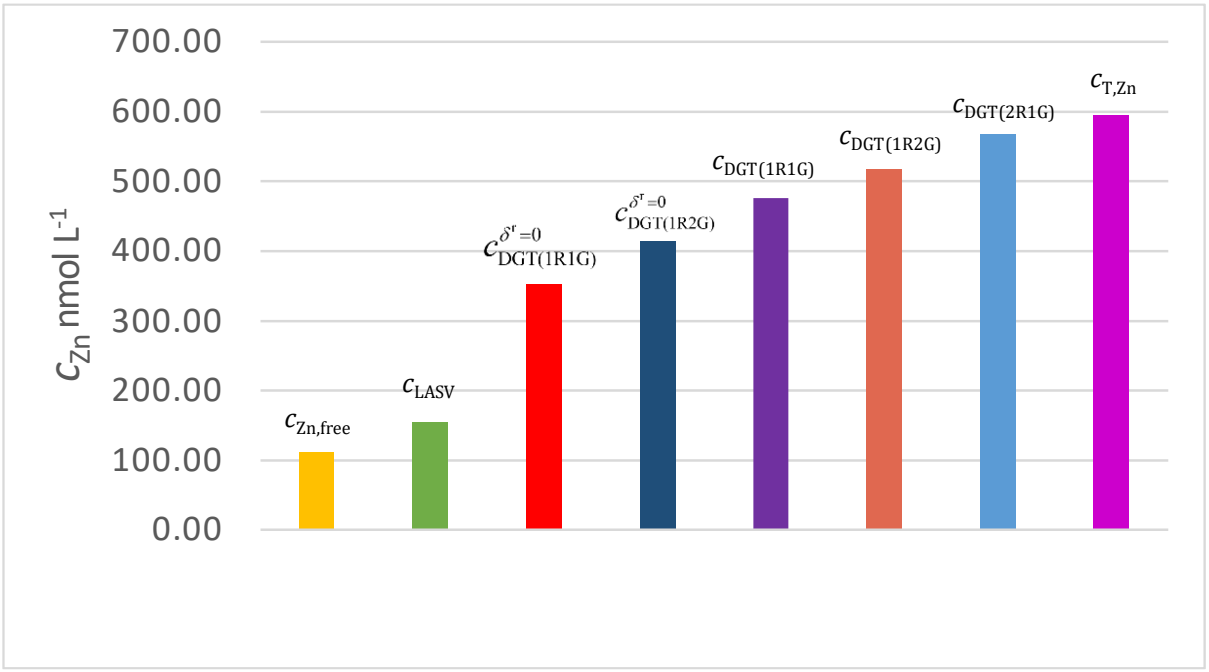

Figure 7.4 Span of Zn concentrations measured by different analytical techniques. For the case of $c^{\delta^r=0}_{DGT(1R1G)}$ *and* $c^{\delta^r=0}_{DGT(1R2G)}$ *they are calculated by using a model without penetration in the resin layer.*

In Figure 7.4, we compare the set of available concentrations that would be measured by different dynamic sensors in our sample of the Osor stream. Notice that values ranging from the free Zn concentration to the total Zn concentration present in the Osor stream can be available depending on the sensor used for the measurement. All the measurements are correct even though they differ in the available concentration indicating that the lability of a system is not an intrinsic property of the system but a property that also depends on the sensor used in the measurement. The results of Figure 7.4 are relevant to illustrate the

effective concentration that an organism would uptake depending on the thickness of the diffusive layer, when diffusion limiting conditions apply. In these conditions, although DGT technique reproduces the physical phenomena, in principle, it may not be best tool to assess the available concentration for macroorganisms such bivalves or plants. For the case of plants, even though we could assume that the diffusive thickness is the same as in a DGT 1R1G, their membrane receptors only react with free metal ion and the complex does not penetrate inside the membrane where an hypothetic shift to the dissociation reaction process would increase the total metal flux inside the organism. Therefore, even in this suitable scenario, the contribution of complexes to the total metal flux in a DGT device would be higher than in plants [7].

To solve this problem, we can recalculate $\xi_{DGT,1R1G}$, $\xi_{DGT,1R2G}$ by using Eq. (7.6) and using the value k_d =2.68x10^{-3} s^{-1} and K'=4.70 which have been obtained based in our experimental measurements. Once we have recalculated the lability degree considering a model without penetration, the calculation of $c^{\delta^r=0}_{DGT(1R1G)}$ and $c^{\delta^r=0}_{DGT(1R2G)}$ is straightforward by using Eq.(7.8). Notice, that $c^{\delta^r=0}_{DGT(2R1G)}$ would give the exact same value as a $c^{\delta^r=0}_{DGT(1R1G)}$, so it is not worth to include it in Figure 7.4. Now, to give a quantitative idea of the impact of the resin on the effective concentration, $c_{DGT(1R1G)}$ and $c_{DGT(1R2G)}$ represent 80% and 87 % of the total concentration while $c^{\delta^r=0}_{DGT(1R1G)}$ and $c^{\delta^r=0}_{DGT(1R2G)}$ represent a 59% and 70% of the total concentration. Therefore, $c^{\delta^r=0}_{DGT(1R1G)}$ and $c^{\delta^r=0}_{DGT(1R2G)}$ offer a more realistic approach to the effective concentration relevant to an organism such as a plant, in the case of diffusion limiting conditions and with the same diffusive length as these devices.

Periphyton have been found to uptake under diffusion limited conditions with a maximum diffusion layer of 1 mm and a minimum diffusion layer of 0.1 mm [18]. For the case of a diffusion layer of 1mm, the effective concentration that the organism would uptake is very similar to a $c_{DGT(1R1G),\Delta r=0}$ (352 nM). But for the case of a diffusion layer of 0.1 mm, the effective concentration would be in the range of c_{LASV} (155 nM) and a $c_{DGT(1R1G),\Delta r=0}$ (352 nM).

For microorganisms, such as Prorocentrum minimum (6.3 µm radius) or many species of phytoplankton, whose diffusive layer is related to their own size, thus much smaller than DGT devices, the prediction of the uptake can be ranged from LASV (155 nmol L^{-1}) to the free concentration(111 nmol L^{-1}).

7.5 References

1. Zhang, Z. S.; Buffle, J.; Town, R. M.; Puy, J.; van Leeuwen, H. P., Metal Flux in Ligand Mixtures. 2. Flux Enhancement Due to Kinetic Interplay: Comparison of the Reaction Layer Approximation with a Rigorous Approach. *Journal of Physical Chemistry A* **2009,** *113* (24), 6572-6580.
2. van Leeuwen, H. P.; Town, R. M.; Buffle, J.; Cleven, R.; Davison, W.; Puy, J.; van Riemsdijk, W. H.; Sigg, L., Dynamic speciation analysis and bioavailability of metals in Aquatic Systems. *Environmental Science and Technology* **2005,** *39*, 8545-8585.
3. Worms, I.; Simon, D. F.; Hassler, C. S.; Wilkinson, K. J., Bioavailability of trace metals to aquatic microorganisms: importance of chemical, biological and physical processes on biouptake. *Biochimie* **2006,** *88* (11), 1721-1731.
4. Galceran, J.; Companys, E.; Puy, J.; Cecília, J.; Garcés, J. L., AGNES: a new electroanalytical technique for measuring free metal ion concentration. *Journal of Electroanalytical Chemistry* **2004,** *566*, 95-109.
5. Temminghoff, E. J. M.; Plette, A. C. C.; van Eck, R.; van Riemsdijk, W. H., Determination of the chemical speciation of trace metals in aqueous systems by the Wageningen Donnan Membrane Technique. *Analytica Chimica Acta* **2000,** *417* (2), 149-157.
6. Degryse, F.; Smolders, E.; Merckx, R., Labile Cd complexes increase Cd availability to plants. *Environmental Science and Technology* **2006,** *40* (3), 830-836.
7. Degryse, F.; Smolders, E.; Parker, D. R., Metal complexes increase uptake of Zn and Cu by plants: implications for uptake and deficiency studies in chelator-buffered solutions. *Plant and Soil* **2006,** *289* (1-2), 171-185.
8. Navarro, A.; Font, X.; Viladevall, M., Metal Mobilization and Zinc-Rich Circumneutral Mine Drainage from the Abandoned Mining Area of Osor (Girona, NE Spain). *Mine Water and the Environment* **2015,** *34* (3), 329-342.
9. Kinniburgh, D. G.; van Riemsdijk, W. H.; Koopal, L. K.; Borkovec, M.; Benedetti, M. F.; Avena, M. J., Ion binding to natural organic matter: competition, heterogeneity, stoichiometry and thermodynamic consistency. *Colloids And Surfaces A-Physicochemical And Engineering Aspects* **1999,** *151* (1-2), 147-166.
10. Milne, C. J.; Kinniburgh, D. G.; van Riemsdijk, W. H.; Tipping, E., Generic NICA-Donnan model parameters for metal-ion binding by humic substances. *Environmental Science and Technology* **2003,** *37* (5), 958-971.
11. Sans-Duñó, J.; Cecilia, J.; Galceran, J.; Puy, J., Availability of metals to DGT devices with different configurations. The case of sequential Ni complexation. *Science of The Total Environment* **2021,** *779*, 146277.
12. Uribe, R.; Mongin, S.; Puy, J.; Cecilia, J.; Galceran, J.; Zhang, H.; Davison, W., Contribution of partially labile complexes to the DGT metal flux. *Environmental Science and Technology* **2011,** *45* (12), 5317-5322.
13. Baeyens, W.; Gao, Y.; Davison, W.; Galceran, J.; Leermakers, M.; Puy, J.; Superville, P. J.; Beguery, L., In situ measurements of micronutrient dynamics in open seawater show that complex dissociation rates may limit diatom growth. *Scientific Reports* **2018,** *8*.
14. Galceran, J.; Gao, Y.; Puy, J.; Leermakers, M.; Rey-Castro, C.; Zhou, C.; Baeyens, W., Speciation of Inorganic Compounds in Aquatic Systems Using Diffusive Gradients in Thin-Films: A Review. *Frontiers in Chemistry* **2021,** *9* (170).
15. Galceran, J.; Puy, J., Interpretation of diffusion gradients in thin films (DGT) measurements: a systematic approach. *Environmental Chemistry* **2015,** *12* (2), 112-122.

16. Zhao, J. J.; Cornett, R. J.; Chakrabarti, C. L., Assessing the uranium DGT-available fraction in model solutions. *Journal of Hazardous Materials* **2020,** *384*.
17. Research, W. Find Root. https://reference.wolfram.com/language/ref/FindRoot.html.
18. Bradac, P.; Behra, R.; Sigg, L., Accumulation of Cadmium in Periphyton under Various Freshwater Speciation Conditions. *Environmental Science and Technology* **2009,** *43* (19), 7291-7296.

8 Conclusions

Dynamic analytical techniques provide a way to assess the chemical availability of trace-metals. In limited diffusion conditions, this is a reliable approach to better understand the bioavailability of trace-metals by biota.

In this thesis, a theoretical framework to model availability by DGT devices has been set up. Numerical simulation has been used to solve the resulting systems of equations with the final aim of assessing the processes influencing DGT accumulations in laboratory experiments with well defined compositions. These simulation tools have then been used to simulate the processes in natural waters.

Concomitantly, we have developed new strategies to determine physicochemical parameters of natural waters relevant to understand chemical availability. Special attention is devoted to determine dissociation rate constants of complexes and diffusion coefficients of chemical species.

Altogether, the simulation tools and the knowledge of the physicochemical parameters allow us to make an important step further in predicting nutritive or toxic properties of natural waters. The main results follow:

- We have set up new procedures to determine diffusion coefficients of free metal ion and complexes from experimental measurements in the diffusion cell device. The relevance of a DBL at both sites of the gel can be assessed with a reference metal ion whose diffusion coefficient is known.

- We have shown that a simple steady-state equation that considers an independent diffusion of the species holds to model the steady state diffusion of metal species coupled by chemical reactions from a donor solution to an acceptor one separated by a gel which defines a diffusion layer.

- Experimental measurements at different ligand concentrations allow us to determine the diffusion coefficients through the diffusive gel of free metals and complexes relevant in the speciation of the donor solution. The diffusion coefficient of NiNTA (3.78×10^{-10} m^2 s^{-1}) and $NiNTA_2$ (1.38×10^{-10} m^2 s^{-1}) in a gel of polyacrylamide at T=25°C has been obtained with this procedure.

- When concentrations at the donor and acceptor cell cannot be considered time independent during an experiment in a diffusive cell, i.e, when finite volume effects are non-negligible, new expressions describing the accumulation in the acceptor cell are reported based on an instantaneous steady-state approximation. These expressions set up a theoretical framework

that is helpful to determine the diffusion coefficient from linear regression of appropriate magnitudes. This approach can be very useful to measure the diffusion coefficients of trace-metals that are scarce in nature (especially at some pH ranges).

- The application of the lability degree in excess of ligand, perfect sink and steady-state conditions has been used to determine the kinetic dissociation constant of NiNTA complex.

- The flux at the interface of the resin-gel layer for the chemical system of Ni +NTA which endures the following sequential complexation reaction $\mathrm{Ni+NTA} \underset{k_d}{\overset{k_a}{\rightleftarrows}} \mathrm{NiNTA+NTA} \underset{k_{d,2}}{\overset{k_{a,2}}{\rightleftarrows}} \mathrm{Ni(NTA)_2}$ can be defined as the flux of a single formal complex. This definition holds because the rate limiting step in the dissociation reaction of the species $Ni(NTA)_2$ to Ni^{+2} corresponds to the dissociation of NiNTA to Ni^{+2}.

- The diffusion coefficient and the dissociation rate constant of the formal species “bound Ni” depends on the diffusion coefficient of both, NiNTA and $Ni(NTA)_2$ as well as on the conditional stability of the complexation reaction $\mathrm{NiNTA+NTA} \underset{k_{d,2}}{\overset{k_{a,2}}{\rightleftarrows}} \mathrm{Ni(NTA)_2}$

- The diffusion-reaction equations of a simple system $\mathrm{M+L} \underset{k_d}{\overset{k_a}{\rightleftarrows}} \mathrm{ML}$ have been solved considering the boundary conditions of the DGT devices with a heterogeneous distribution of the resin beads in the resin disc. DGT devices with one or two resin discs have been considered and the solution has been obtained from numerical simulation or with analytical expressions assuming perfect sink and excess of ligand conditions.

- An expression that relates the dissociation rate constant of a metal complex with the *%back* of metal accumulation in a DGT device with a stack of two homogeneous or heterogeneous resin discs has been derived.

- Physicochemical inequalities to assess whether the flux of free metal arriving to the DGT device is negligible in comparison to the flux of complex as well as to assess the relevance of the settling of the resin beads in the back accumulation are reported. Simplified procedures to determine the dissociation rate constant of a complex from the measurement of the *%back* are reported for each results of the inequalities above mentioned. In this framework, it has been obtained the effective value of the dissociation rate constant of a pool of inorganic complexes in a Osor stream. The dissociation rate constant thus obtained agree with the value that can be obtained from the measurement of the lability degree of this pool of complexes.

- The diffusion of complexes in the resin domain increases the accumulation in comparison with the accumulation expected when the resin domain was a hard and impenetrable disc. Accordingly, DGT fluxes can overestimate the flux received by biota in a given natural water. This assertion is supported by: i) the fact that biota (e.g bacteria, plants) that assimilates trace-metals by diffusion usually have a smaller thickness of the diffusion layer where complexes behave more inert than in DGT devices. ii) Penetration of complexes in the cell membranes is, in general, not allowed since only free metals have carriers to help them to be transported through the membrane. The fact that the resin layer is permeable to complexes along all the volume of the resin and the lack of free metal concentration in the resin domain shifts the complex towards the dissociation reaction. Whereas, in the case of biota, the free metal is adsorbed by the membrane proteins and the complexes cannot go through the cell membrane. Thus, the reaction layer is highly reduced and consequently the lability of the complexes decreases.

- A better estimation of the availability by biota can be obtained using $\delta^r=0$ in the expression that models the availability in DGT devices.

- A decrease of the reducible Hg concentration ($c_{red,Hg}$) in solution is found when the DOM/Hg ratio is increased. A similar result holds for the labile concentration which suggests a certain correlation between reducible and labile.

- In the case of Hg-SRFA, $c_{labile} \approx c_{T,Hg}$ indicating that the Hg-SRFA complexes in solution were almost fully labile. For this case, the reducible Hg concentration is not a good predictor of the lability properties of the complex, as only a 30% of Hg-SRFA in the sample is found to be reducible in all the DOM/Hg ratio studied.

- Speciation calculated by VMinteq with the NICA-Donnan model suggests that for the concentrations of Hg and humic acids used in this work, almost all the Hg in solution is complexed to the humic substances. This speciation agree well with the reported high affinity of Hg for humic and fulvic substances. Nevertheless, the fitted affinity parameters are based on trends and not on actual Hg-binding data. Thus, there is a need to fit a new set of NICA-Donnan binding parameters based on experimental binding data of Hg to humic substances.

- Based on the current binding parameters, the conditional affinity spectrum (CAS) allows to visualize the range of affinities where the Hg bound to SRHA is labile as well as the range of affinities at which the lability is lost for a given concentration of SRHA.

- The water from Osor stream right after the location of the former mine shows a total zinc concentration ($c_{T,Zn}$) and c_{DGT} significantly higher than the water in the Osor stream sampled several km up the position of the mine.

- A set of different DGT devices with different configurations have unravelled the presence of partially labile inorganic zinc complexes in the Osor stream. The lability degree of this pool of inorganic complexes is close to a 70% when DGT devices with 1 resin layer and 1 diffusive gel are considered and close to a 80% when DGT devices with 1 resin layer and 2 diffusive gels are considered.

- A *%back*=29% recorded in 2R1G DGT devices also supports the presence of partially labile Zn inorganic complexes in the Osor stream. From this data, the dissociation rate constant of the pool of inorganic complexes has been determined.

- The theoretical framework that relates the DGT concentration (c_{DGT}) with the concentration of the real species ($c_{DGT} = c_M^* + \sum_{i=1}^{h} \varepsilon_i c_{ML}^* \xi_i$) has been successfully applied to determine dissociation rate constant of a pool of inorganic zinc complexes and its effective diffusion coefficient from its application in Osor stream. The results showed that the pool of inorganic zinc complexes diffuse at the same rate than free metal ion and a dissociation rate constant k_d=1.2x10^{-3} s^{-1} has been estimated.

- The concept of effective concentration signature is introduced to quantitatively assess the concentration of zinc that biota would feel depending on uptake conditions and diffusion layer thickness.

- The concept of the characteristic thickness is introduced to label the thickness of a diffusion domain that a certain biota would need in order to feel a concentration equal to c_{DGT}. For all the configurations of DGT devices, the characteristic thickness is greater than the diffusive

gel layer of the DGT device considered. Moreover, the characteristic thickness is greater as the thickness of the diffusive gel layer of the DGT device considered is increased.